FOUNDED 1894

SAIMM

JOURNAL OF THE SOUTHERN AFRICAN INSTITUTE OF MINING AND METALLURGY

VOLUME 116 NO. 8 AUGUST 2016

THE top line matters...

The current economic climate means companies need to work more efficiently to reap the benefit of an upswing in the market.

"This has been one of the key pillars of the success of MIP Process during the last few years. We are able to maximise our resources and this allows us to provide faster and more cost efficient solutions"

says Philip Hoff, Managing Director

MIP Process is one of few Level 1 BEE Contributors in the industry they serve. We are proud of this and have strategies in place to maintain this status, Hoff affirms.

In order to strengthen the staff complement, a General Manager was appointed together with experienced engineers in various fields. This has enhanced the top structure of the organisation. This strategy together with client partnerships has proved to be successful if one looks at the amount of repeat customers we have, says Hoff.

MIP Process has executed numerous projects outside the African continent. They have supplied a flocculant plant to the Philippines, numerous thickeners and flocculant plants to Asia. MIP recently supplied an order for counter-current decantation (CCD) thickeners for a Copper Project in the Democratic Republic of Congo, which has expanded MIP's thickener solutions offering.

The acquisition of Alliance Dust Control (ADCS) secured in 2013, enhanced MIP's product range and they offer the complete dust extraction including bagfilters, scrubbers and dry cyclones.

The success of this acquisition can be seen in that two scrubber plants, for the removal of sulphur dioxide, was recently supplied for two different Copper/Cobalt projects in the DRC.

A contract for the supply of a taphole extraction system, for a larger chrome producer, with a substantial size bagfilter, is presently being executed.

MIP Process will be exhibiting at Electra Mining again in 2016. This is taking place from 12th to 16th September 2016 at Nasrec and is one of the biggest of its kind in the world. "MIP Process will be in Hall 6, Stand No. H05 as usual", concludes Hoff.

Our Current product range includes:

- Attrition Scrubbers
- Agitators
- Bagfilters
- Clarifiers
- Cyclones for dust extraction
- Depressant Pumps
- Horizontal Linear Screens
- Mixers
- Reagent Make-up Plants
- Screen-covers for vibrating screens
- Slurry Samplers
- Thickeners
- Wet Scrubbers

mip | PROCESS TECHNOLOGIES

MIP Process Technologies (Pty) Ltd. | P.O. BOX 677, Kelvin 2054 | Tel + (0) 11 234 1007
Fax: +27 (11) 86 682 2394 | E mail: sales@mipprocess.com | Website: www.mipprocess.com
MIP House, 4A Coombe Place, Rivonia, 2128

Reduced oscillation. Improved precision.

The Demag V-type girder – less is more.

The revolutionary architecture of the Demag V-type girder provides greater load handling efficiency. Thanks to tapered diaphragm joints, the oscillation characteristics are reduced by up to 30%. That cuts cycle times, boosts load handling rates and ensures improved precision in handling operations – above all in the upper load capacity range. This means that heavy loads can also be positioned even faster and more precisely without the need for electronic control systems.

Visit us at Electra Mining 2016, Stand B19, Hall 8.

Enquiry.sa@terex.com

DEMAG
A TEREX BRAND

OFFICE BEARERS AND COUNCIL FOR THE 2015/2016 SESSION

Honorary President
Mike Teke
President, Chamber of Mines of South Africa

Honorary Vice-Presidents
Mosebenzi Zwane
Minister of Mineral Resources, South Africa

Rob Davies
Minister of Trade and Industry, South Africa

Naledi Pandor
Minister of Science and Technology, South Africa

President
R.T. Jones

President Elect
C. Musingwini

Vice-Presidents
S. Ndlovu
A.S. Macfarlane

Immediate Past President
J.L. Porter

Honorary Treasurer
C. Musingwini

Ordinary Members on Council
Z. Botha
V.G. Duke
I.J. Geldenhuys
M.F. Handley
W.C. Joughin
M. Motuku
D.D. Munro
G. Njowa
A.G. Smith
M.H. Solomon
J.D. Steenkamp
M.R. Tlala
D. Tudor
D.J. van Niekerk

Past Presidents Serving on Council
N.A. Barcza
R.D. Beck
J.R. Dixon
M. Dworzanowski
F.M.G. Egerton
H.E. James
G.V.R. Landman
J.C. Ngoma
S.J. Ramokgopa
M.H. Rogers
G.L. Smith
W.H. van Niekerk

Branch Chairmen

Botswana	L.E. Dimbungu
DRC	S. Maleba
Johannesburg	I. Ashmole
Namibia	N.M. Namate
Northern Cape	C.A. van Wyk
Pretoria	P. Bredell
Western Cape	A. Mainza
Zambia	D. Muma
Zimbabwe	S. Ndiyamba
Zululand	C.W. Mienie

Corresponding Members of Council

Australia:	I.J. Corrans, R.J. Dippenaar, A. Croll, C. Workman-Davies
Austria:	H. Wagner
Botswana:	S.D. Williams
United Kingdom:	J.J.L. Cilliers, N.A. Barcza
USA:	J-M.M. Rendu, P.C. Pistorius

PAST PRESIDENTS

*Deceased

* W. Bettel (1894–1895)
* A.F. Crosse (1895–1896)
* W.R. Feldtmann (1896–1897)
* C. Butters (1897–1898)
* J. Loevy (1898–1899)
* J.R. Williams (1899–1903)
* S.H. Pearce (1903–1904)
* W.A. Caldecott (1904–1905)
* W. Cullen (1905–1906)
* E.H. Johnson (1906–1907)
* J. Yates (1907–1908)
* R.G. Bevington (1908–1909)
* A. McA. Johnston (1909–1910)
* J. Moir (1910–1911)
* C.B. Saner (1911–1912)
* W.R. Dowling (1912–1913)
* A. Richardson (1913–1914)
* G.H. Stanley (1914–1915)
* J.E. Thomas (1915–1916)
* J.A. Wilkinson (1916–1917)
* G. Hildick-Smith (1917–1918)
* H.S. Meyer (1918–1919)
* J. Gray (1919–1920)
* J. Chilton (1920–1921)
* F. Wartenweiler (1921–1922)
* G.A. Watermeyer (1922–1923)
* F.W. Watson (1923–1924)
* C.J. Gray (1924–1925)
* H.A. White (1925–1926)
* H.R. Adam (1926–1927)
* Sir Robert Kotze (1927–1928)
* J.A. Woodburn (1928–1929)
* H. Pirow (1929–1930)
* J. Henderson (1930–1931)
* A. King (1931–1932)
* V. Nimmo-Dewar (1932–1933)
* P.N. Lategan (1933–1934)
* E.C. Ranson (1934–1935)
* R.A. Flugge-De-Smidt (1935–1936)
* T.K. Prentice (1936–1937)
* R.S.G. Stokes (1937–1938)
* P.E. Hall (1938–1939)
* E.H.A. Joseph (1939–1940)
* J.H. Dobson (1940–1941)
* Theo Meyer (1941–1942)
* John V. Muller (1942–1943)
* C. Biccard Jeppe (1943–1944)
* P.J. Louis Bok (1944–1945)
* J.T. McIntyre (1945–1946)
* M. Falcon (1946–1947)
* A. Clemens (1947–1948)
* F.G. Hill (1948–1949)
* O.A.E. Jackson (1949–1950)
* W.E. Gooday (1950–1951)
* C.J. Irving (1951–1952)
* D.D. Stitt (1952–1953)
* M.C.G. Meyer (1953–1954)
* L.A. Bushell (1954–1955)
* H. Britten (1955–1956)
* Wm. Bleloch (1956–1957)
* H. Simon (1957–1958)
* M. Barcza (1958–1959)
* R.J. Adamson (1959–1960)
* W.S. Findlay (1960–1961)
D.G. Maxwell (1961–1962)
* J. de V. Lambrechts (1962–1963)
* J.F. Reid (1963–1964)
* D.M. Jamieson (1964–1965)
* H.E. Cross (1965–1966)
* D. Gordon Jones (1966–1967)
* P. Lambooy (1967–1968)
* R.C.J. Goode (1968–1969)
* J.K.E. Douglas (1969–1970)
* V.C. Robinson (1970–1971)
* D.D. Howat (1971–1972)
J.P. Hugo (1972–1973)
* P.W.J. van Rensburg (1973–1974)
* R.P. Plewman (1974–1975)
* R.E. Robinson (1975–1976)
* M.D.G. Salamon (1976–1977)
* P.A. Von Wielligh (1977–1978)
* M.G. Atmore (1978–1979)
* D.A. Viljoen (1979–1980)
* P.R. Jochens (1980–1981)
G.Y. Nisbet (1981–1982)
A.N. Brown (1982–1983)
* R.P. King (1983–1984)
J.D. Austin (1984–1985)
H.E. James (1985–1986)
H. Wagner (1986–1987)
* B.C. Alberts (1987–1988)
C.E. Fivaz (1988–1989)
O.K.H. Steffen (1989–1990)
* H.G. Mosenthal (1990–1991)
R.D. Beck (1991–1992)
* J.P. Hoffman (1992–1993)
* H. Scott-Russell (1993–1994)
J.A. Cruise (1994–1995)
D.A.J. Ross-Watt (1995–1996)
N.A. Barcza (1996–1997)
* R.P. Mohring (1997–1998)
J.R. Dixon (1998–1999)
M.H. Rogers (1999–2000)
L.A. Cramer (2000–2001)
* A.A.B. Douglas (2001–2002)
S.J. Ramokgopa (2002-2003)
T.R. Stacey (2003–2004)
F.M.G. Egerton (2004–2005)
W.H. van Niekerk (2005–2006)
R.P.H. Willis (2006–2007)
R.G.B. Pickering (2007–2008)
A.M. Garbers-Craig (2008–2009)
J.C. Ngoma (2009–2010)
G.V.R. Landman (2010–2011)
J.N. van der Merwe (2011–2012)
G.L. Smith (2012–2013)
M. Dworzanowski (2013–2014)
J.L. Porter (2014–2015)

Honorary Legal Advisers
Van Hulsteyns Attorneys

Auditors
Messrs R.H. Kitching

Secretaries
The Southern African Institute of Mining and Metallurgy
Fifth Floor, Chamber of Mines Building
5 Hollard Street, Johannesburg 2001 • P.O. Box 61127, Marshalltown 2107
Telephone (011) 834-1273/7 • Fax (011) 838-5923 or (011) 833-8156
E-mail: journal@saimm.co.za

Typeset and Published by
The Southern African Institute of Mining and Metallurgy
P.O. Box 61127
Marshalltown 2107
Telephone (011) 834-1273/7
Fax (011) 838-5923
E-mail: journal@saimm.co.za

Printed by
Camera Press, Johannesburg

Advertising Representative
Barbara Spence
Avenue Advertising
Telephone (011) 463-7940
E-mail: barbara@avenue.co.za

The Secretariat
The Southern African Institute of Mining and Metallurgy

ISSN 2225-6253 (print)
ISSN 2411-9717 (online)

SAIMM
JOURNAL OF THE SOUTHERN AFRICAN INSTITUTE OF MINING AND METALLURGY
VOLUME 116 NO. 8 AUGUST 2016

Contents

Journal Comment

Diamonds still Sparkling Conference 2016

What an apt name for this conference, given the current turmoil in the mining industry as a whole and particularly here in southern Africa. While the rest of the industry battles through its routine commodity cycle, diamonds seem able to maintain a certain sparkle. That is not to say that diamonds do not experience their own cycles, but rather that diamonds have always stood apart from other minerals commodities and seem to have that little bit extra. With the De Beers's 'Diamonds are Forever' catchline and 'Diamonds are a girl's best friend' slogan keeping the allure of diamonds up there apart from the other commodities.

In southern Africa, the impact of diamonds and diamond mining has been immense, from the humble beginnings in the mid-1860s in Kimberley, which led to the industrialization of the subcontinent, to the empowerment of important leaders of their generations who, although somewhat controversial, made a significant impact – Barney Barnato and Cecil John Rhodes, and the long-lasting Oppenheimer legacy, spanning four generation to the creation of the mining giant De Beers – through to the discovery of diamonds in Botswana, which underpinned the successful and sustainable growth of this country, to the more recent, probably less sustainable Marowa/Marange fields in Zimbabwe.

Diamonds and diamond mining have also been at the forefront of mining industry for many decades, leading the way with mechanization and innovation. In addition to this, the discovery of large, 'magical' diamonds really adds another dimension to their 'sparkling nature'. Never more so than in recent years, with a number of these finds that have really added some sparkle, the likes of the Lesotho Promise, from Letseng, the Cullinan Heritage, and most recently the 1111 carat Lesedi La Rona recovered at Karowe in Botswana.

The challenges that face the diamond industry in the next few decades are complex and cover a broad spectrum. Some of these are:

- Lower availability of high-grade, massive orebodies
- The technical challenges of profitably extracting diamonds from greater depths
- The ever-increasing limits on natural resources, water and power in particular
- An ever-increasing and complicated social and political environment, putting additional pressure on the industry
- The conflict between the inherent drive to mechanize *versus* the backdrop of ever-increasing unemployment
- The rapidly increasing capacity of technology and its ability to communicate in real time
- The threat that conflict and/or synthetic diamonds poses to the real diamond sparkle.

These challenges make for an exciting future, one that will require the kind of leadership, innovation, and belief in the 'big picture' that have sustained this industry for its first 150 years, to ensure that these challenges are overcome and that the diamond industry sparkles, shines, and lives up to its name for the next 150 years.

This conference was successful through the participation of all those who attended. That success will continue to drive us, encouraging us to take future challenges head-on, so that we can all leave our mark on the industry so it continues to sparkle.

On behalf of the Diamonds Conference Organizing Committee, I would like to take this opportunity to thank all of the presenters and speakers who so graciously share their knowledge with all of us; the sponsors who made the event possible; the organizing committee for its hard work and effort to create the conference; and lastly I would like to thank all delegates for their attendance and support

I trust that this special issue of the SAIMM *Journal* will benefit your own operations and, ultimately, our industry as a whole, and that you will be fired up to sparkle.

H. Marsden
Conference Convener

Goals, Systems, and Plans

On 12 May 1964 Don Shepherd, a 48-year-old gold miner (actually an underground locomotive driver) from Crown Mines in Johannesburg, set out from the Los Angeles City Hall to begin a solo coast-to-coast run across America. At the time, this was the longest run in the world by an amateur runner. Part of his preparation involved running from Johannesburg to Cape Town. He ran alone, completely unaided, with no backup vehicle, and only a small transistor radio for company. He had no financial sponsorship, and did the trip on a shoestring budget, allowing himself $10 daily to pay for his food and accommodation. He had spent much time saving for and planning the trip. He carried a small backpack containing a spare shirt, socks, plastic raincoat, shoe patching equipment and scissors, petroleum jelly, toothbrush and toiletries, a small water bottle, and a map. Because he didn't trust the American style of running shoes, he posted a parcel containing a spare pair of canvas takkies to the postmaster in Lincoln, Nebraska, to be collected halfway through his journey. Don completed his 3200 mile (5100 km) journey to New York City in 73 days, 8 hours, and 20 minutes, averaging 70 km per day, typically running for nine to fourteen hours a day. His amazing story is told in his book «My Run Across the United States', published in 1970.

I met Don Shepherd and read his book while I was in primary school, and was inspired by the story. However, not everyone can undertake such a feat. Many years later, in 2010, I visited Guernsey (one of the Channel Islands), and remembered the story of the coast-to-coast run, and realized that sometimes one needs to re-frame grand ideas into goals that can actually be accomplished. A coast-to-coast run across the USA is beyond my reach, but Guernsey was small enough for me to fulfil my long-standing ambition to do a coast-to-coast run (not quite LA to New York, but still lots of fun). I started my run touching the ocean on the east coast at St Peter Port, Guernsey's capital, and headed west running along scenic tree-lined leafy narrow roads until I reached the ocean on the west coast less than ten kilometres later. The biggest challenge was finding the correct bus to get back to my hotel afterwards.

Goals are so important to many people, and can indeed provide direction and motivation to accomplish great things. Yet, they can also lead to disappointment if they are not achieved. All too often, life interferes with the plans we make. In the words of Robert Burns: 'The best-laid schemes o' mice an' men gang aft agley'. Dilbert cartoonist Scott Adams has written numerous articles and a book on the benefits of systems over goals, saying that 'goals are for losers and systems are for winners'. When trying to improve at something, it is perhaps better to implement a system (that can grow into a habit) than to set goals that often remain unmet. A system is something you do on a regular basis that will inevitably lead to improvement in the long run, whereas goals provide only occasional moments of great satisfaction, punctuating a more common state of non-accomplishment. Working to a system means that you focus on things you can control, rather than aiming at goals that are missed because of extraneous circumstances. Back to my running story: I prefer to run along trails that are enjoyable and pleasurable to me, rather than setting a goal of a certain distance per week. In this way, no willpower is required to exercise, and I have continued to participate actively in this sport over many years.

Time has passed so quickly over this past year, and my time as President of SAIMM is almost at an end. When I look back over the year, I see great strides of progress that have been made in certain areas, along with limitations brought about by the difficult state of the mining industry at present. Some plans have taken shape, some goals have been achieved, and some things have had to be deferred until better times. However, the structure of the Institute is a very sound one in that it ensures a steady flow of new ideas and energy into the organization, while retaining continuity for existing initiatives. I believe we have a very good system in place.

William Shakespeare (in his story of Troilus and Cressida) said: 'Things won are done; joy's soul lies in the doing'. We should take pleasure in real achievements and not only in the accolades that sometimes accompany them. It has been a great pleasure to work with a wonderful team in carrying out the business of the Institute during this past year.

R.T. Jones
President, SAIMM

Obituary

Johannes Paulus Hoffman the Technical Father of 3CR12

Hannes Hoffman, a past President of the Institute, passed away on 16 August 2016 in hospital in George after a short illness.

Hannes Hoffman was born on 9 of March 1933. He obtained a BSc in iron and steel technology, a BSc (Hons) and MSc in metallurgy, as well as an MBA. After working at Iscor, the University of Pretoria and O'okiep Copper Co., he moved to Southern Cross Steel in 1973 to take up the position of head of Metallurgy, later called the manager of Materials Science. In 1988 he was transferred to New Process Development as manager and in 1995 he became the manager of Research and Development. From 1992 to 1993 he was the President of the South (now Southern) African Institute of Mining and Metallurgy (SAIMM). He retired in 1996.

Lucien Matthews in offering his condolences, said that 'Columbus Stainless also recognizes and pays tribute to Hannes for the work he did with numerous other players in developing 3CR12. Their sterling and groundbreaking work led to 3CR12 becoming a world-recognized and accepted material of first choice for building rail wagons for transporting coal. Hannes, Columbus Stainless appreciates your contribution over the years and salutes you.'

Dave Smith remembers working closely with Hannes. He says: 'He was a great mentor for me. I spent many an hour in Hannes's office discussing stainless steels, particularly the ferritics. He was always approachable and never held back in imparting his knowledge. Hannes was very old-school and was held in high regard by everyone. Process changes would be made on the basis of a short memo from Hannes: he was never questioned and never needed to be. If there was a Mr Stainless Steel South Africa, Hannes was it.'

John Tarboton also remembers Hoffman well. He says: 'When I first worked in the lab in 1986, Hannes was the go-to person for technical matters on stainless steel in general, but 3CR12 in particular. Hannes would always take the time to discuss the latest theory or to give guidance or suggest what to look out for and what tests to conduct. He was a great mentor for me when I first joined MS&A.'

Rob White confirmed that 'whilst being technically competent and very driven, he had a very wry sense of humour. I have no doubt that this kept the team together during some of the many exploratory heats where many surprises were encountered. He took what he did seriously but was always sufficiently light-hearted within himself to be open to most approaches.'

Obituary *(continued)*

Hannes Hoffman was regarded as the Technical Father of 3CR12 and here is his story.

In the early 1970s, a group of men at Southern Cross (SX) set their minds to finding a solution to the cost/efficiency conundrum of the steel industry. They knew what they were looking for: a utility, corrosion-resisting steel to replace mild steel at a fraction of the cost of stainless steel. However, they didn't quite know how to get it. Hannes Hoffman was the project leader tasked with finding the solution. The team consisted of Ken Dewar and Dr Rainer Dietrich. The starting point was 409 stainless steel. Hannes introduced the Kaltenhauser equation to calculate the ferrite factor (FF), a means to predict the microstructure. Initially he aimed for a FF to make the steel fully ferritic. A trial plant heat of 409T78 (T78 for temporary specification 78), was made without 'washing' the vessel after an austenitic heat, resulting in a higher-than-planned nickel content. The heat was processed and when samples came to the laboratory for 'hammer testing', a test designed to measure toughness, the steel was discovered to be extremely tough and ductile in thick gauges. Dr Rainer Dietrich came into Hannes' office one morning with a strip of steel that he had gripped with a vice and given a few twists, to prove the ductility. They had discovered that the higher amount of nickel moved the steel from the fully ferritic into a dual-phase realm. The team immediately introduced a nickel target content of 0.6% to move the composition into the dual phase (ferrite and austenite at high temperatures to produce ferrite and martensite on cooling). Ken Dewar had correctly identified that the resulting microstructure was ferritic-martensitic. The martensite in 3CR12 was tough and its presence prevented the normal embrittlement problems seen in conventional ferritic stainless steels. After further tweaking and toning, as well as taking the meltshop's capabilities into account, 3CR12 had arrived.

A tribute from the SAIMM and Mintek

Hannes Hoffman's Presidential address and paper published in the SAIMM *Journal* in August/September 1992 entitled 'Oxygen-coal in-bath smelting reduction - a future process for the production of iron and stainless steel?' (http://www.saimm.co.za/Journal/v092n08p253.pdf) reflects his outstanding ability to contribute to the pyrometallurgical and physical metallurgy/material science and engineering fields, while paying careful attention to environmental aspects of processes. This ability relates directly to his work initially at ISCOR and subsequently at Middelburg Steel and Alloys (MS&A), which produced both ferrochrome alloys and stainless steel. The former activity is now part of Samancor Chrome and the latter of Columbus Stainless, where Hannes continued his illustrious career. His interest in direct stainless steelmaking technologies and the properties of ferrochrome and stainless steels led to the very valuable interactions that Hannes and his colleagues had with universities such as Pretoria and Wits, as well as research councils such as the CSIR and Mintek, over many years. The contribution that Hannes made to the steel industry has endured long after his retirement and will no doubt continue well into the future.

J. Tarboton
Southern Africa Stainless Steel Development Association

PAPERS IN THIS EDITION

These papers have been refereed and edited according to internationally accepted standards and are accredited for rating purposes by the South African Department of Higher Education and Training

Papers – Diamonds Conference

These papers will be available on the SAIMM website
http://www.saimm.co.za

PAPERS IN THIS EDITION

These papers have been refereed and edited according to internationally accepted standards and are accredited for rating purposes by the South African Department of Higher Education and Training

Papers of General Interest

These papers will be available on the SAIMM website
http://www.saimm.co.za

http://dx.doi.org/10.17159/2411-9717/2016/v116n8a1

Pioneering large diamond recovery at Karowe diamond mine

by L.M. van Niekerk*, A. Olivier†, J. Armstrong‡, and N.A. Sikwa§

Synopsis

Historically, the recovery of large diamonds in conventional treatment plant flow sheets has been associated with dense media separation (DMS). This is attributed mainly to DMS's highly efficient and proven track record in the concentration and separation of ores with variable solids densities. In most instances, DMS has been utilized as a pre-concentration step ahead of any recovery plant, due to its ability and versatility in reducing feed within a specific size range to manageable volumes for downstream X-ray processing and subsequent diamond recovery. The benefit of using carbon-signature-based detection equipment for retrieving large stones upfront in the flow sheet not only equates to earlier recovery of diamonds from the system, but also lessens the exposure of diamond-bearing ore to additional materials handling, pumping, and/or crushing, which has been known to damage or even break diamonds and decrease revenue.

Keywords
diamond recovery, preconcentration, sorting, X-ray transmission.

Introduction

The selection of X-ray transmission (XRT) technology for kimberlite sorting lies in the advantage of the material presentation. Detection with XRT is dependent on the atomic number of the material. The sorting ability and effectiveness of XRT is based on the difference in the atomic numbers of the materials that need to be separated. The advantage of this technique is that the presentation of the material is of lesser importance. Unlike near-infrared (NIR) and X-ray luminescence (XRL), XRT is not dependent on a visible colour difference or clean, reflective particle surfaces. XRT technology has a significantly higher detection rate for Type II diamonds compared to traditional XRL sorters, with an order-of-magnitude lower concentrate yield percentage. XRT sorters deliver a significantly lower percentage yield than traditional DMS plants, with a vastly reduced running costs relating to consumables and utilities. Figure 1 summarizes the characteristics of the various sorting technologies and their applications.

A broadband electrical X-ray beam is impinged on the material to be sorted (Riedel and Dehler, 2010) while it is moving along a belt (Figure 2). The X-ray sensor system below the material produces a digital image of the material being sorted, using two different energy bands (Figure 3). The X-ray attenuation through the material is different for the two bands and depends on the material's thickness and density. A transformation of the density images of the two bands then enables the classification of each pixel according to the average atomic density of the particle (Figure 4).

Each pixel is classified relative to a reference density against which the system has been calibrated. A complete particle will then be classified according to the overall classification of the pixels within the particle. Depending on the classification, the selected particles are either 'ejects', diverted upwards by air jets out of the overall material stream (material stream B) or 'accepts' in the other stream (material stream A) (Figure 5). It is important to note that 'eject' refers to the material that the system has been configured to blow out of the material stream; this can be either the waste or the product.

XRT circuit design, commissioning, and performance

The Karowe XRT section, part of the greater Karowe Plant Upgrade circuit, is situated after autogenous (AG) milling (van Niekerk *et al.*, 2013), where a DMS/bulk sorter sizing screen is utilized to separate the XRT feed envelope from the –8 mm DMS feed. Any –1.5 mm fine effluent generated in the circuit due to particle breakdown by materials handling, transfers, and recycling is also separated.

* *DRA Mineral Projects, Johannesburg, South Africa.*
† *Tomra Sorting Solutions, Randburg, South Africa.*
‡ *Mineral Resources, Lucara Diamond Corp, Vancouver BC, Canada.*
§ *Karowe Diamond Mine, Letlhakane, Botswana.*

 ISSN 2225-6253. This paper was first presented at the Diamonds still Sparkling 2016 Conference, *14–17 March 2016, Gaborone International Convention Centre.*

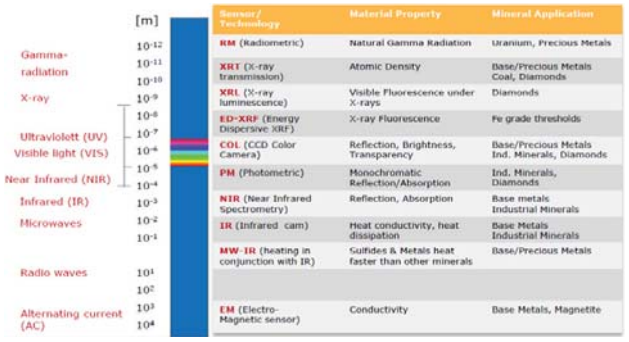

Figure 1—Sensor technology applications (von Ketelhodt, 2012)

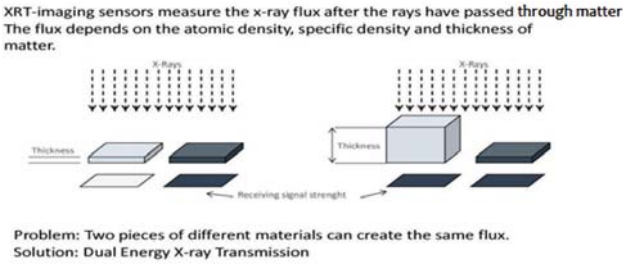

Figure 2—Principle of material discrimination by XRT sorter

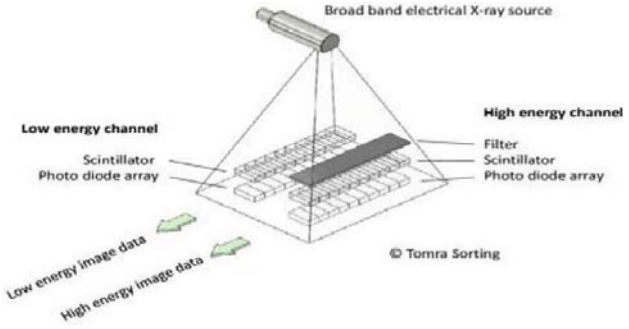

Figure 3—Dual XRT sensing

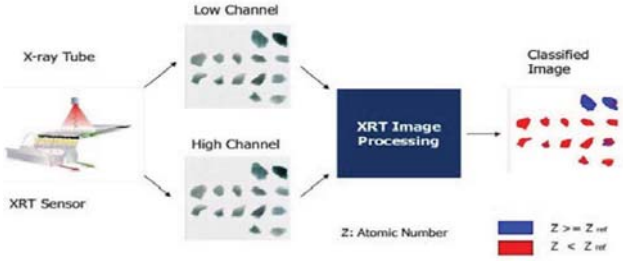

Figure 4—XRT imaging (Riedel and Dehler, 2010)

The DMS/bulk sorter sizing screen is key to the circuit (Figures 6, 7, and 8) due to its central positioning in receiving milled ore, tertiary crusher product, and pebble crusher 'bleed' fraction (pebble crusher recycle bypass not re-directed back to mill feed for load management requirements). From the DMS/bulk sorter sizing screen, the feed is split into the following three streams:

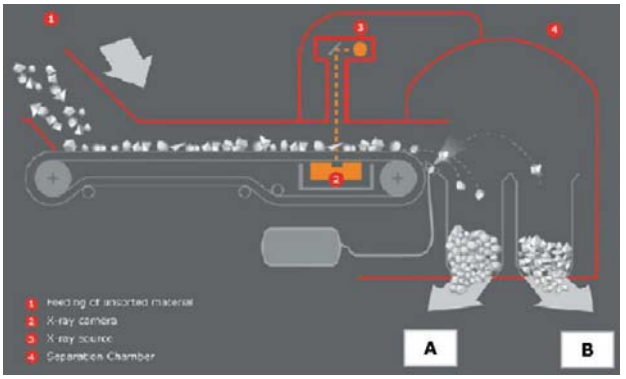

Figure 5—XRT automated sorting principle

- –60 +8 mm fraction, which is wet-screened and fed to the XRT section
- –8 +1.5 mm fraction, which is wet-screened and fed to the existing DMS for gravity concentration
- –1.5 mm envelope, which is removed as effluent to the degrit circuit for grit removal and dewatering. There is little to no value in the effluent stream, hence the reason for removal and dewatering.

In the XRT section, the –60 +8 mm is further separated via the bulk sorter sizing screen at the top of the XRT building into the following streams:

- Large diamond recovery (one stream) –60 +32 mm
- Coarse XRT (two streams) –32 +14 mm
- Middles XRT (two streams) –14 +8 mm.

To recover large diamonds in the various XRT size fractions as described above, the processing route for each individual size fraction stream utilizes bins and variable-speed belt feeders to 'match' each associated XRT sorter's size-specific throughput. Feed presentation ahead of each XRT machine was a critical factor evaluated during the design phase: a vibrating feeder ahead of the XRT machine accepts feed from the upstream belt feeder and introduces an evenly distributed monolayer feed to the XRT feed belt, which typically runs at speeds of up to 3 m/s. Table I illustrates the throughput to size fraction relationship applicable to Karowe's bulk sorting section.

Feed moisture content from upstream washing/sizing was also crucial to the design, as more than 8% surface moisture (by weight) will cause unnecessary build-up of fines in the bulk sorting section and detrimentally affect the machine's performance. Supporting utility services were also essential in order for each sorter to perform at its optimum efficiency – by utilizing compressed air and chilled water as essential services to the machines, diamond concentrate could be adequately 'ejected' from each sized stream with chiller water, effectively cooling the X-ray tubes for continuous successful operation. Tables II and III capture the chiller water and compressed air services data. The data was developed during design and subsequent operation of the Karowe XRT sorter machines.

Cold commissioning of the Karowe XRT machines was completed on 15 April 2015. This included the following vendor-specific activities:

- Splicing of new sorter belts

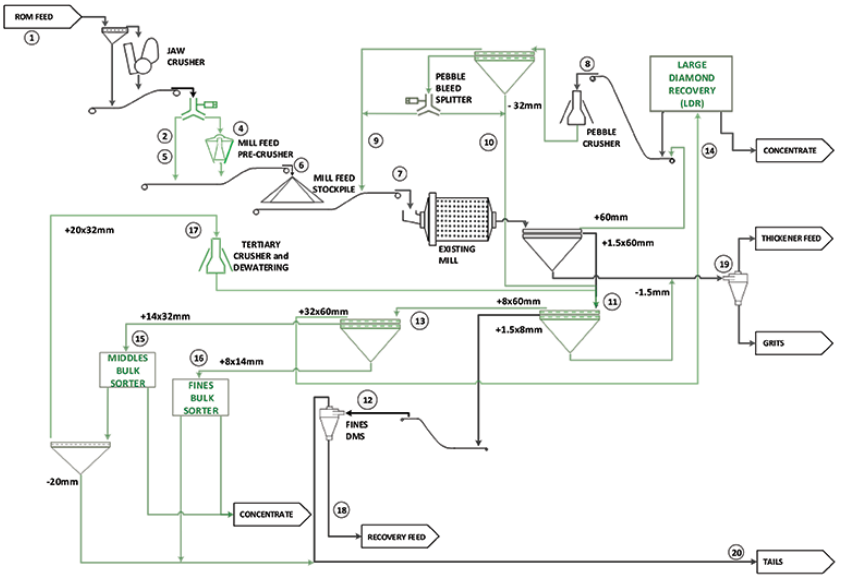

Figure 6—XRT treatment section in relation to the Karowe Plant Upgrade Project circuit (Morgan *et al.*, 2015)

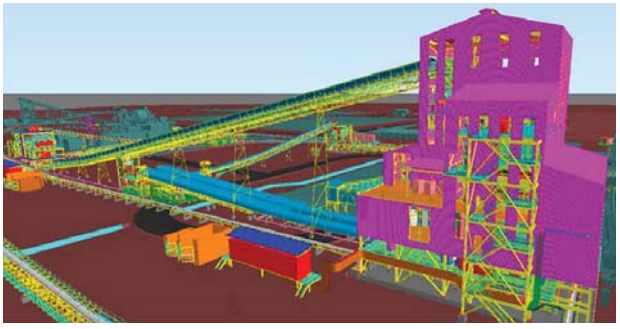

Figure 7—3D model of Karowe's XRT section (in foreground, with purple shading)

Figure 8—Karowe's XRT section during construction in Q2 2015

- Electrical wiring of the sorters
- Sorter calibrations and sorting algorithms
- Tracer testing without material
- Diamond testing without material.

Table I

XRT throughput *vs* size fraction treatment

Maximum machine throughput – Karowe plant-specific		
Description	**Size fraction**	**Throughput (t/h)**
Large diamond recovery (LDR) XRT bulk sorting	–60 +32 mm	150
Coarse XRT bulk sorting	–32 +14 mm	100
Middles XRT bulk sorting	–14 +8 mm	60

Table II

Chiller water requirements per Karowe XRT sorter

Description	Value/comment
Water circuit flow rate (l/min)	10
Water pressure at machine inlet (bar)	4.5
Maximum operating temperature (˚C)	40
Water inlet temperature (˚C) (Chiller pipes require isolation lagging to keep fluid temperature to a minimum before feed entry into machines)	25
Cooling capacity required (kW, accumulated heating energy) 4 kW X-ray source 4 kW generator	8
Coolant	High glycol content; ≤ 10%concentration

During the tracer and diamond testing without material, the tracer and diamond quantities with specifications in Table IV were utilized to calibrate, set up, and test the performance of individual machines. Aspects requiring set-up and testing included white balance, nozzle to pixel mapping, divergence, and establishing the various calibration curves.

Table III

Consumed air requirements per ton of feed ejected

Description	Value
Large diamond recovery (LDR) XRT bulk sorting (m3/h)	20 (Based on 1% material ejection rate)
Coarse XRT (m^3/h)	25 (Based on 1% material ejection rate)
Middles XRT (m^3/h)	50 (Based on 1% material ejection rate)
Operating air pressure (bar)	9.5–10.0

Table IV

Karowe XRT tracer and diamond specifications used during cold commissioning

Material size fraction (mm)	Number of cubic carbon tracers used	Tracer dimensions (mm)	Minimum diamond size range (mm)
LDR: –60 +32 mm at 150 t/h	500 at 98% expected recovery	50 × 50 × 50	24.26 × 20.12 × 24.12 (tracer diamond #52)
Coarse: –32 +14 mm at 100/200 t/h (throughput per sorter / overall throughput)	500 at 98% expected recovery	15 × 15 × 15	11.14 × 11.03 × 9.51 (tracer diamond #25)
Middles: –14 +8 mm at 43/86 t/h (throughput per sorter / overall throughput)	500 at 98% expected recovery	10 × 10 x 10	6.54 × 6.83 × 6.99 (tracer diamond #52)

Table V

Karowe LDR (–60 +32 mm) XRT sorter tracer test results

Tracer test no.	Totalizer start (t)	Totalizer stop (t)	Tons treated during tracer test	Number of tracers added to ore feed	% tracer recovery
1	5.8	14.0	8.2	100	100
2	14.0	26.2	12.2	100	100
3	26.2	33.9	7.7	100	100
4	33.9	46.5	12.6	100	100
5	46.5	54.3	7.8	100	100
Total / average	—	—	48.5 (total)	500 (total)	100 (average)
Average throughput range during all tracer test runs (t/h)	100–153				
% VSD setting on belt feeder feeding XRT sorter	20 (tests 1, 2) and 38 – 42 (Tests 3, 4, and 5)				

Following cold commissioning, which was completed on 15 April, the project moved into a hot commissioning phase with the following activities:

- Tracer testing with material feed
- Production ramp-up
- Production optimization.

Tracer results obtained during hot commissioning of the XRT sorters can be seen in Tables V to IX.

Average yields achieved during tracer tests in material feed were in the order of 1.3–8.0 × 10^{-5}%, with an associated calculated product yield range of 0.3–1.2 kg/d. Hot commissioning was completed on 27 April 2015, and the XRT sorters were handed over to the client for normal production running. Production performance monitoring continued after XRT handover for a further 28 days. Further XRT optimization was required to address the challenges experienced post-production running. These challenges were:

- Low air consumption and air inlet pressure: mitigating action involved separating the LDR XRT separator from the rest of the XRT compressed air circuit with its own dedicated compressor unit
- Low chiller water inlet flow: matter resolved on-site through small system adjustments
- Occasional fines carry-over from DMS/bulk sorter sizing screen: this was alleviated by optimizing the spray and wash water requirements associated upstream with the DMS/bulk sorter sizing screen.

On 18 November 2015, Karowe mine made history when Lucara Diamond Corporation reported the recovery of an 1111 carat, white Type IIa stone weighing 222 g and measuring 65 mm × 56 mm × 40 mm (Financial Post, 2015). This is the second-largest gem-quality stone in history – beaten only by the massive Cullinan diamond discovered in 1905 and weighing 3106 carats. Karowe mine also recovered an 813 carat, white Type IIa diamond soon after the 1111 carat find – which is the sixth-largest gem-quality stone also ever recovered.

Future XRT upgrades envisaged at Karowe mine

Due to the prevalence of very large diamonds at Karowe, the mine has opted to evaluate the possibility of a very large

Table VI

Karowe Coarse 1 (–32 +14 mm) XRT sorter tracer test results

Tracer test no.	Totalizer start (t)	Totalizer stop (t)	Tons treated during tracer test	Number of tracers added to ore feed	% tracer recovery
1	12.4	18.6	6.2	100	100
2	18.6	24.1	5.5	100	100
3	24.1	29.0	4.9	100	100
4	29.0	33.6	4.6	100	100
5	33.6	37.4	3.8	100	100
Total / average	—	—	25.0 (total)	500 (total)	100 (average)
Average throughput range during all tracer test runs (t/h)	100–120				
% VSD setting on belt feeder feeding XRT sorter	25				

Table VII

Karowe Coarse 2 (–32 +14 mm) XRT sorter tracer test results

Tracer test no.	Totalizer start (t)	Totalizer stop (t)	Tons treated during tracer test	Number of tracers added to ore feed	% tracer recovery
1	3.0	8.8	5.8	100	100
2	8.8	13.8	5.0	100	100
3	13.8	18.6	4.8	100	100
4	18.6	24.8	6.2	100	100
5	24.8	29.4	4.6	100	100
Total / average	—	—	26.4 (total)	500 (total)	100 (average)
Average throughput range during all tracer test runs (t/h)	90–130				
% VSD setting on belt feeder feeding XRT sorter	25				

Table VIII

Karowe Middles 1 (–14 +8 mm) XRT sorter tracer test results

Tracer test no.	Totalizer start (t)	Totalizer stop (t)	Tons treated during tracer test	Number of tracers added to ore feed	% tracer recovery
1	34.8	38.3	3.5	100	100
2	38.3	41.0	2.7	100	98
3	41.0	44.3	3.3	100	100
4	44.3	47.0	2.7	100	100
5	47.0	49.4	2.4	100	99
Total / average	—	—	14.6 (total)	500 (total)	99.4 (average)
Average throughput range during all tracer test runs (t/h)	40–43				
% VSD setting on belt feeder feeding XRT sorter	13				

Table IX

Karowe Middles 2 (–14 +8 mm) XRT sorter tracer test results

Tracer test no.	Totalizer start (t)	Totalizer stop (t)	Tons treated during tracer test	Number of tracers added to ore feed	% tracer recovery
1	46.9	50.9	1.3	100	100
2	50.9	52.1	1.2	100	100
3	52.1	53.3	1.2	100	99
4	53.3	54.6	1.3	100	100
5	54.6	55.8	1.2	100	100
Total / average	—	—	6.2 (total)	500 (total)	99.8 (average)
Average throughput range during all tracer test runs (t/h)	41–44				
% VSD setting on belt feeder feeding XRT sorter	13				

diamond recovery (VLDR) section close to the current secondary crushing area. A potential design would entail keeping the sorting and comminution aspects separate from a process perspective, so that the undersize scalping associated with comminution can be changed independently of the VLDR sorter. In a nutshell, a proposed design will consider:

- Scalping of all primary crusher ROM product at 60 mm or even 50 mm, with the –60/50 mm undersize reporting directly to the AG mill
- Inclusion of a 125 mm grizzly screen ahead of secondary crushing to treat the oversize fraction from the scalping screen, with the –125 +50 mm middles envelope directed to the VLDR sorter(s) for diamond recovery
- Tailings from the new VLDR sorter(s) will subsequently recombine with the +125 mm grizzly oversize material and be subjected to the existing proportional splitter ahead of the secondary crushing section, undergoing the same crusher/bypass operational split flexibility of 25, 50, or 75% as is currently the case.

Acknowledgements

The authors are grateful to the following individuals:

- William Lamb, Lucara Diamond Corp
- Paul Day, Lucara Diamond Corp
- Gerald Ndlovu, Boteti Mining
- John Maketo, Boteti Mining
- Boteti Process, Lab, and Security teams
- Fabien Riedel, Tomra Sorting Solutions
- Geoffrey Madderson, Tomra Sorting Solutions
- Gavin Underwood, Minopex Botswana
- Paul Morgan, DRA Mineral Projects
- Matthew Duddy, DRA Mineral Projects
- Bennie Viljoen, DRA Mineral Projects
- Reuben Moalosi, DRA Mineral Projects
- Cornelius Ntsomeng, DRA Mineral Projects
- Gavin Outhwaite, DRA Mineral Projects
- DRA construction and commissioning teams.

References

Financial Post. 2015. Canadian miner Lucara finds 1,111-carat diamond – believed to be second largest ever. http://business.financialpost.com/news/mining/canadian-miner-lucara-uncovers-1111-carat-diamond-believed-to-be-second-largest-ever-found [Accessed 14 Dec. 2015].

Morgan, P., Van Niekerk, L.M., Underwood, G., and Paz, A. 2015. Introduction of Turbo-lifter System at Karowe Diamond Mine and comminution circuit upgrade. *Proceedings of the Sixth International Conference on Semi-autogenous and High Pressure Grinding Technology*. Vancouver, Canada.

Riedel, F. and Dehler, M. 2010. Recovery of unliberated diamonds by X-ray transmission sorting. *Proceedings of the Fourth Diamonds: Source to Use Conference*, Gaborone, Botswana. Southern African Institute of Mining and Metallurgy, Johannesburg. pp. 193–200.

Van Niekerk, L.M., Ndlovu, G.N., and Sikwa, N.A. 2013. Commissioning and operating an autogenous mill at Karowe Diamond Mine. *Proceedings of the Fifth Diamonds: Source to Use Conference*, Muldersdrift, South Africa. Southern African Institute of Mining and Metallurgy, Johannesburg. pp. 175–192.

Von Ketelhodt, L. 2012. Presentation: Tomra Sorting Solutions. *Regional Meeting*. Southern African Institute of Mining and Metallurgy, Johannesburg. ◆

http://dx.doi.org/10.17159/2411-9717/2016/v116n8a2

The CCUT block cave design for Cullinan Diamond Mine

by H. Tukker*, A. Holder†, B. Swarts†, T. van Strijp†, and E. Grobler†

Synopsis

Petra Diamonds' Cullinan Diamond Mine (CDM) is currently producing from two mining blocks that are nearly depleted and highly diluted. CDM is developing the CCUT mining block as a mechanized block cave with an advance undercut that would replace the current mining blocks and increase production to approximately 4 Mt/a. The CCUT block production level on 839 m level is approximately 200 m below the current production areas on the 630 and 645 m levels.

The planning of the CCUT block with a lift height of approximately 194 m at CDM under Petra's ownership commenced in 2008. The access declines to the block started in 2009 and 2010. Most of the shaft deepening and waste development have been completed, with the planned 'deep' shaft and ground-handling system planned for commissioning in June 2016. The first undercut ring was blasted in July 2015.

This paper reports on the design process and evolution of the project, including:

- Geotechnical design criteria
- Advance undercutting sequence and strategy
- Undercut advance rates, slot designs, and rings designs to achieve the undercutting objectives (of high early tonnages and high undercut advance rates)
- The production level development philosophy in utilizing advance undercutting, production level design and drawbell opening sequence.

Keywords

block, cave design, advance undercut, rock mass characteristics, support regime.

History and background

Premier Mine, as it was known then, was registered in 1902 and open pit mining activities commenced in 1903 (see timeline in Figure 1). The Cullinan Diamond, the largest rough diamond of gem quality in the world at 3106 ct, was found 9 m below surface (mbs) in 1905. De Beers acquired a controlling interest in Premier Mine in 1917 and open pit activities progressed down to 189 mbs. The mine closed during the Great Depression of 1932 and re-opened only after the Second World War. Dewatering of the pit began in 1945 and underground mining started in 1947 using variations of sublevel open-bench mining. Conventional-type cave mining started in the early 1970s, and sublevel open stoping was attempted in the early 1980s but was changed to mechanized panel retreat block caving. The BA5 and BB1E blocks (Figure 2) below the sill on elevations 630 mbs and 732 mbs respectively were changed from post-undercut panel retreat caves to advance undercut block caves to reduce the tunnel deformation and failures caused by high abutment stresses on the production level infrastructure, which was developed and constructed ahead of the undercut face. The BA5 block cave can be considered a success, with high extractions achieved, especially in the hard western Hypabyssal Kimberlite, albeit with significant tunnel failures in the softer Grey Kimberlite zones close to the contact. The BB1E and AUC mining blocks that lie within the soft eastern Brown and Grey kimberlites respectively experienced massive tunnel failures early in their lives and a recovery level on 747 mbs had to be established to recover the remaining BB1E resource tons (see Figure 2).

The mine was renamed Cullinan Diamond Mine (CDM) after the Cullinan Diamond as part of its centenary celebrations in 2003. Petra Diamonds acquired CDM from De Beers in November 2007. Petra initiated mining studies in 2008 to mine the CCUT resource defined down to 1073 mbs. Two declines to access the lower CCUT mining block were started in 2009 and 2010.

Historical production from CDM ranged from 2 to 5 Mt/a). More than 360 Mt of kimberlite ore have been mined to date over 113 years, yielding approximately 128 million carats at 35 carats per hundred tons (cpht). CDM has produced over 750 stones that are

* *Ukwazi Mining Solutions, Johannesburg, South Africa.*

† *Petra Diamonds Group, Johannesburg, South Africa.*

 ISSN 2225-6253. This paper was first presented at the Diamonds still Sparkling 2016 Conference, *14–17 March 2016, Gaborone International Convention Centre.*

The CCUT block cave design for Cullinan Diamond Mine

Figure 1—History of Cullinan Diamond Mine (CDM)

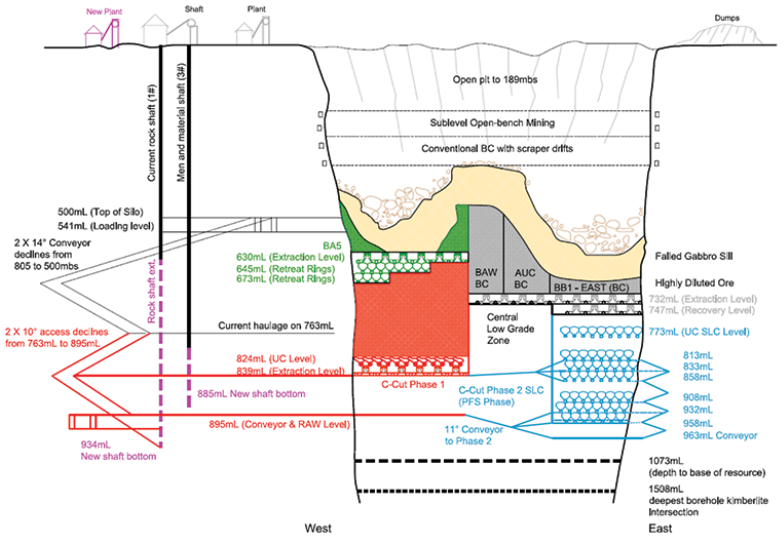

Figure 2—Schematic section of CDM showing mining blocks and infrastructure

greater than 100 carats and more than a quarter of the world's diamonds that are greater than 400 carats in size. It is furthermore also the only significant source of blue diamonds in the world.

Current CDM mine infrastructure includes a rock shaft (No. 1 Shaft) for waste and ore hoisting from 541 m level (mL) and a men and a material shaft (No. 3 Shaft) that provides access down to 763 mL. Production from underground mining sections is currently from highly diluted block cave drawpoints on 747 mL and retreat rings on 645, 673, and 732 mL at a rate of approximately 2.6 Mt/a. 645 and 673 mL were old ventilation levels for the BA5 block and these levels were converted to longhole retreat production sections to serve as tonnage gap-fillers between the current blocks and the CCUT. 732 mL was the extraction level for the BB1E, AUC, and BAW blocks and the remaining production planned from these blocks will be retreat rings recovering the major apex pillars above the old production tunnels. BAW was abandoned due to the low grades reporting from this area.

With the current ground-handling system ore is loaded with load haul dumpers (LHDs) from production section and tipped into rock-passes from where it is trammed with locos and hoppers on 763 mL to the north and south jaw crushers. The two crushers feed two conveyors positioned on 805 mL that convey the rock to the top of the No. 1 Shaft silos at 500 mL. The loading level on 541 mL feeds the No. 1 Shaft loading flasks, from where rock is hoisted to surface. On surface, the ore is conveyed to the processing plant, which was constructed in 1947 but has been continuously modified and upgraded to recover large and small diamonds.

The CCUT project entailed establishing new surface and underground infrastructure to extract the next mining block below the depleted BA5 mining block using block caving with an advance undercut at a production rate of 4 Mt/a. This project required major recapitalization that included:

- Extending the existing shafts to provide access, services, and rock hoisting on the CCUT horizon as shown in Figure 2. This includes two new shaft bottoms, a loading level, pumping infrastructure, underground workshops, and underground stores
- No. 1 Shaft winder upgrade to increase the hoisting capacity to 4 Mt/a from 934 mbs
- Extending two declines down from 763 mL to the CCUT ground handling level on 895 mL
- A new block cave with undercut level on 824 mL (measurement from the undercut gives an effective lift height of 194 m to 630 mL), production level on 839 mL, and ground-handling on 895 mL, as shown in Figure 2.

Geology

The CDM kimberlite pipe has a kidney-shaped exposure on surface and measures 860 m by 400 m, elongated along a NW-SE axis. The surface area of the pipe is approximately 32 ha, decreasing progressively to 22 ha at 500 mbs and 12 ha at 1000 mbs. Subsidence caused by the mining

operations has increased the surface rim size more than 40 ha. It has been estimated that the top 300 m of the original pipe has been removed by erosion since its intrusion 1 200 million years ago. The diatreme zone of the pipe is fairly unique in that it has been cut by a younger 75 m thick gabbro sill that dips shallowly from north to south between elevations 350 mbs and 525 mbs, as indicated in Figure 3. The country rock around the pipe consists of Waterberg quartzites, felsite, norite, and Transvaal Supergroup meta-sediments, as shown in Figure 3. Three major kimberlite intrusions have been identified within the pipe. Two of these are typical volcaniclastic kimberlites (previously identified as tuffsitic kimberlite breccia or TKB), while the final phase of intrusion is a hypabyssal kimberlite core complex in which four kimberlite types and late-stage carbonaceous dykes have been identified.

- Brown Kimberlite is a volcaniclastic kimberlite that has the highest clay content and is the weakest kimberlite at CDM. It represents the first intrusion and has the highest grade, which varies from 60-115 carats per hundred tons (cpht). It also contains diamonds with the highest average value
- Grey Kimberlite is also a volcaniclastic kimberlite, and can be classified as weak kimberlite with high clay content. This facies has the lowest grade and lowest value diamonds, especially close to the centre of the pipe where there is significant internal waste (the 'Grey Waste' sub-facies), and grades are estimated to be generally below 30 cpht. This area has remained mostly unmined below the sill due to its low payability
- The hypabyssal core is made up of Pale and Dark Piebald hypabyssal kimberlite surrounded by Black and Green transitional kimberlite. It is more competent than the two volcaniclastic kimberlite facies, with almost no clay content. This kimberlite is believed to be responsible for producing the majority of large (>100 ct) stones at CDM, including the Type 2a and blue boron-bearing Type 2b diamonds perceived to occur close to the internal Grey/Hypabyssal and Grey/Waste contacts on the western side of the pipe. The grade within this facies varies from 30–70 cpht. The project footprint consists mostly of the Hypabyssal Kimberlite core surrounded by Grey Kimberlite, as shown in Figure 4.

The late-stage carbonaceous kimberlite dykes at CDM are widespread and intrude into all kimberlite facies. In some cases where these dykes occur parallel to, or on, internal facies contacts and close to pipe contacts they can cause major instability in the form of shear planes that can fail uncontrollably if not supported timeously and correctly during the development phase.

Geotechnical setting and design parameters

Table I indicates the rock mass characteristics for the project area at CDM. Note that the uniaxial compressive strength (UCS) and the mining rock mass rating (MRMR) values for the Grey and Hypabyssal kimberlites have large ranges, and the average values indicate that the ground for the CCUT project should be fairly competent with minimal expected

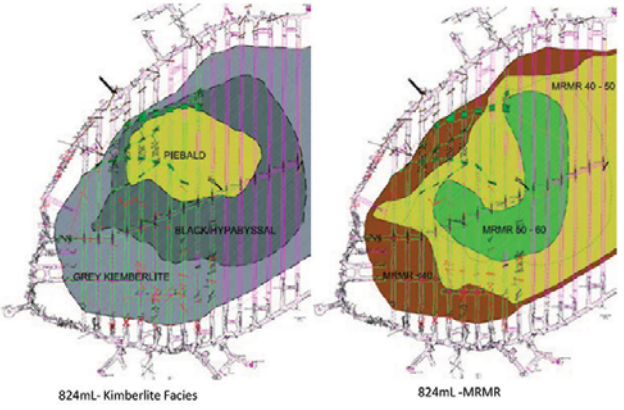

Figure 4—Kimberlite facies and the MRMR interpretation for the undercut level (824 mL)

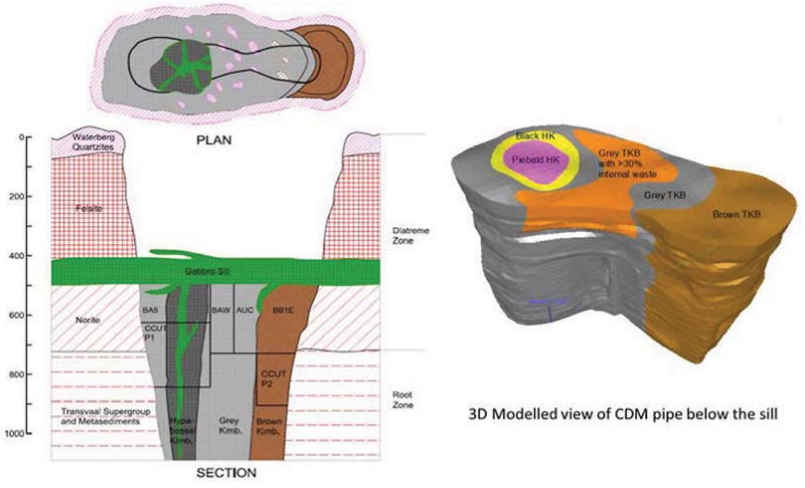

Figure 3—Plan and section of the generalized geology of the CDM pipe below the sill (after Bartlett and Kroll, 2000), and 3D geological interpretation of the pipe

Table I

Rock mass characteristics at CDM relevant to CCUT

Rock classification	Value
Kimberlite density (SG)	2.66 Grey 2.71 Hypabyssal
Country rock density (SG)	2.85 Norite 2.65 Metasediments
Av. UCS of kimberlite (MPa)	80–130 Grey 73–193 Hypabyssal
Av. UCS country rock (MPa)	140–220 Norite 60–240 Metasediments
Mining rock mass rating	30–50 (Grey) and 25-35 (at contacts, some internal dykes and shear zones) 40–60 (Hypabyssal)
Hydraulic radius	BA5 above CCUT caved at 30, but the CCUT undercut is started in the weak Grey Kimberlite. Expected HR between 20 and 25 for average MRMR of 35

problems. The localized weak mining zones with lower-end MRMRs close to the pipe and internal contacts as shown in Figure 3 do, however, suggest that ground conditions pose a significant geotechnical risk if not managed properly, as experienced in the BA5 directly above the CCUT. The current generic tunnel support regime for the CCUT block includes bolts, sealant, welded mesh, and shotcrete. The contacts and drawpoints will have site-specific recommendations, usually including stiff brow steel sets.

Figure 4 shows that the weaker (lower MRMR) areas are generally close to the contact zones, with the hypabyssal core being competent. All the undercut and production tunnels intersect the contact or weaker zones and the mine design, sequence, and tunnel support standards have to ensure that these areas stay open for the life of the production block. With this in mind a back-analysis was done on the AUC block cave, which is located in the Grey Kimberlite as shown in Figure 3. This block sat down halfway through the undercutting process and most of the undercut tunnels crushed within a short space of time. The process entailed simulating the mining steps that were followed in a geotechnical modelling package and calibrating the model until the results replicated the actual events that followed.

The model was then re-calibrated for CCUT conditions, including rock characteristics depth, pipe geometry etc. Different scenarios were designed, sequenced, and modelled to achieve the optimal outcome. Some of the model outcomes at different stages of undercutting and production drawbell construction are shown in Figure 5.

This paper does not report on the specifics of the geotechnical modelling, which are covered elsewhere, but focuses on the recommendations incorporated into mine design and schedule. The geotechnical recommendations were as follows:

- The undercut tunnels were sized to 4 m wide and 4 m high and the extraction level development to 4.2 m wide by 4.2 m high
- The El Teniente layout was chosen as the preferred block cave layout as this resulted in improved development efficiencies and quality while reducing the planned drawbell construction and opening times compared to the herringbone layout
- The undercut tunnel spacing of 16 m and production tunnel spacing of 32 m used in the modelling were found to be appropriate
- The extraction level drawpoint spacing of 16 m had to be increased to 18 m. It was furthermore recommended that the spacing be increased to 21 m for the last third of the footprint to avoid the deformation shown in Figure 5. Local underground observations will, however, guide geotechnical simulations and subsequent recommendations going forward
- The analysis shows that the undercut deformation was normal until undercutting was around 65–75% complete. The final corner showed significant levels of deformation due to the pipe geometry. Wrecking of the final problematic undercut zone might be an appropriate strategy, but observations going forward will dictate the final recommendations
- The southern contact appears to be problematic with fringing occurring (see Figure 5). The presence of a local shear zone is another complication that might amplify the problems highlighted by the modelling
- The initial undercut strategy, consisting of an advance undercut with production drifts and drawpoint stubs ahead of the undercut face, was revised to having only the first four tunnels (without any stubs) developed

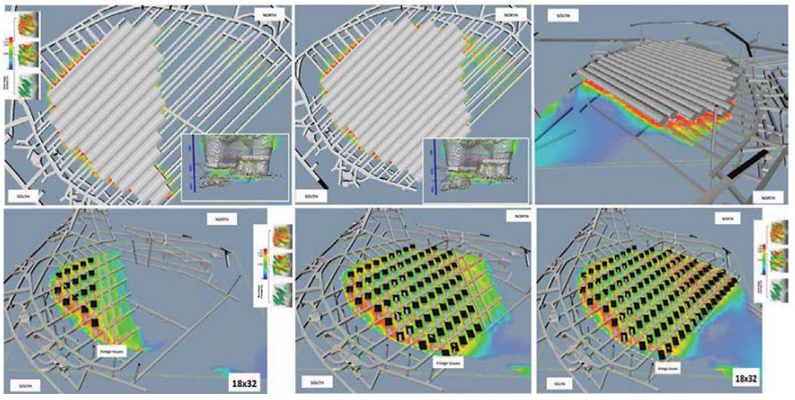

Figure 5—Geotechnical modelling outputs for different steps in mining sequence, damage shown as expected deformation (source: Beck Engineering)

ahead of the undercut face. Of the remaining four tunnels, only every second tunnel can be developed ahead of the undercut

- Local ground conditions must be re-interpreted continuously and the mine design and sequence adapted accordingly.

Underground infrastructure

The CCUT project consists of three major levels: an undercut, production, and conveyor/ventilation (RAW) level. The main underground infrastructure entails:

- Ground handling (see Figure 6 to Figure 8):
  - 13 × 9 t LHDs (100 t/h or 33333 t/month per LHD) loading from development, rings, rim loading, and production level drawpoints. Total capacity of 13 LHDs is 5.2 Mt/a
  - Undercut level: 4 × tips with 600 mm grizzly, rockbreaker, and orepass configuration, each feeding one of four crushers
  - Production level: 4 × double-tip 600 mm grizzly, rockbreaker, and orepass configuration, each feeding one of four crushers
  - 4 × 450 t/h (100 kt/month or 1.2 Mt/a each) jaw crushers positioned below the production level. Enough space was allowed above the crushers to introduce a recovery level if required without changing the ground-handling system materially

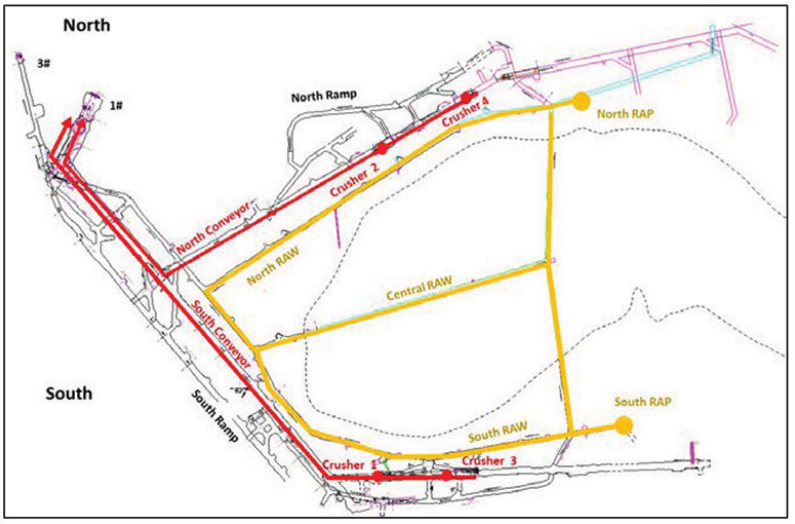

Figure 6—895 mL conveyor and RAW level with crusher excavations

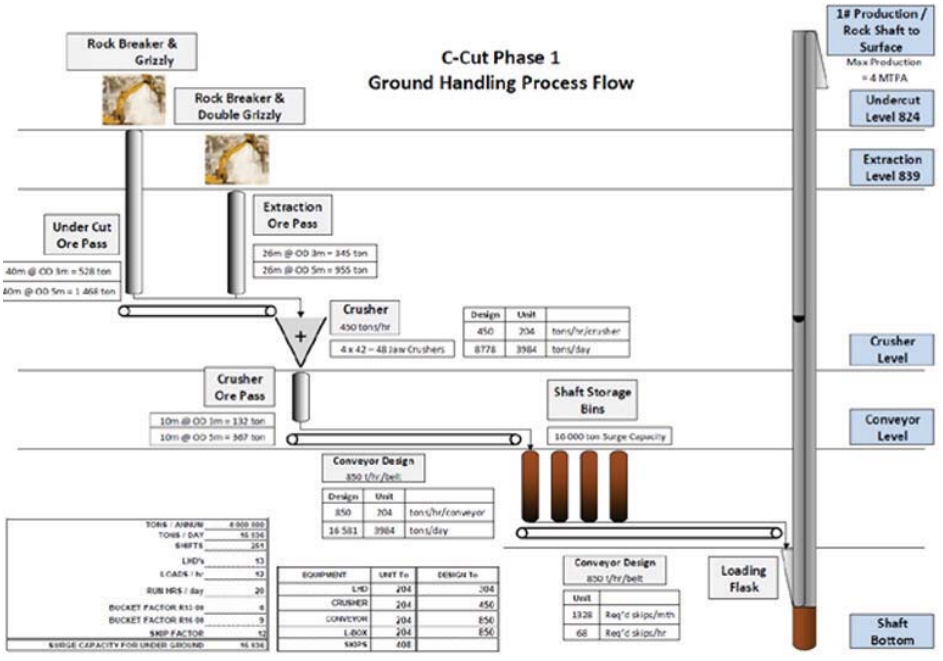

Figure 7—CCUT ground-handling process flow

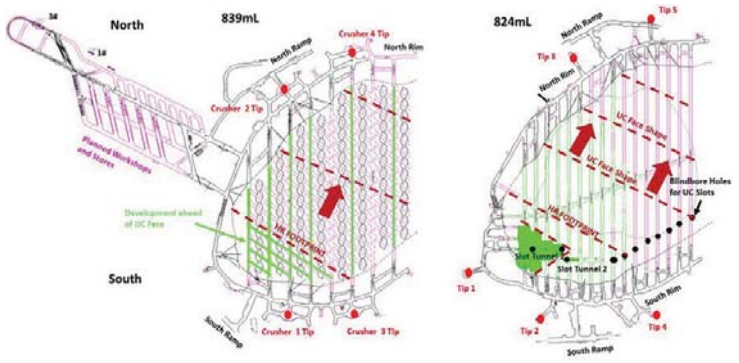

Figure 8—839 mL production level (left) and 824 mL undercut level (right)

  - 2 × 1200 mm strike conveyors (850 t/h or 3.6 Mt/a each) below the crushers convey the ore to the new shafts silos
  - The No. 1 Shaft hoisting capacity of 4 Mt/a is the limiting factor on the ground-handling configuration
- Ventilation (see Figure 6 and Figure 8):
  - The shafts and declines accessing the block facilitate air intake for the mining section. The dirty production air is directed from the production tunnels down raisebore holes to the return airway level (RAW level) on 895 mL. The dirty air in the RAW is then directed to the central return airpasses (RAPs) that link into the main mine returns
- Trackless maintenance and shaft logistics (see Figure 8):
  - Temporary workshops constructed on 763 mL will serve until the new centralized workshop on 839 mL has been developed and equipped
  - All the material will be dispatched via No. 3 Shaft to the 839 mL laydown area and store facility, from where it will be issued to mining crews
  - Production personnel will access the production level via No. 3 Shaft on 839 mL

Undercut design and schedule

The weakest zone within the project area is the southwestern zone, as shown in Figure 4, with MRMR ratings below 40 and in some instances 30–35. The hydraulic radius (HR) for the area is estimated to be 20–25 m. In assessing the overall risk of undercutting the entire footprint, the decision was taken to initiate the undercut slot in the southwest to ensure that the higher risk area was undercut before the HR with associated high abutment stresses was reached. Initiating the undercut in the weaker ground would also allow for higher initial cave propagation and production rates. The undercut slot tunnel was positioned 30 m from the southwest contact to enable high undercutting rates towards the south and north to reach the HR footprint within the first nine months of undercutting, and by doing so reach the more competent zones early in the undercutting process as shown in Figure 9. The undercut face shape can be described as diagonal, with 6–8 m lead-lags being maintained while the face advances in a northeast direction. The lead-lags will also be adjusted in response to local ground conditions observed, especially close to shear zones, tunnel intersections, internal contacts, and pipe contacts. The rings advancing to the southern contact were initially planned to have a height of 12 m. However, to improve stability close to the contacts and to increase production capability, being close to the south tips, the required undercut height was increased from 12 m to 20 m on the south of the slot tunnel. The ring height on the northern side was reduced to 6 m, as shown in Figure 10, for the following reasons:

- Required longhole drilling metres: only 75 m per ring allows for quick drilling turnaround time
- Low probability of pillars with a low undercut and ease of ability to fix potential problems, *i.e.* large rings big problems and small rings small problems'
- Tonnage per ring reduced from almost 1500 t to approximately 500 t *in situ* considering the long tramming distance to the northern tips
- Low logistical requirements enabling high advance rates.

The average monthly required undercut advance rate is four rings (or 8 m) and the total output for the undercut per month is 48 rings, 1400–1800 m2, 17 000 t (at 60–70% draw of blasted tons), and approximately 4000 longhole metres with 10% re-drill. The powder factor using bulk emulsion is 0.75–1.0 kg/t for the undercut rings (2 m burden, 2–2.3 m toe spacing using 76 mm blast-holes).

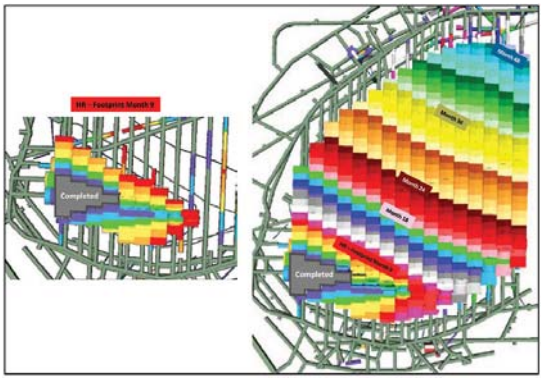

Figure 9—Undercut level sequence as planned in Mine2-4D - HR is reached in month 9

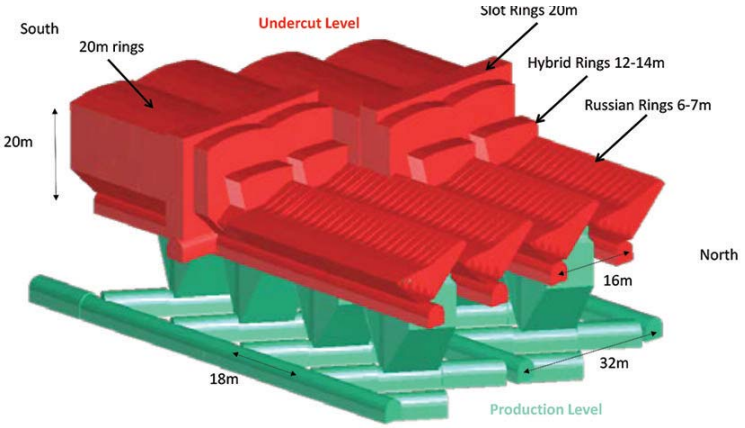

Figure 10—Undercut and production level model with ring configuration

Production level design and schedule

The production level has a tunnel spacing of 32 m and a drawpoint spacing of 18 m as shown in Figure 11. The production level construction strategy employed at the CCUT project entails constructing the drawbells within the HR footprint ahead of the undercut face, which includes the first 4 bell rows or 10 drawbells in total, while the abutment stresses are considered to be low.

The remaining footprint will be constructed as an advance undercut that entails constructing only tunnels 1–4, 6, and 8 ahead of the undercut face and all the other drawbells and tunnels 5 and 7 in the de-stress shadow of the undercut face, as shown in Figure 8, to avoid abutment stresses damaging production level infrastructure. The re-compaction time guideline used in determining the construction cycles and resource requirements is 6 months, which is the time to open up a drawbell from the time the undercut advances over the area. Two months is required for the undercut moving at 8 m per month (16 m) to create the de-stress shadow, and another four months for development and construction (see Figure 12). If this timeline is not adhered to and the undercut runs away from the production level, the area already undercut might re-compact and the abutment stresses re-configure over these zones and be transmitted down onto the production level.

The training of the production level construction crews entails using the initial 10 drawbells inside the HR boundary as a school to acquire the appropriate skills to complete the required activities within a set sequence and timeframe. The activities include development, tunnel support, placement of footwall concrete, construction of stiff-brow sets, blindboring, longhole drilling, longhole charging, and production loading as shown in Table II. Most of these activities must occur within the space of one month in a production tunnel.

The individual activities and durations allowed for are not difficult to achieve, but the combination of all the required activities in a set sequence in one tunnel makes the scheduling extremely complex, rigid, and difficult to achieve. In an advance undercut scenario the emphasis is on tunnel utilization and not necessarily resource utilization or efficiency, which means that the activities have to be over-resourced at lower efficiencies to ensure that the required cycle is achieved. CDM has opted for a 5-day three-shift configuration and has populated its micro-schedules according to this shift configuration. This shift arrangement equates to 62 available shifts, an average of 1.5 activities per

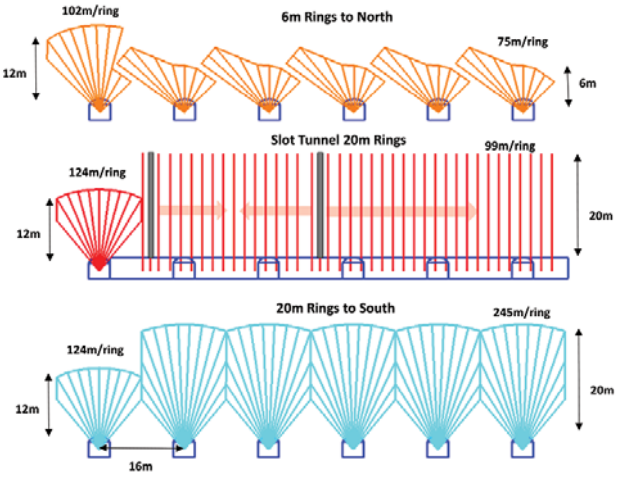

Figure 11—Generic ring designs for the undercut level

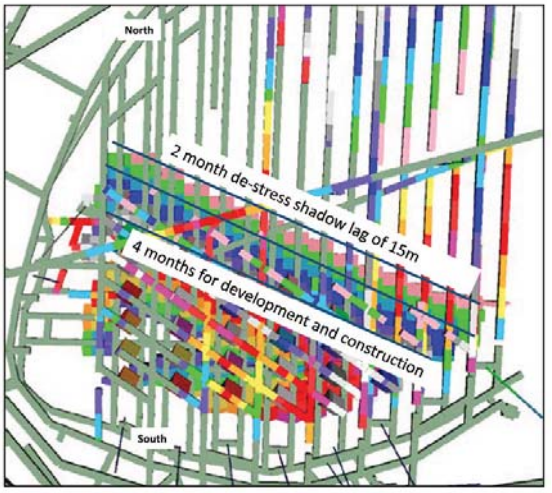

Figure 12—View from below looking up at the production and undercut level leading by 6 months

Table II

Production level construction activities to establish three drawbells per month

Activity	Total block	Per production tunnel or access	Time per activity per tunnel
Development	80–100 m/month	15–20 m/month	10 shifts
Tunnel support	80–100 m/month	15–20 m/month	10 shifts
Footwall concrete	60–80 m/month	12–15 m/month	5 shifts
Stiff-brow drawpoint sets	6 × sets	1 set	10 shifts
Blindbore metres	3 × 25 m holes	0.5 holes—12.5 m	6 shifts
Longhole drilling	3 × drawbells at 1200 m/bell = 3600 m/month	0.5 bells—600 m	6 shifts
Longhole dharging	3 × drawbells at 3 blasts per bell = 9 blasts 27 drawbell rings	0.5 bells—2 blasts	2 shifts
Production doading	All open drawpoints	Minimum 1 shift per day per tunnel	20 shifts
Time required in tunnel		69 shifts (single activity in the tunnel) 35 shifts (two activities in the tunnel)	
Redundancy		20%	
Total time required in a tunnel		83 shifts (single activity in the tunnel) 42 shifts (two activities in the tunnel)	
Time available		5 days, 2 shifts/day—41 shifts 5 days, 3 shifts/day—62 shifts 11 days, 2 shifts/day—46 shifts 11 days, 3 shifts/day—69 shifts FULCO × 3 shifts/day—90 shifts	

tunnel (with the focus on getting the ventilation in place to allow multiple activities in a tunnel, not all the activities can be carried out in parallel), and overtime to recover any slip in the schedule. The first 6 months will serve as a trial, and if required the CCUT crews can convert to a FULCO shift configuration as a last resort to ensure that the schedule is achieved.

Production level drawpoint maturity rules

The expected fragmentation for the CCUT is 30% >2 m^3 (oversize) initially and 7–12% >2 m^3 after 20% draw. The maturity rules have been adjusted to allow for lower initial draw rates in the build-up and higher rates on reaching maturity to avoid excessive percentages of oversize that must be blasted or handled by the the grizzly. The drawpoint maturity rules as applied in mining scheduling software packages (Mine2-4D and PCBC) can be viewed in Table III. A total of 184 drawpoints will be in production at steady-state, allowing for sufficient redundancy when producing at a rate of 4 Mt/a.

Conclusion

CDM's CCUT block cave will be one of the deepest mechanized kimberlite block caves in production when it reaches steady state at 4 Mt/a in three years' time. The first undercut rings were blasted in July 2015 and the first drawbell will be opened in January 2016. The fundamentals of the mine design and schedule seem appropriate thus far, with development and ring blasting being on schedule, although problems were encountered in handling waste tonnage and getting the ventilation infrastructure in place. Future planning at CDM entails implementing more detailed micro-schedules in the production level construction environment to ensure that timetables are achieved on an hour-by-hour, day-by-day, and month-to-month basis. Up-skilling and build-up of specialized longhole, development, and construction crews is also a priority to ensure that the production level targets are achieved, thereby ensuring the successful tonnage ramp-up of the CCUT block.

Table III

CCUT drawpoint maturity rules

Drawpoint age (months)	Accumulated mined (t)	Max. capacity (t/d)	Max. draw (mm/d)
0	0	50	71
3	3000	75	107
6	7500	100	142
12	19500	155	220

Acknowledgements

The authors thank Petra Diamonds for allowing us to publish this paper, and in particular the CCUT project team at CDM. Contributions and technical input were provided by Andrew Rogers.

References

Bartlett, P.J. and Croll, A. 2000. Cave mining at Premier Diamond Mine. *Proceedings of Massmin 2000*, Brisbane, Queensland, 29 October – 2 November 2000. *Australasian Institute of Mining Metallurgy*, Melbourne. pp. 227–235.

Beck, D. 2010. Premier Mine Stability 824/839 Level.

Beck, D. 2014. Assessment of stability of proposed designs for CCUT Phase 1 and 2.

Laubscher, D.H. 1994. Cave mining – the state of the art. *Journal of the South African Institute of Mining and Metallurgy*, vol. 94, October. pp. 279–293

Marsden, H. 2006. Observations of damage in the AUC undercut, Premier Mine. ◆

http://dx.doi.org/10.17159/2411-9717/2016/v116n8a3

Design and implementation of steeper slope angles on a kimberlite open pit diamond operation—a practical approach

by A. Madowe*

Synopsis

The steepening of slope angles on an open pit mining operation has a material impact on improving the economics of mining. Steepening of slope angles can also increase the risk of slope failure. Slope failures are inherently costly events, because they can be catastrophic, resulting in multiple fatalities, equipment damage, and temporary or permanent closure of a mine. The steepening of the basalt slope angles at Letšeng Diamond Mine followed operational improvements that were introduced through improved blasting practices and geotechnical controls. The steeper slope design resulted in a 6 Mt/a reduction in the peak waste mining compared with the previous mine plan coupled with an increase in the net present value and life of mine. This paper is an outline of the steps that were taken at Letšeng to increase slope angles in waste and the resulting improvements to the mine plan.

Keywords
slope stability, slope design, mine plan.

Introduction

Letšeng Diamonds (Pty) Ltd is a mining operation situated at Letšeng-la-Terae in the Kingdom of Lesotho (Figure 1). Gem Diamonds at 70% is the majority shareholder with the remaining 30% shareholding held by the Government of Lesotho. Letšeng is known for producing large, top colour, exceptional white diamonds, with the highest percentage of large (+10.8 carat) diamonds of any kimberlite mine, making Letšeng the highest average dollar per carat kimberlite diamond mine in the world. Letšeng production is characterized by a uniquely high proportion of D colour type II diamonds, which are the purest form of diamonds. Historic stones from Letšeng include 550, 478, 603, 493 and 601 carat diamonds.

Letšeng employs a conventional open-pit mining method. Mining and ore treatment are on a continuous two-shift cycle. Drilling, loading, hauling and dewatering are operated by a mining contractor while blasting is done by the owners of the mine. Treatment plants are operated and maintained by a contractor while the Diamond Recovery Plant is owner-operated.

Geology

Letšeng has two kimberlite pipes (Main and Satellite) adjacent to each other, with cone-shaped sections to confirmed vertical depths of 798 m and 849 m respectively (Figure 2).

The surface impression of the Satellite Pipe is approximately 5 ha including a large basalt raft. The Satellite Pipe comprises two phases of kimberlite, namely North Volcaniclastic Kimberlite (NVK) and South Volcaniclastic Kimberlite (SVK). The Main pipe is approximately 17 ha, consisting of three kimberlite phases: KMain, K6, and K4. Letšeng's pipes are near vertical and hosted in unweathered basaltic lavas. The kimberlites have sharp contacts with the basalt country rock and are characteristically carrot-shaped in section, comprising volatile-rich, potassic, and ultrabasic igneous rocks.

The Letšeng mineral resource consists of approximately 5 million carats at an average value of over US$2 000 per carat. The resource is classified into Indicated and Inferred with the Indicated category extending from surface to 504 m below the datum elevation – Figure 2. 63% of the Letšeng mineral resource is Indicated with the balance being Inferred.

Slope stabilitiy risk management at Letšeng

The steepening of the slopes angle in waste was enabled by operational improvements in the areas affecting pit slope stability. This section provides an overview of these improvements.

The purpose of slope stability risk management is to assist in providing a safe working environment for the open pit mining operation by managing the geotechnical risk. Letšeng seeks external assurance from world-renowned geotechnical consultants on the determination of the optimal slope designs for the pits.

* *Gem Diamond Technical Services.*

Design and implementation of steeper slope angles on a kimberlite open pit

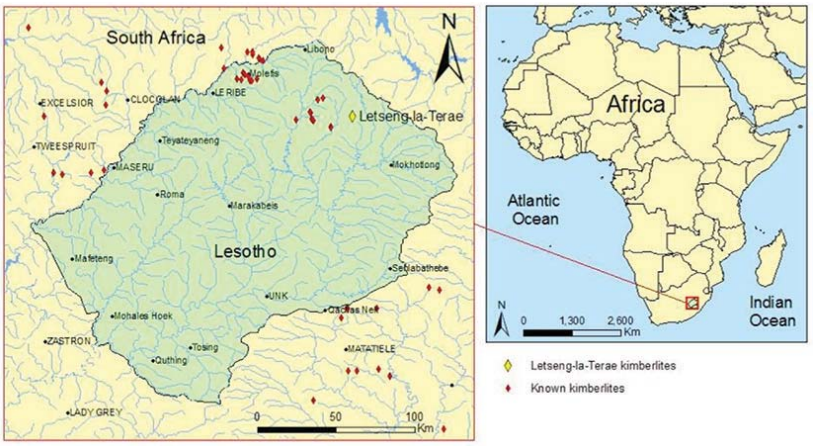

Figure 1—Locality map of Letšeng Diamond Mine

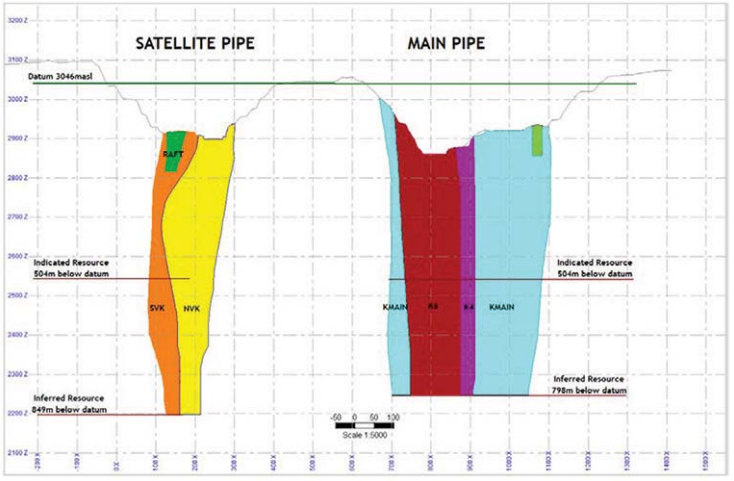

Figure 2—A vertical section through the Letšeng kimberlite pipes

Aspects of the Letšeng slope stability risk management are as follows:

- *Hazard identification*—involves a range of geotechnical monitoring activities comprising instrumentation, survey, and visual inspection by geotechnical personnel. Lidar scanners were purchased for the purpose of monitoring slope deformation that might not be picked up by visual observation. Hazard plans are used to define potentially hazardous situations in the pits
- *Exposure assessment*—involving a study of historical trends from monitoring and comparisons with predicted performance from the geotechnical models
- *Consequence assessment*—with respect to safety of personnel and equipment in the pits is determined with reference to assessment of the impact and severity of the risk from the identified hazard
- *Mitigation*—involves a range of options such as evacuation, buttressing (construction of berms), installation of ground support, changes to pit designs, as well as installation of survey prisms and utilization of scanners to monitor the identified high-risk areas
- *Standardized procedures*—covering aspects such as data collection and record management, operation of lidar scanners, mining practices, evacuation, working under highwalls, and pit design changes. The procedures include a '*Code of Practice to combat rock fall and slope instability accidents at Letšeng Diamonds*'.

Pit slope management

The management of the slopes is enforced throughout the mining operations. Discussions and necessary recommendations on operational procedures and awareness of identified geotechnical hazards are made in the form of verbal and written reports. The discussions take place in daily production meetings as well as monthly pit safety meetings.

Geotechnical data collection

The stability of an excavation is dependent on the rock strength and rock mass quality in which it is located. Geotechnical data is collected routinely through face mapping, core logging, and field and laboratory sample testing. The data, comprising uniaxial compressive strength measurements, spacing, orientation and condition of discontinuities is used for rock mass characterization and slope stability analysis. Detailed structural mapping on final walls is undertaken along each face that is exposed and updated onto the geotechnical database. Intact rock strength plays an

important role in rock mass characterization, thus a comprehensive rock test database improves the confidence in the rock mass characterization. A geotechnical model has been created from the geotechnical field data and the interpolated geotechnical parameters, calculated slopes angles, and blasting parameters.

Sign-off of pit walls

Once loading has taken place close to a highwall, a sign-off form is filled out by the geotechnical personnel. There are two forms which are available to be signed off. The red form is filled in when the area does not comply with the geotechnical standards. The blue form in is filled when the area has passed geotechnical standards. The purpose of the sign-off form is to ensure that the highwall on the previous bench is clean and stable before proceeding to the next bench.

Pit monitoring

Visual inspections

Visual inspections are carried out to evaluate appropriateness of the slope design and to identify areas of potential rockfall. Visual inspections around working areas in the pits are carried out daily by geotechnical personnel and Pit Superintendents. The geotechnical engineer conducts detailed inspections in the areas of high risk and after falls of ground for back analysis. A monthly inspection is carried out by geotechnical personnel and Pit Superintendents to build a monthly hazard plan, which provides an indication of areas of potential geotechnical risk. An inspection around the perimeter of the pits is carried out once a month to identify new cracks and monitor old cracks around the pits should they develop during the month.

Monitoring instrumentation – scanners

Monitoring of the pit walls using the scanners is a quantitative method to supplement the qualitative methods described. Letšeng introduced pit scanning to monitor progressive slope movements. The scanners have the capability to detect small-scale slope movements in the order of millimetres. It is now known that it is these small-scale movements characterized by temporal evolutions ranging from several hours to several weeks, that usually precede large slope failures in open pits. A procedure for the operation of the scanners was developed that among other issues, stipulates the necessary response in the event that rock movement is detected. These responses include visual inspection to determine cause of movement, increasing the frequency of monitoring, and in the event of continued acceleration of movement closure of the pit until the situation is fully investigated. The capability of providing advance notice of impending instability conditions through accurate and timely measurement of precursors to slope collapses clearly represents an outstanding benefit for the pit personnel.

Blasting

The release of energy during blasting produces reactive forces that may cause the deterioration of the rock face behind the mine design line. Blast damage is created by the transfer of explosive energy into the rock mass resulting in the propagation of fractures. Pre-splitting, trim and buffer blasting are the key blasting techniques adopted at Letšeng to protect the final walls. The main parameters within the control of the blasting engineer are type and amount of explosive energy in a hole, drill pattern design, hole depth, hole diameter, hole angle, bench geometry, and blast timing. The correct parameters to use at Letšeng mine has been determined through the application of theory, experience, consultations with renowned blasting experts, and trials on the mining faces.

A short-term mining plan developed and updated weekly includes of the schedule of activities and time required for wall control blasting. The mine planner ensures that pre-split lines are marked in accordance with the approved cutback design from the long-term planner.

Pre-splitting

Pre-splitting is one of the key techniques applied at Letšeng to protect mine design walls. Pre-splitting provides a preferential fracture plane behind the blast to terminate cracks emanating from blast-holes (Cunningham, 2000). Pre-splits have been designed in accordance with the signed-off geotechnical recommendations for a double bench of 28 m in waste, and single bench of 14 m in kimberlite. The Letšeng pre-splits were designed on 1.0 m spacing between holes with a 1.0 m sub-drill. The pr-split holes are blasted ahead of production holes. Caution is taken while loading explosives (emulsion) in wet holes to prevent primers floating above the explosive charge, thereby resulting in misfired holes and frozen pre-splits. The blasts of pre-split holes are initiated simultaneously using detonating cord that has a detonation speed of more than 6 km/. Figure 3 shows a typical highwall face at Letšeng mine for a double bench pre-split.

Trim and buffer blasting

Trim and buffer blasting techniques are aimed at reducing the rate of energy release against the mine design wall. Trim blasts are designed along the excavation limit at reduced pattern and charge mass, and timed to achieve single-hole firing. Timing delays should be 'long enough for the strain waves from neighbouring holes to disperse individually' (Cunningham, 2000). Trim blasts at Letšeng are marked at a 4.5 m burden and 5 m spacing on a rectangular pattern after which the production holes continue with the burden and spacing of 5.0 x 6.0 m on a staggered pattern. The minimum

Figure 3—Single-pass 28 m pre-split on basalt

width of a trim is 20 m and the length generally limited to 100 m. Figure 4 illustrates the layout of a typical waste rock blast at the Minm. The sequence of blasting starts with the firing of the presplit line, followed by the firing and mining of the production blast, after which the trim is blasted and mined.

In cases where the geometry of the pit does not allow for a trim blast, a buffer/cushion blasting technique is applied. The first two rows of the production blast along the excavation limit are charged at reduced charge mass and drilled at reduced hole spacing to cushion/buffer the final wall from damage by the heavily charged production holes. At the mine, the first buffer line is designed with the standoff position of 1.6 m from the pre-split at blast-hole spacing of 2.5 m. The second buffer line is designed at burden and spacing of 4.0 x 4.0 m.

Electronics in blasting

Damage of highwalls is maximized when the maximum number of holes is detonated simultaneously. Timing is the key to controlling both the rate at which the available energy is released, and the direction of thrust of the blast. Cunningham (2000) states that the lack of precision of pyrotechnic timing systems requires the use of fairly long inter-hole delays to avoid crowding or out-of-sequence shots. He further notes that these 'long delays can result in ground movement interfering with the functioning of holes around each shot, and in excessive fracture and movement between shots'. The application of electronic blasting at Letšeng is aimed at achieving more precise timing in comparison to pyrotechnic timing. The blasting engineers at the mine utilize electronic detonators to achieve faster timing between holes and slower timing between rows than pyrotechnic blasting initiation systems can achieve. The use of electronic detonators at Letšeng allowed enhanced precision on blast timing, thereby protecting highwalls against blast damage and contributing to slope stability.

Highwall scaling

The purpose-made scaler at the mine is a standard CAT-385 excavator with two major modifications: a longer arm for greater reach and the replacement of the excavator bucket with a ripper for a CAT-D8 dozer for use as a prying tool. The scaler, with a reach of 15 m, is used to dislodge loose rocks on bench faces. This machine forms an integral part of the mine's slope stability management. Figure 5 shows the scaler dislodging loose rocks from highwalls and also removing rocks that are occasionally frozen onto the pre-splits. Due care is taken in the scaling operation to ensure the safety of the machine and operator in the cab.

Slope design

Geotechnical rock mass characterization

The basalt host rock at Letšeng mine is generally competent with relatively widely spaced joint sets. Based on drilling records and observations in both pits, it is apparent that the basalt reports as a relatively dry unit with little or no risk of high pore-water pressures (Terbrugge, 2015). The estimation of the rock mass strengths and joint strength parameters was based on the geotechnical borehole logs, in-pit mapping, and the results of the laboratory testing programme carried out for the stability analysis conducted in June 2012 by SRK Consulting. A summary of the rock mass strength parameters from geotechnical borehole logging and laboratory testing is presented in Table I. These parameters were used in the slope stability analysis.

Slope stability analysis

The stability analysis was based on the Hoek-Brown criterion, which was used to represent the strength of both

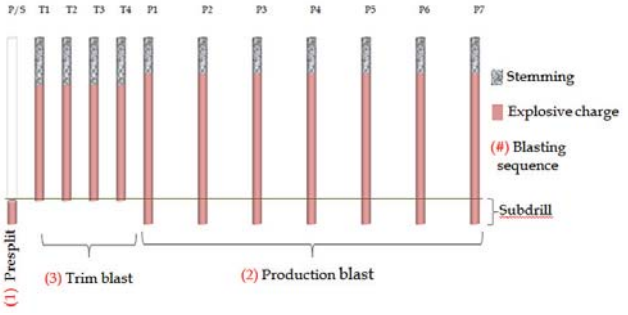

Figure 4—Vertical section through a blast

Figure 5—Scaler working on highwalls

Table I

Summary of the rock mass strength parameter

Geotechnical unit	Hoek-Brown Geomechanical Parameters							Equivalent Mohr-Coulomb strength Parameters		
	UCS (MPa)	GSI	mi	MR (1)	D	E (GPA)	v	σ_3 max (MPa)	c (KPa)	Φ (°)
Basalt	126	70	14	350	0.7	14.9	0.23	1.0	185	59
Kimberlite	41	50	5	300	0.8	1.1	0.25	1.0	285	33

the basalt and the kimberlite rock units (Terbrugge, 2015). The criterion starts from the properties of intact rock and then introduces factors to reduce these properties on the basis of the characteristics of joints in the rock mass and geological observations (Hoek, Carranza-Torres, and Corkum, 2002). The estimation of joint strength parameters was based on the Barton-Bandis criterion, which enabled the estimation of equivalent Mohr-Coulomb friction angles and cohesive strengths of each rock mass. The analysis of sensitivity of the rock slopes, as well as the evaluation of the overall stability of the slopes, was carried out with the program SLIDE from Rocscience based on the limit equilibrium method. The results were verified with a stress deformation analysis using the program PHASE 2 using the shear strength reduction technique in the finite element model.

Limit equilibrium analysis

Limit equilibrium analysis is used to determine the stability of sliding planes, blocks, and wedges for a single free body and does not depend on the distribution of effective normal stresses along the failure surface. Limit equilibrium methods are relatively easy and fast to use, and also consider rock mass or step-path type failures.

Stress deformation analysis

The deficiency in limit equilibrium analysis of a jointed rock mass is that the analysis cannot quantify deformation and/ or displacement of the failing rock mass, which of course can be modelled by numerical methods that include the complex conditions found in rock slopes such as nonlinear stress-strain behaviour, anisotropy and changes in geometry. Numerical models divide the rock mass into elements, with each element assigned an idealized stress-strain relation together with the properties that describe the rock mass behaviour. Elements may be connected in a continuum model or separated by discontinuities in a discontinuum model, which will allow slip and separation at explicitly located surfaces within the model.

Recommended slope design

The main objective of the geotechnical slope design is to design fully optimized slopes at all stages of the mining operation utilizing available geotechnical data. The results of the limit equilibrium and stress deformation analysis all appeared to meet the acceptance criteria with a factor of safety greater than 1.3. Based on the geotechnical analysis, Figure 6 illustrates the recommended slope design in waste rock (basalt) for Letšeng pit designs.

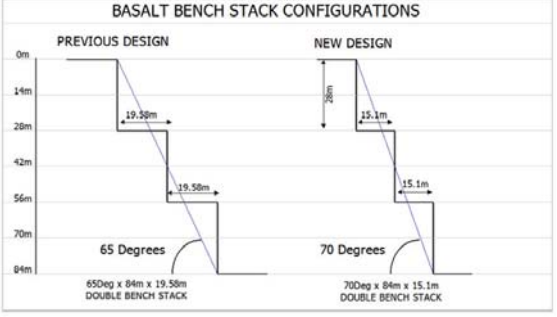

Figure 6—Letšeng bench stack configurations in waste

The 15.1 m berm was regarded as the minimum with respect to a rockfall that could report to the berm from a 28 m high bench. The new 2015 slope design in basalt resulted in a 5° steepening of the inter-ramp angle from the 2012 basalt slope design. The 84 m double bench stacks are separated by ramps or 25 m catchberms in the absence of a ramp.

Figure 7 shows the slope geometry with a 52° stack angle in kimberlite. This design has remained unchanged as the steepening of slope angles was to be carried out only in waste.

Incorporation of steeper slope design into the mine plan

A review of the mine plans was required to evaluate the economics of the new pit slope angles. At the beginning of the Life-of-Mine (LoM) planning process, a 'Mine Planning Input Parameters' document is created as a repository of the mine design and planning input parameters.

The mine planning inputs

- The latest geological model that defines the grades, diamond price per kimberlite phase and tons of the various rock types in and around the deposit. The geological model also defines the classification (measured, indicated or inferred) of the various blocks in the model in accordance with the SAMREC Code
- Pit slope design parameters such as bench height, berm width and batter angles
- Financial data consisting of exchange rates, annual diamond price escalations, royalties, marketing and selling costs, discount rate, mining and treatment unit costs, overhead (fixed) costs, and capital costs
- Haul road design, minimum mining widths, mining dilution, and mining recovery. The minimum mining width is the minimum cutback width that allows the selected fleet to operate efficiently
- Plant recovery and annual plant capacity
- Any other relevant parameters such as environmental, legal, social, and governmental factors.

The inputs are compiled in collaboration with heads of relevant departments, which include finance, MRM, mining and the treatment sections of the mine. The input document is signed off before the parameters are used for mine planning. The consultative process and sign-off of planning parameters ensures that there is buy-in to the plan by all stakeholders. The evaluation of the economics of the new

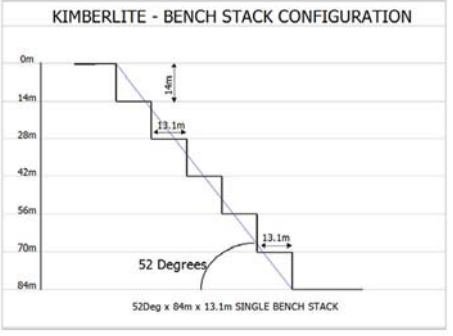

Figure 7—Bench stack configuration in kimberlite

(steeper) slope design required the update of only the pit slope design parameters, all other parameters from the previous mine plan remaining unchanged.

Mine design

Mining options for a steeper slope – cost versus values

There are at least three mining options for a steeper slope angle. One obvious option is to save mining costs by mining less waste for the same amount of ore on the shallower slope, as illustrated in Figure 8.

The second option, as illustrated in Figure 9, is to mine more ore for the same amount of waste.

In a third option more ore is exposed by mining even more waste (Figure 10). This option makes better use of the difference in the cost of mining a ton of waste against the net value (excludes ore mining, processing and fixed costs) in a ton of ore. The net value in a ton of ore is much higher than the cost of mining a ton of waste, hence there is more value in mining more tons of ore than having a cost saving on waste.

Pit optimization

The mine design process starts with the update to the pit optimization exercise where a new optimum pit shell (Figure 11) is determined in Whittle software based on the steeper basalt slope angles. All other optimization parameters were kept constant from the previous optimization. The optimum shell was used as a guide in the pit design process. The optimization for the shallower slope, which formed the base case, yielded an optimal pit with 374 Mt of waste and 140 Mt of ore. Table II compares the pit optimization results for the three mining options for the steeper slope as discussed against the base case.

The value of a ton of ore at Letšeng is approximately ten times the unit cost of waste mining, underlining the fact that accessing more ore is more valuable than saving waste. Consequently, mining option 3 yielded the highest NPV.

Pit designs

Pit design made use of the optimized/steeper basalt slope design parameters based on the stack angle of 70° in basalt and 52° in kimberlite over stack heights of 84 m. The major change from the previous design is the reduction of the berm from 19.58 m to 15.10 m. Pit designs were done using Gems software on a split shell design concept.

The split shell design subdivides the concentric cutback into two (or more) cutbacks as shown in Figure 12. The Letšeng cutbacks are subdivided on a north-south split axis. The split axis was determined based primarily on the value distribution in the kimberlite pipes.

The fundamental advantages of this design concept include:

- Deferred waste mining and a reduced waste peak and hence an increased Net Present Value (NPV) of the mine
- Decongestion of mining operations through the separation of waste and ore mining activities leading to increased mining efficiencies and safer operations

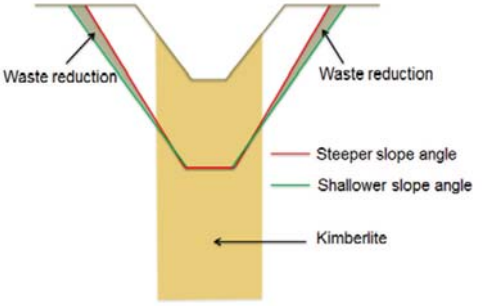

Figure 8—Mining option 1: mine less waste for the same amount of ore

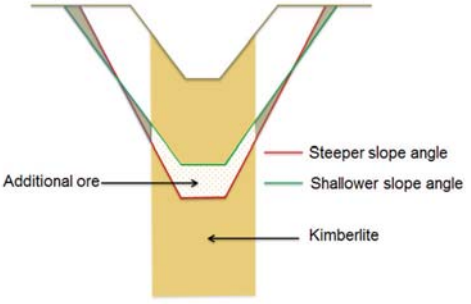

Figure 9—Mining option 2: mine more ore for the same amount of waste

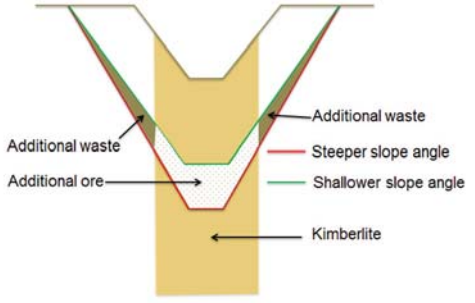

Figure 10—Mining option 3: mine more waste for more ore

Table II

Comparison of mining options for a steeper slope

Mining options for steeper slope	Change in waste / (Mt)	Additional ore / (Mt)
Option 1: Mine less waste for same amount of ore	–57	0
Option 2: Mine more ore for same amount of waste	0	14
Option 3: (New Optimal Pit) Mine more waste for more ore	77	27

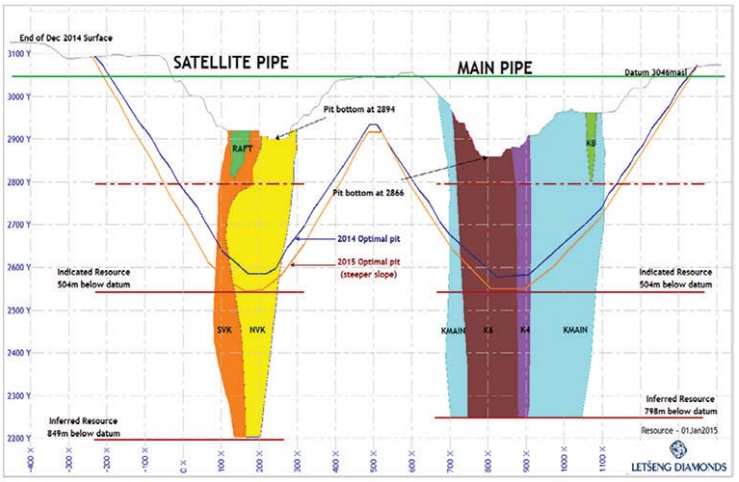

Figure 11—Comparison of optimal pit shells for the steeper slopes against shallower slopes on a W-E section of the Letšeng kimberlite pipes

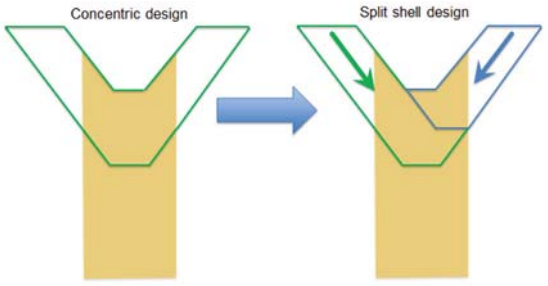

Figure 12—Split shell design concept

- The elimination of waste spillage on ore ramps, thereby minimizing ore hauling stoppages and enhancing safety.

A disadvantage of the concept is merging of cutbacks, potentially leading to the development of bullnoses which can present stability issues.

A section through the Letšeng pit designs is shown in Figure 13.

Development of LoM schedules

Upon completion of pit designs, block model data constrained to different cutbacks is exported to XPAC software for the development of LoM schedule scenarios. The LoM plans have to satisfy conflicting objectives of maximizing NPV through deferring waste and ensuring the continuity of ore supply to the plants. This is achieved by planning through mining bottlenecks, keeping a minimum of six months of stripped reserves available. This is especially important during the time when the cutback being stripped starts to expose ore and the preceding cutback ore is nearing exhaustion.

Mine plan improvements

The schedule scenarios for the steeper slope and the shallower slope were input into the company NPV model for comparison. The LoM plan for the steeper slope design yielded the following improvements:

- Improved stripping ratios in the various pit cutbacks
- A reduction in the peak waste profile from 42 Mt/a to 36 Mt/a, leading to a significant reduction in fleet size
- The improved stripping ratios allowed for an increased ore contribution to plant feed from the higher grade Satellite pipe.
- A 14% improvement in the life-of-mine NPV
- An extension to the life of mine of three years.

Conclusions

The steepening of the slope angles in waste led to significant improvements in the mine plans and NPV. The steepening of the slopes was enabled through the improvements that were introduced in blasting, geotechnical controls, data collection and communication of geotechnical hazards.

- Improvements in blasting:
  - The introduction and advances in trim or buffer blasting and pre-splitting around the final pit perimeter enhanced the protection of final pit walls
  - Introduction of electronic timing systems in blasting led to improved blasting by exploiting the flexibility and greater accuracy of the electronic systems

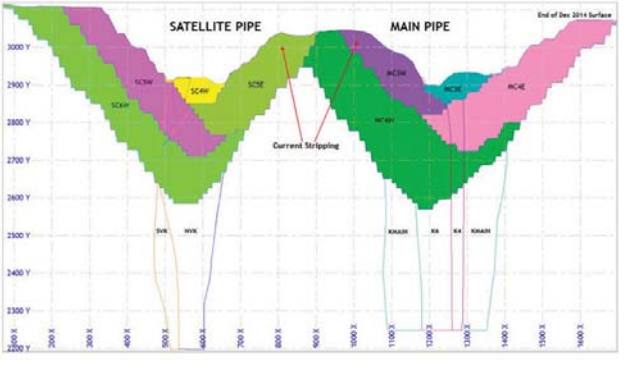

Figure 13—W-E Section though the Letšeng pit designs

  - Introduction of multiple primers in blast-holes to improve fragmentation
- ➤ Improvements in geotechnical controls:
  - The initiation of a process of geotechnical sign-off for each highwall immediately after completion of mining in order to ascertain that the wall has been mined to standard and will not pose future risks to mining personnel and equipment
  - Improved geotechnical data collection that resulted in better rock mass characterization
  - The introduction of slope monitoring using lidar scanners, including the formulation and adoption of a pit clearing procedure in the case of a detection of a slope movement beyond set threshold limits
  - Commissioning of a purpose-built scaler for dislodging loose rocks on the pit highwalls.

However, the steeper slope requires the mine to be more vigilant in the areas of geotechnical control. An ongoing pit slope angle reconciliation on both basalt and kimberlite slopes will be required to be carried out on a regular basis, with decisions taken on the performance of the slopes and modifications to the slopes, as and when required. Quality assurance and quality control on the pit limit blast design patterns remain one of the most important factors in ensuring that the limit blasts are carried out in the most effective manner.

Acknowledgements

Thanks to my wife Fungai Kwangwari, to my colleagues, Bob Burrell, Obed Matlala, Dr Gerard Letlatsa, Nkopane Lefu, and Tinodashe Nyikavaranda, to SRK Consulting for their invaluable input, and to the Letšeng management for giving permission for this paper to be published.

References

Akisa, D., and Gyimah, D. 2015. Application of Surpac and Whittle Software in Open Pit optimisation and Design. *Ghana Mining Journal.* pp. 35–43.

Armstrong, R. and Terbrugge, P. 2012. Slope design feasibility study for Letseng Diamond Mine, Lesotho. Johannesburg: Unpublished report.

Chiappetta, F. 2015. Letseng Blast Training. Maseru: Unpublished report.

Cunningham, C. 2000. The Use of Blast Timing to Iimprove Slope Stability (1st edn.). Colorado: Society for Mining, Metallurgy, and Exploration, Inc. (SME) Littleton, co.

Eberhardt, E. 2012. The Hoek–Brown Failure Criterion. Springer-Verlag.

Hoek, E., Carranza-Torres, C., and Corkum, B. 2002. Hoek-Brown failure criterion - 2002 Edition. *Proceedings of NARMS-TAC Conference,* Vancouver. University of Toronto. pp. 267–273.

Hustrulid, W., Kuchta, M., and Martin, R. 2013. Open Pit Mine Planning and Design. Volume 1 Fundamentals. CRC Press, Boca Raton, Florida.

Letlatsa, G., Madowe, A., Lefu, N., and Chitate, W. (2015). Slope stability risk management at Letseng. Letseng Diamond Mine internal document.

SAMREC. 2009. South African Mineral Resource Committee. The South African Code for Reporting of Exploration Results, Mineral Resources and Mineral Reserves (the SAMREC Code). 2007 Edition as amended July 2009. http://www.samcode.co.za/downloads/samrec2009.pdf.

Terbrugge, P. 2015. Proposed basalt slope angles. Johannesburg: Unpublished report.

Wooler, R. 2001. Taking Whittle Four-X to the limits. *Proceedings of the Fourth Biennial Conference on Strategic Mine Planning Conference,* Perth, 26–28 March 2001. Australasian Institute of Mining and Metallurgy, Melborne. pp. 163–169. ◆

http://dx.doi.org/10.17159/2411-9717/2016/v116n8a4

Using the proportion of barren samples as a proxy for minimum grade in a diamondiferous linear beach deposit—an application of the Nachman model

by J. Jacob*

Synopsis

Over the past 80 years, the Namibian diamondiferous marine placer has been studied extensively to develop solutions for mining and sampling challenges. The types of studies include the statistical modelling of the distributions of the stone counts per sample; investigating the relationship between geology and the grade distribution; assessing the quality potential of the entrapment of the available diamond pulse; using predetermined acceptability of barren samples (zero proportion (Z_p) samples) to model distributions; optimal sample sizes; and more. During early-stage project evaluation it is more important to find out if a particular area is likely to be above a specific cut-off grade than to focus on sampling for the purpose of accurate resource estimation. Previous work using mixed Poisson and Sichel distributions to model the abundant onshore diamond data has been very successful in modelling the long-tailed nature of these linear beach deposits. The means of these distributions are, however, sensitive to extreme values. Technical and cost constraints prevent a similar scale of sample collection in an adjacent, geologically equivalent, submerged beach environment. A method not sensitive to extreme values is thus required to make early-stage assessments of the likelihood that the grade of a particular target is above a minimum cut-off grade. The Nachman model describes the functional relationship between the mean population density and proportion of barren patches (Z_p) in a patchy environment. A prerequisite for using the Nachman model is that the underlying data must be modelled using a negative binomial distribution (NBD). The case study data is from an analogous area adjacent to the exploration target and meets the NBD requirement. It is thus appropriate to apply the Nachman model. The Nachman model provides an opportunity to use the observed Z_p to predict the mean grade for an area at the very early stage of an exploration project. In future, early-stage exploration data from a homogenous geological zone exhibiting characteristics of the Nachman model assumptions can thus be used to rank and target those areas that show potential to be above the minimum required grade cut-off for follow-up sampling and inclusion in the mine planning cycle.

Keywords
diamond sampling, marine placer, diamond distribution, Nachman model.

Introduction

Diamond mining of linear beaches along the southwestern coast of Namibia has been carried out since the early 1930s. The onshore raised beaches, stretching 100 km north of the Orange River mouth, have been virtually mined out. Mining of the extension of the raised onshore beaches continues below present-day sea level using a process of beach accretion (Jacob *et al.*, 2013).

Between the 1930s and the 1960s some 26 000 samples were collected during the initial delineation of the diamondiferous raised beach deposit along the 100 km coastal strip north of the Orange River mouth. The delineation took the form of 1 m wide coast-perpendicular trenches sampled at 5 m intervals, resulting in a sample support size of 5 m² (1 m × 5 m). These trenches are mostly spaced 500 m apart along the coast (Figure 1). Detailed logging and record keeping of the exact locations where diamonds were found are preserved in hand-drawn trench sections. During this delineation trenching campaign, six raised beaches, A- to F-beach, were identified, with the A-beach closest to the present-day shoreline and the F-beach the furthest inland.

Overview of previous statistical work on diamondiferous marine placers

The Namibian diamondiferous marine placer has been studied extensively over the past 80 years to develop solutions for mining and sampling challenges. The types of studies include (a) statistical modelling of stone count distributions per sample; (b) using mixed distributions to describe the occurrence of diamonds in trapsites; (c) investigating the relationship between geology and sample grade; (d) determining an optimal sample size using a preselected sample zero proportions (Z_p); (e) determining optimal sample sizes, and more. A summary of these studies is given below.

Statistical modelling of the stone count per sample

The grade valuation of diamond populations is governed by two aspects: the number of individual stones per sample and the size

* *Namdeb Diamond Corporation.*
 This paper was first presented at the Diamonds still Sparkling 2016 Conference *14–17 March 2016, Gaborone International Convention Centre.*

Using the proportion of barren samples as a proxy for minimum grade

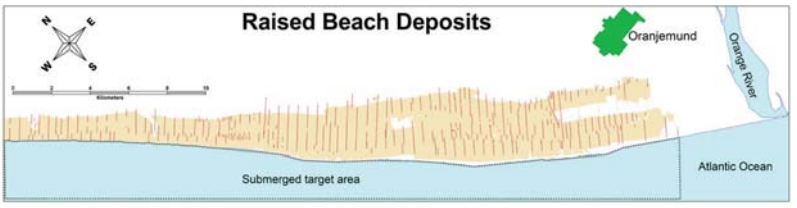

Figure 1—Overview map of the southern portion of diamondiferous raised linear beach deposits north of the Orange River mouth, showing 1 m wide delineation trenches and the submerged target area

distribution of the individual stones. Sichel (1973) derived a distribution function that could successfully model the number of stones per sample using a mixed Poisson probability distribution. This distribution is especially useful in modelling populations with a high Z_p and a long positive tail.

Sichel's distribution function (Sichel, 1973) for the number of stones is given by:

$$\phi(r) = \sqrt{2\alpha/\pi}\exp\left(\alpha\sqrt{1-2\beta/\alpha}\right)\frac{\beta^r}{r!}K_{r-\frac{1}{2}}(\alpha)$$

$$r = 0,1,2,3\ldots, \alpha > 0, \beta > 0$$

with $K\gamma$ (.) the modified Bessel function of the second kind of order γ, with $\gamma = r\frac{1}{2}$, and

$$\hat{\alpha} = \left[-\ln\hat{\phi}(0)\right]\left[1 - \frac{\ln\hat{\phi}(0)}{2\left[\bar{r} + \ln\hat{\phi}(0)\right]}\right] \quad \text{and}$$

$$\hat{\beta} = \frac{\bar{r}}{\hat{\alpha}}\sqrt{\bar{r}^2 + \hat{\alpha}^2} - \bar{r} \quad \text{and}$$

$$\hat{\theta} = \frac{\hat{\beta}}{\hat{\alpha}}$$

where $\bar{r}$ is the average number of stones per sample.

The expected frequencies are calculated from the recurrence formula:

$$\phi(r) = \frac{\beta}{\alpha}\left(\frac{2r-3}{r}\right)\phi(r-1) + \frac{\beta^2}{r(r-1)}\phi(r-2) \quad r > 1$$

starting with the first two frequencies:

$$\phi(0) = \exp\left[-\alpha\left(1-\sqrt{1-\theta}\right)\right]$$

$$\phi(1) = \beta\phi(0) \qquad 0 < \theta < 1$$

Sufficient samples are required to define the parameters of the distribution in order to determine the estimated proportion of barren samples, $\hat{\phi}(0)$, and the mean r with reasonable confidence. Once such a distribution has been fitted, the mean and associated confidence limits can be determined.

Using mixed distributions to describe the occurrence of diamonds in trapsites

Diamond (discrete particle) concentration in a marine placer environment is influenced by the quality of diamond pulses available to be concentrated and the quality of the trapsites. A concept of regionalized potential described by Kleingeld (1987) combines the impact of dependent factors influencing diamond concentration. The geological processes at play during diamond deposition are complex. One scenario could be that a diamond pulse containing a relatively high proportion of diamonds is deposited over an area with poor trapsites. A different scenario could be that a high diamond content pulse of gravel is deposited over an area with good trapsites, but that subsequent marine reworking processes could have removed diamonds from these trapsites. The model developed by Kleingeld (1987) makes use of the hypothesis that the number of particles within any region is considered to be a sum of Poisson pockets, with the particles per trapsite randomly distributed.

Kleingeld (1987) used $\phi(r)=\int_0^\infty P(r|\lambda)f(\lambda)d\lambda$, with $P(r|\lambda)$ a Poisson and $f(\lambda)$ a gamma distribution function, to model the number of particles per sample and the distribution of the trapsites. Kleingeld concluded that when applying Sichel's model, $\hat{\theta}$ can be estimated with some degree of accuracy only by using large numbers of samples so that a good statistical chance exists for encountering the richer trapsites. Also, through exhaustive testing, Kleingeld determined that using the Z_p of samples and the mean to determine the Sichel distribution parameters is far superior to using the method of moments.

With $\bar{r}$ the sample mean and $\phi(0)$ the sample Z_p, $\hat{\alpha}$ and $\hat{\theta}$ can be determined from:

$$\hat{\alpha} = -\tfrac{1}{2}\log\left(\phi(0)\right)\left(1 + \frac{\bar{r}}{\bar{r} + \log\left(\phi(0)\right)}\right)$$

$$\hat{\theta} = 1 - \left[\frac{-\log\left(\phi(0)\right)}{2\bar{r} + \log\left(\phi(0)\right)}\right]^2$$

For early-stage exploration decisions, when only a few data points are available, it will be challenging to model the Sichel distribution with confidence.

Relationship between geology and sample grade

The complexity of diamondiferous marine placer geological models cannot be overstated. Oosterveld *et al.* (1987) made an attempt to determine the relationship between the geology and statistical parameters obtained from diamond sampling for the diamondiferous marine placer of southwestern Namibia. It was found that those highly complex geological controls influencing the distribution of diamonds could only be described in broad terms by the statistical parameters. For this reason, blocks up to 5 km in length along the coast were estimated (Oosterveld *et al.*, 1987). The large blocks were subsequently sub-blocked into 500 m lengths situated between 1 m trenches and 100 m to 300 m widths perpendicular to the coast. Two smoothed parameters of the Sichel

distribution are used as follows: the contribution is associated with the quantity of trapsites and the θ contribution with the abundance of diamonds in trapsites (*i.e.* the quality of trapsites). Oosterveld *et al.* (1987) stabilized the term by smoothing $\theta/\sqrt{1-\theta}$ along the coastline with a moving average, based on groups of at least 50 samples. The parameter is calculated with θ fixed *a priori*. The estimation of Sichel's mean (Sichel, 1973) is log-transformed into:

$$\log(D) = \log(\beta) + \log(1/\sqrt{1-\theta})$$

where

$$D = \alpha\theta/2(\sqrt{1-\theta})$$

$$= \beta(\sqrt{1-\theta})$$

and

$$\beta = \alpha\theta/2$$

Oosterveld *et al.* (1987) related the smoothed parameters to broad-scale geological observations, diamond pulse, and footwall conditions determining the abundance of trapsites. It was concluded that the highly complex geological controls influencing the spatial distribution of diamonds could only be modelled in broad terms by the statistical parameters (Figure 2).

Determining an optimal sample size using a preselected sample Z_p

A challenge that exists prior to the modelling of the individual stone data is the decision about an appropriate sample support size for data collection. In determining a sample size, Sutherland and Dale (1984) developed an approach based on Sichel's mixed Poisson distribution, where an acceptable sample Z_p is preselected. Based on assumptions about the underlying probability distribution and mean number of stones per sample, a minimum sample size can be determined. In early-stage resource exploration, prior to sufficient number of samples being available, it is difficult to quantify the mean value $\bar{r}$ of the target. If, however, a reasonable value for $\bar{r}$ can be determined early on in a project, then Figure 3 (after Sutherland and Dale, 1984) is very helpful in determining a minimum sample size. This approach does not, however, guide early-stage decision-making regarding continuing with or abandoning an exploration target when there is still insufficient data available and the mean and tail of a target's distribution have not yet been well established.

Determining an optimal sample size using Pierre Gy's sample theory

The application of Pierre Gy's sampling formula to express the sampling error when a volume of material is considered is used by Royle (1986) in an alluvial diamond deposit example. The formula makes use of the physical characteristics of the material being sampled, with the mean squared sampling error expressed as:

$$e = \frac{cflg\ d^3A^2}{M}$$

with $c = D_m/a$, D_m the density of the mineral, a the proportion of the mineral, f a shape factor, l expressing liberation, g a size range factor, d the mesh size, A the mean value of the sampled material, and M the mass of the sample. Royle (1986) outlines detail regarding values to be used for these constants.

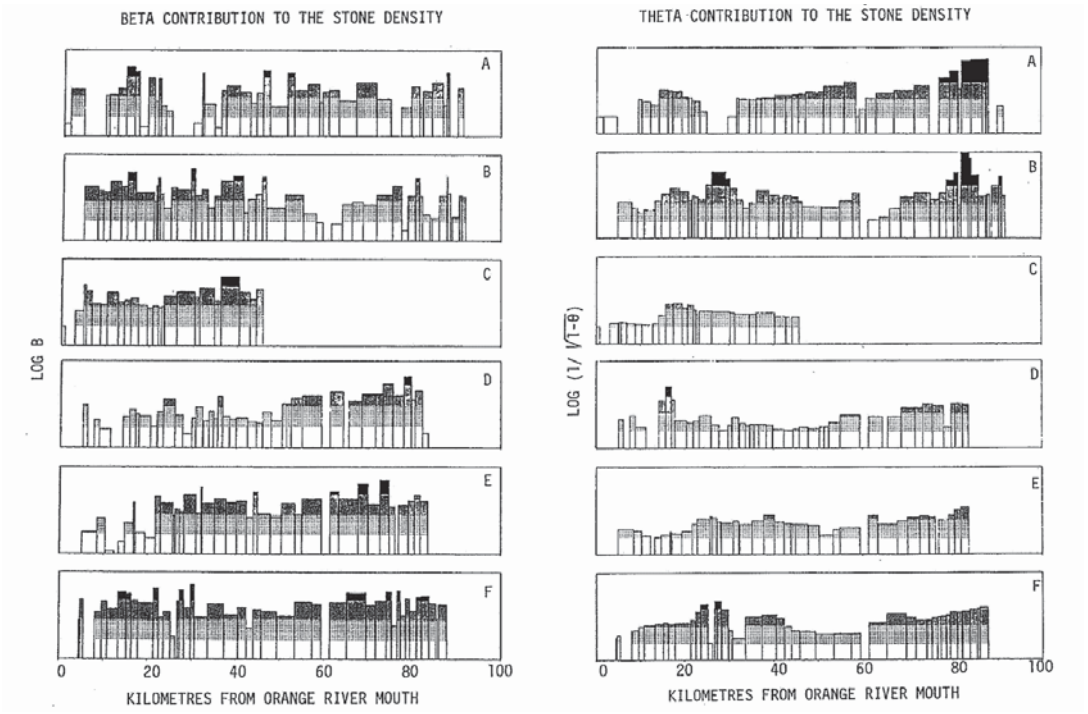

Figure 2—The β and θ contributions plotted along the coastline, split into data groups containing at least 50 samples (after Oosterveld *et al.*, 1987)

Using the proportion of barren samples as a proxy for minimum grade

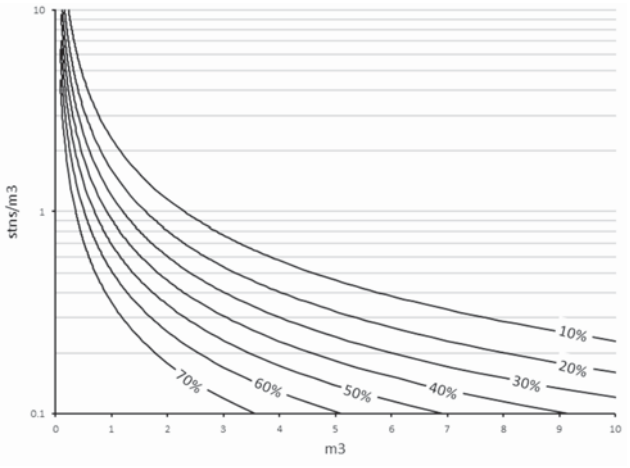

Figure 3—Determining a minimum sample size using a preselected sample Z_p (lines represent Z_p as % here) and $\bar{r}$ (after Sutherland and Dale, 1984)

From an indication of the expected grade of a deposit, or making use of a minimum economically required cut-off grade, the sample error can be determined. By changing the sample volume and making use of an assumed $1.96\sqrt{e}$, the error variance can be used to adjust and express 95% confidence limits for the mean value of the material.

Royle (1986) notes that Gy's formula gives an order-of-magnitude sample size and that, if possible, larger samples would be better. Of utmost importance, however, is the fact that no mathematical or statistical procedure can improve poor quality samples. All effort should be focused on ensuring sample integrity and minimizing the introduction of sample error.

Problem statement

Technical and cost constraints will always be present in exploration efforts targeting diamondiferous submerged beaches. During early-stage project evaluation it is more important to find out if a particular area is likely to be above a selected cut-off grade than to focus on sampling for the purpose of accurate resource estimation. Previous work on statistical distributions of diamonds was based on abundant onshore data, which has been used very successfully in modelling the long-tailed nature of these linear beach deposits. Technical and cost constraints militate against using a similar sampling campaign in a geologically equivalent submerged beach target environment. A method not sensitive to the occurrence of extreme values and reliant on less data is thus required in order to make early-stage assessments as to the likelihood that the grade of a particular target is above a certain cut-off grade.

Proposed method of applying the Nachman model to diamond occurrences

Description of the Nachman model

Nachman (1981) described the functional relationship between the mean population density and the proportion of unoccupied (mite-free) patches (Z_p) in a patchy environment, as initially applied to mite counts observed on cucumbers in glasshouses. The Nachman model assumes that the underlying population follows a NBD distribution. Plotting the following transformations against each other shows a linear relationship between the mean discrete counts and the zero proportion.

Zero proportion (Z_p) transformation: $\log [\ln (\frac{1}{Z_p})]$

Mean number of occurrences (m) transformation: $\log (m)$

This linear relationship can then be plotted and used to predict the mean of the data based on the observed Z_p.

Case study

As discussed previously, the Sichel distribution fits the long-tailed linear beach data reasonably well. Looking at the 26 000 sample results per trench spaced at about 500 m intervals along the 100 km long coastal strip (discarding any grouping containing fewer than 30 samples, where a grouping represents a section of the beach covered by a trench), the two-parameter NBD also shows a reasonable good fit to the data (Figure 4).

The two-parameter NBD depends on parameters ν and p (Kleingeld, 1987) with the probability density function given by:

$$P(X = i) = q^{\nu} \frac{\Gamma(\nu + i)}{\Gamma(\nu)} \frac{p^i}{i!}$$

$$i = 0,1,2,3,\ldots \quad \text{and} \quad p, q, \nu > 0$$

The mean m and variance σ^2 can be determined from its moments (Kleingeld, 1987):

$$m = \nu\, p/q \text{ and } \sigma^2 = \nu \frac{p}{q^2}$$

from which

$$p = \frac{\sigma^2 - m}{\sigma^2} \text{ and } \nu = \frac{m^2}{\sigma^2 - m}$$

The assumption required for using a Nachman model, that the data can be modelled by a NBD, is thus valid. For this reason it is thus reasonable to use the Nachman model to guide exploration effort based on the Z_p of data collected.

Results

Recognizing that there would be measurement error in both Z_p and the mean, a Deming regression (Deming, 1943) is fitted to the Nachman-transformed data (Figure 5a). The regression line is subsequently shifted by changing the y-axis intercept in such a way that 95% of the data falls above it (Figure 5a). The back-transformed Deming regression line (Figure 5b) illustrates that if, for example, Z_p is equal to 0.60 then 95% of the data will be above a mean of 0.67 stones per

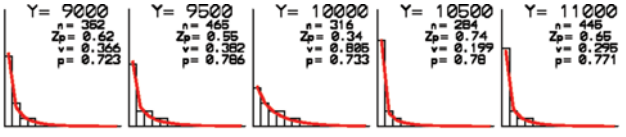

Figure 4—Snapshot of the NBD distribution fitted to diamondiferous linear beach sample data grouped per trench. Y represents the distance from the Orange River mouth northwards along the coast in metres

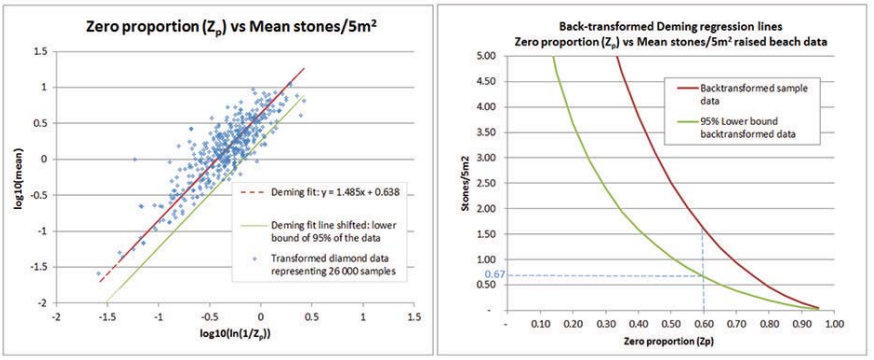

Figure 5—Transformed (a) and back-transformed (b) linear beach diamond data of the Nachman model based on raised onshore beach data

5 m². Based on these results it is perhaps thus not surprising that more than 95% of the onshore diamondiferous raised beach deposit along the 100 km strip north of the Orange River mouth has been mined out to date, because it is above the cut-off grade of 0.05 stones per 5 m². An application of this method applied to limited submerged beach data is shown in the Appendix.

Discussion and conclusion

Previous publications (Sichel, 1966; Sutherland and Dale, 1984;, Sichel, 1987; Kleingeld, 1987; Oosterveld *et al.*, 1987) described diamond distributions using variations of the mixed Poisson model. The means of these distributions are, however, sensitive to extreme values and many data points are needed to stabilize the results.

The Nachman model (Nachman, 1981) describes the functional relationship between the mean population density and proportion of unoccupied patches (Z_p). In the case study, the available analogous data from an area adjacent to the exploration target can be modelled using a NBD. It is thus reasonable to apply the Nachman model. The Nachman model approach provides an opportunity to use the proportion of barren samples to predict the mean grade for an area during the very early stage of an exploration project. In future, early-stage exploration data from a homogenous geological zone exhibiting characteristics associated with the Nachman model assumptions can thus be used to rank and target those areas that show potential to be above the minimum critical grade cut-off for follow-up sampling and inclusion in the mine planning cycle.

Comparing Sutherland's approach for determining a minimum sample size using a preselected sample Z_p and mean (Figure 3) and the outcome of applying the Nachman model (Figure 5), the following is observed:

- A Z_p of 0.60 (according to the Nachman model) predicts a minimum grade of 0.67 stones per 5 m² or 0.134 stones per m²
- Considering a diamondiferous gravel thickness of 1 m, Sutherland's model based on Sichel's distribution at a 5 m² support predicts a grade of 0.10 stones per m² for Z_p equal to 0.60
- The minimum grade predicted by the Nachman model is higher than that by Sutherland's theoretical model based on the Sichel distribution. Since the Nachman model results are based on actual empirical data, it is deemed more appropriate compared to the theoretical Sichel model results. This affirms the reasonableness of using the Nachman model's Z_p to predict a potential minimum grade based on samples obtained from a single geological zone.

Acknowledgements

The author gratefully acknowledges the assistance of Chris Prins (Anglo American Corporation/ University of the Witwatersrand) in preparing this paper. The author would like to thank the De Beers Group of Companies, Anglo American Corporation, and Namdeb Diamond Corporation Mineral Resource Departments for their support, providing access to data and permission to publish this work. The research presented in this paper forms part of a greater resource development project, also incorporated in a PhD study '*Contextualized risk mitigation based on geological proxies in alluvial diamond mining using geostatistical techniques*' at the University of the Witwatersrand. The author appreciates the comments and helpful suggestions from the reviewers.

References

Deming, W.E. 1943. Statistical Adjustment of Data. Wiley, New York.

Jacob, J., Prins, C., and Oelofsen, A. 2013. Determination of sampling configuration for diamondiferous gravel occurrence using geostatistical methods - applied to a probe drill platform. *Proceedings of Sampling and Analysis: Best Practice in African Mining*, Misty Hills, Mulderdrift, Gauteng, South Africa, 4–6 June 2013. Southern African Institute of Mining, Johannesburg.

Kleingeld, W.J. 1987. La géostatistique pour des variables discrète. PhD thesis, School of Mines, Paris.

Nachman, G. 1981. A mathematical model of the functional relationship between density and spatial distribution of a population. *Journal of Animal Ecology*, vol. 50, no. 2. pp. 453–460.

Oosterveld, M.M. 1972. Ore reserve estimation and depletion planning for a beach diamond deposit. *Proceedings of the Tenth International Symposium on Application of Computer Methods in Mineral Industry*. South African Institute of Mining and Metallurgy, Johannesburg, South Africa. pp. 65–71.

Oosterveld, M.M., Campbell, D., and Hazell, K.R. 1987. Geology related to statistical evaluation parameters for a diamondiferous beach deposit. *Proceedings of APCOM 87: Geostatistics. 87. Proceedings of the Twentieth International Symposium on the Application of Computers and Mathematics in the Mineral Industries*. Vol. 3. Lemmer, I.C. (ed.). South African Institute of Mining and Metallurgy in association with the Council for Mineral Technology, Johannesburg. pp. 129–136.

ROYLE, A.G. 1986. Alluvial sampling formula and recent advances in alluvial deposit valuation. *Transactions of the Institution of Mining and Metallurgy Section B: Applied Earth Science*. pp. B179–B182.

SICHEL, H.S. 1966. The estimation of means and associated confidence limits for small samples from lognormal populations. *Proceedings of the Symposium on Mathematical Statistics and Computer Applications in Ore Evaluation*. South African Institute of Mining and Metallurgy, Johannesburg. pp. 106–122.

SICHEL, H.S. 1973. Statistical valuation of diamondiferous deposits. *Journal of the South African Institute of Mining and Metallurgy*, vol. 73. pp. 235–243.

SICHEL, H. S. 1987. Some advances in lognormal theory. *APCOM 87: Geostatistics. 87. Proceedings of the Twentieth International Symposium on the Application of Computers and Mathematics in the Mineral Industries*. Vol. 3. Lemmer, I.C. (ed.). South African Institute of Mining and Metallurgy in association with the Council for Mineral Technology, Johannesburg. pp. 3–8.

SUTHERLAND, D.G. and DALE, M.L. 1984. Method of establishing the minimum sample size for sampling alluvial diamond deposits. *Transactions of the Institute of Mining and Metallurgy Section B: Applied Earth Science*, vol. 93. pp. B55–B58. ◆

Appendix

Owing to a process of beach accretion (Jacob *et al.*, 2013), areas previously not accessible for sampling could recently be sampled. Figure A1 shows a NBD distribution fitted to 613 sample results from beach accretion areas. The 613 sample results are spatially grouped into 13 groups. Each group contains a minimum of 40 samples (Figure A2a).

- A Z_p of 0.60 (according to the Nachman model) predicts a minimum grade of 0.80 stones per 5 m² or 0.16 stones per m² (Figure A2b)
- In this example the minimum grade predicted by the Nachman model of 0.16 stones per m² is higher than Sutherland's theoretical model prediction of 0.10 stones per m² based on the Sichel distribution (Figure 3). Since the Nachman model results are based on actual empirical data, it is deemed more appropriate compared to the theoretical Sichel model results. This affirms the use of the Nachman model's Z_p to predict a potential minimum grade based on samples.

As more sample data become available the application of the Nachman model to predict a potential minimum grade will be assessed and used.

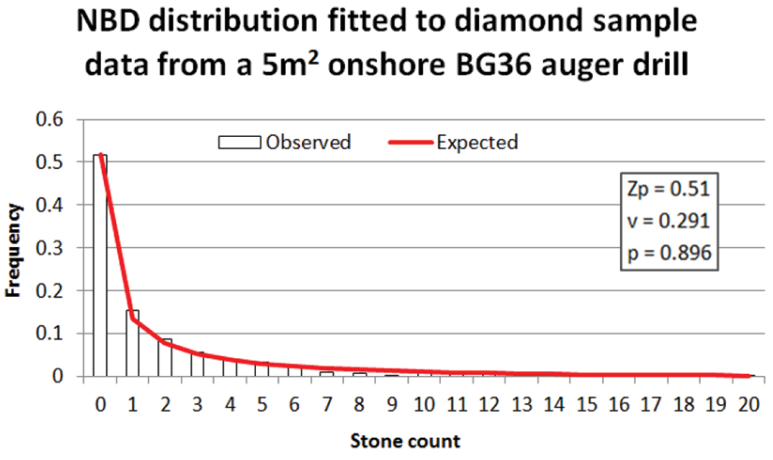

Figure A1—NBD distribution fitted to diamondiferous submerged linear beach sample data

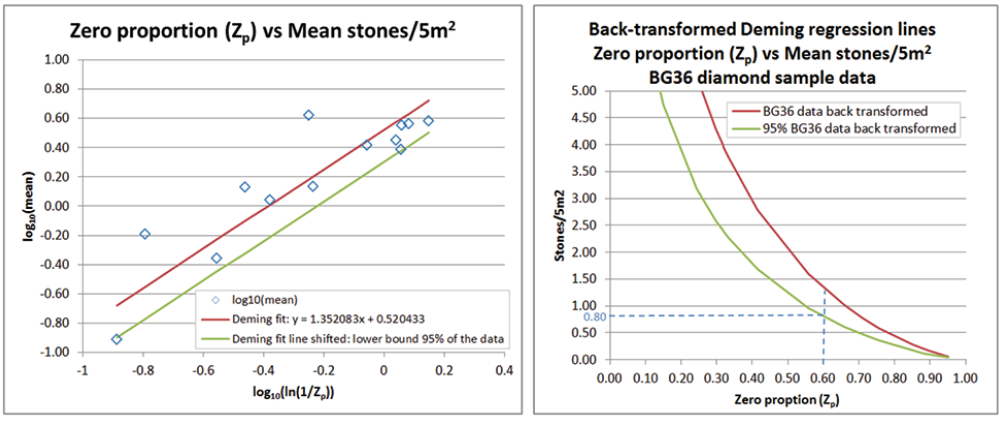

Figure A2—Transformed (a) and back-transformed (b) linear beach diamond data of the Nachman model based on submerged beach data

http://dx.doi.org/10.17159/2411-9717/2016/v116n8a5

Microdiamond analysis—a method for estimating the size frequency distribution of the macrodiamonds

by J. Danoczi* and S. Creighton*

Synopsis

Estimating the size frequency distribution of the macrodiamonds on a new deposit is important for both economic reasons and for the design of the processing plant. Millions of dollars can be lost due to incorrectly sized comminution circuits. This report analyses an alternative methodology for macrodiamond grade estimation using the cumulative results from small parcels of microdiamonds and plotting them on a log-log scale. The method was first evaluated mathematically for diamond populations to assess the confidence for data extrapolation. Macrodiamond size distributions and grades were predicted using microdiamond data from three kimberlites, and the actual macrodiamond grades compared to the the predicted grades. The predicted grades were found to replicate the actual grades closely, showing that a high degree of confidence can be ascribed to the results from this method of analysis. This analysis can be used both for resource estimates and for predicting the diamond size distribution information needed for designing a new operation.

Keywords

diamond resource estimation, microdiamond distribution, macrodiamond grade, probability density function, grade-size plot.

Introduction

Microdiamonds are defined as diamonds having the largest dimension smaller than 0.85 mm; too small for cutting into gemstones. Although these small diamonds are suitable only for industrial purposes, they can provide valuable information during exploration for new diamond deposits. Microdiamond abundance data is used to estimate the macrodiamond size frequency distribution and thus provides information relevant to the deposit's economics, eventual plant design, and equipment selection.

Macrodiamonds are diamonds larger than 0.85 mm that may be suitable for cutting into gemstones, depending on their colour and clarity. Macrodiamond recovery from bulk samples is carried out once the microdiamond tests are positive. Macrodiamond recovery confirms that a kimberlite contains macrodiamonds.

Determinations of the micro/macro diamond size relationship are typically based on grade-size plots (Ferreira, 2013). However, this method requires a large data-set in order to obtain reasonable confidence in the results. This report analyses an alternative method that does not require such a large data-set, but instead requires microdiamond occurance (data) in at least seven different size intevals to obtain reasonable confidence.

Microdiamond recovery

Microdiamond recovery is carried out to confirm that a kimberlite contains diamonds. The information used in microdiamond analysis is the number of diamonds per size fraction greater than 75 μm that reside in a sample of the ore (McCandless, 2013). The diamonds are recovered from the kimberlite samples by dissolving small quantities of kimberlite, usually <20 kg per sample, in hydrofluoric (HF) acid or molten sodium hydroxide (NaOH) (also known as caustic fusion). Since diamonds are chemically inert (do not dissolve in acids or alkalis), the small amount of residue from the dissolution process includes some poorly soluble oxide and silicate minerals as well as all of the diamonds. Final recovery of the microdiamonds is carried out by hand-sorting under a binocular microscope.

Macrodiamond recovery

If the microdiamond results indicate that the kimberlite is diamondiferous, macrodiamond recovery is undertaken. Macrodiamonds are recovered in bulk sampling exercises ranging from surficial extraction of a few trenches to drill samples and even to small underground mining projects. The bulk samples are crushed and concentrated through a dense medium separation plant capable of processing several tons of ore. The recovered concentrate is then sent to a laboratory for X-ray sorting and grease table recovery. The final recovery is carried out by hand-sorting in a secure facility.

* *Saskatchewan Research Council, Saskatoon, SK, Canada.*

 ISSN 2225-6253. This paper was first presented at the Diamonds still Sparkling 2016 Conference *14–17 March 2016, Gaborone International Convention Centre.*

If the results for both the microdiamond analysis and the macrodiamond numbers meet the required economic predictors, a diamond processing plant is built and the deposit is mined.

Microdiamond and Macrodiamond Analysis

Diamond count *vs.* size data from both the microdiamonds and the macrodiamonds typically defines a quadratic curve on a log-log plot. The mathematical fitting of a quadratic equation can be accomplished with only three points. In principle, these three points can be from the microdiamond abundances, impliying that the macrodiamond grade can be calculated using only three microdiamond data-points. In practice, more than three points of data are required, since the errors in the microdiamond data can be quite large as the diamonds do not populate the ore in a homogeous manner. The accuracy of macrodiamond abundance predictions from microdiamond data can be evaluated by calculating the 'diamond abundance *vs.* size' curve from the microdiamond data, extrapolating to predict macrodiamond abundance, and comparing the results to the actual recovered macrodiamonds.

The lognormal probability density function (PDF) and the diamond population

The diamond population of a diamondiferous kimberlite has a typical lognormal distribution. The diamond distribution, or probability density function (PDF), comprises positive real values with the majority of the diamonds occuring in the smaller size fractions, causing the diamond population to be skewed to the smaller sizes. An example of a typical diamond lognormal distribution is depicted in Figure 1.

In Figure 1, the blue diamonds depict the number of microdiamonds per hundred tons per unit interval (Dpht/ui), and the purple circles depict the number of macrodiamonds per hundred tons per unit interval (Dpht/ui). The microdiamonds were recovered by caustic fusion (NaOH), ensuring total liberation of all diamonds, whereas the macrodiamonds were recovered by a bulk sampling programme and hence there are inefficiencies (diamond losses) in the number of macrodiamonds recovered smaller than 0.1 carat. The causes of the poor recoveries of the small macrodiamonds include increased the probability of diamond lock-up and plant inefficiencies for this size fraction.

The red squares are the hypothetical estimates of the number of microdiamonds in the kimberlite that are smaller than 75 μm. The green curve is the mathematical model obtained from *only* the microdiamond data and extrapolated into the macrodiamond size fractions, and shows how well the microdiamond curve predicts the actual macrodiamond data.

Properties of the lognormal probability density function (PDF)

Figure 2 is an illustration of a set of lognormal PDFs that have been drawn on an X-Y axis with linear scales.

The lognormal formula used to generate these curves is given by Equation [1], where x is the variable and the parameters used are Coefficient = 1, $u = 0$, and $a \in \{1, 0.5, 0.25\}$ (Montgomery, 2011).

$$\frac{\text{Coefficient}}{xa\sqrt{2\pi}}\, e^{(\ln x - u)^2/2a^2} \qquad [1]$$

The characteristics of the lognormal curve given in Equation [1] are:

Median= e^u
Mean = $e^u+a^2/2$
Mode = e^u-a^2

In Figure 2, the curve most skewed to the left (blue) provides the best representation of a diamond population distribution. This curve also has the highest a-value of the three examples with $a = 1$. The mode of the PDF for a lognormal curve occurs at an X-value where the function (Y-value) is the greatest and is a different value to that of the mean (average) as illustrated in Figure 2. The long and short dashed lines represent the mode and mean, respectively, for each of the three functions depicted in Figure 2.

The lognormal formula that best represents the diamond population represented in Figure 1 is Equation [1] with the parameters:

$$\text{Coefficient} = 60 \qquad u = -4 \qquad a = 2.4$$

and is depicted in Figure 3 as a dark green dashed curve overlain on the diamond data from Figure 1.

The mode of this diamond population occurs at a size (in carats) where the numbers of diamonds in a unit inteval (UI) is the greatest, and occurs at

$$e^{u-a^2} = e^{-4-2.4^2} = 5.8 \times 10^{-5} \text{ carats}$$

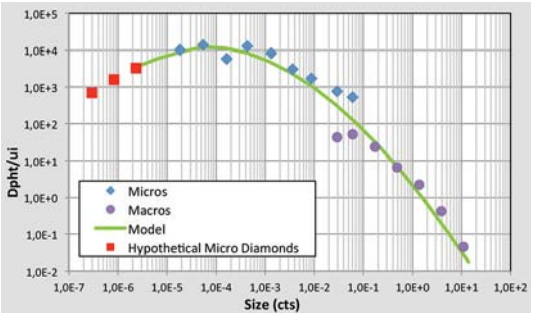

Figure 1—Example of a lognormal distribution of diamond distribution data expressed in units of diamonds per hundred tons (Dpht) per size unit interval for a diamondiferous kimberlite

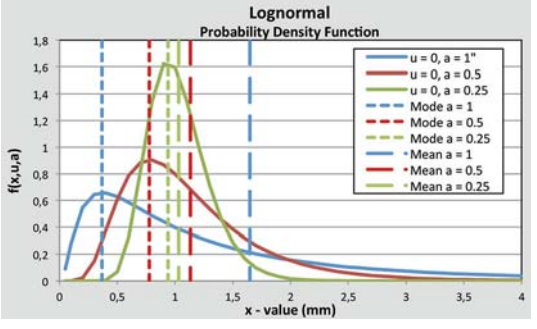

Figure 2—Lognormal curves showing the probability density functions for the same locator parameter 'u' but with different scale parameters of 'a'

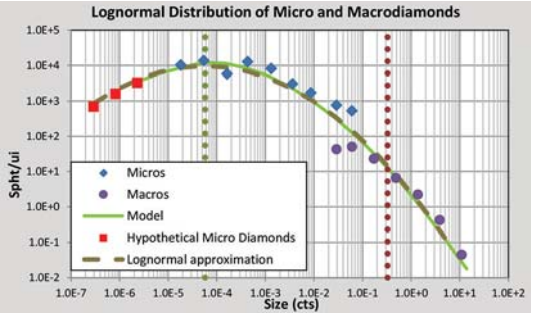

Figure 3—The lognormal formula that best approximates the diamond data is represented by the dark green dashed line

while the average size or mean is at

$$e^{u+a^2/2} = e^{-4+2.4^2/2} = 0.33 \text{ carats}$$

as depicted by the green and brown vertical dotted lines in Figure 3, respectively. This information is useful when comparing different diamond populations and is absent from a grade-size plot.

The lognormal cumulative distribution function (CDF)

The lognormal cumulative distribution function (CDF) is the summation/integral of the data in the PDF from the maximum X-value to the X-value of interest. The CDF is a simpler mathematical progession for modelling of the lognormal data, since the data is always decreasing as X increases and there are no points of inflexion in the graph.

Taking the log of both the X-values and the function values (Y-values) of the lognormal CDF allows the data to be approximated by a quadratic equation with a high degree of confidence, as illustrated in Figure 4. Of importance is the fact that the best quadratic approximation occurs for the lognormal CDF curve with $a = 1$ (the data in blue). The coefficient of determination (R^2) for this quadratic equation is greater than 0.999, illustrating that the lognormal distributions, with scale parameters of 'a' greater than 1 can be approximated by a quadratic equation with a high degree of confidence. The scale parameter (parameter 'a' in Equation [1]) for the diamond population given in Figure 1 was estimated at 2.4, significantly higher than unity. It can

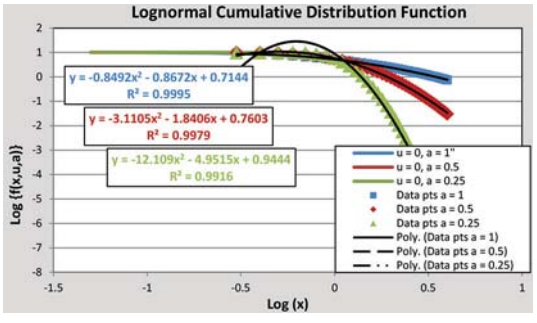

Figure 4—Quadratic equations approximating lognormal curves and their associated coefficient of determination (R^2) when the X-axis and Y-axis are converted to logarithms

therefore be concluded that the CDF for diamond populations can be approximated by a quadratic equation with a high degree of acuracy.

Microdiamond analysis method

Bottom size (75 μm)

Liberating all the +75 μm microdiamonds from a kimberlite sample using HF or NaOH is an expensive and hazardous undertaking. The concentrate from the process has to be neutralized and is then laboriously sorted by hand under a binocular microscope. The cost and time for microdiamond sorting increase in as the size of the microdiamonds decreases. Test work has shown that small diamond losses occur with both the HF and NaOH processes, and the percentage volume loss increases as the diamond size decreases, resulting in errors (Kruger, 2004). From an analytical perspective, analysing only microdiamonds larger than 75 μm ensures that the quadratic approximation of the CDF retains a high coefficient of determination and the level of confidence in the analysis is high. Hence, the accepted lower limit used in microdiamond analysis is 75 μm or 5×10^{-6} carats.

Top size (10 carats)

The top size for valuing diamonds from bulk samples is generally 10 carats, which is the limit to which the microdiamond grade data has been extrapolated. The confidence in the extrapolated data decreases as the range of the extrapolation increases, but if macrodiamond data from bulk samples is included, the data can be extrapolated further in order to predict a top diamond size for the diamond population – information that is necessary for plant design.

Unit intervals

Microdiamonds are sized using a set of progressive sieve sizes, starting ideally at 75 μm and increasing by a factor of √2 up to 1.70 mm. If macrodiamonds are recovered when processing kimberlite using chemical digestion, these diamonds must be included in the analysis in their relevant unit interval (UI). The UIs generally used for reporting diamonds recovered from total chemical digestion processes are given in the first column of Table I.

Analysis of publicly available microdiamond data revealed that different laboratories use different sieve sizes; some start at 75 μm while others start at 106 μm or even 100 μm. Sieving inefficiencies were also encountered when comparing the microdiamond dimensions and mass to the sieve size. For these reasons, the microdiamond data in this study was sorted according to the mass from which the diamond's size was calculated (at the Saskatchewan Research Centre (SRC) all microdiamonds are weighed individually). The diameters of the sorted microdiamonds increase in size by a factor of √2 for subsequent UIs. The microdiamond counts are then normalized to a 100 t sample per UI.

Calculating the mean diamond size per unit interval

The mean diamond size in each unit interval is measured in carats, and is the summation of all the diamond masses in a particular UI divided by the number of diamonds in that UI, as seen in Table I, where column 4 is the mean diamond size

Table I

Microdiamond data for the Unit 1 kimberlite

Sieve size (mm)	Total ct/UI (ct)	Diamonds (units)	Mean diamond size (ct)	Log (MDS)	Dpht (units)	Cumulative Dpht (units)	Log (cumulative)
0.075	0.0017	174	0.00001	-5.0445	10 263	60 352	4.781
0.106	0.0053	233	0.00002	-4.6442	13 743	50 089	4.700
0.150	0.0108	158	0.00007	-4.1666	9 319	36 346	4.560
0.212	0.0439	215	0.00020	-3.6902	12 681	27 026	4.432
0.300	0.0753	139	0.00054	-3.2664	8 199	14 345	4.157
0.425	0.0861	52	0.00165	-2.7812	3 067	6 166	3.789
0.600	0.1310	29	0.00452	-2.3451	1 711	3 079	3.488
0.850	0.1841	17	0.01083	-1.9653	1 003	1 369	3.136
1.180	0.1461	4	0.03652	-1.4375	236	366	2.563
1.700		0	0.07405	-1.1304		130	2.114
Totals	0.6841	1021			60222		

(Kimberlite processed = 1695.4 kg, factor = 58.983 units to calculate Dpht in column 7)

(MDS) and is calculated by dividing column 2 by column 3. The MDS provides information on the size of the diamonds in each UI.

Tabulating the comulative data

The cumulative data is the total number of diamonds that occur in a 100 t sample with sizes ranging from 75 μm (0.000 005 ct) to 10 mm (10 ct). The cumulative data starts adding from the largest UI (9.6–13.6 mm) to the smallest UI (75–106 μm), which is the final value for the smallest UI. This last value is also the sum of all the diamonds. The cumulative data either decreases or stays the same as the UIs increase, as seen in column 7 of Table I. Representing the data in this manner reduces the amount of variation 'noise' in the data, so making it easier to observe trends.

When calculating the cumulative data for a microdiamond population, an estimate is made for the total number of macrodiamonds expected in the kimberlite, known as the 'projection factor'. This projection factor is based on the cumulative distribution of the microdiamonds and the coefficient of determination (R2), which includes the projection factor point. The projection factor is placed in the preceeding UI, as highlighted in yellow in Table I. The projection factor for the Unit 1 kimberlite was; 130 diamonds of size of 1.7 mm and produced an R2 value of 0.99891.

Converting to logarithms and fitting the quadratic curve

In order to analyse the lognormal data in a spreadsheet, both the MDS (in carats) and the cumulative number of diamonds, for each UI were converted to logarithms as shown in columns 5 and 8 of Table I. The data was plotted as denoted by the blue diamonds, including the projection factor, as seen in Figure 5, and a quadratic curve fitted to the data. In the case of the Unit 1 kimberlite, the quadratic formula is:

$$Y = 0.15478x^2 - 1.62205x + 0.5183 \quad [2]$$

with an R^2 value of 0.99891.

Applying the quadratic formula to the required macrodiamond distribution

The formula for the quadratic curve seen in Figure 5 and given in Equation [2] was applied to the size intervals for the macrodiamonds as seen in column 3 of Table II. The macrodiamond distribution used was based on the standard size intervals employed for valuing the diamonds. This was feasible since the formula for cumulative data is not restricted to UIs.

To calculate the number of diamonds in each size fraction (column 5), the cumulative logarithmic data (column 3) was first calculated as an exponent of 10, as seen in column 4 of Table II, and the difference between consecutive size intervals was determined, as seen in column 5 of Table II. The grade of each size interval, column 6, was calculated by multiplying the number of diamonds in the size interval by the mass of diamonds for that interval. The summation of column 6 is the macrodiamond grade, assuming 100% recovery.

However, in an operating diamond processing plant not all the diamonds will be fully liberated and recovered. In particular, the smaller the diamond the lower the probability of liberation and recovery. This loss is evident from the fact that the number of the smaller diamonds recovered by the processing plant (24 Dpht) is less than 6% of the number recovered by chemical dissolution method (439 Dpht).

Finally, the estimated production grade is calculated by correcting for the plant losses by subtracting decreasing percentages of subsequent size intervals from the total, starting at 90% for the 1 mm diamonds, 70% for 1.4 mm diamonds, 50% for the 1.7 mm, and 30% for the 2.3 mm diamonds.

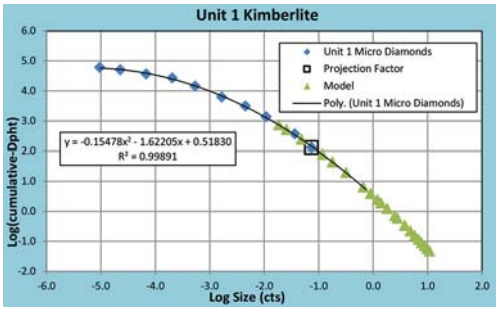

Figure 5—The logarithmic cumulative number of diamonds plotted against the logarithmic mean diamond size

Table II

The modelled macrodiamond data for the Unit 1 kimberlite

Diamond size categories	Log (MDS)	Log (cumulative)	Cumulative (Dpht/size) (units)	Dpht/size (units)	Grade (cpht/size) (ct)
>10 ct	1.0000	-1.2585	0.055	0.055	0.0930
9 ct	0.9542	-1.1705	0.068	0.012	0.1116
8 ct	0.9031	-1.0728	0.085	0.017	0.1363
7 ct	0.8451	-0.9630	0.109	0.024	0.1702
6 ct	0.7782	-0.8376	0.145	0.036	0.2187
5 ct	0.6990	-0.6911	0.204	0.058	0.2916
4 ct	0.6021	-0.5144	0.306	0.102	0.4091
3 ct	0.4771	-0.2908	0.512	0.206	0.6178
10 gr	0.3979	-0.1517	0.705	0.193	0.4833
8 gr	0.3010	0.0160	1.038	0.332	0.6646
6 gr	0.2041	0.1808	1.516	0.479	0.7659
5 gr	0.1139	0.3315	2.145	0.629	0.8177
4 gr	0.0000	0.5183	3.298	1.153	1.1532
3 gr	-0.0969	0.6740	4.721	1.423	1.1381
+11	-0.4559	1.2257	16.814	12.093	4.2325
+9	-0.7447	1.6404	43.696	26.882	4.8388
+7	-0.9586	1.9310	85.306	41.610	4.5771
+5	-1.0458	2.0453	110.995	25.689	2.3120
+3	-1.3010	2.3666	232.618	121.623	6.0812
+1	-1.6990	2.8273	671.958	439.340	8.7868
Total					37.899
Estimated macro grade (cpht)			22.766		

The microdiamond and macrodiamond distributions

In this study, natural diamond populations from three prospective deposits were used to evaluate the suitability of the data modelling methodology outlined above for predicting macrodiamond counts.

The macrodiamonds from each of these three propective deposits were recovered via three different methods. The first method was a small underground mining exercise, the second was a large-diameter drill (LDD) programme, and the third method was a high-voltage pulse-power fragmentation process.

Unit 1 kimberlite

The microdiamond grade analysis of the Unit 1 kimberlite is seen in Figure 5 and again in Figure 6. The microdiamond distribution is represented by the blue diamonds, including the calculated 'projection factor' which has a square around the data-point. The modelled macrodiamond distribution is represented by the green triangles and the actual macrodiamond distribution, as obtained from conventional mining processes, by the purple circles. The macrodiamond distribution deviates significantly from the modelled macrodiamond distribution in the smaller size range (1–3 mm) due to inefficiencies in the liberation and recovery of these smaller, low-value diamonds. The list of Unit 1 macrodiamonds recovered in the bulk sample is given in the Appendix.

The accuracy of this cumulative methodology to estimate the recovery grade of the Unit 1 kimberlite, is demonstrated by how closely the actual recovery curve tracks the modelled curve. Furthermore, the results predicted that 144 diamonds >1 mm in size with a combined mass of 22.766 ct would be liberated and recovered for every 100 t of kimberlite mined and processed. The actual number of >1 mm macrodiamonds recovered for each 100 t of kimberlite processed was 129, with a mass of 17.047 ct. The results also predicted that at least one 1.8 ct diamond would be recovered with every 104 t processed, while in reality, at least a 1.8 ct diamond was recovered with every 106 t processed – this last observation being the more accurate prediction of the methodology.

Unit 2 kimberlite

The microdiamond grade analysis of the Unit 2 kimberlite is seen in Figure 7. The microdiamond distribution is represented by the blue diamonds, including the calculated 'projection factor' which has a square around the data-point. The modelled macrodiamond distribution is represented by the green triangles and the actual macrodiamond distribution, as obtained from the LDD programme, is represented by the red squares. Again we see the macrodiamond distribution deviate from the modelled macrodiamond distribution in the smaller size range due to inefficiencies in the liberation and recovery of these smaller diamonds. There were also a number of broken diamonds due to the mining process, and this is observed in the deviation of the red squares from the green triangles in the larger size fractions. The list of Unit 2 macrodiamonds recovered in the LDD programme is given in the Appendix.

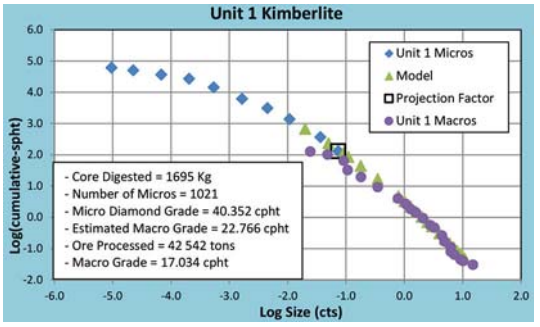

Figure 6—Cumulative distribution of; microdiamonds, modelled macrodiamonds, and actual macrodiamonds for the Unit 1 kimberlite

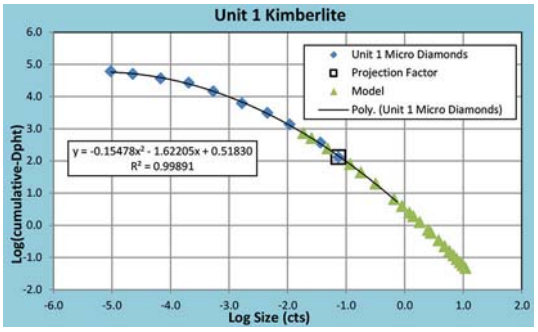

Figure 7—Ccumulative distribution of; microdiamonds, modelled macrodiamonds, and actual macrodiamonds for the Unit 2 kimberlite

In this example, the predicted number of >1 mm macrodiamonds that would be recovered for every 100 t of kimberlite processed is 55, with a combined mass of 7.493 ct. The actual number of >1 mm diamonds recovered was 63, with a combined mass of 5.526 ct. The results also predicted that at least one 0.9 ct diamond would be recovered with every 100 t processed, while in reality, 180 t were required for the recovery of a 0.9 ct diamond.

Unit 3 kimberlite

The microdiamond grade analysis of the Unit 3 kimberlite is seen in Figure 8. The microdiamond distribution is represented by the blue diamonds, the modelled macrodiamond distribution by the green triangles, and the actual macrodiamond distribution, as obtained from a high-voltage pulse-power fragmentation process, is represented by the red stars. We note that the high-voltage pulse-power fragmentation process is able to liberate all the diamonds, althugh recovery was still by dense media separation (DMS) and hand-sorting. The list of Unit 3 macrodiamonds recovered is given in the Appendix.

High-voltage pulse-power fragmentation is an expensive process and only 20 t of kimberlite was processed using this technology. In the model, the predicted number of >1 mm macrodiamonds for 20 t of the Unit 3 kimberlite was 194 with a total mass of 36.636 ct. The actual number of >1 mm macrodiamonds recovered from the 20 t sample was 194, with a total mass of 30.695 ct. The results also predicted that at least one 6 ct diamond would be recovered in a 20 t sample, while in reality, a 6.5 ct diamond was recovered.

Discussion

Using the cumulative data ensures that data arrays either always increase, always decrease, or remain constant, thus reducing the amount of variation 'noise' in a data-set. Using cumulative data-sets and quadratic approximations permits the calculation of trends within the microdiamond results, which in turn enables the extrapolation of the data at a higher level of confidence.

An advantage of using the cumulative method for representing the data is that the quadratic formula is independent of the sieve sizes used. The cumulative data can then be used against various size scales such as the valuation scale, the UIs for assessing recovery efficiency, or against the millimetre screen sizes used in the production plant, provided that the start and end sizes are the same.

The microdiamonds were sized into their UIs based on their masses. The UIs were initially a millimetre measurement, but were converted to carats by determining the MDS for the UI. If all the microdiamonds are weighed and the data captured electronically, one should be able to classify the microdiamonds based on their weights in carats directly, without sieving. Sieving requires shaking the diamonds, resulting in diamond-on-diamond contact, potential breakages, and reduced diamond sizes. Lastly, sieving of small particles incurs inefficiencies and errors and is not recommended for such important economic studies.

Conclusions

Arranging the microdiamond distribution data in a cumulative manner, converting the data to logarithms, determining a projection factor by using the quadratic equations with the highest R^2 value, and extrapolating this quadratic equation into the macrodiamond region has enabled the macrodiamond grade of Unit 1, Unit 2, and Unit 3 kimberlites to be modelled with a high degree of accuracy.

The same mathematical model established with the microdiamonds can be added to when moving into the bulk sampling phase, and again used in the production phase when plant upgrades are investigated.

From this analysis, the following recommendations are suggested when analysing future data-sets.

- Sizing and tabulating the microdiamonds per UI should be carried out in a simple spreadsheet, according to the mass of the microdiamonds
- The conditions for a microdiamond data-set to be accurately extrapolated are:
  - At least 300 microdiamonds in the data-set (though only 200 were used for the Unit 3 kimberite)
  - At least seven of the nine UIs to contain microdiamonds
  - At least two microdiamonds larger than 0.6 mm to be present in the data-set.

References

FERRIERA, J. 2013. Sampling and estimation of diamond content in kimberlite based on microdiamonds. Ecole Nationale Superieure des Mines de Paris. [In English].

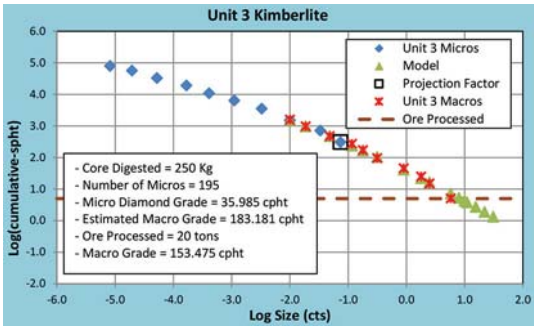

Figure 8—Cumulative distribution of the microdiamonds, modelled macrodiamonds, and actual macrodiamonds for the Unit 3 kimberlite

KRUGER, L. 2004. Discussions on the advantages and disadvantages of HF and NaOH. Kimberley Micro Diamond Laboratory Pilot Plant project. De Beers.

LIMPERT, E., STAHEL, W.A., and ABBT, M. 2001. Log-normal distributions across the sciences: keys and clues. American Institute of Biological Sciences. *BioScience Article*, vol. 51, no. 5. May 2001.

MCCANDLESS, T.E. 2013. The mystery of microdiamonds. Presentation at UBC Robson Square, Vancouver, 10 April 2013. MCC Geoscience Inc.

MONTGOMERY, D.C. and RUNGER, G.C. 2011. Applied Statistics and Probability for Engineers. 5th edn. Wiley, New York.

ROMBOUTS, L. 2002. Assessing the Diamond Potential of Kimberlites from Discovery to Evaluation Bulk Sampling. Springer-Verlag. ◆

Appendix

The microdiamonds recovered from the three kimberlites

		Unit 1		Unit 2		Unit 3	
NaHO (kg)		1695.40		1598.53		250.00	
Microdiamond grade (cpht)		40.352		27.358		35.618	
Number of UIs		9		9		9	
Total microdiamonds		1021		1038		195	
Size (ct)	**Sieve (mm)**	**Number (units)**	**No. per 100 t (units)**	**Number (units)**	**No. per 100 t (units)**	**Number (units)**	**No. per 100 t (units)**
0.00001	0.075	174	10.263	143	8946	56	22 400
0.00002	0.106	233	13.743	246	15 389	58	23 200
0.00007	0.150	158	9.319	196	12 261	34	13 600
0.00020	0.212	215	12.681	277	17 328	21	8400
0.00054	0.300	139	8.199	117	7319	11	4400
0.00165	0.425	52	3.067	34	2127	7	2800
0.00452	0.600	29	1.711	12	751	5	2000
0.01083	0.850	17	1.003	8	450	2	800
0.03652	1.180	4	236	5	200	1	400

The macrodiamonds recovered from the three kimberlites

			Unit 1		Unit 2		Unit 3	
Tonnage processed			42.542		1.803		20	
Grade (cpht)			17.047		5.525		153.475	
Largest stone recovered (ct)			19.706		3.418		6.500	
Size (ct)	**Sieve (mm)**	**DTC**	**Number (units)**	**No. per 100 t (units)**	**Number (units)**	**No. per 100 t (units)**	**Number (units)**	**No. per 100 t (units)**
0.0186	1.09	+1 & +2	10318	24.254	214	11.869	100	500
0.0256	1.47	+3 & +4	15940	37.469	424	23.516		
0.0485	1.83	+5 & +6	13681	32.159	345	19.135	40	200
0.1170	2.46	+7 & +8	5571	13.095	79	4.382	20	100
0.1790	2.85	+9& +10	4286	10.075	42	2.329	15	75
0.3170	3.45	+11	2234	5.251	31	1.719	10	50
0.6600	4.15	3 gr	554	1.302	2	0.111		
0.9000	4.61	4 gr	368	0.865	4	0.222	4	20
1.2000	5.07	5 gr	167	0.393	0	0.000		
1.4000	5.34	6 gr	206	0.484	1	0.055		
1.8000	5.80	8 gr	163	0.383	3	0.166	2	10
2.5000	6.47	10 gr	40	0.094	1	0.055	2	10
2.8000	6.72	3ct	86	0.202	1	0.055	1	5
3.8000	7.44	4ct	40	0.094	0	0.000	0	0.000
4.8000	8.05	5ct	24	0.056	0	0.000	0	0.000
5.8000	8.57	6ct	13	0.031	0	0.000	0	0.000
6.8000	9.04	7ct	7	0.016	0	0.000	0	0.000
7.8000	9.46	8ct	8	0.019	0	0.000	0	0.000
8.8000	9.85	9ct	2	0.005	0	0.000	0	0.000
9.8000	10.21	10ct	17	0.040	0	0.000	0	0.000
			54745	129	1147	64	194	970

Terex® Minerals Processing Systems

Not just equipment. A complete solution.

ELB Equipment, the sub-Sahara Africa distributor of a complete range of Terex® Minerals Processing Systems, understands your business and with Terex® are dedicated to offering cost-effective solutions for your needs.

In today's competitive environment, you need high quality equipment backed by an outstanding support network locally and internationally. Our sales and after-market teams are trained to provide customers with outstanding crushing and screening process knowledge and service.

As a member of the ELB Group, we have a century of experience in the mining industry that you can depend on. Customer satisfaction is our ultimate goal.

H/OFFICE:
14 Atlas Road, Anderbolt, Boksburg • **Tel:** (011) 306-0700 • **Fax:** (011) 918-7208
e-mail: Elb@elbquip.co.za • **Website:** www.elbequipment.com

BRANCHES & DEALERS – SOUTH AFRICA: BRITS: (012) 250-1565 • CAPE TOWN: (021) 933-2383
DURBAN: (031) 464-6522 • EAST LONDON: (043) 740-4530 • GEORGE: (044) 878-0874
KIMBERLEY & KATHU : (053) 841-0040 • MIDDELBURG: (013) 246-2312 • POLOKWANE: (082) 334-1564

SUBSIDIARY: ELB EAST AFRICA: NAIROBI, KENYA: (00254) (0) 20 807-0728

DEALERS – SOUTHERN AFRICA: BOTSWANA: (00267) 390-9972 • LESOTHO: (00266) 2831-3926 • MOZAMBIQUE: (00258) 219-00469
NAMIBIA: (00264) 61-234-052 • SWAZILAND: (00268) 518-5348 • ZAMBIA: (00260) 212-210-642 • ZIMBABWE: (00263) (4) 448-990-3

Distribution and Product Support by:

ELB EQUIPMENT
A Member of the ELB Group

http://dx.doi.org/10.17159/2411-9717/2016/v116n8a6

Extension of the Cullinan Diamond Mine No. 1 Shaft underneath the existing operating shaft, with emphasis on rock engineering considerations

by G. Judeel*, T. Swanepoel†, A. Holder†, B. Swarts†, T. van Strijp†, and A. Cloete†

Synopsis

In 2012, Cullinan Diamond Mine began an expansion programme with the shaft deepening and development of access to the C-Cut 1 block at approximately 839 m below surface. The expansion programme is funded by a combination of bank loans and retained operating profit generated by the mine. Continuous production during deepening of the No. 1 Shaft, which is the rock hoisting shaft, was therefore critical for sustainability and efficiency as well as overall funding of the project. The deepening method, support design and verification, as well as learning outcomes pertaining to the extension of the No. 1 Shaft underneath the existing operating shaft are summarized, with emphasis on the importance of gaining some understanding of the shaft's host rock mass.

Keywords

shaft sinking, shaft extension, rock mass properties, field stress distribution, numerical modelling, support design.

Introduction

Cullinan Diamond Mine (CDM) is an underground block cave diamond mine located 37 km northeast of Pretoria in South Africa's Gauteng Province. CDM has been operated by Petra Diamonds since it was acquired from De Beers in July 2008. CDM, a successful and long-lived kimberlite-hosted diamond mine, has produced many of the world's largest and most famous diamonds, including a quarter of all diamonds over 400 carats (ct). It earned its place in history with the discovery of the well-known Cullinan Diamond in 1905. The kimberlite pipe still contains the world's second-largest Indicated Diamond Resource. CDM is capitalizing on this by undertaking an expansion programme with the objective of taking production from just over 850 000 ct per annum (ctpa) to 2.4 million ctpa by FY 2019. The expansion programme is optimized by the extension of the CDM No. 1 Shaft beneath the existing operating shaft, allowing for normal production while the No. 1 shaft is extended.

The CDM expansion programme requires huge amounts of capital. The aim is to sustainably extend the life of the mine and therefore ensure extended socioeconomic community empowerment, employment opportunities, and stakeholder benefits from the mine for many years to come. The expansion programme is funded by a combination of bank loans and retained operating profit generated by the mine. Continuous production while extending the shaft was therefore critical for the sustainability and overall funding of the project.

Extending the shaft required the development of temporary excavations and leaving an *in situ* plug to enable safe sinking below the existing operating shaft. The host rock of the shaft deepening section consists of igneous rocks of the Bushveld Complex and Transvaal Supergroup metasediments, which are of a blocky nature due to their being intersected by four prominent joint sets. The Laubsher mining rock mass rating (MRMR) ranges between 21 and 80. The deepening section of the shaft is also subjected to varying field stresses brought about by the shaft's position relative to the open pit. The deepening method, support design, and verification as well as learning outcomes pertaining to the extension of the No. 1 Shaft are described, with emphasis on the importance of gaining some understanding of the shaft's host rock mass. This understanding of the rock mass in turn served to explain why the north-northwestern pit wall, where the No. 1 Shaft is located, is stable while the south-southeastern pit wall is not stable.

Mine layout

The kimberlite orebody is currently exploited by mining blocks BA5, BB1E, and AUC and BAW Phase 1. The new C-Cut Phase 1 block is located on the northwestern side of the

* *Consulting Rock Engineer, GeoSindile, Johannesburg, South Africa.*

† *Petra Diamonds, Johannesburg, South Africa.*

 ISSN 2225-6253. This paper was first presented at the Diamonds still Sparkling 2016 Conference *14–17 March 2016, Gaborone International Convention Centre.*

kimberlite pipe with extraction planned on 839 Level, as illustrated in Figure 1. The upper portions of the kimberlite orebody have been depleted by open-pit mining activities, and current mining operations are concentrated between 630 m and 747 m below surface, where the block caving mining method is applied. In block caving, an undercut level is developed to allow the orebody to be undermined by drilling and blasting. When a sufficiently large area of the undercut level has been opened, *i.e.* an area covering a critical hydraulic radius, caving is initiated. This undercutting allows the rock to fracture and cave under its own weight. The caved ore is extracted from a level developed below the undercut, called the extraction level, through a series of systematic drawpoints by means of load haul dumpers.

No. 1 Shaft extension plan and execution

Mining of the new C-Cut Phase 1 block requires the CDM No. 1 Shaft to be extended by 354 m from its present depth of 580 m below surface to 934 m, while the existing shaft above it remains in operation (Figure 2). The circular 6.6 m final diameter concrete-lined No. 3 Shaft is also extended, but only by 75 m, and its extension is not dealt with in this paper. The No. 1 Shaft is a rectangular shaft and its extension will have minimum final dimensions of 9.6 m × 2.3 m after being lined with wetcrete. Sinking is made easier by a 2.5 m diameter raisebore hole, which was drilled from the new shaft bottom at 934 Level to the present shaft bottom at 580 Level (Figure 2). The raisebore hole served as an orepass, breaking point for blasting, and for ventilation during the sinking of the shaft extension. Sinking also required the development of temporary excavations and leaving an *in situ* plug to enable the safe sinking of the extension below the existing operating shaft (Figure 3). The temporary excavations include a hoist chamber for the sinking hoist, a rope raise, and a chamber of suitable shape and size to house the sinking headgear situated just below the plug. The excavation of the headgear chamber and deepening of the shaft commenced below the plug at 583 m below surface with the raisebore hole as access (Figures 2 and 3). Sinking progressed conventionally vertically downward towards 645 Level concurrent with sinking (winzing) of the rope raise at an angle towards the winder chamber (Figure 3). After the shaft and the rope raise holed, preparations commenced with permanent sinking arrangements to enable sinking to continue conventionally from 645 Level to 934 Level; the new shaft bottom (Figure 2). Silo development from the South Decline, which also forms an integral part of the No. 1 Shaft commissioning process, commenced concurrently with the sinking operations, and as a result of being ahead of schedule, early sinking of the No. 1 Shaft loading box on 895 Level could be done concurrently with the vertical sinking of No. 1 Shaft.

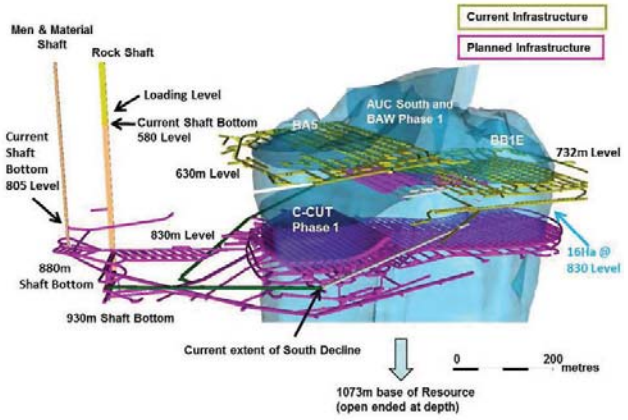

Figure 1—The deeper, currently operating, and planned mining areas of CDM

Shaft host rock – geological setting

The CDM No. 1 Shaft extension below 580 Level is located in igneous rocks of the Bushveld Complex and Transvaal

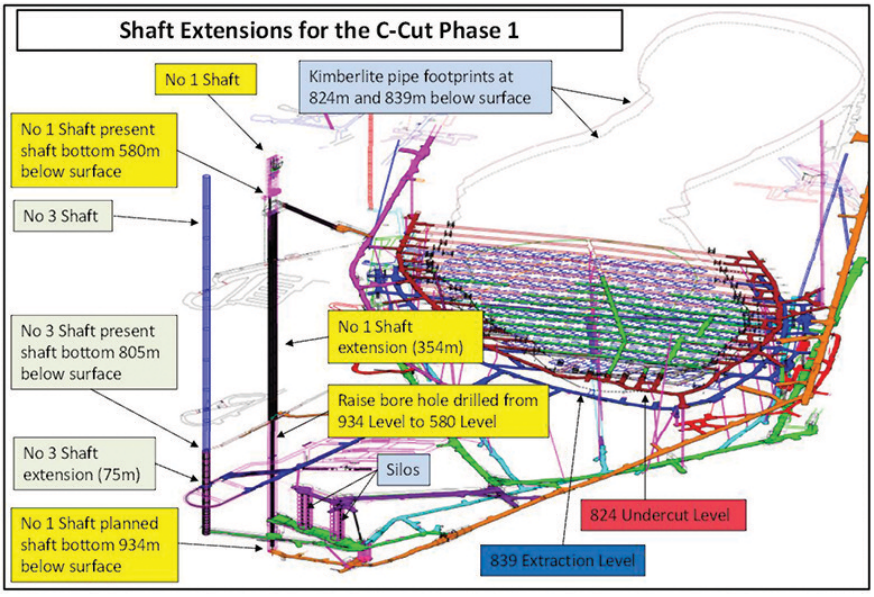

Figure 2—Shaft extensions for the C-Cut Phase 1

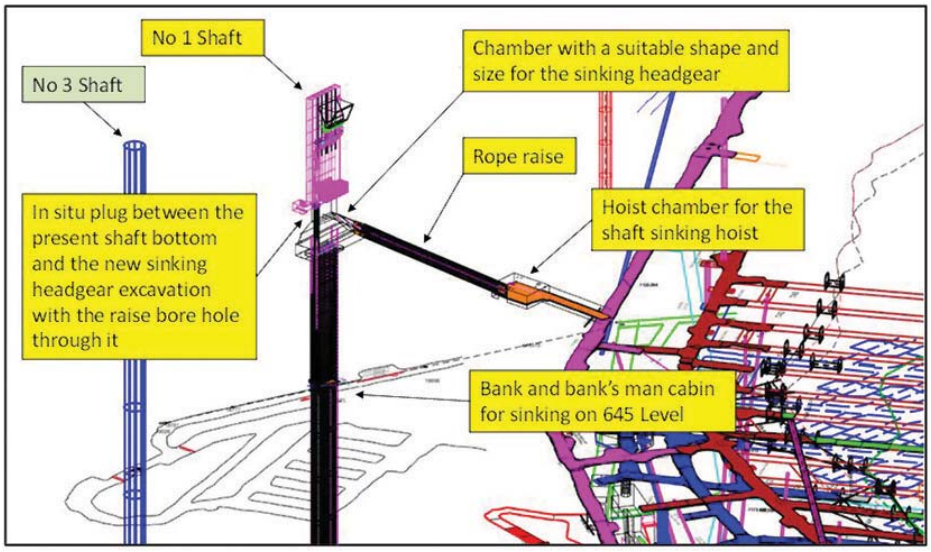

Figure 3—Temporary excavations for sinking the 354 m CDM No. 1 Shaft extension

Supergroup metasediments. Based on the C-Cut drill-hole data, the rock mass was characterized as follows.

- The country rock changes from Bushveld Complex norite to Transvaal Supergroup metasediments. The transition zone seems to be intercalated norite and metasediments at around 810 Level to 830 Level. Based on 736 Level exposures, the upper transitional quartzite contacts are welded and competent contacts
- The lower norite (including quartzite) is a competent rock mass with typical Bieniawski (1973) rock mass rating (RMR) values of 50–70 and uniaxial compressive strength (UCS) values ranging from 160 to 280 MPa, averaging 200 Mpa
- The metasediments are very variable, ranging from competent quartzite to shale/mudstone of low competency. The RMR values range from 30 to 60 and UCS values from 60 to 180 MPa, averaging 120 MPa.

Some of the CDM geotechnical average rock properties for the CDM No. 1 Shaft extension are presented in Table I.

Structural geology

Joint sets

There are four prominent joint sets in the country rock mass, and hence also in the host rock mass of the No. 1 Shaft. These joints are also visible in many surface rock outcrops close to and further away from CDM. The average dip directions and dip angles of the four joint sets are shown in Table II and in Figure 4. The four joint sets were recorded and defined by SRK Consulting (2005).

Effects of joint sets on the shaft extension

Some effects that the orientations of the four joint sets have on the shaft are depicted in Figure 5. For example, some minor overbreak resulting from the very weak, slippery, and striated serpentine infill associated with J4 occurred on the eastern sidewall of the shaft (Figure 5). Some minor wedge failures also occurred as a result of dislodgement from between J1 and J3 on the eastern sidewall of the shaft, regardless of smooth wall blasting that had being practised (Figure 5).

Table II

Average dip directions and dip angles of the four prominent joint sets in the host rock mass of the No. 1 Shaft extension

Set reference	Dip direction (azimuth) (°)	Dip angle (°)
J1 (dominant – rock fabric)	300 (strike approx. north-south)	80
J2 (dominant)	260	80
J3	180	85
J4 (associated with intrusive or weak infill material *i.e.*, serpentine)	035 (Dip in a northerly direction)	16

Table I

Average country rock properties

Rock type	RMR	UCS (MPa)	Density (kg/m³)	Young's modulus (GPa)	Poisson's ratio	Bulk modulus (GPa)	Shear modulus (GPa)	Cohesion (MPa)
Norite	55	200	2850	13.4	0.2	8.5	5.4	4.5
Metasediment	51	120	2650	10.7	0.2	6.9	4.3	3.5
Lower norite	55	200	2850	13.4	0.2	8.5	5.4	4.5

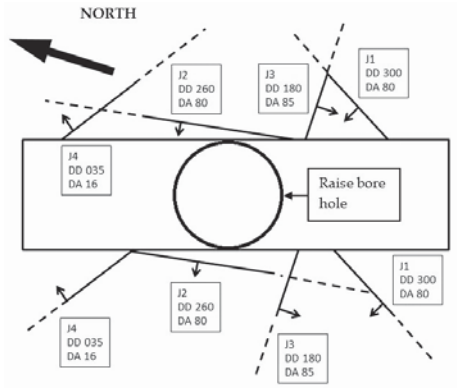

Figure 4—Plan view of the rectangular 9.8×2.5 m shaft, depicting the average dip directions and dip angles of the four prominent joint sets

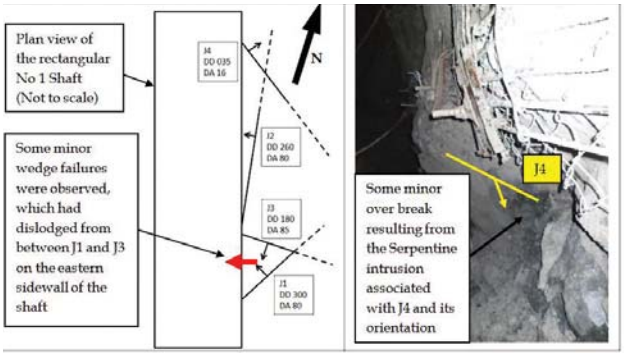

Figure 5—Effects of the joint sets on the eastern sidewall of No. 1 Shaft

In some vertical sections of the shaft, due to prominent joints of the J4 set, which dip at approximately 16° in a northerly direction, the shaft bottom on the southern side of the raisebore hole advanced more rapidly than the depth of the blastholes. In the same vertical sections of the shaft on the northern side of the raisebore hole, the advance per blast was less and normal blasthole sockets occurred in the shaft bottom.

Host rock classification by ground condition

The host rock of the No. 1 Shaft extension was classified into three different categories, *i.e.* competent (1), intermediate competent (2), and least competent (3), using the mining rock mass rating (MRMR) system of Laubscher (1990). The MRMR system is based on joint spacing, joint infill, and degree of prominence of the joints etc. The relationship between the MRMR ratings of the Laubscher classes from I to V and the ratings of the three CDM classes is shown in Table III. For each of the three classes a different shaft support standard was designed to suit the different ground conditions. From the commencement of sinking, the standards have remained mostly unchanged, except for changing the anchor installations from a square pattern to staggered pattern and from welded square mesh to more robust expanded metal sheets, which have smaller apertures than the welded square mesh.

J-Block modelling

Construction of the J-Block model

J-Block software was used to simulate the effects of the four prominent joint sets, shown in Table II, on the CDM No. 1 Shaft extension without and with the shaft standard support. Since J-Block is generally used for horizontal to subhorizontal excavations, Esterhuizen (2015) pointed out that a vertical rectangular shaft can be modelled with J-Block when the shaft sidewalls are simulated to be dipping at 89°. The worst-case scenario was selected to model all the joints as having zero cohesion because of the presence of serpentine infill on the joint sets.

J-Block modelling results

The J-Block results indicate that even though the rockbolts reduce the number of unstable key blocks remarkably, compared to when no support is installed, there are still unstable key blocks of up to 0.002 m³ (approx. 25×10×8 cm) that could cause serious injuries if areal support is not used (Figure 6). The J-Block results also indicated that the eastern sidewall of the shaft has the highest probability of unstable key blocks, which corresponds with the observations shown in Figure 5.

Effects of varying field stresses

From approximately 679 m to 726 m below surface, excessive fracturing (typical dog-earing, as can be seen in Figure 7) of the eastern and western sides of the raisebore hole was observed. In this section, due to overbreak and scaling out of

Table III

Relationship between the MRMR ratings of Laubscher's classes I to V and those of CDM No. 1 Shaft extension classes 1, 2, and 3

MRMR rock mass classes determined from total ratings (after Laubscher, 1990)					
Rating Class no. Description	100←81 I Very good	80←61 II Good	60←41 III Fair	40←21 IV Poor	<20 V Very poor
CDM rock mass classes determined from total ratings for the No. 1 Shaft					
Laubscher's MRMR rating CDM No. 1 Shaft class no. Host rock competence		80←61 1 Competent	60←41 2 Intermediate	40←21 3 Least competent	

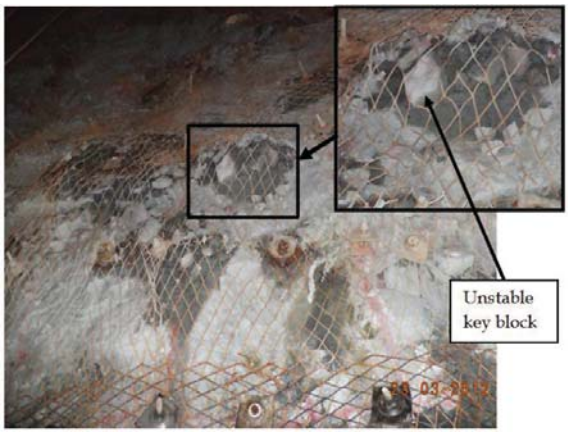

Figure 6—Unstable key block (approx. 0.002 m³) corresponding with the J-Block results

loose rocks – regardless of the smooth wall blasting that had been employed, the overall shape of the shaft changed from rectangular to almost elliptical, as can be seen in Figure 7 (as described by Judeel, 2014a). Below 726 m in the shaft extension, the ground conditions improved, again without excessive visible stress-induced fracturing. These observations indicated that the horizontal to subhorizontal field stress acting on the shaft was higher in the north-south direction than in the east-west direction. An investigation was carried out to determine the possible reasons for this.

Possible causes of the varying field stresses

In an attempt to find out and understand what caused the dog-earing, the following three reasons were considered.

1. The depth of the shaft where the dog-earing occurred, from 679 m to 726 m below surface, corresponds with the anticipated concentrated subhorizontal mining-induced stress field at the bottom corner below the open pit and block caves. Therefore, at the position of the shaft relative to the open pit and at depths from 679 m to 726 m below surface, this stress field can be expected to be acting in a north-south direction, which explains the dog-earing on the eastern and western sides of the raisebore hole as well as the shape to which the shaft scaled out to (Figure 7)
2. Due to the approximately north-south strike direction of the two most prominent joint sets, there may be high tectonic horizontal stresses acting in the NS direction, which could also explain the dog-earing on the eastern and western sides of the raisebore hole and the overbreak in the shaft. Stacey and Wesseloo (1998), who carried out an investigation of the *in situ* stresses in mining areas in South Africa, found that the major horizontal stresses are also oriented roughly in a north-south direction, which further confirms this reasoning
3. The dog-earing is probably due to the combined effect of the higher mining-induced and tectonic horizontal stresses, which both act in a north-south direction, as described under points 1 and 2 above.

Combined effects of the varying field stresses and poor rock mass conditions

Van de Steen *et al.* (2003) investigated the application of a flaw model to the fracturing around a vertical circular shaft. They found that dog-earing occurs when there is a variance of ±40% in the magnitude of the horizontal stress acting on a vertical circular shaft. Therefore, in the case of the CDM No. 1 Shaft extension, the magnitude of the stress acting in a north-south direction should be approximately 40% higher than that in the east-west direction. The extent of the dog-earing or the fracturing of rock around the raisebore hole, as well as around the rectangular shaft, depends on the stress magnitudes, geological rock mass conditions, and rock strength. However, the geological rock mass conditions have the most influence over the size or volume of the fractured rock around the raisebore hole and the shaft, since the stress-induced fracturing around the excavations follows the path of least resistance along joints in the rock mass. An example of this, lower down in the raisebore hole, can be seen in Figure 7. It is thus very important to classify the shaft host rock into one of the three rock mass classes as shown in Table III. and to select the corresponding support standard.

Modelling the stress distribution around the shaft

Two different field stress scenarios were simulated with Examine 2D to investigate and confirm the expected different induced stress distributions around the shaft. The horizontal stress magnitudes for the two field stress scenarios were also investigated by simulating a cross-section of the open pit. When considering the possible causes of the varying horizontal field stresses, as discussed above, and the geometry of the open pit, the determination of the field

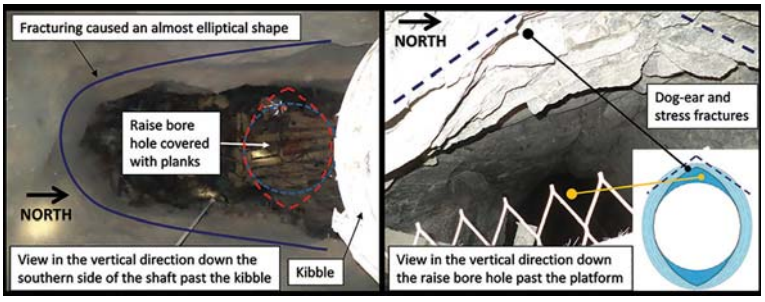

Figure 7—Effects of the horizontal to subhorizontal field stresses on the CDM No. 1 Shaft extension, with higher magnitudes in the north-south direction compared to the east-west direction

stresses that acts on the shaft with a two-dimensional modelling package may seem rather over-simplistic. However, since the aim of the modelling is mainly to investigate and confirm the expected different induced stress distributions around the shaft brought about by the two scenarios, it is reasoned that the estimated magnitudes of the field stresses, as shown below, will for this purpose be accurate enough.

- *Possible scenario*—East-west field stress (11 MPa) higher than the north-south field stress (6 MPa). Figure 8a shows the distribution of the induced stresses around the shaft calculated by Examine 2D-.
- *Predicted scenario*—North-south field stress (11 MPa) higher than the east-west field stress (6 MPa). Figure 8b shows the Examine 2D-calculated induced stresses around the shaft.

Discussion of the modelling results

Shaft

Since the shaft is a rectangular excavation it is not symmetrical in all directions, and therefore the magnitudes of the induced stresses are different for both the first and second scenarios, as can be seen in Figure 8a and 8b. The Examine 2D results indicate that the possible scenario, where the east-west field stress is higher than the north-south field stress, is the worst regarding the induced stresses around the shaft, *i.e.* it will cause high tensile stresses deep into the eastern and western sidewalls of the shaft, as can be seen in Figure 8a. At this depth below surface and with the present pit and mining geometry, all the indications are that the north-south field stress is higher than the east-west field stress, which results in a more favourable induced stress distribution around the shaft, *i.e.* all the induced stresses are compressive, as can be seen in Figure 8b. However, just to be on the safe side, the anchor lengths were verified for the possible situation (east-west stresses higher than north-south stresses, as indicated in Figure 8a). It was reasoned that should the possible scenario occur, it could cause the sections of the shaft host rock mass that were classified as having a class 2 or class 3 MRMR to deteriorate even further if it was not timeously supported with areal support, consisting of expanded metal cladding and wetcrete. According to the shaft support standards, these sections of the shaft's host rock mass, with a class 2 or class 3 MRMR, require the installation of anchor support. Figure 8a indicates that the anchors are long enough to extend past the modelled induced tensile stress zone. The SAIMM's referee of this paper pointed out that as the cave develops adjacent to the shaft that there is a possibility that the north-south stress component will reduce and that the east-west stress component may increase. The author agrees that this is indeed what can be expected as the cave develops and the depth of the pit increases. Therefore, the previously envisaged unlikely scenario becomes the possible scenario. This points out the necessity to investigate stress distributions in three dimensions; and hence to improve the level of confidence of the shaft support verification further, 3D numerical modelling is recommended.

Raisebore hole

The raisebore hole was also modelled with Examine 2D, and the results are shown in Figure 9a and Figure 9b. The modelling also indicates, as expected, that when the horizontal stress acting on the raisebore is higher in the north-south direction, high induced compressive stresses act on the eastern and western sidewalls of the raisebore hole. This confirms that in reality the north-south field stress from 679 m to 726 m below surface was higher than the east-west field stress, which caused the dog-earing on the eastern and western sides of the raisebore hole as shown in Figures 7.

Stability of the No. 1 Shaft regarding its location relative to the open pit

The south-southeastern pit wall had been unstable since before 2005, as described by SRK Consulting (2005) and Judeel (2014c). This led to the recent closure of a section of the R513 public road and a fuel service station, which were located close to the unstable south-southeastern pit wall. On the other hand, mine personnel reported that the north-northwestern pit wall, where the No. 1 Shaft is located, had been stable since the changeover from opencast to underground mining. This is evident from the fact that some

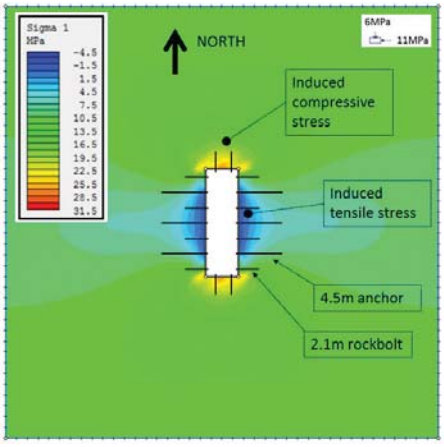

Figure 8a—Examine 2D modelling results for the No. 1 Shaft where the east-west field stress is higher than the north-south field stress

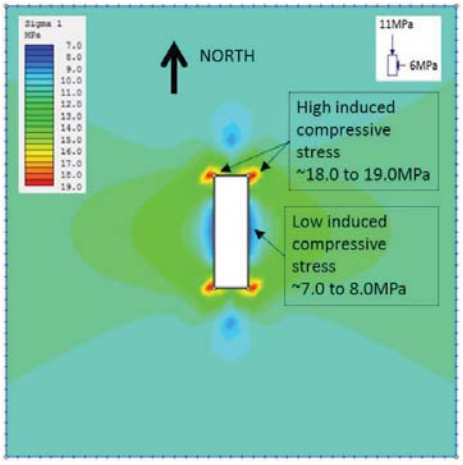

Figure 8b—Examine 2D modelling results for the No. 1 Shaft where the north-south field stress is higher than the east-west field stress

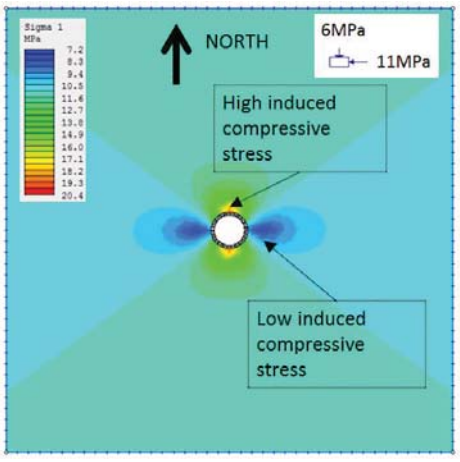

Figure 9a—Examine 2D modelling results for the raisebore hole where the east-west field stress is higher than the north-south field stress

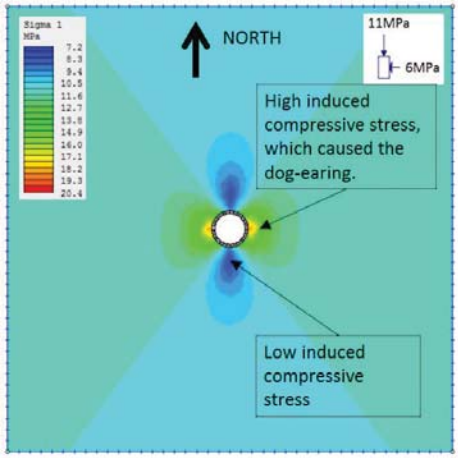

Figure 9b—Examine 2D modelling results for the raisebore hole where the north-south field stress is higher than the east-west field stress

remains of infrastructure that was used for the opencast mine are still intact on the edge of the north-northwestern pit wall. So the question arose; why is the north-northwestern sidewall, where the No. 1 Shaft is located, stable while the south-southeastern sidewall is not. This question led to the reasoning that the orientations of J4 and J3 are the main contributors to the instability of the south-southeastern pit wall, and that these orientations actually promote the stability of the north-northwestern pit wall, as described by Judeel (2015). As mentioned earlier, the joints as indicated in Table II are visible on many surface rock outcrops close to and further away from CDM. The most prominent surface exposure of the joint sets, especially J4, can be seen on the smooth wall blasted road cutting for the N4 Witbank (Emalahleni)/Pretoria Highway, which is located to the south of CDM (Figures 10, 11, and 12).

In Figures 11 and 12 wedge failures are visible, which occurred regardless of the smooth wall blasted road cutting due to rock wedges that slid down the joint surfaces of the J4 joint set and from between the more steeply dipping joints of the J3, J2, and J1 joint sets. The same type of wedge failure also occurs on the south-southeastern highwall of the open pit, but on a much larger scale due to the size and depth below surface of the highwall.

It is clear from the sketch in Figure 13 that the orientations of J3 and J4 are causing rock wedges/blocks on the south-southeastern highwall of the pit to tend to slide out on the weak infill material of J4, while the same rock wedges/blocks on the north-northwestern sidewall are locked in by gravity on the slope of the highwall. The instability of the south-southeastern sidewall is thus caused by the unfavourable orientation of J3 and J4 as well as time-dependent deformation occurring on the weak infill material of J4 at the bottom of the pit, where the vertical stress increases with depth. The time-dependent deformation occurs when the weak infill material is pushed out from between the

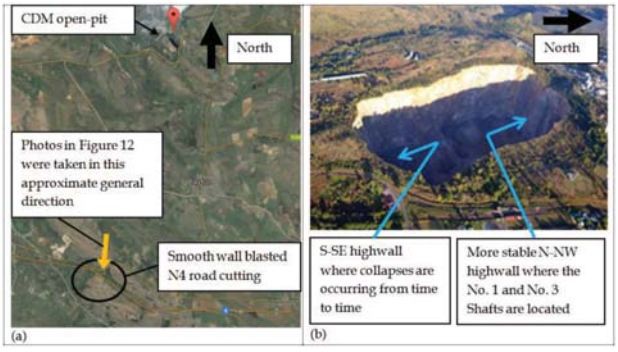

Figure 10—(a) Aerial view of the positions of the N4 road cutting and the CDM open pit, (b) closer aerial view of the pit

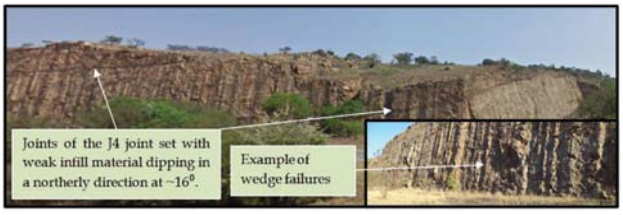

Figure 11—A view of the N4 road cutting in the southerly direction, where some of the four prominent joint sets are visible. J4, with its weak infill, is the most prominent

Figure 12—Closer views in the southerly direction of the smooth wall blasted N4 road cutting, in which some wedge failures are visible

joint planes by the constant vertical stress at a given depth, which in turn causes the wedges/blocks bounded by J3 and J4 to start sliding and toppling from the bottom up on the south-southeastern highwall, resulting in an unstable slope as shown in Figure 13.

Conclusions

1. Even though some sections of the No. 1 Shaft extension are located in poor quality rock masses, caused by excessive jointing, the J-Block results indicate that the 2.1 m rockbolt support alone, *i.e.* without anchors but with areal support, is sufficient to support the shaft when the effects of the shaft's field stresses are not taken into account
2. This is also confirmed by the continuous monitoring of the wetcrete in the completed deepened sections of the shaft, as described by Judeel (2014b), which indicates that no fracturing of the wetcrete that may indicate support failure has been observed to date
3. The investigation of the possible varying field stresses that may be intersected by the shaft during deepening revealed that the magnitude of the north-south field stress is higher than that of the east-west field stress, which results in more favourable induced stresses around the shaft
4. Even in the possible event, due to the increasing depth of the open pit, that the shaft be subjected to a horizontal field stress that change at a later stage so that the magnitude of the east-west field stress is higher than that of the north-south field stress, which will result in unfavourable tensile stress in the eastern and western sidewalls of the shaft, the installed shaft support is still adequate
5. The favourable orientation of the J3 and J4 joint sets on the north-northwestern highwall of the open pit, where the No. 1 Shaft is located, results in a more stable slope compared to the south-southeastern highwall, where the orientation of the J3 and J4 joint sets is unfavourable, thus causing the south-southeastern highwall to collapse from time to time. This led to the recent closure of a section of the R513 public road and a fuel service station, which were located close to the unstable south-southeastern pit wall. At present, there is no other infrastructure close to this pit wall
6. It is generally accepted that the key to the successful execution of the project so far has been the collaboration and cooperation between the geotechnical and project teams and the disciplined execution of the plan. Some important learning outcomes are that most of the reactions of the rock mass to the excavations can be explained by and predicted from the characteristics of the major joint sets of the rock mass
7. An understanding of the induced stresses that are caused by the excavations, and the resulting stress fields to which other excavations are subjected, by initially two-dimensional investigations, and later progressing to three dimensions for an improved understanding, is also required to explain and predict the reactions of the rock mass.

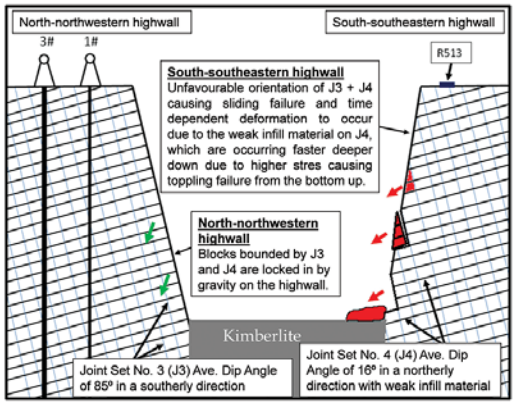

Figure 13—Indicating the reasoning why the north-northwestern highwall, where the No. 1 and No. 3 Shafts are located, is more stable in comparison to the south-southeastern highwall, where collapses occur periodically

Acknowledgements

The knowledge and skill of the project management team, under the leadership of Mr André Cloete, contributed largely to the successful execution thus far of the extension of the Cullinan Diamond Mine No. 1 Shaft beneath the existing operating shaft. The authors also acknowledge the permission of Petra Diamonds to publish this paper.

References

Bieniawski, Z.T. 1973. Engineering classification of jointed rock masses. *Transactions of the South African Institution of Civil Engineers*, vol. 15. pp. 335–344.

Esterhuizen, G.S. 2015. Personal communication.

Judeel, G. du T. 2014a. Support and numerical modelling recommendations for the No 1 Shaft in the areas where dog-earing of the raise bore hole is occurring. *Report no.* GS0003/28 rev 02. GeoSindile Geotechnical and Rock Engineering Services. Johannesburg, South Africa. 9 pp.

Judeel, G. du T. 2014b. Shaft host rock deformation monitoring procedure for No. 1 Shaft and No. 3 Shaft. *Report No.* GS0003/29 rev 02. GeoSindile Geotechnical and Rock Engineering Services. Johannesburg, South Africa. 5 pp.

Judeel, G. du T. 2014c. Cullinan Diamond Mine – R513 high wall stability and risk review. *Report no.* GS0006/1 rev 05. GeoSindile Geotechnical and Rock Engineering Services. Johannesburg, South Africa. 25 pp.

Judeel, G. du T. 2015. Cullinan Diamond Mine - No 1 Shaft deepening support and general shaft stability review. *Report No.* GS0003/41 rev 02. GeoSindile Geotechnical and Rock Engineering Services. Johannesburg, South Africa. 42 pp.

Laubscher, D.H. 1990. A geomechanics classification system for the rating of rock mass in mine design. *Journal of the South African Institute of Mining and Metallurgy*, vol. 90, no. 10. pp. 257–273.

SRK Consulting. 2005. East wall stability: Impact on the R513 road - Report on a geotechnical study of surface ground movements associated with pit sidewall failures. *Report no.* 352650. SRK Consulting. Johannesburg, South Africa. 54 pp.

Stacey, T.R. and Wesseloo, J. 1998. In situ stresses in mining areas in South Africa. *Journal of the South African Institute of Mining and Metallurgy*, vol. 98, no. 7. pp. 365–368.

Van de Steen, B., Vervoort, A., Napier, J.A.L., and Durrheim, R.J. 2003. Implementation of a flaw model to the fracturing around a vertical shaft. *Rock Mechanics and Rock Engineering*, vol. 36, no. 2. pp. 143–161. ◆

http://dx.doi.org/10.17159/2411-9717/2016/v116n8a7

Fracture banding in caving mines

by D. Cumming-Potvin*, J. Wesseloo*, S.W. Jacobsz†, and E. Kearsley†

Synopsis

The Duplancic model of caving is widely accepted in industry and is the framework within which most monitoring and numerical modelling results in caving mines are interpreted. As a result, the damage profile ahead of the cave back is often interpreted as continuously decreasing damage with increasing distance ahead of the cave back. Physical modelling of the caving process performed in a centrifuge did not support this expected behaviour, but instead suggested a discontinuous damage profile ahead of the cave caused by fracture banding. Some support is found in the literature to suggest that the behaviour observed in the models may also be present in the field. This notion is further supported by banding behaviour observed from microseismic monitoring at two block cave mines. Combining the information from the physical models, field observations referred to in the literature, and the microseismic analyses, it is concluded that the Duplancic model needs to be extended to include the phenomenon of fracture banding. It is also reasonable to expect that fracture banding may play a more important role in the caving process than has previously been recognized.

Keywords

block caving, caving mechanics, fracture banding, extensional fracturing, centrifuge, physical modelling.

Introduction

The Duplancic model of caving (Duplancic, 2001) is widely accepted in industry and is the framework within which most monitoring and numerical modelling results in caving mines are interpreted. The Duplancic model was created based primarily on simple microseismic analysis and linear elastic numerical modelling of one case study. At the time, it provided a much-needed interpretation framework and, as a result, has been applied to numerous mines. The model is generally interpreted as indicating that the damage ahead of the cave back in block caving mines continuously decreases with increasing distance from the cave back. From basic seismic analysis and with the assumption that slip along pre-existing discontinuities will take place preferentially to intact rock failure, Duplancic found that the most likely failure mechanism in the cave crown was slip along pre-existing discontinuities. As such, the model downplays the role of intact rock failure, including extensional failure. Extensional fracturing occurs parallel to the major principal stress and perpendicular to the maximum extensional strain. This may occur under a compressive macro-stress regime (Stacey, 1981).

Physical modelling of cave development in a centrifuge was carried out, and the results of the physical modelling did not correspond with the expectation of the Duplancic model. The main mechanism of cave propagation observed in the physical models was via a series of extensional fractures parallel to the cave back.

This discrepancy between the Duplancic model and the physical model raises the question whether the governing mechanism evident in the physical models is also present in the field, and whether the Duplancic conceptual model for caving mechanics should be reviewed.

A literature review revealed that several observations that were made in the past support the existence in the field of the mechanism evident in the physical models, although it seems that the importance and the full implication of these observations were not appreciated by the respective authors.

In addition to the physical models and literature review, an investigation was performed in order to establish whether any banding formation can be supported by the interpretation of microseismic monitoring data in modern block caving mines. Analysis of microseismicity was conducted at two large copper-gold porphyry block cave operations. The results of the analysis indicated that the mechanism seen in the physical model may have occurred at both mines.

This paper discusses the Duplancic model and presents an overview of the results from the physical modelling, literature review, and microseismic event monitoring.

* *Australian Centre for Geomechanics, University of Western Australia, Australia.*

† *University of Pretoria, Pretoria, South Africa.*

 ISSN 2225-6253. Paper received Apr. 2016; revised paper received Jun. 2016.

The Duplancic model

The Duplancic conceptual model of caving (Duplancic and Brady, 1999; Duplancic, 2001) is illustrated in Figure 1. The model is composed of five caving zones, which together describe the caving profile from the initiation of self-propagation until the cave breakthrough. These zones were developed based on research using data from Northparkes E26 Lift 1 block cave mine. The five zones are defined by Duplancic (2001) as:

(1) *Caved zone*—The region of displaced (caved material) that has fallen from the cave and provides support to the walls
(2) *Air gap*—A gap between the caved zone and the cave back
(3) *Zone of loosening*—A zone of fractured rock that provides no support to the overlying rock mass and where disintegration of the rock mass occurs. Loss of confinement controls failure in this region. The failure in this region is aseismic
(4) *Seismogenic zone*—An active stress front where seismic failure of the rock mass occurs. It was determined that the most likely mode of failure in this region is slip along pre-existing discontinuities
(5) *Pseudo-continuous domain*—The volume of rock ahead of the seismogenic zone. Only elastic deformation occurs in this region.

This conceptual caving model has been widely accepted by the mining industry and is the framework within which most monitoring results are interpreted (*e.g.* Brown, 2007; Pfitzner *et al.*, 2010). However, the model does not appear to have been rigorously and independently verified.

This conceptual model implies that the rock ahead of the cave back progresses through each of these zones consecutively as the cave propagates. Hence, the damage ahead of the cave back at any point in time decreases continuously with increasing distance from the back (*i.e.*, the damage profile is continuous in space). This is how the model had been interpreted in the industry, as evidenced by Brown (2007) who stated that 'the boundaries between these regions are diffuse rather than sharp' and 'the rock mass undergoes a gradual reduction in strength from its in situ state to its caved state'.

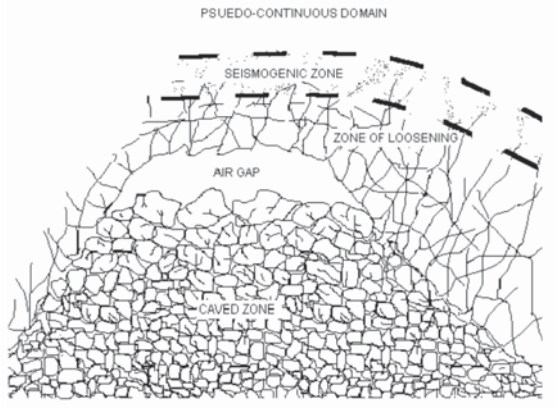

Figure 1—Conceptual model of caving (Duplancic, 2001)

In assuming that slip along pre-existing discontinuities will occur preferentially to intact rock failure (including through an extensional mechanism), Duplancic also emphasizes the hypothesis that failure in the cave back is due to the former and downplays the role of the latter in the caving process.

It is important to note that the Duplancic model of caving is based on one case study, Northparkes E26 Lift 1. Duplancic did not have any instrumentation in the cave back, nor access to any areas of the cave back for visual observation. He relied on the interpretation of linear elastic numerical modelling and simple analysis of seismicity (focal plane analysis, event locations on sections, and S to P wave energy ratio). While the analyses conducted were relatively simple compared with current capabilities, it should be noted that Northparkes was one of the first mines to use a microseismic monitoring system to better understand cave mechanics.

Despite being based on a single case study, the Duplancic model has been applied to monitoring results from many other caving mines (Hudyma and Potvin, 2008; Pfitzner *et al.*, 2010; Westman *et. al.*, 2012, Abolfazlzadeh, 2013). However, the universality of the conclusions that Duplancic draws are called into question by the results of the physical modelling described in this paper.

Centrifuge modelling

Overview

Cumming-Potvin *et al.* (2016) developed a series of physical models with the aim of creating representative examples of cave propagation. Physical testing was performed in the geotechnical centrifuge facility at the University of Pretoria (Jacobsz *et. al.*, 2014). Samples for the caving material were created using weakly cemented sand and fly ash mixtures and a network of fully closed (healed) joints was cut into the sample while it was curing. The fly ash was included in the sample mix in order to increase the brittleness of the material to better mimic the stress-strain behaviour of rock. To date, no specific tests of brittleness have been conducted and further research would be needed to determine the effect of brittleness on the results of the tests.

Horizontal stress was applied through water-filled bladders on the sides of the samples. The samples were tested at 80 times the acceleration due to earth's gravity, and the cave mining undercut was simulated by the retraction of five hydraulic pistons. The tests were essentially two-dimensional, allowing visual observations of the caving process to be made using the digital single-lens reflex (DSLR) camera on board the centrifuge.

The two-dimensionality of the test, together with the restraints in front of and behind the samples, creates a situation that is close to plane strain. The test was inherently limited in its ability to simulate the stresses and expansion of the cave in the third dimension; however, the two-dimensionality allows visual observation of the caving mechanisms and cave growth.

During the design and execution of the physical modelling programme, the expectation was that the caving in the physical model would resemble (and independently verify) the Duplancic conceptual model. However, the results

did not correspond with this expected behaviour. Instead, a series of fractures developed parallel to and ahead of the cave front and the cave periphery. These fractures were judged to be extensional, due to the direction of movement and lack of damage to the asperities along the fractures. The cave progressed as a series of 'jumps' to successive parallel fractures. This created a discontinuous damage profile ahead of the cave back, contrasting with the common interpretation of a continuous damage profile in the Duplancic model.

For convenience, the phenomenon of parallel fracturing ahead of the cave back is referred to herein as *fracture banding*. Although the evidence is not definitive, it suggests that these fractures form in extension.

Some results of physical modelling

The test programme was conducted using five samples. Fracture banding resulted in all of the tests.

Photographs at the ends of the tests on samples 1–4 are shown in Figures 2–5, respectively. Figure 6 is a photograph of the test on sample 5 at the stage when the last undercut piston was extracted. The upward progression of the cave through the fracture banding process is demonstrated in Figure 7 at several stages in the test on sample 3. Two images are shown in each of Figures 2–5; the one, labelled A, without any markings and the other, labelled B, with the markings delineating fractures as described below.

In Figures 2–6, the parallel fractures in each test are highlighted by solid red lines. In Figures 3 and 5 (tests 2 and 4), large pre-existing discontinuities (analogous to faults) gave rise to large shear movements, as shown in blue lines.

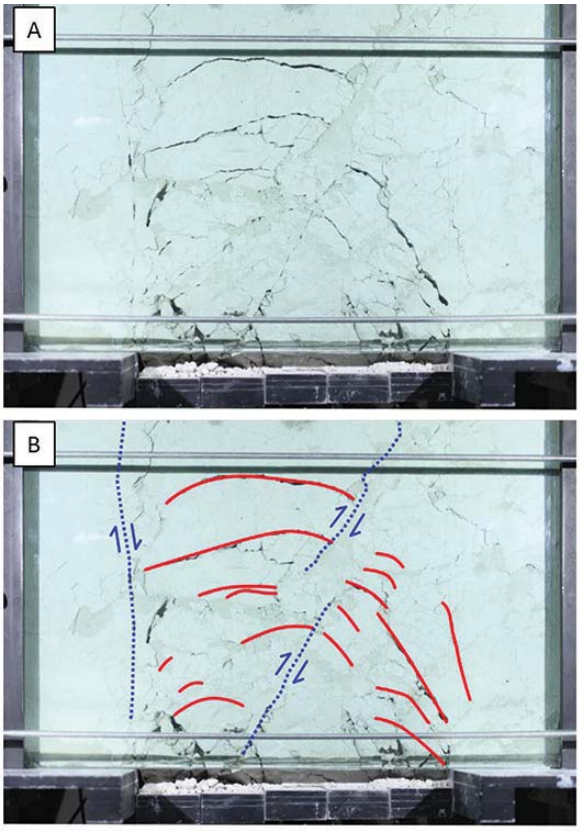

Figure 3—Parallel fractures ahead of the cave front and on the cave periphery, together with major shear discontinuities (test 2)

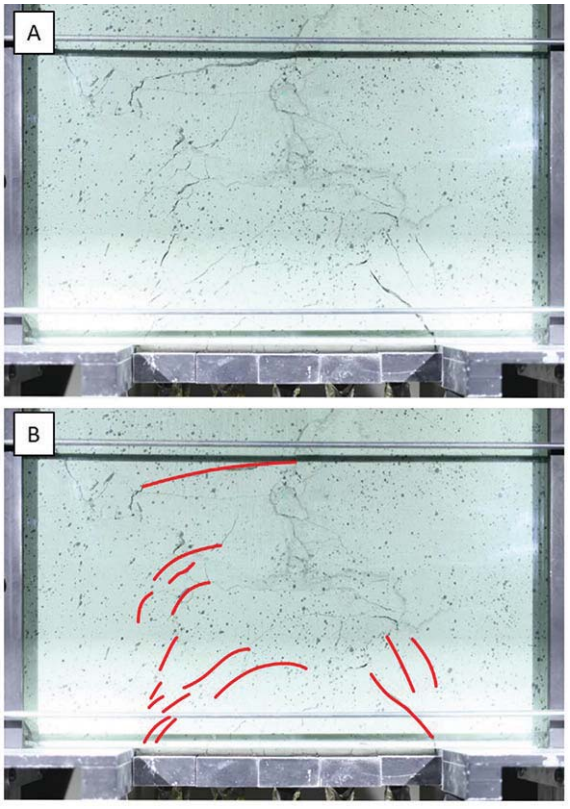

Figure 2—Parallel fractures ahead of the cave front and on the cave periphery (test 1)

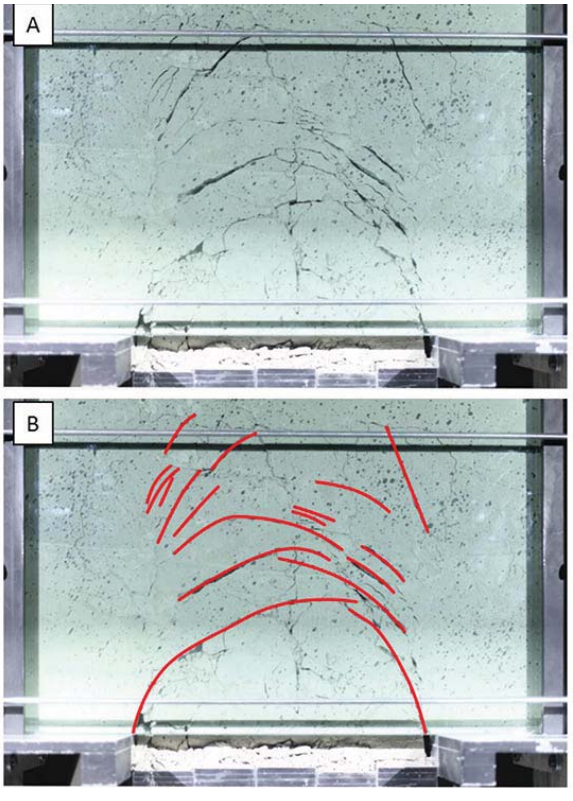

Figure 4—Parallel fractures ahead of the cave front and on the cave periphery (test 3)

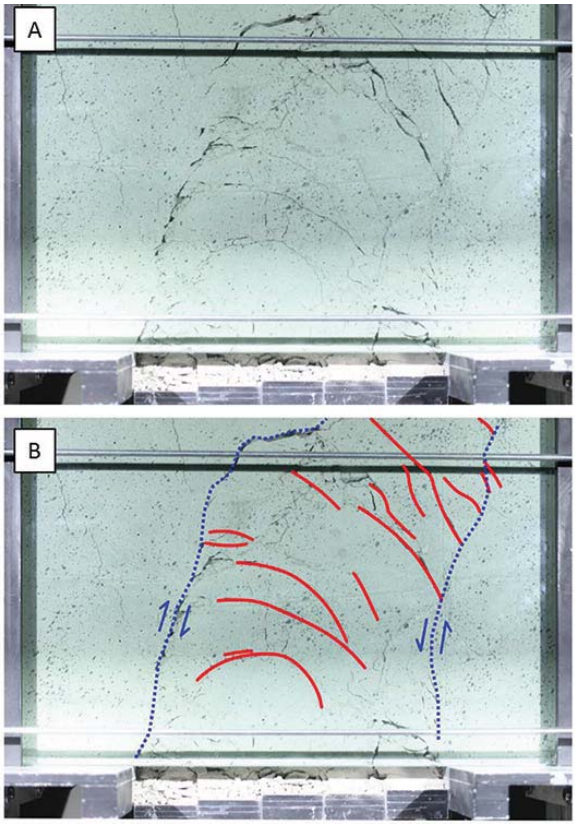

Figure 5—Parallel fractures ahead of the cave front and on the cave periphery, together with major shear discontinuities (test 4)

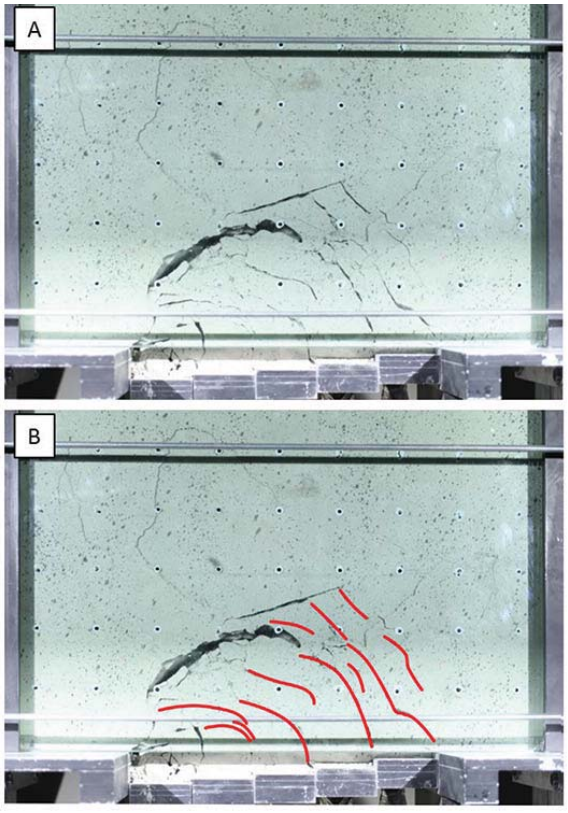

Figure 6—Parallel fractures ahead of the cave front and on the cave periphery (test 5)

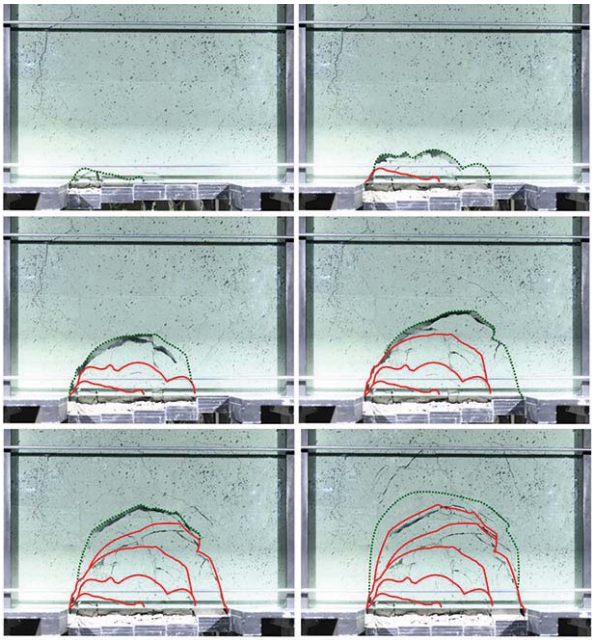

Figure 7—Cave progression (test 3)

In Figure 7, the current cave outlines at the various stages are highlighted with dashed green lines while the previous cave outlines are highlighted with solid red lines.

It is worth noting that although the spacing of the fractures was not consistent between tests, it was relatively consistent within each test, indicating that the spacing might be a function of the material properties and stress state. As some of the fractures terminated at the edge of the pistons, this may create the impression that the fracture banding is an artificial by-product of the fact that the 'undercutting' was performed with comparatively wide pistons. A careful investigation of the data, however, does not support such an interpretation. While the retraction of the pistons may have affected the termination point of the fractures, there were many parallel fractures that did not coincide with the edge of the pistons (shown in dashed orange lines in Figure 8), confirming that the pistons had little influence on the initiation and propagation of the fractures in the early stages. In addition, fracture banding in Figure 3 formed between the two 'faults', some distance away from the 'undercut', and in an area and during a time period when the undercut method could not have influenced the mode of cave propagation.

Literature on cave mechanics

The discrepancy between the expected Duplancic behaviour and the observed fracture banding behaviour prompted a thorough literature review on caving mechanics. The review included three focus areas, namely literature on other physical models, observations from caving mines, and numerical models.

Physical modelling in the literature

Most physical modelling experiments in caving have focused on draw control, and there have been very few physical

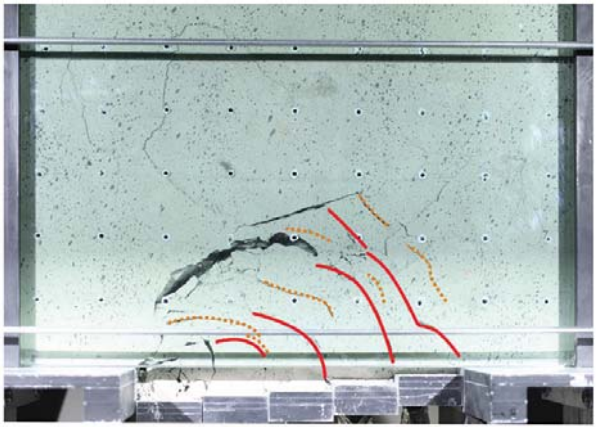

Figure 8—Fractures lining up with edges of pistons (solid red lines) and those that do not (dashed orange lines)

models that investigated the caving process itself. McNearny and Abel (1993) created a two-dimensional model of caving using layers of bricks, primarily to investigate the effect of drawpoint spacing. Duplancic (2001) points out the limitations of the model, stating that 'the regular jointing formed in the model is not representative of the random nature of a real jointing pattern' and 'the lack of horizontal confining stresses limits its contribution to the understanding of caving mechanics'. Although the test had significant flaws, limiting its ability to increase the understanding of caving mechanics, it is interesting to note that the bricks separated from each other parallel to and ahead of the caving void surface; this was interpreted as representing extensional fractures similar to the pattern observed by Panek (1981) at San Manuel Mine. These results, in principle, support the phenomenon of fracture banding as an important mechanism in cave propagation.

Nishida *et al.* (1986) created a base friction model that included horizontal stress applied using hydraulic jacks in order to study subsidence from cave-ins in Japan. The formation of these sinkholes is not an equivalent situation to that of a block caving mine, representing low-strength material at shallow depths and a single jointing pattern. Despite these differences, there are still some similarities between the two cases. Figure 9 shows a typical test of the cave-in using the base friction model. The fracture pattern reveals a discontinuous damage profile, with a series of parallel fractures ahead of the cave surface (*i.e.* fracture banding). These fractures do not coincide with the boundaries between the layers in the sample and thus are not a failure mechanism controlled by the layered nature of the model. The authors were primarily focused on the final subsidence profile, and as such presented no discussion on the failure mechanism and damage profile ahead of the cave.

While the two studies listed here are not particularly representative of modern block caving operations, some knowledge can still be extracted from them. The observation of what appears to be fracture banding give further indications that the importance of this phenomenon in cave evolution has not been recognized to date.

Although these studies indicate that fracture banding is reproducible by different researchers using different materials and different testing methods (centrifuge and friction table), this cannot be used on its own to support the idea that the phenomenon would also occur in real cave mines, nor does it give any indication of its importance in the caving process in a real cave. For this reason, studies that include field observations are essential.

Observations at caving mines

A number of authors have noted tensile fractures in both the crown and the periphery of block caves and open stopes that have caved (Heslop, 1976; Panek, 1981; Lorig *et al.*, 1989; Sharrock *et al.*, 2002; Carlson and Golden, 2008). These tensile fractures were found using direct visual observations, extensometers, time domain reflectometry (TDR) cables, and borehole camera observations.

Heslop (1976) found horizontal tensile fractures developing above the cave back through visual observations of old cut-and-fill workings above the cave back, which were also inferred through extensometer measurement. He made important strides in defining stress and subsidence caving; however, he did not create a conceptual model for the damage ahead of the cave back. The direct observations of tensile fractures are significant in that they reveal the importance of this failure mechanism in the caving process.

Using TDR monitoring, Carlson and Golden (2008) identified multiple instances of potential tension cracks parallel to the cave advance in the periphery of the Henderson 7210 cave.

Using in-hole camera surveys, Sharrock *et al.* (2002) observed two types of rock mass failure above an open stope that had caved at the Mt Isa Mines lead mine. The first was large, widely spaced extensional fractures at a distance from the stope crown and parallel to the excavation surface. The second was a composite failure between discontinuities and intact rock observed within 10 m of the crown.

Lorig *et al.* (1989) investigated caving of an open stope at Falconbridge East mine. They noted that core discing in boreholes above the stope back supported the idea that high stress caused shear and tensile failure.

Several of these authors found that the tensile fractures manifested as a series of discontinuities parallel to the cave front (Panek, 1981; Sharrock *et al.*, 2002; Carlson and Golden, 2008). It appears that these may be observations of fracture banding.

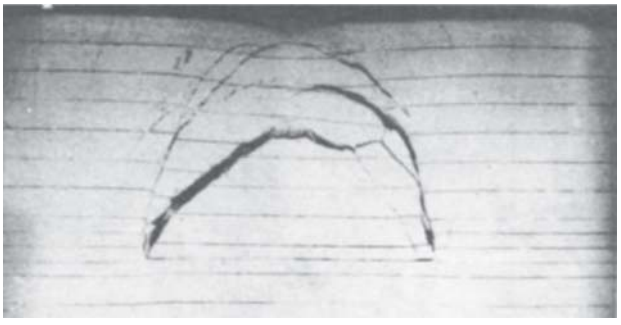

Figure 9—Typical cave-in test (Nishida *et al.*, 1986)

Of these studies, only Panek (1981) included an in-depth discussion of the importance of the parallel extensile fractures he observed in the caving process. The results of Panek's monitoring programme at San Manuel mine suggested a series of parallel extension fractures with strike angles tangential to the cave boundary, forming a 'roughly circular fractured zone of expansion about each active cave'. This concept is illustrated in Figure 10.

Panek stated that, in theory, the same extensional fractures tangential to the cave boundary should occur above and below the caved block. However, no measurements were made directly above the cave. Panek also postulated that this fracturing pattern can influence the potential for the rock mass to cave upward toward the surface, which would have a significant impact on the viability of caving projects. No further studies were conducted to verify if the fracturing extended above and below the active cave, nor were any efforts made to determine why the failure manifested as a series of parallel fractures. Panek's interpretation was based on direct observations, making it an important contribution, which seems to have been lost in the modern understanding of cave mechanics.

Studies using numerical modelling

While there is an abundance of literature dealing with numerical modelling of block caving, the existing literature tends to interpret results within the Duplancic model of caving and often focuses on the ability of numerical models to predict the cave geometry or subsidence profile. There is limited literature that attempts to better understand caving mechanics and the fracture pattern ahead of the cave using numerical models.

A notable exception is the work of Garza Cruz and Pierce (2014), who investigated the failure mechanisms in the crown of cave mines. They modelled a cube with sides of 8 m, with a material model simulating a massive, veined rock mass. Loading conditions analogous to those in a cave back were introduced. Significant maximum and intermediate principal stresses (horizontal) were applied while the minimum principal stress (vertical) was unloaded in increments at the bottom of the cube while being maintained at the top of the cube.

Figure 10—Parallel fractures in a circular zone around an active cave (after Panek, 1981)

The authors found that as the vertical stresses at the cave back decrease, high differential stresses induce shear failure and tensile fractures develop simultaneously sub-parallel to the face. These tensile fractures sub-parallel to the caving face could be interpreted as fracture banding. It was noted that the cave back showed progressive spalling as the back failed and stress was shed upwards. No further details were given on the importance of the tensile fractures during the cave progression.

There are several other studies, focusing on areas other than cave mechanics, that contain illustrations showing discontinuous damage ahead of the cave back, often in the form of a series of fractures parallel to the cave back (Vyazmensky i., 2007; Lisjak *et al.*, 2012; Li *et al.*, 2014). All of these examples use combined continuum-discontinuum (finite-discrete element method) codes. An example of this can be seen in Figure 11. These cases give yet another indication that fracture banding may be an important mechanism in cave development, but that its significance has not been recognized.

The study by Li *et al.* (2014) was the only one of these studies to look at the damage profile ahead of the propagating cave in some detail. The authors describe the failure ahead of the cave as a series of pressure-balancing arches and stress-release zones. It was postulated that in order for the cave to grow, the pressure-balancing arches must be broken, either by extension of the undercut or by further drawing of caved material. The failure in the model was primarily intact rock failure between existing joints that formed the pressure-balancing arches. While this numerical model shows some evidence for it, the authors do not specifically address the discontinuity of the damage, nor do they try to relate the phenomenon to any field data.

It appears that fracture banding propagation occurs only in contimuum-discontinuum hybrid models where the fracturing precess is explicitly modelled. We could not find

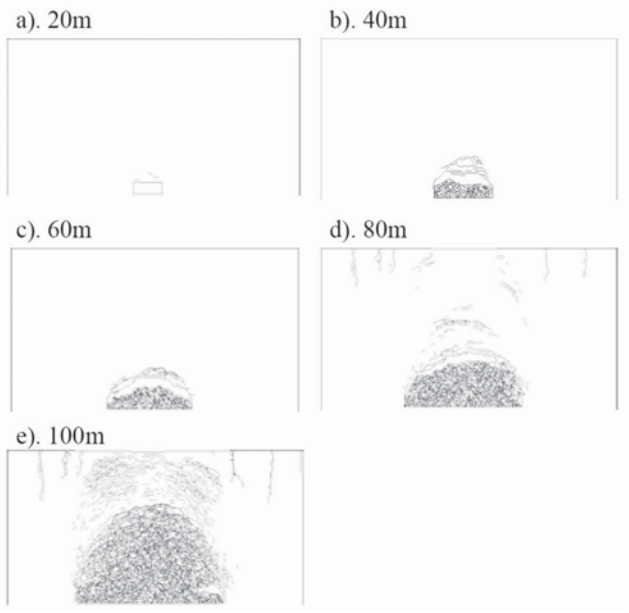

Figure 11—Cave growth for different undercut widths using an equivalent continuum approach (Vyazmensky *et al.*, 2007)

any example in the literature where a fracture banding phenomenon was modelled using a purely continuum modelling approach, without any explicit modelling of fracturing.

Analysis of microseismicity

Since the Duplancic (2001) publication, microseismic monitoring has become commonplace in caving mines. A study was performed to look for evidence from microseismic monitoring that could support the notion of fracture banding occurring in real cave operations.

For this purpose, analysis of microseismicity at two larger copper-gold porphyry block cave operations was undertaken. The analysis revealed indications that fracture banding was taking place as part of cave evolution. There were many instances where 'bands' of high microseismic event density alternated with 'bands' of low microseismic event density. This can be seen in Figure 12 to Figure 14, with the bands being highlighted in Figure 12B to Figure 14B. The microseismic events are coloured according to the date on which they occurred.

This pattern of microseismicity is not always observable at all times and in all locations in the crown and periphery of both mines. There are several possible explanations for this. The first is that conditions necessary for fracture banding to occur are not always met and that, at times, the cave propagates via another failure mechanism. It is also possible that the spacing of the fractures is closer to, or in the same order of magnitude as, the general location accuracy of the system. Another possible explanation is that the parallel extensional fractures form a beam, which subsequently begins to fail, creating microseismic events throughout the spatial volume.

Based on consultation with site personnel, there is no reason to believe that the bands of microseismicity are related to geology or were caused by any artefact of the seismic system. This is most likely due to the caving process created by the upwards expansion of the cave.

These examples of bands of microseismicity imply that fracture banding may be present at both Mine A and Mine B and, in turn, that it may be an important mechanism in cave propagation in general. The authors have also found indications in the microseismic records of other mines that bands of microseismicity may be forming.

Conclusions

Multiple sources indicate that fracture banding is an important mechanism in cave evolution. Physical models of caving tested in a geotechnical centrifuge suggested that the primary mechanism for cave evolution is through a series of fractures parallel to and ahead of the cave back, creating a clearly discontinuous damage profile.

In the literature there are examples from observations, instrumentation, and numerical models that indicate extensile fracturing and discontinuous damage ahead of the cave back. This suggests that the phenomenon observed in the laboratory is present in the field, although its significance may not have been appreciated by the individual observers.

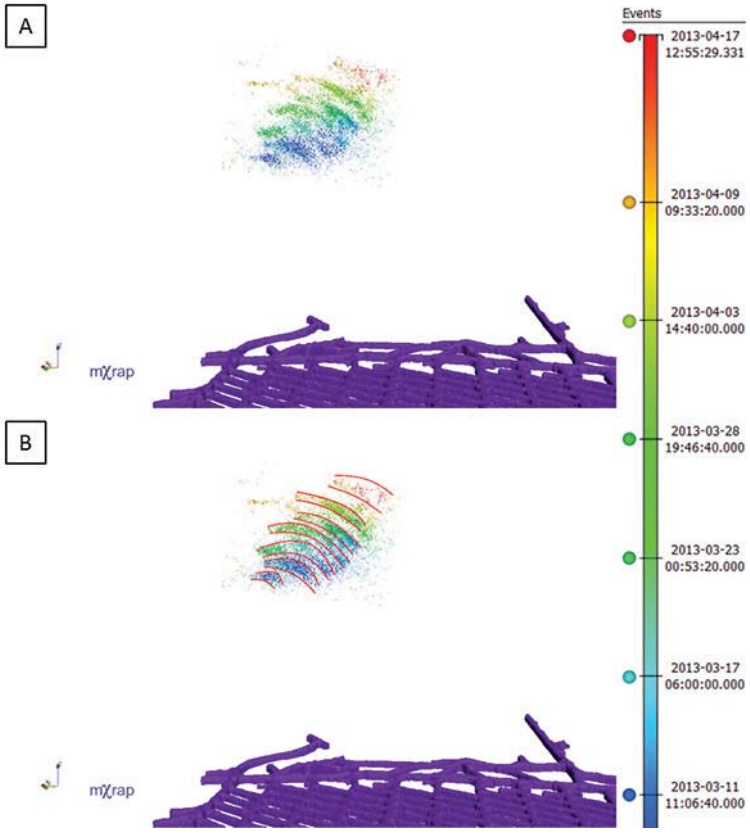

Figure 12—First example of bands of microseismicity at Mine A, with the production level shown in purple

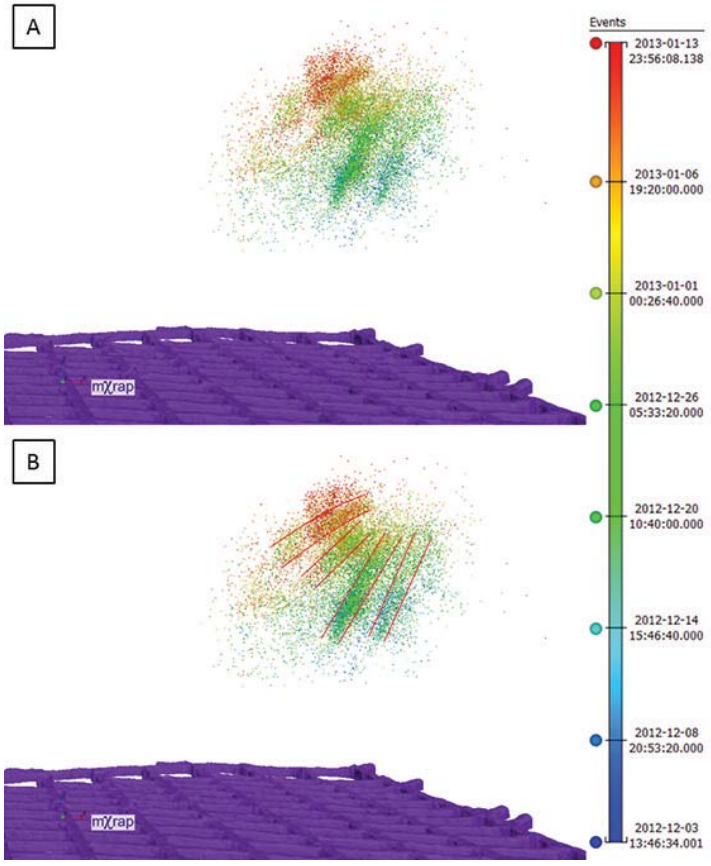

Figure 13—Second example of bands of microseismicity at Mine A, with the production level shown in purple

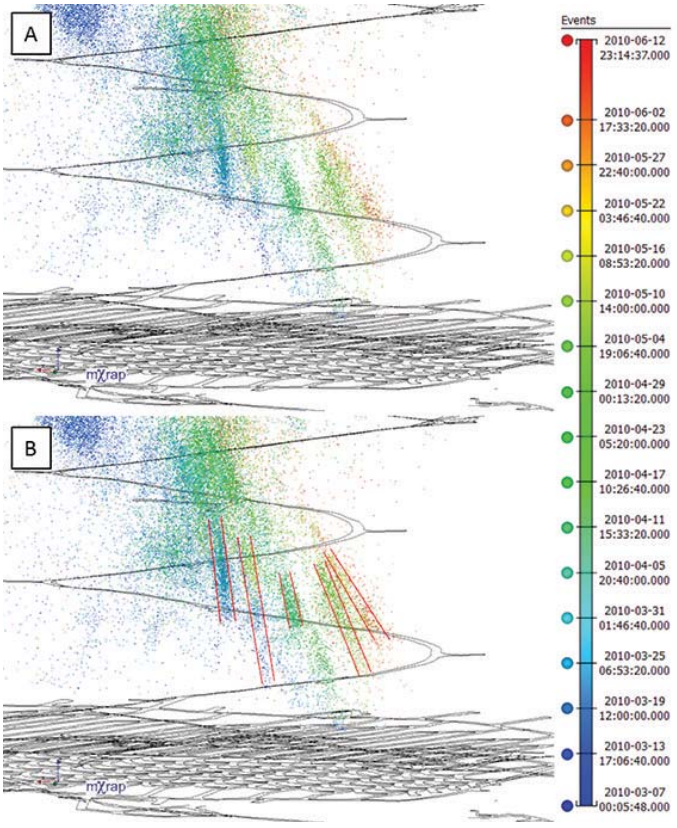

Figure 14—Example of bands of microseismicity at Mine B, with development shown as black lines

Analysis of microseismicity also revealed that in some circumstances, repeated bands of microseismicity alternating with low or no microseismicity occur that may be interpreted to represent fracture banding.

Considering the evidence from physical models, direct field observation, and microseismic monitoring, it appears that fracture banding is a mechanism that contributes to cave propagation. The Duplancic model of caving, which is commonly interpreted as implying a continuous damage profile and downplaying the role of extensional failure, is not applicable in all cases and needs to be extended.

Access to the cave back and direct observation of the caving process is limited and the phenomenon of fracture banding is difficult to observe. These facts, in combination with the important role that fracture banding plays in caving propagation in the physical models, make it reasonable to expect that this process may play a much larger role in the field than has previously been recognized.

Further research needs to be conducted in order to determine the conditions under which fracture banding occurs and its significance with respect to cave design and management.

References

Abolfazlzadeh, Y. 2013. Application of seismic monitoring in caving mines - case study of Telfer Gold Mine. MSc thesis, Laurentian University.

Brown, E.T. 2007. Block Caving Geomechanics. 2nd edn. Julius Kruttschnitt Mineral Research Centre, University of Queensland.

Carlson, G. and Golden, R. 2008. Initiation, growth, monitoring and management of the 7210 cave at Henderson Mine - a case study. *Proceedings of the 5th International Conference and Exhibition on Mass Mining (MassMin 2008)*, Luleå, Sweden, 9–11 June 2008. Schunnesson, H. and Nordlund, E. (eds.). Luleå University of Technology. pp. 97–106.

Cumming-Potvin, D., Wesseloo, J., Jacobsz, S.W., and Kearsley, E.P. 2016. Results from physical models of block caving. *Proceedings of the 7th International Conference and Exhibition on Mass Mining (MassMin 2016)*, Sydney, Australia, 9–11 May 2016. Australasian Institute of Mining and Metallurgy, Melbourne. pp. 329–340.

Duplancic, P. 2001. Characterisation of caving mechanisms through analysis of stress and seismicity. PhD thesis, University of Western Australia.

Duplancic, P. and Brady, B.H. 1999. Characterisation of caving mechanisms by analysis of seismicity and rock stress. *Proceedings of the 9th ISRM Congress*, Paris, France, 25–28 August 1999. International Society for Rock Mechanics. pp. 1049–1053.

Garza Cruz, T.V. and Pierce, M. 2014. A 3DEC model for heavily veined massive rock masses. *Proceedings of the 48th US Rock Mechanics/Geomechanics Symposium*, Minneapolis, 1–4 June 2014. American Rock Mechanics Association.

Heslop, T.G. 1976. Rock mechanics aspects of block caving chrysotile asbestos orebodies at Shabanie mine, Rhodesia. MSc thesis, University of the Witwatersrand.

Hudyma, M. and Potvin, Y. 2008. Characterizing caving induced seismicity at Ridgeway gold mine. *Proceedings of the 5th International Conference and Exhibition on Mass Mining (MassMin 2008)*, Luleå, Sweden, 9-11 June 2008. Schunnesson, H. and Nordlund, E. (eds.). Luleå University of Technology. pp. 931–942.

Jacobsz, S.W., Kearsley, E.P., and Kock, J.H.L. 2014. The geotechnical centrifuge facility at the University of Pretoria. *Proceedings of the 8th International Conference on Physical Modelling in Geotechnics*, Perth, Australia. Gaudin, C. and White, D. J. (eds.). Taylor and Francis, Boca Raton, FL. pp. 169–174.

Li, L.C., Tang, C.A., Zhao, X.D., and Cai, M. 2014. Block caving-induced strata movement and associated surface subsidence: a numerical study based on a demonstration model. *Bulletin of Engineering Geology and the Environment*, vol. 73, no. 4. pp. 1165–1182.

Lisjak, A., Tatone, B., Mahabadi, O., and Grasselli, G. 2012. Block caving modelling using the Y-Geo hybrid finite-discrete element code. *Proceedings of the 6th International Conference and Exhibition on Mass Mining (MassMin 2012)*, Sudbury, 10–14 June 2012. CIM, Montreal.

Lorig, L.J., Hart, R.D., Board, M.P., and Swan, G. 1989. Influence of discontinuity orientations and strength on cavability in a confined environment. *Proceedings of the 30th US Symposium on Rock Mechanics (USRMS)*, Morgantown, West Virginia, 19–22 June 1989. Balkema. pp. 167–174.

Mcnearny, R.L. and Abel, J.F. 1993. Large-scale two-dimensional block caving model tests. *International Journal of Rock Mechanics and Mining Sciences*, vol. 30, no. 2. pp. 93–109.

Nishida, T., Esaki, T., and Kameda, N. 1986. Development of the base friction technique and its application to subsidence engineering. *Proceedings of the International Symposium on Engineering in Complex Rock Formations*, Beijing, China, 3–7 November 1986. LI, C. and Yang, L. (eds.). Science Press. pp. 386-392.

Panek, L.A. 1981. Ground movements near a caving stope. *Design and Operation of Caving and Sublevel Stoping Mines*. Stewart, D. (ed.). Society of Mining Engineers of AIME. New York, USA. pp. 329–354.

Pfitzner, M., Westman, E., Morgan, M., Finn, D., and Beck, D. 2010. Estimation of rock mass changes induced by hydraulic fracturing and cave mining by double difference passive tomography. *Proceedings of the 2nd International Symposium on Block and Sublevel Caving*. Potvin, Y. (ed.). Australian Centre for Geomechanics, Perth. pp. 677–684.

Sharrock, G., Slade, N., Thin, I., and Duplancic, P. 2002. The prediction of stress induced caving on a mining abutment. *Proceedings of the 1st International Seminar on Deep and High Stress Mining*, Perth, Australia, 6–8 November 2002. Potvin, Y., Hadjigeorgiou, J., and Stacey, T. (eds.). Australian Centre for Geomechanics, Perth.

Stacey, T.R. 1981. A simple extension strain criterion for fracture of brittle rock. *International Journal of Rock Mechanics and Mining Sciences & Geomechanics Abstracts*, vol. 18, no. 6. pp. 469–474.

Vyazmensky, A., Elmo, D., Stead, D., and Rance, J.R. 2007. Combined finite-discrete element modelling of surface subsidence associated with block caving mining. *Rock Mechanics: Meeting Society's Challenges and Demands*. Eberhardt, E., Stead, D., and Morrison, T. (eds.). Taylor and Francis, Boca Raton, FL. pp. 467–476.

Westman, E., Luxbacher, K., and Schafrik, S. 2012. Passive seismic tomography for three-dimensional time-lapse imaging of mining-induced rock mass changes. *The Leading Edge*, vol. 31, no. 3. pp. 338–345. ◆

YOUNG PROFESSIONALS COUNCIL

3rd YOUNG PROFESSIONALS CONFERENCE

9–10 MARCH 2017 | INNOVATION HUB | PRETORIA

UNLOCKING THE FUTURE OF THE AFRICAN MINERALS INDUSTRY: VISION 2040

KEYNOTE TOPICS

Leadership | Innovation | Wealth Management
Professional Development

OBJECTIVES

- To provide an opportunity for Young Professionals in the Minerals and Mining Industry to showcase their post-graduate work and experiences.
- To provide opportunities for young professionals to obtain exposure, build reputations, further their careers and network with peers and leaders in the African Minerals Industry.

EXHIBITION/SPONSORSHIP

Sponsorship opportunities are available. Companies wishing to sponsor or exhibit should contact the Conference Co-ordinator.

SAIMM
THE SOUTHERN AFRICAN INSTITUTE OF MINING AND METALLURGY

FOR FURTHER INFORMATION CONTACT:
Conference Co-ordinator: Camielah Jardine
E-mail: camielah@saimm.co.za • **Tel:** +27 11 834 1273/7

http://dx.doi.org/10.17159/2411-9717/2016/v116n8a8

Estimating specific energy from the brittleness indexes in cutting metallic ores

by R. Comakli*, S, Kahraman†, C. Balci‡, and D. Tumac‡

Synopsis

Specific energy (SE) is a very useful parameter for assessing rock excavation by machine. Predicting the SE from the brittleness will be practical, especially for preliminary studies, due to the fact that determining the SE from cutting tests is difficult and expensive. In this study, the predictability of the SE from different brittleness concepts was investigated for metallic ores such as chromite, haematite, galena, and smithsonite. Uniaxial compressive strength, Brazilian tensile strength, impact strength, and small-scale cutting tests were carried out in the laboratory. The SE values were calculated from the cutting tests and correlated with three different brittleness concepts. A significant correlation could not be found between the SE and the brittleness B_3 (the ratio of compressive strength minus tensile strength to compressive strength plus tensile strength). However, strong correlations were found between the SE and the both brittleness B_5 (the product of percentage fines in the impact strength test and compressive strength) and brittleness B_8 (half of the product of compressive strength and tensile strength). The validations of the derived equations were also checked. It is concluded that the SE in ore cutting can be reliably estimated from the brittleness concepts B_5 and B_8.

Keywords
specific energy, ore cutting, brittleness indexes, regression analysis.

Introduction

Specific energy (SE) is an important parameter in mechanical rock excavation. It can be simply used for predicting the performance of roadheaders (Rostami, Ozdemir, and Neil, 1994). However, obtaining the SE from small-scale or full-scale cutting tests is very difficult and expensive. For this reason, some researchers have investigated the relationships between SE and rock properties and suggested empirical equations for the estimation of SE. McFeat-Smith and Fowell (1979) carried out experimental studies for correlating the SE obtained by small-scale cutting tests with some rock properties such as cone indenter index, cementation coefficient, Schmidt hammer rebound value, and compressive strength. They stated that the cone indenter test consistently proved to be the best predictor for SE. Copur *et al.* (2001) correlated the SE with the UCS and BTS for some rock and ore types. They found good correlation between SE and both UCS and BTS. They also showed that the relation between SE and the product of UCS and BTS has a better correlation coefficient than that of the relations between SE and both UCS and BTS. Balci *et al.* (2004) tested 23 different rock and ore types and investigated the predictability of SE from physical and mechanical properties. They found good or very good correlations between the SE and rock properties such as UCS, Brazilian tensile strength, static and dynamic elastic moduli, and the Schmidt hammer value. Tiryaki and Dikmen (2006) carried out mineralogical and petrographic analyses, rock mechanics, and linear rock cutting tests on sandstones. They investigated the relations between SE and rock properties using regression analysis. They showed that the texture coefficient and feldspar content of sandstones affected rock cuttability, evidenced by significant correlations between these parameters and SE. However, the felsic and mafic mineral contents of sandstones exhibited no significant correlation with SE. On the other hand, cementation coefficient, effective porosity, and pore volume indicated good correlations with SE. Poisson's ratio, Brazilian tensile strength, Shore scleroscope hardness, Schmidt hammer hardness, dry density, and point load strength index showed very strong linear correlations with SE. Tumac *et al.* (2007) investigated the predictability of rock cuttability from Shore hardness and compressive strength. They showed that there was a relation between Shore hardness values, optimum specific energy, and compressive strength.

* *Mining Engineering Department, Nigde University, Nigde, Turkey.*
† *Mining Engineering Department, Hacettepe University, Ankara, Turkey.*
‡ *Mining Engineering Department, Istanbul Technical University, Istanbul, Turkey.*

 ISSN 2225-6253. Paper received Jul. 2015; revised paper received Oct. 2015.

Some researchers have investigated the relations between the cuttability or SE and brittleness. Singh (1986) indicated that cuttability, penetrability, and the Protodyakonov strength index of coal strongly depended on the brittleness of coal. Singh (1987) also showed that a directly proportional relation existed between *in situ* SE energy and the brittleness of three Utah coals. Goktan (1991) investigated the relation between SE and a brittleness concept derived from the UCS and BTS and concluded that the brittleness concept adopted in his study might not be a representative measure of specific energy consumption during rock cutting. Altindag (2003) investigated the relations between SE and brittleness concepts using the raw data obtained from previous experimental studies on rocks. He showed that the SE was strongly correlated with the brittleness B_3 (the area under the line relating compressive strength and tensile strength).

In this study, eight different metallic ores such as chromite, haematite, galena, and smithsonite were tested in the laboratory and the predictability of the SE from different brittleness concepts was investigated.

Brittleness

There is no common agreement as to the definition, concept, or measurement of brittleness. Different researchers express and use the concept differently. Morley (1944) and Hetényi (1966) define brittleness as lack of ductility. Materials such as cast iron and many rocks, which usually fail by fracture at or only slightly beyond the yield stress, are defined as brittle by Obert and Duvall (1967). Ramsay (1967) defines brittleness as follows: 'when the internal cohesion of rocks is broken, the rocks are said to be brittle.' The definition of brittleness as a mechanical property varies from author to author. Different definitions of brittleness summarized by Hucka and Das (1974) are formulated as follows:

$$B_1 = \frac{\varepsilon_r}{\varepsilon_t} \quad [1]$$

where B_1 is the brittleness determined from the percentage of reversible strain as determined from the stress-strain curve, ε_r is the reversible strain, and ε_t is the total strain.

$$B_2 = \frac{W_r}{W_t} \quad [2]$$

where B_2 is the brittleness determined from the percentage of reversible energy as determined from the stress-strain curve, W_r is the reversible energy, and W_t is the total energy.

$$B_3 = \frac{\sigma_c - \sigma_t}{\sigma_c + \sigma_t} \quad [3]$$

where B_3 is the brittleness determined from the compressive and tensile strengths, σ_c is the uniaxial compressive strength, and σ_t is the tensile strength.

$$B_4 = \sin\theta \quad [4]$$

where B_4 is the brittleness determined from Mohr's envelope (at $\sigma_n = 0$) , and θ is the angle of internal friction.

$$B_5 = q\sigma_c \quad [5]$$

where, B_5 is the brittleness from the Protodyakonov (1962) impact test, σ_c is the UCS, and q is the percentage of fines (-28 mesh) formed in the Protodyakonov impact test.

$$B_6 = \frac{H_\mu - H}{K} \quad [6]$$

where B_6 is the brittleness from macro-hardness and micro-hardness, $H\mu$ is the micro-indentation hardness, H is the macro-indentation hardness, and K is a constant.

Hucka and Das (11975) defined a brittleness obtained from load-deformation curves. This definition of brittleness can be formulated as follows:

$$B_7 = \frac{W_{rs}}{W_t} \quad [7]$$

where B_7 is the penetration brittleness determined from the percentage of reversible energy in the load-deformation curve, W_{rs} is the reversible strain energy just before failure, and W_t is the total energy supplied just before failure.

Altindag (2000) suggested a brittleness index obtained from compressive and tensile strength. This brittleness index is defined as the area under the curve of compressive strength versus tensile strength and can be formulated as follows:

$$B_8 = \frac{\sigma_c \sigma_t}{2} \quad [8]$$

where B_8 is the brittleness determined from compressive and tensile strength, σ_c is the uniaxial compressive strength, and $\sigma\tau_c$ is the tensile strength.

Recently, Yagiz (2009) introduced a new brittleness index obtained from the punch penetration test:

$$B_9 = \frac{F_{\max}}{P} \quad [9]$$

where B_9 is the brittleness determined from force-penetration curve, $F_{\max}$ is the maximum applied force on a rock sample (kN), and P is the corresponding penetration at maximum force (mm).

Sampling

Mineral deposits are common in the Taurus Mountain Belt, which runs from west to east in the south of Turkey. This mountain belt is subdivided into three parts: the western, the middle, and the eastern Taurus Mountains. The boundary between the middle and the eastern part is the Aladaglar region. Block samples of chromite, haematite, galena, and smithsonite were collected from eight different mines or outcrops in the Aladaglar region (Figure 1). The sampling locations are listed in Table I. Samples 70 mm in diameter were cored from the blocks for cutting tests, and 38 mm diameter samples for physico-mechanical tests.

Experimental studies

Uniaxial compressive strength (UCS) test

Uniaxial compressive strength tests were conducted on trimmed core samples, which had a diameter of 38 mm and a length-to-diameter ratio of 2–2.5. The stress rate was applied within the limits of 0.5–1.0 MPa/s. The tests were repeated at least five times for each ore type and the average value recorded as the UCS.

Table I

Average results of physico-mechanical and cutting tests

Ore type	Location	Uniaxial compressive strength (MPa)	Tensile strength (MPa)	Impact strength index (%)	Specific energy (MJ/m³)
Hematite	Mentes/Yahyali	32.37	4.85	71.3	12.6
Hematite	Dundarli/Nigde	31.47	3.86	78.3	9.4
Hematite	Attepe/Yahyali	27.42	3.99	81.5	12.6
Chromite	Kapiz mine/Pozanti	66.27	7.44	72.1	28.1
Chromite	Guven mine/Aladag	7.89	1.12	40.9	10.1
Chromite	Andizli/Pozanti	58.98	5.98	68.6	20.1
Galena	Delikkaya/Yahyali	19.83	2.93	38.2	9.0
Smithsonite	Derebag/Yahyali	22.35	3.99	66.7	11.5

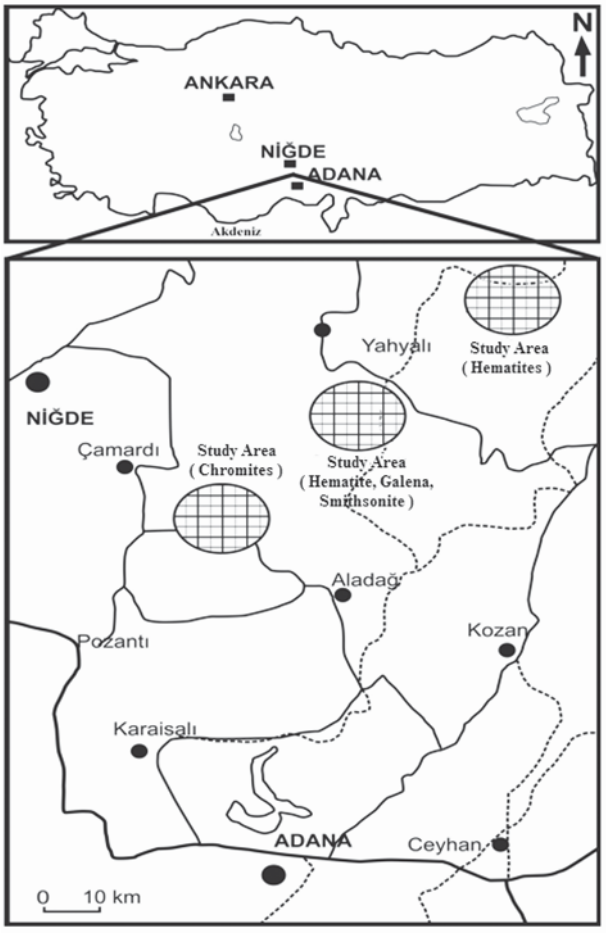

Figure 1—Location map of sampling area

Brazilian tensile strength (BTS) test

Brazilian tensile strength tests were conducted on core samples with a diameter of 38 mm and a height-to-diameter ratio of 0.5–1.0. A tensile loading rate of 200 N/s was applied until failure occurred. At least six samples were tested for each ore type and the results were averaged.

Impact strength test

The impact strength test was first developed by Protodyakonov (1962), and later modified by Evans and Pomeroy (1966). The device designed by Evans and Pomeroy (1966) was used in the impact strength tests in this study. A 100 g sample of rock in the size range 3.175–9.525 mm is placed inside a cylinder 42.86 mm in diameter and a 1.8 kg weight is dropped 20 times from a height of 30.48 cm onto the sample. The amount of rock remaining in the initial size range after the test is termed the impact strength index. The test was repeated three times for each ore type and the average value recorded as the impact strength index (I_s).

Small-scale cutting test

Details of this test were presented by McFeat-Smith and Fowell (1979). In the current study, 70 mm core samples were fixed in the table of a shaping machine (Figure 2) and cut by a chisel pick having a rake angle of –5 degrees, a clearance angle of 5 degrees, and a tool width of 12.7 mm. The depth of cut was selected as 5 mm. The tool forces in three directions were recorded (Figure 3) using a force dynamometer, and the SE calculated by dividing the mean cutting force by the yield (volume of cut material). The cutting tests were repeated three times for each rock type and the results were averaged.

Evaluation of the results

Table I presents the average results of all tests. As shown, the UCS values range from 7.89 MPa for the Guven Mine/Aladag chromite to 66.27 MPa for the Kapiz Mine/Pozanti chromite. The BTS values range from 1.12 MPa for the Guven Mine/Aladag chromite to 7.44 MPa for the Kapiz Mine/Pozanti chromite. I_s values range from 38.2% for the Delikkaya/Yahyali galena to 81.5 % for the Attepe/Yahyali haematite.

The brittleness concepts B_3, B_5, and B_8 were used in the statistical analysis. The calculated brittleness values are given in Table II. The brittleness values and SE values were analysed using least squares regression. Linear, logarithmic, exponential, and power curve fitting approximations were executed and the best approximation equation with the highest correlation coefficient was determined for each regression. No significant correlation between SE and brittleness B_3 was found (Figure 4). However, a strong correlation between SE and brittleness B_5 was found (Figure 5). The relationship follows an exponential function. The SE increases with increasing brittleness B_5. The equation of the curve is

$$SE = 7.64e^{0.0002\,B_5} \quad r = 0.89 \qquad [10]$$

where SE is the specific energy (MJ/m³) and B_5 is the brittleness.

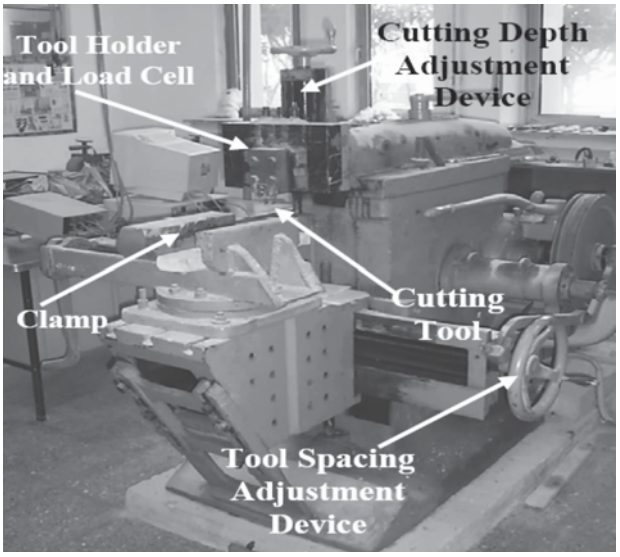

Figure 2—Small-scale cutting rig

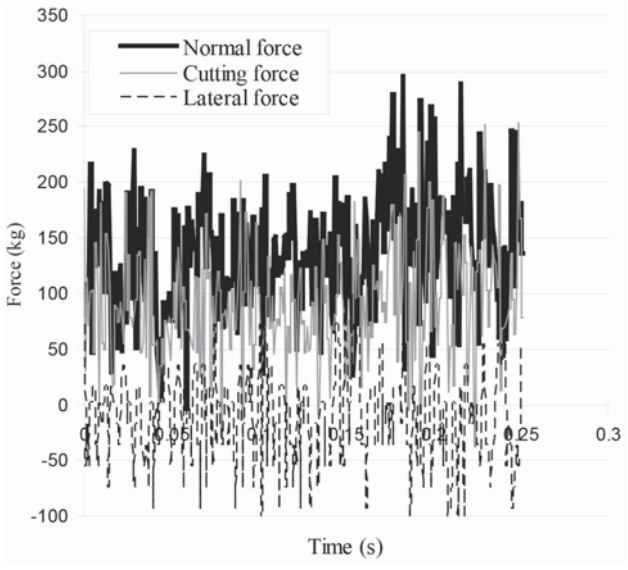

Figure 3—Tool forces in three directions

Table II

Brittleness values

Ore type	Ore location	B_3	B_5	B_8
Hematite	Mentes/Yahyali	0.74	2308.0	78.5
Hematite	Dundarli/ Nigde	0.78	2463.2	60.7
Hematite	Attepe/ Yahyali	0.75	2233.6	54.7
Chromite	Kapiz mine/ Pozanti	0.80	4775.4	246.5
Chromite	Guven mine/ Aladag	0.76	322.4	4.3
Chromite	Andizli/ Pozanti	0.82	4043.7	176.4
Galena	Delikkaya/ Yahyali	0.74	757.5	29.1
Smithsonite	Derebag/ Yahyali	0.70	1490.7	44.6

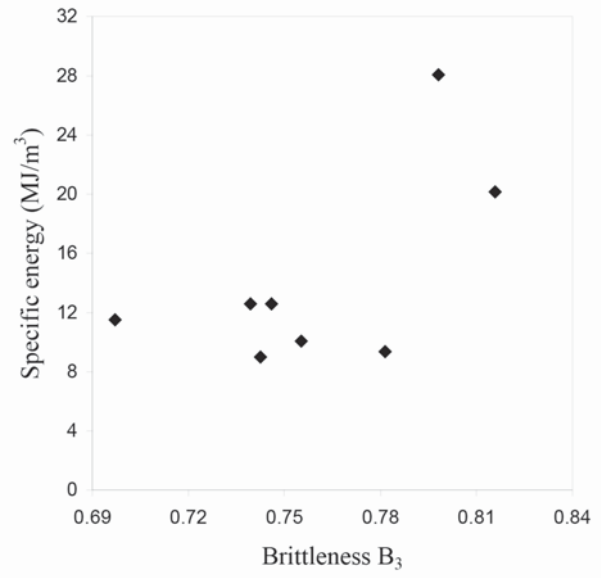

Figure 4—Correlation between specific energy and brittleness B_3

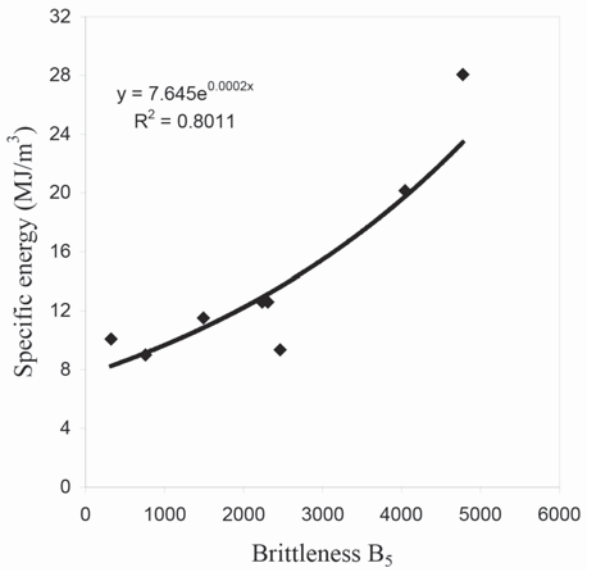

Figure 5—Correlation between specific energy and brittleness B_5

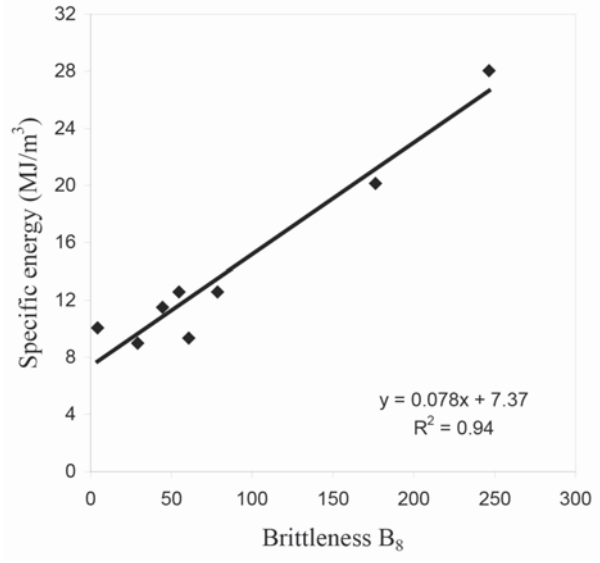

Figure 6—Correlation between specific energy and brittleness B_8

A very strong correlation between SE and the brittleness B_8 was also found (Figure 6). The relation follows a linear function. SE increases with increasing brittleness B_8. The equation of the line is

$$SE = 0.078B_8 + 7.37 \quad r = 0.97 \qquad [11]$$

where SE is the specific energy (MJ/m³) and B_8 is the brittleness.

Altindag (2003) combined some data for the regression analysis and derived the following equation between SE and brittleness B_8:

$$SE = 1.005B_8^{0.61} \quad r = 0.84 \qquad [12]$$

where SE is the specific energy (MJ/m³) and B_8 is the brittleness.

Figure 7 was plotted to compare Equations [11] and [12]. Although Equation [11] is a linear relation and Equation [12] is a power relation, there is not a large difference between the two trends, as shown in Figure 7. The difference between the two trends may be due to the fact that Altindag's data covers a wide strength range. The ores tested in this study have UCS values less than 66 MPa and brittleness B_8 values less than 300. However, Altindag's data includes UCS values up to 559 MPa and brittleness B_8 values up to 2491. An important point is that Altindag's data shows an almost linear trend for rock with brittleness values less than 300. On the other hand, some of the methods for measuring SE are different in Altindag's study. For example, Altindag used published data and some of his data is derived from to disc cutter tests, not a chisel pick test.

As shown above, the correlation coefficients of Equations [10] and [11] are very good, but they do not necessarily identify the valid model. Validation of these equations was checked by the *t*-test and the *F*-test.

The significance of *r*-values can be determined by the *t*-test, assuming that both variables are normally distributed and the observations are chosen randomly. The test compares the computed *t*-value with the tabulated *t*-value using the null hypothesis. In this test, a 95% level of confidence was chosen. If the computed *t*-value is greater than tabulated *t*-value, the null hypothesis is rejected. This means that *r* is significant. If the computed *t*-value is less than the tabulated *t*-value, the null hypothesis is not rejected. In this case, *r* is not significant. As seen in Table III, the computed *t*-values

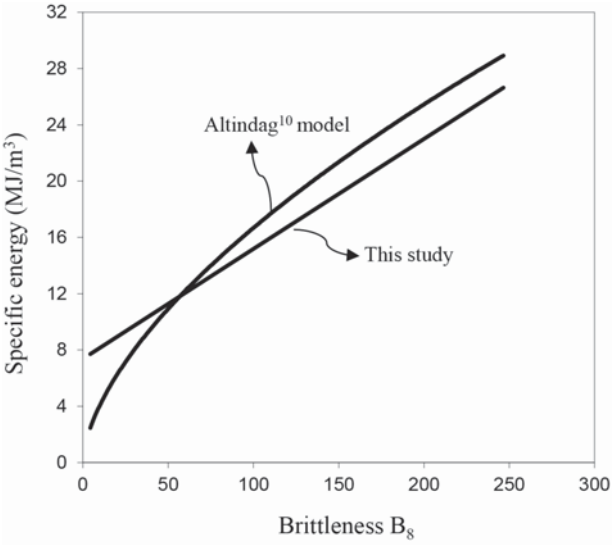

Figure 7—Comparison between Equations [11] and [12]

Table III

t- and F-test results

Equation no.	Tabulated *t*-value	*t*-value	Tabulated *F*-ratio	*F*-ratio
10	± 2.36	4.27	4.60	18.11
11	± 2.36	2.71	4.60	6.22

are greater than the tabulated *t*-values for Equations [10] and [11]. Equation [10] and [11] are therefore valid according to the *t* -test.

The significance of regressions was determined by analysis of variance. In this test, a 95% level of confidence was chosen. If the computed *F*-value is greater than tabulated *F*-value, the null hypothesis is rejected, and there is a real relation between the dependent and independent variables. Since the computed *F*-values are greater than the tabulated *F*-values for Equations [10] and [11], the null hypothesis is rejected (Table III). Therefore, it is concluded that Equations [10] and [11] are valid according to the *F*-test.

Conclusions

The prediction of specific energy (SE) from three different brittleness concepts was investigated for metallic ores such as chromite, haematite, galena, and smithsonite. It was concluded that there is no correlation between SE and the brittleness B_3. However, strong correlations were found between SE and brittleness concepts B_5 and B_8. The derived equations were also checked by the *t*- and *F*-tests and the models were shown to be valid. It was concluded that SE in ore cutting can be reliably predicted from brittleness concepts B_5 and B_8.

Acknowledgement

This study was supported by the Scientific Research Project Unit of Nigde University under the project number FEB 2009/04. The automatic cutting machine used for sample preparation was financed by the Alexander von Humboldt Foundation. The authors thank Professor Nuh Bilgin and his colleagues from Istanbul Technical University for their support in performing the linear cutting tests.

References

Altindag, R. 2000. The role of brittleness on the analysis of percussive drilling performance. *Proceedings of the 5th Turkish National Rock Mechanics Symposium*, Isparta, Turkey, 30-31 October 2000. pp. 105–112.

Altindag, R. 2003. Correlation of specific energy with rock brittleness concepts on rock cutting. *Journal of the South African Institute of Mining and Metallurgy*, vol. 103. pp. 163–171.

Balci, C., Demircin, M.A., Copur, H., and Tuncdemir, H. 2004. Estimation of optimum specific energy based on rock properties for assessment of roadheader performance. *Journal of the South African Institute of Mining and Metallurgy*, vol. 11. pp. 633–641.

Copur, H., Tuncdemir, H., Bilgin N., and Dincer, T. 2001. Specific energy as a criterion for the use of rapid excavation systems in Turkish Mines. *Transactions of the Institution of Mining and Metallurgy Section A: Mining Technology*, vol. 110. pp. A149–157.

Evans, I., and Pomeroy, C.D. 1966. The Strength, Fracture and Workability of Coal. Pergamon Press, London.

Goktan, R.M. 1991. Brittleness and micro-scale rock cutting efficiency. *Mining Science and Technology*, vol. 13. pp. 237–241.

Hetényi, M. 1966. Handbook of Experimental Stress Analysis. Wiley, New York.

Hucka, V. and Das, B. 1974. Brittleness determination of rocks by different methods. *International Journal of Rock Mechanics and Mining Sciences and Geomechanics Abstracts*, vol. 11. pp. 389–392.

Hucka, V., and Das, B. 1975. Laboratory investigations of penetration of complete coal series. *International Journal of Rock Mechanics and Mining Sciences and Geomechanics Abstracts*, vol. 12. pp. 213–217.

Mcfeat-Smith, I. and Fowell, R.J. 1979. The selection and application of roadheaders for rock tunneling. *Proceedings of the Rapid Excavation and Tunnelling Conference*, Atlanta, GA. Maevis, A.C. and Hustrulid, W.A. (eds). AIME. pp. 261–279.

Morley, A. 1944. Strength of Materials. Longman, London.

Obert, L. and Duvall, W.I. 1967. Rock Mechanics and the Design of Structures in Rock. Wiley, New York.

Protodyakonov, M.M. 1962. Mechanical properties and drillability of rocks. *Proceedings of the 5th Symposium on Rock Mechanics*, University of Minnesota. Fairhurst, C. (ed.). Pergamon Press, Oxford. pp. 103–118.

Ramsay, J.G. 1967. Folding and Fracturing of Rocks. McGraw-Hill, London.

Rostami, J., Ozdemir, L., and Neil, D.M. 1994. Performance prediction: a key issue in mechanical hard rock mining. *Mining Engineering*, November 1994. pp. 1263–1267.

Singh, S.P. 1986. Brittleness and the mechanical winning of coal. *Mining Science and Technology*, vol. 3. pp. 173–180.

Singh, S.P. 1987. Criterion for the assessment of the cuttability of coal. *Underground Mining Methods and Technology*, vol. 8. pp. 225–239.

Tiryaki, B. and Dikmen, A.C. 2006. Effects of rock properties on specific cutting energy in linear cutting of sandstones by picks. *Rock Mechanics and Rock Engineering*, vol. 39, no. 2. pp. 89–120.

Tumac, D., Bilgin, N., Feridunoglu, C., and Ergin, H. 2007. Estimation of rock cuttability from shore hardness and compressive strength properties. *Rock Mechanics and Rock Engineering*, vol. 40, no. 5. pp. 477–490.

Yagiz, S. 2009. Assessment of brittleness using rock strength and density with punch penetration test. *Tunneling and Underground Space Technology*, vol. 24. pp. 66–74. ◆

http://dx.doi.org/10.17159/2411-9717/2016/v116n8a9

The globalization of the South African mining industry

by I. Robinson*

Synopsis

In 1990 the South African mining industry was predominantly domestically based and was dominated by six mining houses, which all had their head offices in Johannesburg with their primary listings on the Johannesburg Stock Exchange (JSE). However, radical changes in the domestic and international political and economic environments during the 1990s resulted in the demise of the domestic mining house system and the two largest mining houses, Anglo American and Gencor (which was incorporated into Billiton) moved their head offices and primary listings to London.

Unfortunately, this move led to massive disinvestment from South African mining and industrial assets by both Anglo American and BHP Billiton. It also resulted in a loss of financial and technological capacity, which during the last century had made a massive contribution not only to the mining industry but also the development of the manufacturing industry. After their London listings both these companies placed their international interests well above the national interests of the host country, South Africa. This raises serious questions regarding foreign ownership of the South African mining industry.

Thus, although foreign-owned companies are still playing an important role, the history of our mining industry during the new century suggests that South Africa should not place excessive reliance on foreign-based companies to develop its mining industry and national economy.

Keywords
mining houses, Anglo American, BHP Billiton, globalization, foreign ownership, disinvestment.

The road to London

South Africa's mining industry has undergone drastic changes since the 1980s. There has been a persistent decline in the economic viability of the most important sector and the foundation on which the mining house system had been based – the gold industry. In real terms the rand gold price started to fall from 1987 and the working profit per ton of ore milled declined from R182 600 in 1981 to R41 200 in 1993, expressed in 1990 prices (Nattrass, 1995). Despite only a small decline in production from 655.8 t in 1981 to 619.3 t in 1993, gold's contribution to South Africa's exports fell from 45.7% to 28.3%.

Over-staffing of head offices added significantly to rising overheads on the mines, and one of the first casualties of the decline in the gold industry in the early 1990s was engineering capabilities. Mining houses were paying for engineering staff that they were not fully using, and many engineers were eventually transferred to specialist engineering companies.

The release of Nelson Mandela in February 1990, which represented the first step on the road to democracy in South Africa, signalled the beginning of the end of isolation for the South African mining industry. South Africa's emergence from isolation exposed its mining industry to changes in the global mining industry and changes in investor perceptions, from which it had been protected during the previous decade by isolation and sanctions. The conglomerate corporate structure, which had been popular internationally during the 1960s and 1970s, came under increasing attack and London brokers identified the mining house system as a value trap. London brokers and banks complained that the mining houses were charging excessive fees for their services to Group mines – fees that could be paid out as dividends to shareholders.

Investors therefore placed massive pressure on South African mining houses to break up their conglomerate structure to become focused mining companies. The process started in 1985 when, following an analysis of Gencor's management structure by the American consultancy firm Arthur D. Little, Derek Keys was appointed the new chairman of Gencor to replace Ted Pavitt. At the time, commerce, industry, and finance contributed about half of Gencor's income. Keys' appointment was the beginning of a new

* *PhD University of the Witwatersrand, Johannesburg, South Africa.*
 ISSN 2225-6253. Paper received Dec. 2013; revised paper received Mar. 2016.

era for Gencor, which led inexorably to its internationalization as he embarked on a new strategy of 'unbundling' in order to get rid of the conglomerate structure that was alleged to be responsible for the discount in the value of a pyramid organization. The unbundling process involved the sale of non-core, non-mining divisions and enabled Gencor to focus fully on its core business – mining.

Gencor's example of unbundling its non-mining assets was followed by other mining houses in the 1990s. In September 1992, the Barlow Rand industrial and mining conglomerate announced a restructuring that dismantled the Rand Mines mining house, and in 1996 Anglovaal split the group into two companies – industrial and mining. Anglo American clung to its conglomerate structure longer, but undertook an immense re-organization over two years prior to its move to London in May 1999 in order to make itself marketable as a focused global natural resources player.

The decline in the gold industry and the lack of major new mineral discoveries meant that new opportunities for mining and metallurgical projects in South Africa were limited, which encouraged the mining houses to look for expansion opportunities offshore. Political uncertainty and the legacy of distrust between the African National Congress (ANC) and the mining houses provided a further incentive for the mining houses to move offshore, and Mbeki (2009) alleged that there was an agreement between South Africa's 'economic oligarchs, that handful of white businessmen and their families who control the commanding heights of the country's economy, that is, mining and its associated chemical and engineering industries and finance' and 'the leaders of the black resistance' to pay reparations by introducing Black Economic Empowerment (BEE).

Aluminium played a pivotal role in the internationalization of Gencor. Gencor decided to build a massive new smelter at Richards Bay, and this smelter would need to secure adequate supplies of alumina feedstock. One of the potential suppliers was Billiton, based in the Netherlands, which had diverse global assets in the aluminium sector. Billiton was owned by the oil major Shell and, like most of the oil majors at that time, Shell saw its mining portfolio as a non-core business. Negotiations were concluded on 1 December 1995 when Gencor acquired Billiton.

Gencor's acquisition of Billiton was made much more difficult by the exchange controls in force, which limited the sums that Gencor could export to finance the deal. However, Gencor chairman Brian Gilbertson was able to persuade the South African Reserve Bank and the Cabinet to permit the export of the required sums, and in July 1997 Gencor separated its international and South African businesses when it created a wholly-owned London-based company, Billiton plc, leaving only the gold and platinum interests with Gencor Limited, still based in Johannesburg. In March 2001 Billiton merged with the Australian mining group BHP to establish a diversified global resources group, BHP Billiton. BHP Billiton would be run by a unified board with its headquarters in Melbourne, with primary listings on the London and Melbourne stock exchanges and a secondary listing on the JSE. Paul Anderson was the first CEO, with Brian Gilbertson deputy CEO.

In contrast to Gencor, which entered the international arena only in the 1990s, Anglo American had begun its expansion beyond South Africa in the 1920s when it commenced exploration activities in Zambia leading to the discovery of Zambian Copperbelt. The nationalization of the Zambian copper mines at the end of the 1960s forced Anglo to seek alternative sources of base metals and provided capital for the creation of the Minerals and Resource Corporation (Minorco), an offshore company that Anglo used for international acquisitions. The first Anglo American investment outside the African continent was in Canada in 1961, and more than ten years lapsed before Anglo made its second major overseas investment when it acquired a 49% stake in the Morro Vehlo gold mine in Brazil in 1975. During the 1960s and 1970s the closed economy in South Africa had forced Anglo to diversify beyond mining into every sphere of the South African economy, but expansion in South America began in earnest at the end of the 1970s and early 1980s.

White (2008) noted that 'South America provided, to all intents and purposes, an ideal haven for Anglo', and by the late 1990s Anglo American South America (AMSA) had become the largest mining company in South America. 'These (South American) countries' willingness to open their mining sectors to FDI, and their clear commitment to sensible and sustainable economic policies was an attractive "pull" factor that encouraged ongoing investments from Anglo over an extended period of time. Meanwhile, the politically averse and severely challenging operating environment in Africa provided sufficient "push" for Anglo to seek alternative mining opportunities elsewhere and pursue its natural ambition as a truly international mining giant, constantly striving to improve its competitive and strategic capabilities and above all achieve maximum profits' (White, 2008).

In 1996 Anglo American chairman Julian Ogilvie Thompson commented that 'while we see our future as a *mining house rooted in South Africa and are committed to seeking every opportunity of expansion at home* new opportunities opening up in Africa and internationally will facilitate a determined expansion of our mining and selected industrial interests abroad'.

Ogilvie Thompson's 1996 vision of Anglo American as 'a mining house rooted in South Africa' proved to be of short duration, as in May 1999 Anglo American transferred its head office to London and its primary listing to the London Stock Exchange (LSE). White (2008) observed that 'in South Africa, the government and general public interpreted this (transfer of head office) less as a cold business decision that enabled Anglo to better manage its diversity of international interests than a clear expression of Anglo's lack of confidence in the country'.

Ogilvie Thompson (1999) paid tribute to 'the support of the South African government in establishing Anglo American as a global resources company', adding that 'its far sighted understanding of the imperatives of globalization has been rewarded by a growing confidence in South Africa as a

leading emerging market'. He committed Anglo American to '*continue to expand and grow its businesses in South Africa and those other parts of the world that are prospective*'.

Criteria for offshore listings

In a paper in the quarterly bulletin of the South African Reserve Bank (SARB) in September 2002, Walters and Prinsloo evaluated the impact of foreign listings on the South African economy. The companies wishing to change their primary listings argued that offshore listings offered certain advantages that they would be denied if they maintained a primary listing on the JSE. Some of these advantages were:

- Easier access to capital resources at lower cost
- Opportunities to raise efficiencies by competing head-on with global competitors
- The opportunity to promote foreign investment in South Africa
- The opportunity to expand their core business into other countries and regions
- The opportunity to improve South Africa's profile internationally.

The exchange control authorities set guidelines in order to decide whether to grant permission for overseas listings. These included:

- Foreign expansion was necessary and integral to the firm
- There would be definite balance-of-payment benefits to South Africa
- There would be a substantial advantage over alternative approaches to raising the required capital
- South Africa's gross international reserves would not be adversely affected by a net outflow of dividends or any other funds
- All the South African operations and assets of the company would remain in South Africa

The analysis by Walters and Prinsloo was not confined to mining companies (Billiton and Anglo American), but also included South African Breweries, Old Mutual, and Dimension Data. The authors concluded:

'From a macroeconomic perspective it can be argued that the domestic economy was not excessively sensitive to the relocation of the primary listing of South African companies from Johannesburg to London. As all the South African companies that obtained primary listings on the LSE still have secondary listings on the JSE, the market capitalization of the JSE has not been affected adversely by the listings on a foreign stock market. In addition, *none of the companies listed have terminated any of their operations in the geographic area of South Africa*, leaving the aggregate size of the gross domestic product largely unaffected. *The likely expansion of offshore-listed companies in future years in South Africa may give extra impetus to economic growth*'.

However, Walters and Prinsloo's conclusions regarding termination of operations in South Africa and the likely expansion of offshore-listed companies in South Africa proved to be wishful thinking.

BHP Billiton

In 1990 Gencor, based in Johannesburg derived only 45% of its income from mining operations (Stear and Clay, 1992). Gold and platinum each contributed about one-fifth to total mining income, coal contributed 7%, and all other minerals contributed over half.

Following Billiton's listing in London in July 1997, Gencor separated its gold and platinum interests, which remained in South Africa, but all its other mining interests were effectively placed under foreign control when Billiton plc issued shares to acquire the parent company's interests in Alusaf, Samancor, Ingwe Coal, Richards Bay Minerals (RBM), Billiton International, the base metals assets, and the trading businesses. All the platinum interests were housed within Impala Platinum, which became an independent company in early 1998. Effective 1 January 1998, Billiton disposed of its gold interests when Gencor merged its gold assets with those of Gold Fields of South Africa (GFSA) to create a new gold company, Gold Fields Limited. Brian Gilbertson became the first chairman of the new company.

At the end of 2013, BHP Billiton's assets in South Africa were limited to three commodities: aluminium, manganese, and coal. On 19 August 2014 BHP Billiton announced plans to create an independent global metals and mining company, South32, based on a selection of its alumina, aluminium, coal, manganese, nickel, silver, lead, and zinc assets. All BHP Billiton's southern African (South Africa and Mozambique) assets were transferred into South32, with its headquarters in Perth, Australia.

BHP Billiton's major contribution to the growth of mining/metallurgical production capacity in the Southern African Development Community (SADC) had been in aluminium. In September 2000 Billiton opened the Mozal aluminium smelter in Mozambique and during its financial year (FY) 2003 the company doubled Mozal's annual capacity from 250 kt to 500 kt. BHP Billiton made a further massive investment in aluminium smelter capacity in southern Africa when it added a third potline at its Hillside smelter at Richards Bay during 2004, raising annual capacity from about 500 kt to a nominal capacity of 704 kt. Production of aluminium in FY 2015 was 265 kt at Mozal and 699 kt at Hillside.

BHP Billiton also increased the capacity of its manganese mining and alloy operations in South Africa, which are now controlled by South32. South Africa Manganese comprises Hotazel Manganese Mines (HMM) and Metalloys. HMM has two operations, the Wessels and Mamatwan mines, and production of ore reached a record level of 1 636 kt during FY 2015. At Metalloys, a new furnace (M14) was completed in March 2013 which added 130 kt/a capacity of high-carbon ferromanganese but replaced the now closed 120 kt/a silico-manganese South Plant, taking Metalloys' total capacity to 500 kt/a. Production in FY 2015 was 246 kt.

In FY2007 (year ended 30 June) BHP Billiton's wholly–owned South African coal subsidiary BHP Billiton Energy Coal South Africa (BECSA) operated six coal mines in Mpumalanga which supplied 30 Mt to Eskom and exported

the bulk of the remaining 22 Mt produced. However, production fell drastically after the sale of Optimum mine to local buyers in early 2007. During FY 2009 the Group disposed of other coal interests in South Africa – the Koornfontein mine, an interest in the Eyesizwe mine, and 1 Mt/a of capacity at the Richards Bay Coal Terminal. The Douglas-Middelburg optimization project, which was completed in July 2010, was a replacement project to enable the Group to maintain energy coal exports at about 10 Mt/a while also fulfilling its domestic contractual obligations. BECSA's total production in FY2013 was 30.4 Mt, a decline of over 40% compared to the FY2007 level.

South32's subsidiary South Africa Energy Coal now operates four coal mines (Khutala, Klipspruit, Middelburg, and Wolwekrans) and three processing plants. Total production in FY2015 was 34.3 Mt.

Before transferring its aluminium, manganese, and coal assets to South32, BHP Billiton had drastically reduced its footprint in South Africa and reduced South Africa's domestic ownership and control of its mining industry.

After its London listing, Billiton moved swiftly to internationalize its chrome and manganese businesses through the takeover of the leading South African ferro-alloys producer Samancor. In December 1998 Samancor was de-listed from the JSE and established as the vehicle for Billiton's global manganese and chrome businesses. Billiton's manganese division became the global industry leader when Billiton and Anglo American acquired the manganese assets of the Broken Hill Proprietary Company (BHP Manganese) in Australia.

In order to align Samancor Chrome's marketing division with its new international profile, Billiton transferred members of the former marketing department of Samancor, which had been based in Johannesburg, to the Hague in Holland. However, BHP Billiton's commitment to chrome did not last long and in June 2005 it sold its majority interest in Samancor Chrome to the Kermas Group, a company domiciled in the UK with substantial interests in the chrome industry in Kazakhstan.

In 2001 BHP Billiton announced the sell-down of its interest in the Columbus Stainless Steel Joint Venture, which was acquired by Spanish producer Acerinox.

South Africa's subservient role in the BHP Billiton group was demonstrated in December 2008 when, on instructions from Melbourne, the Johannesburg office closed its Information Centre and its R&D facility adjacent to Mintek in Randburg. These facilities did not conform to the Group's business model.

The decline in South Africa's role in BHP Billiton's global business was reflected in the decline in South Africa's percentage contribution to its global revenue and in the number of employees. In FY 2013 South African coal contributed only 2% of the Group's total annual revenue; aluminium (South Africa and Brazil) contributed 3%, and manganese (South Africa and Australia) also contributed 3%. As the revenue earned by the aluminium and manganese operations is not broken down according to country, it is not possible to accurately estimate South Africa's percentage contribution to BHP Billiton's global revenue in FY 2013, but it was probably about 6%.

There was also a sharp fall in the number of BHP Billiton's employees in southern Africa, from 15 928 in FY2004 to 9 280 in FY2013 – a fall of over 40%.

Anglo American

In 1990 Anglo American, based in Johannesburg, derived only 54% of its income from mining operations (Stear and Clay, 1992). Gold contributed about one-third of Anglo American's income from mining, diamonds approximately one-quarter, and other minerals about 40%, with coal's contribution only 4%.

Like BHP Billiton, Anglo American took the path of reducing its assets in South Africa following its listing on the LSE in May 1999 as it progressively refined what it considered to be its core business. Nevertheless, it retained a much larger presence in South Africa than BHP Billiton and, to some extent, compensated for the disposal of its non-core assets in South Africa through acquiring control of Kumba Iron Ore and maintaining a strong presence in other commodities that were considered to be core businesses – platinum, coal, and diamonds.

One of Anglo American plc's first actions was to dismantle the Anglo American/De Beers crossholding, and De Beers was then controlled by three shareholders – Anglo American (45%), Central Holdings (40%, representing the Oppenheimer family), and the Government of the Republic of Botswana (15%). De Beers de-listed from the JSE in 2001 and became a private company no longer administered by Anglo American.

However, in August 2010 Anglo American completed its acquisition of Central Holdings' 40% share of De Beers, thereby increasing its holding to 85% and regaining control of the company.

De Beers, too, had progressively disposed of its assets in South Africa. After completing a full feasibility study in 2001, De Beers decided that it would not proceed with the C-Cut project (estimated to cost R10 billion) at its Premier mine and put the mine up for sale in October 2007. The mine was acquired by Petra Diamonds, based in the UK. At the end of 2010 De Beers had reduced the number of operations in South Africa from seven in 2005 to only three (Venetia, Voorspoed, and the Combined Treatment Plant outside Kimberley), and in mid-2015 also sold the Kimberley operation. However, in November 2013 Anglo American made another major (R20 billion) commitment to South Africa when De Beers commenced development of the Venetia Underground Project.

In January 2002, Anglo American's global interests prevailed over its historic ties to Africa when it withdrew from the Konkola Deep copper project in Zambia. However, the company renewed its commitment to southern Africa in 2003 when it commissioned the Skorpion zinc project in Namibia.

In October 2005 Anglo American announced the outcome of its strategic review, which concluded that the Group should focus on its core mining portfolio. Boart Longyear and Anglo's interest in Samancor Chrome were sold in mid-2005.

One of the decisions resulting from the strategy review was to reduce the Group's shareholding in AngloGold Ashanti, and in July 2006 Anglo disposed of its majority stake in Highveld Steel and Vanadium, leading to the takeover of the company by Luxembourg-based Evraz, controlled by Russian oligarch Roman Abramovich.

After a long series of disinvestments, in November 2006 Anglo committed itself to a new project in South Africa when it listed Kumba Iron Ore, in which it held a 64% share, on the JSE.

However, Anglo re-affirmed its de-South Africanization and globalized status when on 1 March 2007 Canadian citizen Cynthia Carroll succeeded Tony Trahar who retired as chief executive.

Anglo continued to dispose of its non-core South African assets during 2008. In October it completed the sale of its Namakwa Sands mineral sands business to Exxaro Resources, and in November sold its interests in both the Black Mountain lead-zinc-copper operation and Gamsberg zinc project, also to Exxaro. In March 2009 Anglo sold its remaining share in AngloGold Ashanti.

In February 2009 Anglo announced that it had suspended dividends for the first time since 1939 and that it would cut 19 000 jobs worldwide, with 10 000 of these jobs lost at its South African subsidiary and 9 000 at operations spread around the world. When this move attracted criticism from South Africa from ex-Anglo staff who questioned the company's decision to abandon diversification in South Africa in favour of becoming a globally focused mining company, Anglo spokesman Nick von Schirnding asserted that the company's current strategy, to be a focused mining company with interests primarily in platinum, coal, diamonds, base metals and iron ore, 'is very clear and *endorsed by our institutional shareholders*' (Rose, 2009).

In October 2012 Cynthia Carroll announced her intention to resign as CEO, and she was replaced by Mark Cutifani, formerly CEO of Johannesburg-based AngloGold Ashanti and also president of the South African Chamber of Mines for the year 2013. In South Africa, the Public Investment Corporation (PIC) and the Government Employees Pension Fund (GEPF) issued a joint statement in response to Carroll's resignation (*Star Business Report*, 2012). The PIC was the largest South African shareholder in Anglo American, with a holding of 7% of the shares on behalf of the GEPF. The PIC-GEPF statement accused Carroll of 'a disappointing operational performance' and because 'around 37 per cent of group assets are still based in South Africa and generate 55 per cent of group operating profit .... the composition of the board (should be) more reflective of the geographic positioning of the company'.

Anglo's operations both in South Africa and worldwide are supported by R&D conducted by the Anglo Technical Division, which is based in Booysens, Johannesburg.

Anglo still produces four commodities in South Africa – platinum, coal, iron ore, and diamonds – and during calendar year (also FY) 2015 69% of Anglo's total global expenditure was spent in South Africa, followed by Chile with 11% and Brazil with 10%.

However, in December 2015, in response to a collapse in global commodity prices Anglo announced plans to sell 60% of its assets and was expected to reduce its global workforce by about 85 000 over the next few years to only 50 000. The company would now focus on only three commodities – platinum, diamonds, and copper. In February 2016 it announced that it would sell its coal assets and Kumba Iron Ore. This would reduce Anglo's involvement in South Africa to only two commodities – platinum and diamonds. Its subsidiary De Beers now has only two operating mines in South Africa – Venetia and the much smaller Voorspoed in the Free State.

After resuming the payment of dividends in 2010, Anglo announced that it would not pay dividends for the second half of 2016 and during the whole of 2017.

Disadvantages of foreign ownership

Foreign ownership of companies involves four major disadvantages to the host country relative to domestic ownership:

- International interests prevail over national interests
- May limit opportunities for local investors
- Development is restricted to mining projects
- Countries lose their 'economic champions'.

International interests

The record of BHP Billiton and Anglo American in South Africa since their overseas listing in the late 1990s highlights how international interests prevail over national interest when companies are foreign-owned. Divestment from all projects apart from those regarded as 'core business' is dictated by their head offices overseas. In contrast, the old mining houses (which were domestically-based conglomerates) did not limit themselves to 'core businesses' and would not have disposed of profitable businesses.

Overseas operations must conform to the parent companies' business models, which are ruthlessly imposed. BHP Billiton had no compunction about breaking up the giant South African ferro-alloys producer Samancor (which had its origins in Amcor, which was established in 1937) to suit its international interests and closing the Information Centre in Johannesburg.

Operations are also vulnerable to the perceptions of overseas investors; for example, the frequent complaint of London investors that 'Anglo American is too exposed to South Africa'.

Arcelor Mittal's record in South Africa has highlighted the potential dangers of foreign control of strategic domestic assets. In 2001 the London-based Arcelor Mittal, headed by its founder Lakshmi Mittal, gained control of the former state-owned steel producer Iscor. Since its takeover of Iscor Arcelor Mittal has shown itself to be totally insensitive to

local and national interests, while Lakshmi Mittal himself indulged his personal family interests on a scale that dwarfed his commitment to his company's employees. It has been alleged that Lakshmi Mittal spent approximately as much money on his daughter's wedding in London in 2004 as it would have cost to completely rehabilitate the highly polluted area around the Vanderbijl steel plant known as 'Steel Valley' (Armstrong, 2010). Furthermore, the company has turned a deaf ear to the government's plea to discuss a pricing system ('developmental pricing') for steel that would promote industrial development through supplying cheaper steel to domestic manufacturing companies.

Local investment

When foreign-based companies do not list on local stock exchanges, local investors (both individuals and institutions) are deprived of opportunities to invest in the development and growth of companies in their own countries. Furthermore, because of limited access to journalists and analysts, these companies are not subject to public scrutiny. Foreign-based companies operating large projects in South Africa and which are not listed on the JSE include Kermas, South Africa's largest ferrochrome producer and Acerinox, South Africa's only stainless steel producer. Without exposure to public scrutiny, it is impossible to know whether the foreign owners are operating these large projects to favour national or their own international interests.

Therefore, the secondary listing of Glencore Xstrata on the JSE on 13 November 2013 was particularly welcome. The company was the fourth largest global mining company and had its primary listing on the LSE. The company had a diversified portfolio across 50 countries and interests in coal, chrome, vanadium, and platinum (via a 25% share in Lonmin) in South Africa.

Linkages

Whereas domestically based companies tend to widen their investment horizons in their own countries beyond their original projects, overseas-based companies tend to confine their investments to specific projects. The mining houses made a major contribution to the manufacturing industry in South Africa through linkages emanating from the needs of the mining industry. Two examples of manufacturing industries established by Anglo American are AE&CI and Boart & Hard Metals. AE&CI was formed by a merger between African Explosives and ICI in 1924 and, through diversification into a wide range of chemical products, had become South Africa's largest industrial company by 1969. Anglo established Boart & Hard Metals in 1936 to investigate uses and markets for industrial diamonds. It developed the use of industrial diamonds in drilling applications, and after the Second World War expanded into the related fields of carbide cutting tools and abrasives.

From its foundation in 1933, Anglovaal 'resolved to give as much attention to establishing secondary industries as to mining' (Anglovaal, 1970). Industrial projects established by Anglovaal included Anglo Alpha Cement, Irvin & Johnson, and Consolidated Glass.

Innes (1984) observed that AE&CI and Boart & Hard Metals were classic examples of how 'the development of a major primary industry can set in motion a number of industries which are initially totally dependent on it but which subsequently branch out into other fields and become relatively more independent. However, as these cases suggest, it is the existence of the primary industry which is the sine qua non of industrial growth'.

Thus, the offshore listings of its two largest mining houses and the demise of the domestic mining house system has deprived South Africa of enormous financial and technical capacity for the development of the country beyond the narrow confines of the mining industry.

Loss of our champion

Anglo American, born in South Africa in 1917, became the dominant mining company and economic power in South Africa during the second half of the 20th century. In 1976, Anglo group companies held top positions in all South Africa's economic sectors except agriculture – these being mining, manufacturing, property, and finance (Innes, 1984). Anglo had the capacity and the drive to tackle highly complex projects such as Highveld Steel and Vanadium. Innes wrote how during the late 1950s Anglo had expressed an interest in developing South Africa's vast vanadium resources and, after buying Transvaal Vanadium Company, the only company in South Africa at the time engaged in the production of vanadium pentoxide, undertook intensive research and in 1963 built a full-scale plant, becoming one of the largest vanadium producers in the world and the second largest producer of steel (after Iscor) in South Africa. It is difficult to imagine that any private company in South Africa today would have the capacity to tackle a project of comparable size and complexity.

In an interview with the Financial Mail in 1969, Harry Oppenheimer said 'I think if there had never been exchange control, we would probably have expanded more in overseas mining ..... Of course we would have participated actively in industrial development but in the absence of exchange control the emphasis would have been more on sticking to mining, wherever it was in the world, *and building up an international mining house based in South Africa*'.

The flight of Anglo American's head office and primary listing to London is in marked contrast to the Australian government's approach to the possibility that after its merger with Billiton, the head office of the 'Big Australian' BHP, Australia's largest mining company, might move to London. Pressure by the Australian government ensured that BHP Billiton's remains 'headquartered in Australia' (as proudly proclaimed on the company's letterheads).

Conclusions

The imbalance between BHP Billiton's and Anglo American's disinvestment from existing projects and investment in new projects since their London listings in the late 1990s and transfer of their head offices overseas has made a mockery of Walters and Prinsloo's expectation that 'the likely expansion

of offshore-listed companies in future years may give extra impetus to economic growth'. It appears that the government exchange control authorities who gave permission for these overseas listing did not foresee the total dominance that the international interests of these companies would have over South Africa's national interests.

There is currently an intense national debate over the proposed Minerals and Petroleum Resources Development Amendment (MPRDA) Bill and the need to attract foreign investment in the South African mining industry. There is concern over the South African mining industry's poor rating as an investment destination by the prestigious Fraser Institute based in Vancouver, Canada.

Politicians and commentators are fond of quoting the Citi report of April 2010, which estimated that South Africa is the richest country in the world in terms of the *in situ* value of its mineral reserves. The implication of quoting this report is that because it is endowed with such mineral wealth, South Africa should be a very attractive destination for foreign investors in its mining industry. However, this is a simplistic conclusion and a more careful reading of the report gives cause for concern as it shows that platinum reserves comprise 90% of the total value of South Africa's *in situ* reserves. Therefore, South Africa's mineral wealth apart from platinum – according to the Citi report – is limited. However, the Citi report does not reflect the full picture as South Africa's chrome, manganese, and vanadium resources, which play such an important role in actual and potential beneficiation projects, are not included in the mineral reserve estimates.

However, even if the legislation and the jurisdiction were improved to make South Africa a more attractive destination for foreign investment in the mining industry, the records of BHP Billiton and Anglo American suggest that such investment would always be constrained by the companies' international interests, and investors would be reluctant to expand operations beyond the narrow interests of their mining projects or specialized metallurgical projects (such as ferrochrome).

The proposed MPRDA Amendment Act places much emphasis on the promotion of minerals beneficiation. However, the reaction of many of the mining companies is that mining – not beneficiation – is their business. This is in strong contrast to the mining houses' attitude before the demise of the system in the 1990s, when they actively sought opportunities to develop beneficiation projects.

Thus, South Africa has lost much of the private sector's capacity to beneficiate its mineral production and most of the burden now falls on the State. The Industrial Development Corporation (IDC) has a proud record of promoting beneficiation through its involvement in projects such as Alusaf and Sasol, and could play a major role in future beneficiation projects.

This analysis has shown that although foreign-owned companies are still playing an important role in the South African mining industry, South Africa cannot place excessive reliance on foreigners to develop our mining industry. While foreign investment can make an important contribution to our mining industry and, therefore, we should endeavour to make South Africa an attractive destination for foreign investment, it is not a panacea and we should not rely on foreign-owned companies to develop our mining industry.

South Africa needs to take responsibility for developing its own mineral resources and beneficiating its mineral production through partnerships between domestically based companies and the State, with foreign-owned companies playing a supplementary rather than a principal role.

References

Anglovaal. 1970. A South African financial, industrial and mining group. Anglovaal Today.

Armstrong, S. 2010. The Super-Rich shall Inherit the Earth. *Constable and Robinson*, London. p. 8

CITI. 2010. Metals & Mining Strategy – The Richest Country in the World is....? 26 April 2010.

Financial Mail. 1969. Special Survey. *Inside the Anglo power house*. p. 10.

Innes, D. 1984. Anglo American and the Rise of Modern South Africa. Ravan Press, Johannesburg. pp. 176, 195, 221.

Mbeki, M. 2009. Architects of Poverty – Why African Capitalism Needs Changing. Picador Africa, Johannesburg. p. 66.

Nattrass, N. 1995. The Crisis in South African Gold Mining. University of Cape Town. pp. 858, 859.

Ogilvie Thompson, J. 1996. Anglo American Annual Report – Chairman's Statement.

Ogilvie Thompson, J. 1999. Anglo American Annual Report – Chairman's Statement.

Rose, R. 2009. Former Anglo bosses are grumbling. *Business Times*, 4 July 2009.

The Star Business Report. 2012. PIC, GEPF support resignation of Anglo's Carroll. 28 October 2012.

Stear, W.M. and Clay, A.M. 1992. Project Phoenix. A Venmyn Rand report commissioned by Gold Fields of South Africa (GFSA). Figure 4A.

Walters, S.S. and Prinsloo, J.W. 2002. The impact of offshore listings on the South African economy. *SA Reserve Bank Quarterly Bulletin*, September.

White, L. 2008. The case of Anglo American Corporation in Latin America. PhD thesis, University of Cape Town. pp. 51, 52, 53, 75, 76. ◆

http://dx.doi.org/10.17159/2411-9717/2016/v116n8a10

A systems approach to mining safety: an application of the Swiss Cheese Model

by J. Bonsu*, W. van Dyk†, J-P. Franzidis*, F. Petersen‡, and A. Isafiade*

Synopsis

Achieving zero harm in the mining industry is still a big challenge worldwide. A potential major step towards remedying the situation is a good understanding of the processes that lead to accidents in the industry. The Swiss Cheese Model has had a significant impact on the understanding of the causes of accidents in high-risk industries. In this paper, an accident analysis framework based on the Swiss Cheese Model is developed and tested against a previous mining disaster. The developed framework has the potential to enhance the understanding of the factors that contribute to accidents in the mining sector.

Keywords

Safety, accident causality, risk assessment, Swiss Cheese Model, analysis framework.

Introduction

It is well known that safety is still a big challenge in mining operations worldwide. This assertion is supported by recent mining disasters such as the Crandall Canyon disaster in the USA (6 August 2007), the Harmony Gold mine deaths in South Africa (June, 2009), the Soma mining disaster in Turkey (May, 2014), the Chile mining accident (5 August 2010), and the Xiaojiawan coal mine disaster in China (29 August 2012). Although mining employees represent only 1% of the global workforce, they account for about 8% of workplace fatalities. Workplace injuries in the mining industry worldwide have also been reported to be very high by the International Labour Organization (ILO, 2010).

The understanding of accident causality is a major step in the quest to reduce accidents. Accident modelling techniques provide the necessary platform for the interpretation and understanding of accidents at workplaces. Accident models provide a conceptualization of the characteristics of the accident process by showing the relationship between causes and effects. They explain why accidents occur, and are used as techniques for risk assessment during system development (Qureshi, 2008). During accident investigations, accident models impose patterns on the understanding of the accidents and influence both the data collected and the factors identified as causative. Since accident models influence the factors considered in any accident investigation, they may either act as a sieve and bias toward allowing for only certain events and conditions, or they may broaden the scope of the investigation by forcing consideration of factors that are often left out (Leveson, 2004). The importance of accident models in the quest for safer work environments makes the choice of the right model a crucial decision.

The Swiss Cheese Model developed by Reason (1990) is widely known for its contribution to the understanding of the factors that need to be considered during the investigation of accidents in a complex system. The model incorporates the basic components of all successful production systems such as decision-makers, line management, preconditions for effective work, production activities, and safeguards against known hazards. Effective production is achieved only when the right decisions are taken at each level of the production system. Under certain circumstances, the accident process starts when fallible decisions taken at the executive and management level are propagated through the various components of the production system. These decisions create 'holes' in the barriers put in place to prevent accidents. An accident is likely to occur when holes in the various layers of safeguards line up for the accident trajectory to be complete.

Although the Swiss Cheese Model is generally accepted as being able to depict situations leading to accidents in production systems, it has also been criticized as lacking sufficient details for practical applications

* *Department of Chemical Engineering, University of Cape Town, South Africa.*
† *Arete Consultants (Pty) Ltd.*
‡ *Faculty of Engineering and the Built Environment, University of Cape Town, South Africa.*
 ISSN 2225-6253. Paper received Apr. 2015; revised paper received Feb. 2016.

(Shappell and Wiegmann, 2000). A further publication by Reason, Hollnagel, and Paries (2006) admitted that the Swiss Cheese Model was not intended for such details, but is a simplification intended to make it easier to understand the essential features of an accident in an organization. In an attempt to deal with this deficiency, various analysis techniques based on the Swiss Cheese Model have been developed to meet the specific needs of various industries. Examples of such techniques available in the literature are the Human Factor Analysis and Classification System (HFACS) by Wiegmann and Shappell (1997), the Incident Cause and Analysis Model (ICAM) by de Landre *et al.* (2006), the Wheel of Misfortune (O'Hare, 2000), and the Behaviour Safety method (Benedyk and Minister, 1998).

In this paper an accident analysis technique applicable to the mining industry is introduced and explained. The technique is based on the ICAM model (de Landre *et al.*, 2006), which in turn is based on the Swiss Cheese model of Reason.

The accident analysis framework

An analysis framework (Figure 1) was developed to analyse accident data from the mining industry. The need for such a framework stems from the current authors' belief that existing frameworks are overly complex and do not adequately account for all the factors that contribute to accidents in the mining industry. The aim was to develop a systemic framework that is simple but applicable to accident causality in the mining context. The framework has three broad sections, namely: causal analysis, agency and barrier analysis, and metadata. The three sections of the framework are described next.

Causal section

The first section of the framework is responsible for the analysis of accident causality. Accident causality in this framework is described in a similar manner to the Mark III version of the Swiss Cheese Model (Reason, 1997). It is divided into three levels, *viz*. proximal causes, workplace factors, and systemic factors, as described below.

Proximal causes

The first level of the causal section seeks to identify the activities that lead directly to an accident. These activities usually lead to the breaking of safety barriers, leading to accidents. These are subdivided into slips and lapses, mistakes, violations, and non-human causes. The choice to stay with this categorization is due to the fact that these terminologies (slips, lapses, mistakes, and violations) are already being used in the safety parlance. These subdivisions (slips, lapses, mistakes, and violations) cover all possible ways human error can lead to accidents.

Slips and lapses are used in this framework to represent all situations in which an adequate plan fails to achieve its intended purpose due to a distraction while carrying out the original plan, or in which there is a design flaw or a change in the usual situation which is not in the knowledge of the offender. This is synonymous with 'skilled based errors' in the HFACS (Wiegmann and Shappell, 1997) framework or 'action errors' in the Wheel of Misfortune framework (O'Hare, 2000).

The term *mistake* is used in the newly developed framework to describe all situations in which a plan carried out proves to be inadequate. Mistakes are due to wrong judgement, which may in turn be due to inadequate knowledge or a wrong interpretation of a situation. *Mistake* as used in this framework is comparable to 'decision error' in the HFACS framework and 'diagnosis and procedure errors' in the Wheel of Misfortune framework.

Violations are used in this framework to describe situations where there is a deliberate attempt not to follow laid-down procedure or rules. Violations are grouped into *routine violations* and *exceptional/deviant violations*. *Routine violations* involve all the times when rules are breached to save time, reduce effort, or for any other reason; *deviant violations* are out-of-the-blue violations. Routine violations are widespread and are indicative of a flaw in the work system. These are difficult to predict and control. The same terminologies are used in the HFACS framework.

Non-human causes: This category was created to accommodate situations in which human error of the person at the workplace is not directly involved in the cause of an accident. Events such as sudden failure of equipment, structures, natural disasters *etc.*, are classified under this category.

Workplace factors

This level of the framework addresses conditions at the workplace or in the work environment that contribute or lead to human error, which in turn leads to the accident. This level

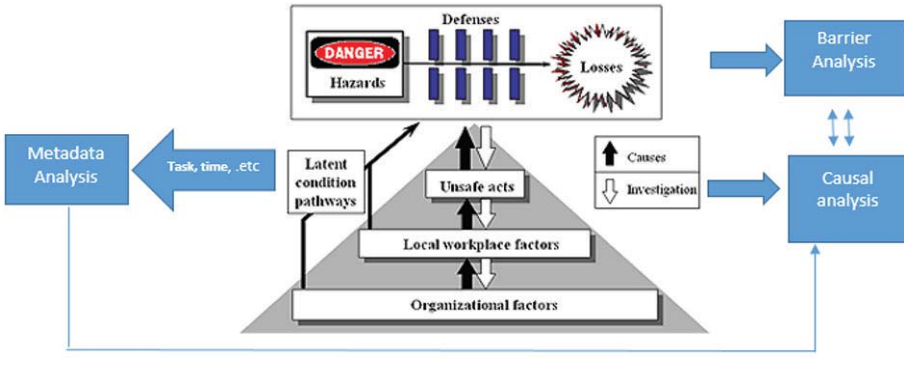

Figure 1—An analysis framework adapted from the Swiss Cheese Model

is synonymous with *pre-condition for unsafe* act in the HFACS framework (Wiegmann and Shappell, 1997, 2001), *local conditions* in the Wheel of Misfortune framework, and *task/environmental* condition in the ICAM model (de Landre, Gibb, and Walters, 2006).

The de Landre paper clearly shows nine categories under this section, *viz*. working conditions, time pressures, resources, tool availability, job access, task complexity, fitness for work, workload, and task planning. Under workplace factors, the HFACS framework identifies *adverse mental state, adverse physiological state, physical/mental limitation* (sub-categories under condition of operators), *physical environment, technological environment* (sub-categories under environmental factors), *crew resource management, and personal readiness* (sub-categories under personnel factors) as the conditions that can lead to accidents (Wiegmann and Shappell, 1997, 2001). The authors of this paper are of the opinion that the aforementioned categories are overly ramified and hence may defeat the purpose of ease of use. O'Hare (2000) also pointed out the potential conflict when incidents are to be classified under operator conditions and personnel factors.

To be able to choose factors affecting the performance of workers in the mining context, the workplace model, also known as the Nertney Wheel (Bullock, 1979), was adopted for the framework developed in this paper. The Nertney Wheel (Figure 2) identifies four components necessary for every safe and productive system, *i.e. competent people, safe work practices, fit-for-purpose equipment, and a controlled work environment*.

The newly developed framework identifies deficiencies in the above four components as ways in which workplace factors can lead to error- or violation-producing conditions, which lead to accidents or affect performance. The components are described below.

- *Competent people*—The competence of the person used for a particular task is essential for its success or otherwise. This category of the framework is intended to cater for situations in which the quality of the human resource employed leads to the committing of errors. It may be compared to *substandard conditions of operator* in the HFACS framework
- *Fit-for-purpose equipment*—is a necessity for safe production. This category is included in the framework developed in this paper to cater for situations in which the equipment used is not fit for purpose and thereby influences the output of the task or the behaviour of the operators. It is analogous to *technical environment* in the HFACS framework and *resources and interface* in the Wheel of Misfortune framework
- *Safe work practices*—Formal safe work practices, such as operating procedures, are needed for safe production in any organization. This category is included in the framework to cater for situations in which there is no standard procedure on how a particular task is to be carried out or where the standard procedures proves inadequate for safe completion of the task
- *Controlled work environment*—This category of the framework describes situations where the quality of the working environment creates error- or violation-producing conditions. It is further divided into physical and behavioural environments:
  - Physical environment includes, but is not limited to, situations such as a noisy environment, inadequate lighting, poor ventilation, and slippery floors, which could lead to error- or violation-producing conditions. This category is similar to 'physical environment' in the HFACS framework
  - Behavioural environment describes situations in which unsafe behaviours are either condoned or not frowned upon. Behavioural environment as used in this study is analogous to 'crew resource management' in the HFACS framework (which embodies poor leadership and poor coordination). Paul and Maiti (2008) found that safe behaviour is improved by the presence of a social support group.

Figure 2—The Nertney Wheel (Bullock, 1979)

Systemic factors

This layer of the framework identifies ways in which the actions of the top hierarchies of organizations contribute to an accident process. These are similar to those discussed as *organizational factors* in the ICAM model (de Landre, Gibb, and Walters, 2006). According to Reason, Hollnagel, and Paries (2006), there could be two failure pathways – active and latent. In the active failure pathway, the systemic factors create error- and violation-producing conditions in the workplace, which in turn creates errors and violations, leading to the breaching of defences and the accident. In the latent failure pathway, the systemic factors are directly responsible for the failure of the defences, and therefore no active human error is present. This level is synonymous with *organizational factors* in the HFACS framework and *global conditions* in the Wheel of Misfortune. While the last layer of the HFACS framework broadly categorizes such factors into organizational climate, resource management, and organizational process, the Wheel of Misfortune categorizes them into philosophy, policies, and procedures (O'Hare, 2000). In the view of the authors of this paper, none of the aforementioned classifications clearly identifies the exact ways in which the decisions of managers affect the behaviour of their subordinates. To achieve such an aim, elements of every good management safety management system were adopted in the newly developed framework. The authors conclude that deficiencies in these systems represent the various ways in which managements contribute to accidents. The components are discussed below.

- *Training and competence*—This category of the framework addresses situations where the training offered to a worker does not help the worker to perform the required task in a safe way. It also includes situations when a worker has not been found competent before being assigned tasks
- *Contractor management*—This involves situations where the absence of company standards regarding work performed by employees of contractor companies results in unwanted events. This includes making sure that employees of contracting companies have received the necessary training on tasks they perform and that they adhere to the safety standards of the company
- *Design*—This category of the framework represents situations when poor design of equipment or the workplace leads either directly to accidents or to physical environmental problems
- *Management of change*—Changes that occur in organizations introduce new risks into the system. This category covers situations where management's inability to appreciate the full risk that comes with a new project, equipment, or task leads to an accident or error/violation-producing condition in the workplace
- *Hazard identification*—Controls put in place can only protect workers against hazards for which they were designed. This category of the framework represents situations in which there were no organizational controls for a hazard due to lack of identification. This could also be cited in situations in which the controls that were put in place could not contain the magnitude of the event when it occurred. In this case the hazard was identified, but there was a poor understanding of its magnitude and/or mechanism of release
- *Monitoring and auditing*—For safe production there must be systems of control in place. These control systems must be constantly audited and monitored to ensure that they are adhered to and also that they are sufficient to deal with the ever-changing working environment. This category is included in the framework to identify situations in which lack of monitoring and auditing of existing controls leads to accidents or error/violation-producing conditions in the workplace
- *Maintenance management*—This category of the framework covers all situations where poor maintenance of equipment and structures leads to accidents or error/violation-producing condition in the workplace. A culture of poor equipment maintenance can lead to both equipment and workplace deficiencies
- *Resource provision*—This category covers situations in which failure of management to provide the physical resources needed for the accomplishment of tasks leads to accidents or error- or violation-producing condition in the workplace. This usually happens during budget optimization decisions
- *Strategic decision/planning*—There are times in which an organization is faced with conflicting safety and production goals. This category of the framework covers situations in which the organization's choice of which goal should have prominence contributes to the accident process. For example, a decision to maximize profit by reducing the workforce
- *Risk management*—This category of the framework represents situations in which the refusal to deal properly with an identified risk, manage a known problem in the organization, or use effective risk management technique serves as a root cause of an accident
- *Leadership*—This category is included in the framework to cater for situations such as ineffective supervision, failure to correct deviant behaviour, and any other situation in which actions or inactions of leaders could have prevented an incident
- *Work scheduling*—This category is included in the framework as a systemic factor to cater for situations in which work schedule (continuous night shift, overtime, task coinciding with bad weather, *etc.*) serves as a root cause of an accident
- *Emergency response*—This category caters for situations in which the lack of proper emergency procedures exacerbates the effect of an accident or creates another accident.

Hazard and barrier analysis

The hazard and barrier analysis section of the framework was designed to capture information about the accident-causing agents and the safety barriers broken in each accident. This was done with the belief that the information adds meaning to the results obtained from the causal section.

Safety barriers

This section of the framework records the safety barriers that failed during the accident process. Safety barriers can be defined as any means (physical or non-physical) instituted to prevent, control, or mitigate accidents (Hollnagel, 2008). The need for safety barriers in industry arises from the fact that the nature of some industrial activities is such that it is not always possible to remove all hazards by design. In such situations the safety of employees is ensured by placing a barrier between them and the hazard. This implies that the harm from a hazard reaches a target only when there is no safety barrier to prevent it, or the barriers put in place were not effective. The nature of the safety barriers in place also tells a lot about the nature of the industry and the kinds of unsafe acts that will be prevalent in such an industry. The ICAM framework also has a barrier analysis section.

Accident-causing agencies

This section of the framework records information on the hazards/agencies involved in each of the accidents analysed. A hazard is defined as a source of harm to people or damage to property or the environment. A major challenge in the categorization of dangerous occurrences in the mining industry is that there is no standard way of categorization. Different countries classify the same or similar incidents differently. For example the terms 'fall of ground' and 'roof fall' mean the same thing in the South African and the US mining industries. This makes it necessary for any analyst who wants to apply this framework to understand how the country involved classifies its accidents.

Metadata

Metadata can simply be described as data about data or data that describes data. Metadata was chosen to elucidate other factors that may have influenced accidents. For example, knowledge of a particular time in which most human errors/violations occur could help in understanding why those errors/violations are occurring. The variables chosen under this category were time of accident, day of accident, activity the victim was involved in that resulted in the accident, place of the accident (underground, surface *etc.*), status of the victim (contractor or company employee), age of victim, relevant work experience, \and the last vacation period. This information may not be very significant on an individual basis, but when used together proved very useful. Although the studies of Patterson and Shappell (2010) incorporated some situational data, metadata has never been formally integrated into any of the frameworks that have adopted the Reason (1990, 1997) model.

Now that the framework has been explained, its applicability is tested by applying it to an actual mining disaster.

Application of framework to the Jim Walter Resources mine disaster

The Jim Walter Resources mine disaster is one of the worst mining disasters in the USA in recent times. This section starts with a summarized version of the official account provided by the Mine Health and Safety Administration (2001). The causes identified by the investigation are then mapped onto the framework.

On Sunday 23 September 2001, a roof fall followed by two separate explosions occurred in an underground coal mine owned by Jim Walter Resources, leading to the fatal injury of 13 miners. The two explosions occurred at approximately 5:20 pm and 6:15 pm during a non-production afternoon shift.

Prior to the first explosion, three miners (a foreman, a longwall machine operator, and a helper) were building cribs to address deteriorating roof and rib conditions in the entry of a section near a battery charging station. The deteriorating conditions had been identified by earlier shifts and reported for repairs.

While they were building the cribs, the roofing condition continued to deteriorate as small rocks began to fall and water began pouring steadily from the roof. This was followed by several lumps, which caused the three miners undertaking the repair to take a few steps backwards. At approximately 5:17 pm, they heard sounds indicating the possibility of a broken roofbolt. The fall of a large rock and the entire roof followed subsequently.

Within minutes of the roof fall, the first explosion occurred, resulting from the ignition of the methane-air mixture by an arcing damaged battery. The explosion injured four miners (the three building the cribs and a fourth delivering building materials at the time of the explosion) and also disrupted the air flow, allowing methane to accumulate in that section of the mine. The explosion also caused visibility issues at the section of the explosion and other sections of the mine.

The foreman instructed an electrician to ensure that the electrical power to the section was turned off. Though the high-voltage electrical circuit for the section was de-energized, a track haulage block light system that extended into the section remained live. The foreman left the section to inform the control room about the explosion. He was able to inform the people in the control room about the roof fall and explosion via a telephone outside the section. He also told them about the critical condition of one of the injured miners and hence the need for an ambulance, emergency help, and a life-support helicopter.

The people in the control room mobilized other miners who were underground at the time of the first explosion to help with the situation in the affected section. While some miners were made aware of the gravity of the situation and evacuated the mine, most of the other miners who went and helped with the rescue mission were under the impression that an ignition incident had occurred. Five of these miners entered the section affected by the explosion to help rescue the injured miners.

At 6:15 pm, a second methane explosion occurred. This explosion propagated to the other sections of the mine via coal dust, resulting in at least 12 fatalities and widespread destruction of ventilation controls throughout the mine. The second explosion was most likely caused by the ignition of the methane-air mixture by the track haulage block light system. Nineteen miners were able to evacuate the mine.

Mine rescue teams were dispatched to the accident scene. One of the dispatched teams found three fatally injured miners and one severely injured miner. The injured miner died the next day after an operation. By 8 November, the bodies of 12 more victims were discovered by recovery teams.

The MHSA investigation established the following factors as contributing to the accident.

1. During the drilling of the cable bolt holes, the miners failed to fully appreciate the seriousness of the roof condition and hence did not report to their superiors. Had they reported, the roof fall may have been avoided. The miners' failure to report the situation may have been due to the fact that there had not been a previous roof fall in areas where cable bolts had been installed. Hence existing standards did not include checking for abnormal or unexpected roof conditions and drawing the attention of superiors. It was suggested that workers be made to understand the principle of roof anchorage
2. The ignition source for the second explosion was probably the block light system in the section that remained energized. Although the electrician was instructed to de-energize the power to the section following the first explosion, he failed to de-energize the track haulage block light system. He might have thought that de-energizing the high-voltage electrical circuit for the section would also de-energize the haulage block light system that extended into the section of the explosion. The foreman also tried contacting the people at the surface to de-energize all underground power sources, but was unsuccessful because the telephone was not working
3. Analysis showed that rock dust application was inadequate, which might have increased the effect of the second explosion. The mine management had no procedure of routine checks or re-applying dust in

areas of need. They relied on external inspectors. There were 99 violations of the combustible materials and rock dusting standards in the year preceding the incident

4. A timely mine evacuation would have greatly reduced the impact of the accident. The investigation revealed that there was enough information to warrant the order of a mine evacuation, but that did not happen. Miners not trained for emergency rescue missions were used. This exacerbated the consequences of event. In addition, all miners were not participating in fire drills every 90 days, as required by mining regulations.

The following sections apply the various categories of the newly developed framework to the above summary of the Jim Walter Resources mine incident.

Agency and barrier analysis

The agencies identified in this accident include roof fall, methane, and coal dust explosion. The safety barriers that could have prevented the incident include an adequate risk/situational assessment and communication by the miners; roofbolts; a methane monitoring system; a properly isolated electrical system; ignition sources control; adequate rock dust application and ventilation; and good emergency planning (a mitigating barrier). While these agencies are amongst the most common accident-causing agencies, they could have been prevented or their impact reduced. Another understanding that can be obtained from the barrier analysis is that most large-scale accidents are possible only when multiple barriers fail. Reason (1998) suggests that only a poor safety culture can lead to the failure of multiple layers of barriers.

The authors of this paper are of the view that although in this situation there seemed to be enough signals to have warned the miners that the roof was unstable, the act of risk and situational assessment is not a very formidable safety barrier in preventing roof falls. This is based on the fact that there is a limitation to the degree to which visual inspections can adequately identify a roof situation. The authors suggest that a much more advanced technical solution beyond sound testing and visual inspection should be adopted. Another fact that is apparent from the barrier analysis is that most of the barriers are not self-enforcing and hence require cooperation with humans. This makes accident analysis techniques/frameworks developed from human error models very important in the quest to understand accidents in the mining context.

The above analysis has shown that a barrier and hazard analysis has the potential for identifying the preliminary causes of an accident, which can also give hints on important routes that the causal analysis of the accident should follow.

Metadata analysis

Information that qualifies as metadata in this accident includes the following.

- The incident happened during a non-productive maintenance shift
- The activity being carried out when the incident occurred was the building of cribs
- The three incidents happened between 5 pm and 7pm
- The workers involved in the original incident were a foreman, a longwall machine operator, and a helper
- There were several violations of standards by the mine management before the incident.

As stated earlier, this information does not say much about a single incident, but during the analysis of several incidents, patterns can be identified.

Causal analysis

Table I shows the results of mapping the causes of the accident identified by the MHSA investigation onto the new framework. A reason is provided for each framework category cited as contributing to the incident. Every causal factor identified is traced to the systemic factor that might have served as its root cause. For example, the first direct cause identified by the analysis of the accident is failure of the miners to fully understand the seriousness of the roof situation (*a mistake*). The workplace factors identified as leading to the mistake were that the existing procedures did not cover it (unsafe work practices) and that the *requisite competence* to adequately assess the situation was lacking.

Failure in the *hazard identification* process during procedure writing and *inadequate training* were the systemic factors identified as leading to these workplace factors.

From Table I it is also apparent that the complex design of the underground electrical system (*fit-for-purpose equipment*) was the main workplace factor identified as leading to the direct cause (*slips and lapses*). The fact that a single section needed to be de-energized at two different places might have contributed to the error. Failure to carry out adequate rock dusting (*routine violation*) at the complex electrical system and inadequate dusting (*physical environment*) was another human error that exacerbated the effect of the accident. There were 99 prior rock-dusting standard violations, which also confirms the fact that it was a routine error. It can also be inferred that while poor design and poor maintenance management were systemic factors leading to the deficiencies identified at the workplace, adequate emergency procedures could have mitigated the impact of the accident. This direct cause was linked to a workplace environment (*behavioural environment*) where violations were condoned. Another *routine violation* identified in this study was failure to follow proper evacuation procedures. This may have been due to the fact that there were no trained people to conduct the emergency evacuation (*competent people*). These findings support Reason's (1990, 1997) theory that an accident has both direct and indirect causes. It also confirms the assertion that human errors are symptoms of deep deficiencies in the organizational structure rather than the causes of accidents in themselves. From Reason's (1990) theory of accident pathogens, it can be said that poor hazard identification, inadequate training procedures, poor design, poor maintenance management, poor risk management, and inadequate emergency procedures were the root causes of the Jim Walter Resources accident. Saleh and Cummings (2011) also pointed to accident pathogens as the root cause of the accident.

Summary and conclusion

A newly developed accident analysis framework for incidents in the mining industry has been introduced and various

Table I

Mapping of the Jim Walter Resources accident causal factors into the causal section of the new framework

Direct cause	Reasoning	Workplace factor	Reasoning	Systemic factor	Reasoning
Mistake	The miners failed to fully appreciate the seriousness of the roof condition and hence did not report to their superiors	Unsafe work practices	It was a novel situation. However, the standards as they existed did not provide for reporting the roof situation during roofbolting	Hazard identification hence did not cater for it	The hazard identification process during the writing of procedures did not consider the possibility of a roof fall during maintenance,
		Competent people	It was clear that the workers did not fully appreciate what constitutes a stable roof	Training and competence	It seems the existing training was not enough to fully equip workers with the required skills. The MHSA investigation made recommendations to that effect
Slips and lapses	The electrician instructed to de-energize thought the whole section has been de-energized	Fit-for-purpose equipment	To de-energize a single section totally, two separate sources had to be isolated	Design	Poor design of the workplace electrical system is the root cause of the error
			A malfunctioning telephone hampered communication	Maintenance	Proper maintenance of the telephone system could have prevented the second explosion
Routine violation	Failure to apply rock dusting.	Behavioural environmental	It was clear that not meeting the rock dusting requirement had become a norm prior to the accident. 99 previous violations give testimony to that	Monitoring and auditing	Existing controls were not enforced
Routine violation	Failure to follow proper evacuation procedure	Competent people	Miners were not trained for emergency evacuation	Training and competence	Miners were not properly trained or emergency situations
		Behavioural environment	Participation in fire drills was not compulsory	Monitoring and auditing	Existing controls were not enforced

sections compared to those in existing frameworks. The use of this framework has been demonstrated by mapping identified causes of a previous mining disaster onto it. The results showed that the accident had both direct and indirect causes. Systemic factors seem to be the root cause of the direct causes. This agrees with Reason's (1990, 2000) analogy of accidents in high-risk industries being the result as accident pathogens. It is recommended that this framework be applied to a wider range of accident reports.

Limitations

The limitations of this study are those of most *post-hoc* analyses. The accuracy of the analysis depends solely on the accuracy of the accident investigation and report.

Acknowledgement

This work is based on research supported by the South African Research Chairs Initiative of the Department of Science and Technology and National Research Foundation of South Africa, which is gratefully acknowledged.

Any opinion, finding, and conclusion or recommendations expressed in this material is that of the authors and the NRF does not accept any liability in this regard.

References

Benedyk, R. and Minister, S. 1998. Applying the BeSafe method to product safety evaluation. *Applied Ergonomics*, vol. 29, no 1. pp. 5–13.

Bullock, M.G. 1979. Work process control guide. System Safety Development Centre EG and G Idaho Inc., Idaho Falls, Idaho.

De Landre, J., Gibb, G., and Walters, N. 2006. Using incident investigation tools proactively for incident prevention. http://asasi.org/papers/2006/Payne_Stewart_Learjet_Investigation_De%20Landre_Gibb_Walters_DOC.pdf [Accessed 1 Feb. 2012].

Hollnagel, E. 2008. Risk + barriers = safety? *Safety Science*, vol. 46, no. 2. pp. 221–229.

ILO (International Labour Organization). 2010. Mining: a hazardous work. http://www.ilo.org/safework/areasofwork/hazardous-work/WCMS_124598/lang--en/index.htm [Accessed 12 Jan. 2013].

Leveson, N.G. 2004. A new accident model for engineering safer systems. *Safety Science*, vol. 42. pp. 237–270.

Mine Safety and Health Administration. 2001. Report of investigation, fatal underground coal mine explosions. 23 September 2001. http://www.msha.gov/fatals/2001/jwr5/ftl01c2032light.pdf [Accessed 1 Sep. 2013].

O'Hare, D. 2000. The 'Wheel of Misfortune': a taxonomic approach to human factors in accident investigation and analysis in aviation and other complex systems. *Ergonomics*, vol. 43, no. 12. pp. 2001–2019.

Patterson, J.M. and Shappell, S.A. 2010. Operator error and system deficiencies: analysis of 508 mining incidents and accidents from Queensland, Australia using HFACS. *Accident Analysis and Prevention*, vol. 42, no. 4. pp. 1379–1385.

Paul, P.S. and Maiti, J . 2008: The synergic role of sociotechnical and personal characteristics on work injuries in mines. *Ergonomics*, vol. 51, no. 5. pp. 737–767.

QURESHI, Z.H. 2008. A review of accident modeling approaches for complex critical sociotechnical systems. *Report no*. DSTO-TR-2094. Defence Science and Technology Organization, Australia.

REASON, J. 1990. Human Error. Cambridge University Press.

REASON, J. 1997. Managing the Risks of Organizational Accidents. Ashgate Publishng (Taylor & Francis).

REASON, J. 1998. Achieving a safe culture: theory and practice. *Work and Stress*, vol. 12, no. 3. pp. 293–306.

REASON, J. 2000. Safety paradoxes and safety culture. *International Journal of Injury Control and Safety Promotion*, vol. 7, no. 1. pp. 3–14.

REASON, J., HOLLNAGEL, E., and PARIES, J. 2006. Revisiting the "Swiss Cheese" Model of accidents. EUROCONTROL Experimental Centre, Bretiny-sur-Orge Cedex, France.

SALEH, J.H. and CUMMINGS, A.M. 2011. Safety in the mining industry and the unfinished legacy of mining accidents: safety levers and defense-in-depth for addressing mining hazards. *Safety Science*, vol. 49, no. 6. pp. 764–777.

SHAPPELL, S.A. and WIEGMANN, D.A. 2000. The Human Factors Analysis and Classification System (HFACS). *Report no*. DOT/FAA/AM-00/7, Office of Aerospace Medicine, Washington DC. http://hfacs.com/sites/default/files/Shappell%20and%20Wiegmann,%202000.pdf [Accessed 6 April 2013].

WIEGMANN, D.A. and SHAPPELL, S.A. 1997. A human error approach to accident investigation: the taxonomy of unsafe operations. *International Journal of Aviation Psychology*, vol. 7, no. 4. pp. 269–291.

WIEGMANN, D.A. and SHAPPELL, S.A. 2001. Human error analysis of commercial aviation accidents: application of the Human Factors Analysis and Classification System (HFACS). *Aviation, Space, and Environmental Medicine*, vol. 72, no. 11. pp. 1006–1016. ◆

http://dx.doi.org/10.17159/2411-9717/2016/v116n8a11

Optimizing seat selection for LHDs in the underground mining environment

by X. Ji*, T.R. Eger†, and J.P. Dickey*

Synopsis

Whole-body vibration (WBV) occurs when the human body is supported on a surface that is vibrating. Operators and passengers in mobile machinery are exposed to vibration transferred from the seatpan to the body. Excessive vibration exposure is strongly associated with low back pain, therefore seat selection is important for reducing vibration exposure. Recently, we developed an efficient neural network (NN) algorithm that identified the dynamic properties of suspension seats, and then interrogated the models to predict seatpan vertical accelerations for a variety of skidders in the forestry sector. We have expanded this approach to evaluate the influence of different seats on the WBV exposures from load-haul-dump vehicles in the underground mining environment. Of the five seat models that we tested, our results demonstrated that one particular seat model was best able to attenuate vibrations based on the equivalent daily exposure, $A(8)$, and the corresponding working hours to reach the upper limit of the ISO 2631-1 health guidance caution zone for 8-hour operation. We performed a sensitivity analysis to evaluate the influence of the individual vibration frequency components on the $A(8)$ results for each of the seat models. This analysis revealed that each of the industrial seats responded differently to specific vibration frequencies and explained why the seat selection algorithm matched particular seats to specific vibration environments.

Keywords

neural network, seat selection, whole-body vibration, $A(8)$, health guidance caution zone, sensitivity analysis.

Introduction

Whole-body vibration (WBV) occurs when vibration at the seat is transmitted to mobile machinery operators (Morgan and Mansfield, 2011). WBV is associated with an increased risk of low back pain (LBP) when operators are exposed to vibrations while in a sitting posture (Johanning, 2011; Lis *et al.*, 2007). More than 25% of employees are affected by LBP each year (Lee *et al.*, 2001). LBP is considered to be a widespread health problem and is a severe complaint amongst occupational operators exposed to WBV (Bovenzi and Betta, 1994; Davis and Jorgensen, 2005; Seidel, 2005).

Load-haul-dump (LHD) vehicles are commonly used to excavate large quantities of ore or rocks in underground mining environments. ISO 2631-1 standard (1997) presents tools to evaluate the health risk by calculating the frequency-weighted accelerations of vibration exposures. Several studies reported that operators of LHD vehicles are exposed to high-magnitude WBV which often exceed the ISO 2631-1 health guidance caution zone (HGCZ) (Aye and Heyns, 2011; Eger *et al.*, 2006, 2011; Kumar, 2004; Mandal and Srivastava, 2010; Smets, Eger, and Grenier, 2010; van Niekerk, Heyns, and Heyns, 2000; Village, Morrison, and Leong, 1989). LHDs are commonly associated with compensation claims (Burgess-Limerick, 2005), and one study reports that LHD operators experience LBP 4.25 times more frequently than control subjects who are not exposed to occupational WBV (Mandal and Srivastava, 2010).

Vibration exposure is influenced by some individual vibration factors (*e.g.* magnitude) (ISO 2631-1, 1997) and modulating factors (*e.g.* terrain type, vehicle mass, *etc.*) (Donati, 2002). Seats also influence the vibration exposure transmitted to the heavy machine operators (Griffin *et al.*, 2006; Gunaselvam and van Niekerk, 2005). Due to the frequency-dependent properties of the suspension system, industrial seats should be selected appropriately for the specific vehicles or workplaces (Gunaselvam and van Niekerk, 2005). Inappropriate choice of seat or incorrect adjustment of a seat suspension system can amplify vibration exposure (Paddan and Griffin, 2002).

Neural network (NN) models have been utilized in a wide range of applications because of their versatility for describing relationships between variables (May, Zhou, and Lee, 2012; Widrow *et al.*, 2013; Won *et al.*, 2010). NNs can model complex nonlinear relationships between the measured system's

* *Kinesiology/Faculty of Health Sciences, Western University, London, Ontario.*

† *School of Human Kinetics, Laurentian University, Sudbury, Ontario.*

 ISSN 2225-6253. Paper received Dec. 2014; revised paper received Jul. 2015.

input and output signals by adjusting the weights and biases between neurons to optimize the predictions. An efficient NN model approach (Ji, Eger, and Dickey, 2015) has been successfully developed and used to identify the vibration attenuation properties of five commercial industrial seats that are commonly used in heavy mobile machinery. That study determined that one industrial seat was the most suitable for the specific vibration exposure for skidders in forestry workplaces (Ji, Eger, and Dickey, 2015). The primary purpose of the current paper is to apply this NN approach to LHD equipment, and evaluate whether specific industrial seats perform well for LHDs in underground mining environments. A second purpose is to identify the performance of these industrial seats at specific vibration frequencies by evaluating the effects of the individual frequency components on the equivalent daily exposure ($A(8)$) results, and reveal why the seat selection algorithm matched particular seats to specific vibration environments.

Methodology

The development of the NN models for the five industrial seats was described in a previous study (Ji *et al.*, 2015). The essential elements of this process are presented here for completeness.

Each of the industrial seats tested (Access Mining Services model 30019932, model Amobi SM2024; Sears Manufacturing Co. model CAT EW013121; KAB Seating Ltd KAB 301, KAB 525) was mounted to the top surface of a six degree of freedom (6df) robotic platform (R3000, Mikrolar Inc. Hampton, NH, USA), which produced 6df vibrations based on a library of occupational field vibration exposures (Dickey, Eger, and Oliver, 2010) and 3df broadband (0.5-20 Hz, r.m.s. amplitudes between 0.2 and 2.0 m s^2 on all three translational axes) random frequency profiles (Ji, Eger, and Dickey, 2015). Each seat's suspension was appropriately adjusted to its mid-travel position (to avoid hitting the end-stops). Two 6df inertial measurement units (IMUs; MechTrack – analog version, Mechworks Systems Inc., West Vancouver, BC, Canada) were used to record accelerations at the seatpan/operator interface and the centre surface of the robotic platform (chassis) as recommended in ISO 2631-1 (1997). This chassis and seatpan acceleration data was collected from ten subjects with a range of anthropometrics.

The five-layer neural identification NNs' inputs were the recorded time-series translational chassis acceleration data and the *BMI Prime* for each subject. *BMI Prime*, equal to *BMI* divided by 25 (Gadzik, 2006), reflected the machine operators' anthropometrics. Each neuron in the second layer acted as a bandpass filter for the time series chassis data on three translational axes. The root mean square (r.m.s.) values of the recorded chassis acceleration data was calculated in the third layer and were combined with the corresponding *BMI Prime* value from the first layer to predict the vertical r.m.s. accelerations of the seatpan in the fourth layer. Each seat model was represented by the optimal weights and biases that linked the different NN layers. These optimal weighting parameters were determined through a system identification process by matching the predicted outputs (r.m.s. acceleration) to the corresponding measured values in the processing fifth layer. Although the NN structure was identical for each of the seat models, the weighting parameters differed and uniquely described the performance of each of the seats. The NN models robustly described the relationship between measured and predicted seatpan r.m.s. accelerations; the coefficients of determination (r^2) ranged between 0.97–0.99 for the training profiles, and between 0.93–0.96 for the validation profiles.

For the current study, we implemented each of our robust seat models to predict the daily 8-hour equivalent frequency-weighted accelerations (ISO 2631-1, 1997), $A(8)$, for ten LHD vehicles from our library (Dickey, Eger, and Oliver, 2010) of previously reported field data (Eger, Kociolek, and Dickey, 2013) (Table I). The ISO 2631-1 W_d and W_k filters were used to process the horizontal (x- and y-axis) and the vertical (z-axis) chassis acceleration data collected from the mining workplace measurements respectively. Each axis was multiplied by the appropriate k factors for health assessment (*e.g.* k_x=k_y=1.4 and kz=1.0) to obtain the frequency-weighted chassis accelerations (ISO 2631-1, 1997). The r.m.s. values of the weighted chassis vibration data were calculated using bandpass filters (0.5–20 Hz) in the x- and y- axes, and one-third octave filters (0.5–20 Hz) in the z-axis. Three specific *BMI Prime* values (0.74, 1.00, and 1.20) were selected to reflect the influence of machine operator anthropometrics. Then we used these weighted r.m.s. values as inputs of each NN model to predict the weighted r.m.s. accelerations of the seatpan in the vertical direction. Similarly to previous studies (Aye and Heyns, 2011; Eger, Contratto, and Dickey, 2011), $A(8)$ values were calculated from the predicted frequency-weighted seatpan r.m.s. acceleration and the corresponding duration proportion of each machine operation task (Table I). We also estimated the number of working hours to reach the upper acceleration limit (0.9 m/s^2) of the ISO 2631-1 HGCZ for 8 hours of vibration exposure to effectively evaluate the health risk for operators and to select the most suitable seat for this mining environment.

In order to describe the frequency spectra of the vibration data, we calculated the one-third octaves between 0.5 and 20 Hz using the sound and vibration toolkit for LabVIEW (V10.0.1, National Instruments, Austin, TX) for each of the specific mining vehicles. Given the different vibration environment for skidders in the forestry workplace, we also performed this one-third octave analysis on the vibration data from eight skidders for comparison (Ji *et al.*, 2015). We also performed a sensitivity analysis to gain insight into which of the input parameters most strongly influenced the output of each seat NN model. The sensitivity analysis consisted of evaluating the impact of perturbing the amplitudes of specific frequencies of the individual vehicle acceleration profiles; the acceleration magnitude in each of the one-third octave bands was perturbed up and down 50% towards the maximum and minimum range, and the $A(8)$ acceleration magnitude was recalculated. Frequency bands that strongly influenced the output of the NN model will have a large range of $A(8)$ magnitudes when their amplitude is perturbed. The *BMI Prime* was set to 1.0 for these sensitivity analyses.

Results

The predicted seatpan accelerations for this group of 10 LHDs were large; of the 150 scenarios (10 LHDs, 3 operator BMIs, and 5 seats) only two (two operator BMIs for one LHD) were

Table I

Frequency-weighted vibration data (min., max., median) for the 20 s vibration segments for each of the ten LHD vehicles. The size of the vehicle (bucket capacity) and the distribution of machine operations (mucking, dumping, driving loaded, and driving unloaded) are also presented

Vehicle, bucket capacity	Operation	# of 20s segments		Ax (m/s/s)	Ay (m/s/s)	Az (m/s/s)	Roll (rad/s/s)	Pitch (rad/s/s)	Yaw (rad/s/s)
M1									
10 cubic yard	Mucking	10	min.	1.07	1.38	0.90	3.35	3.72	2.98
			max.	2.07	2.08	1.60	3.79	4.71	3.52
			median	1.66	1.82	1.28	3.54	3.99	3.21
	Dumping	1	min.	--	--	--	--	--	--
			max.	--	--	--	--	--	--
			median	1.94	2.20	2.39	4.42	5.97	4.18
	Driving loaded	64	min.	0.99	0.64	0.92	3.37	3.61	2.91
			max.	2.25	2.01	2.57	7.09	6.53	4.59
			median	1.64	1.08	1.25	3.87	4.51	3.36
	Driving unloaded	76	min.	0.96	0.63	0.88	3.35	3.76	2.93
			max.	2.49	2.59	2.93	7.55	7.48	4.75
			median	1.54	1.11	1.14	3.86	4.52	3.39
M2									
10 cubic yard	Mucking	0	min.	--	--	--	--	--	--
			max.	--	--	--	--	--	--
			median	--	--	--	--	--	--
	Dumping	9	min.	1.46	1.73	1.02	3.22	3.98	3.07
			max.	2.11	2.03	1.92	4.26	6.37	4.53
			median	1.82	1.83	1.47	3.64	4.72	3.42
	Driving loaded	28	min.	1.57	1.04	1.16	3.45	4.12	3.10
			max.	2.92	1.98	2.38	4.15	4.88	3.52
			median	2.07	1.22	1.35	3.67	4.34	3.29
	Driving unloaded	23	min.	1.93	0.98	1.43	3.37	4.15	3.06
			max.	2.64	1.82	2.43	4.11	5.33	3.57
			median	2.44	1.19	1.55	3.52	4.55	3.24
M3									
10 cubic yard	Mucking	13	min.	0.78	0.93	1.30	2.88	3.18	3.00
			max.	1.84	1.84	2.56	3.28	3.79	3.24
			median	1.14	1.20	1.66	3.00	3.29	3.10
	Dumping	10	min.	0.67	0.93	0.93	2.80	3.15	2.82
			max.	1.25	1.57	2.14	3.04	3.36	3.20
			median	0.87	1.20	1.43	2.93	3.27	2.96
	Driving loaded	23	min.	0.55	0.61	0.29	2.77	3.07	2.68
			max.	1.13	2.48	2.09	3.12	3.43	3.00
			median	0.83	1.53	0.59	2.87	3.15	2.83
	Driving unloaded	41	min.	0.72	0.32	0.24	2.75	3.08	2.78
			max.	1.84	2.26	1.64	3.03	3.62	3.14
			median	1.11	1.23	0.76	2.89	3.17	2.88
M4									
8 cubic yard	Mucking	21	min.	0.61	0.70	0.42	2.80	2.64	3.27
			max.	2.60	2.78	2.02	6.60	3.51	9.90
			median	1.53	1.71	1.51	3.42	2.90	4.13
	Dumping	4	min.	0.76	1.16	1.32	2.92	2.77	3.38
			max.	1.22	1.22	1.53	3.27	2.87	3.57
			median	0.94	1.20	1.42	3.00	2.81	3.51
	Driving loaded	68	min.	0.22	0.25	0.46	2.73	2.62	3.07
			max.	1.49	1.99	1.45	3.31	2.97	3.85
			median	0.92	0.98	1.01	2.87	2.78	3.22
	Driving unloaded	80	min.	0.51	0.34	0.34	2.71	2.64	3.02
			max.	1.75	1.85	2.60	3.94	3.07	5.33
			median	0.90	0.87	1.09	2.85	2.76	3.22
M5									
8 cubic yard	Mucking	33	min.	0.79	1.07	1.61	2.79	3.46	2.88
			max.	1.78	1.84	4.08	3.30	5.69	3.62
			median	1.21	1.52	2.88	2.96	4.21	3.05
	Dumping	17	min.	0.23	0.63	0.40	2.63	3.30	2.65
			max.	0.93	1.39	1.59	2.87	3.75	3.11
			median	0.56	0.91	0.90	2.71	3.47	2.80
	Driving loaded	38	min.	0.48	0.65	0.68	2.70	3.29	2.71
			max.	1.52	1.37	4.05	2.96	4.27	2.98
			median	1.00	1.04	2.10	2.83	3.57	2.83
	Driving unloaded	41	min.	0.34	0.73	0.47	2.63	3.19	2.63
			max.	1.43	1.94	3.65	3.01	5.26	3.10
			median	1.01	1.10	1.93	2.80	3.53	2.81

Table I (Continued)

Frequency-weighted vibration data (min., max., median) for the 20 s vibration segments for each of the ten LHD vehicles. The size of the vehicle (bucket capacity) and the distribution of machine operations (mucking, dumping, driving loaded, and driving unloaded) are also presented

Vehicle, bucket capacity	Operation	# of 20s segments		Ax (m/s/s)	Ay (m/s/s)	Az (m/s/s)	Roll (rad/s/s)	Pitch (rad/s/s)	Yaw (rad/s/s)
M6									
3.5 cubic yard	Mucking	6	min.	1.10	0.71	0.84	3.00	2.73	2.75
			max.	1.75	1.72	2.20	4.16	3.28	3.27
			median	1.30	1.41	1.65	3.44	2.94	2.83
	Dumping	4	min.	0.76	1.16	1.32	2.92	2.77	3.38
			max.	1.22	1.22	1.53	3.27	2.87	3.57
			median	0.94	1.20	1.42	3.00	2.81	3.51
	Driving loaded	24	min.	0.85	0.72	0.88	3.08	2.77	2.78
			max.	1.64	1.51	2.56	3.82	4.55	3.32
			median	1.33	1.09	1.69	3.33	2.95	2.93
	Driving unloaded	16	min.	1.06	1.23	1.62	3.31	2.99	2.83
			max.	2.49	2.01	3.36	4.95	7.06	3.58
			median	2.00	1.65	2.84	4.05	3.57	3.14
M7									
3.5 cubic yard	Mucking	2	min.	2.10	1.33	2.21	4.93	3.84	3.63
			max.	2.32	1.50	3.07	6.16	7.19	3.80
			median	--	--	--	--	--	--
	Dumping	0	min.	--	--	--	--	--	--
			max.	--	--	--	--	--	--
			median	--	--	--	--	--	--
	Driving loaded	42	min.	2.33	1.18	1.14	4.05	2.67	2.74
			max.	4.00	2.17	2.98	8.23	3.69	4.01
			median	3.34	1.85	1.52	4.72	2.82	2.93
	Driving unloaded	97	min.	1.39	0.61	0.98	3.39	2.71	2.71
			max.	4.37	2.50	5.37	10.35	6.97	5.93
			median	3.33	1.73	1.90	4.87	2.98	3.08
M8									
6 cubic yard	Mucking	7	min.	0.78	0.68	0.87	2.86	3.19	2.72
			max.	1.61	1.33	1.73	3.54	3.55	2.75
			median	1.32	1.07	1.31	3.12	3.36	2.74
	Dumping	5	min.	0.58	0.83	1.31	2.92	3.23	2.65
			max.	0.90	1.16	1.91	3.29	3.58	2.78
			median	0.73	0.98	1.76	3.09	3.32	2.75
	Driving loaded	81	min.	0.72	0.76	0.67	2.88	3.17	2.62
			max.	1.73	2.36	2.39	3.65	3.96	2.86
			median	1.17	1.05	1.34	3.17	3.34	2.73
	Driving unloaded	73	min.	0.91	0.74	0.84	2.94	3.18	2.61
			max.	1.71	1.77	3.04	3.54	3.72	2.89
			median	1.23	1.08	1.72	3.17	3.41	2.73
M9									
2 cubic yard	Mucking	37	min.	0.98	0.87	1.16	2.71	3.12	3.12
			max.	2.20	3.21	3.85	5.19	8.29	5.23
			median	1.54	2.30	2.17	3.16	4.89	3.82
	Dumping	0	min.	--	--	--	--	--	--
			max.	--	--	--	--	--	--
			median	--	--	--	--	--	--
	Driving loaded	22	min.	0.95	1.38	1.32	2.74	3.00	3.00
			max.	1.74	1.88	2.44	3.22	4.11	3.47
			median	1.46	1.73	1.69	2.87	3.35	3.18
	Driving unloaded	24	min.	1.03	1.53	1.51	2.79	3.14	3.08
			max.	2.11	2.78	4.20	3.77	5.86	4.26
			median	1.84	2.36	3.53	3.38	4.91	3.77
M10									
2 cubic yard	Mucking	0	min.	--	--	--	--	--	--
			max.	--	--	--	--	--	--
			median	--	--	--	--	--	--
	Dumping	0	min.	--	--	--	--	--	--
			max.	--	--	--	--	--	--
			median	--	--	--	--	--	--
	Driving loaded	7	min.	1.25	0.86	1.38	3.21	2.90	2.68
			max.	1.53	1.43	1.97	4.23	3.25	3.50
			median	1.42	1.04	1.51	3.31	3.00	2.83
	Driving unloaded	12	min.	1.25	0.83	1.44	3.24	2.95	2.75
			max.	1.69	1.73	2.23	6.46	4.72	6.61
			median	1.59	1.37	1.90	4.72	3.65	3.63

below the lower border of the ISO 2631-1 HGCZ, 30 were within the HGCZ, and 118 were above the HGCZ (Table II). On average, subjects with smaller *BMI Prime* values were predicted to experience larger average daily vibration exposures $A(8)$ than subjects with larger *BMI Primes* (Table II).

One LHD (M4) had lower predicted acceleration levels for all *BMI Prime* values and all seats ($A(8)$ = 0.39–0.69 m/s^2) compared to the other LHDs; all driver and seat combinations could be tolerated for more than 8 hours (Table III). In contrast, several LHDs (M5, M6, M7, M9, M10) had higher acceleration levels ($A(8)$ = 1.05–1.89 m/s^2) such that none of the driver and seat combinations could be tolerated for 8 hours (range from 1.82 to 5.88 hours). Specific seats in some LHDs (M1, M2, M3, M8) reduced the vibration exposure such that exposures could be tolerated for more than 8 hours while other seats in these vehicles could not be tolerated for 8 hours. The KAB301 seat reduced the vibration magnitude to levels that could be tolerated for more than 8 hours more often than the other seats; 14 of the 30 vehicle and driver combinations could be tolerated for more than 8 hours for the KAB301 seat compared to three each for the Access and Amobi seats, and six each for the CAT and KAB525 seats.

For the specific LHD vehicles M1, M2, and M8, the KAB301 seat was the only seat model to attenuate the occupational vibration exposures to below the upper acceleration limit of the ISO 2631-1 HGCZ (0.9 m/s^2); the KAB301 seat attenuated the vibrations approximately twice as well as the CAT seat for these specific vehicles. In contrast, for four other LHD vehicles (M5, M6, M7, M9, and M10), the KAB301 seat and CAT seat performed similarly with all $A(8)$ values larger than 0.9 m/s^2.

Given these differences in performance of the KAB301 seat between vehicles, we examined the frequency spectra of the vibration exposures to evaluate whether there were differences in vibration exposures between vehicles; the chassis acceleration data for the ten LHDs was evaluated in one-third octave proportional frequency bands between 0.5 and 20 Hz. There did not appear to be striking differences in the vibration spectra between the vehicles where the KAB301 seat performed well (M1, M2, and M8) (Figure 1a) and those where the seat did not effectively attenuate the vibrations (M5, M6, M7, M9, and M10) (Figure 1b). For comparison, we also evaluated the chassis acceleration data for eight forestry skidders from our library of industrial vibration exposures (Cation *et al.*, 2008; Jack *et al.*, 2010). Figure 2 represents the data for LHDs M1, M2, and M8 where the KAB301 seat effectively attenuated the vibrations more effectively than the CAT seat, and the data for skidders S4, S5, S6, and S8 where the CAT seat attenuated the vibrations more effectively than

Table II

$A(8)$ results for five industrial seats with different driver anthropometrics (*BMI primes*) in the underground mining environment

LHDs	*BMI Prime*	$A(8)$* (m/s^2)				
		Access	Amobi	CAT	KAB301	KAB525
M1	0.74	1.10	1.20	1.18	0.80	0.96
	1.00	1.06	1.11	1.10	0.74	0.92
	1.20	1.03	1.04	1.05	0.70	0.89
M2	0.74	1.04	1.15	1.21	0.80	0.92
	1.00	1.00	1.06	1.14	0.74	0.88
	1.20	0.97	0.99	1.09	0.69	0.85
M3	0.74	1.11	1.22	0.89	0.92	1.16
	1.00	1.08	1.14	0.82	0.86	1.13
	1.20	1.05	1.07	0.77	0.82	1.10
M4	0.74	0.60	0.69	0.50	0.66	0.69
	1.00	0.56	0.60	0.44	0.60	0.65
	1.20	0.53	0.53	0.39	0.56	0.62
M5	0.74	1.89	1.88	1.46	1.39	1.84
	1.00	1.85	1.79	1.39	1.33	1.81
	1.20	1.82	1.73	1.34	1.29	1.78
M6	0.74	1.54	1.58	1.39	1.15	1.43
	1.00	1.50	1.49	1.32	1.09	1.40
	1.20	1.47	1.42	1.27	1.05	1.37
M7	0.74	1.69	1.73	1.60	1.28	1.52
	1.00	1.65	1.64	1.53	1.22	1.49
	1.20	1.63	1.58	1.48	1.18	1.46
M8	0.74	1.24	1.30	1.15	0.87	1.12
	1.00	1.20	1.21	1.08	0.81	1.08
	1.20	1.16	1.14	1.03	0.77	1.05
M9	0.74	1.80	1.81	1.46	1.49	1.75
	1.00	1.76	1.73	1.39	1.43	1.71
	1.20	1.73	1.66	1.34	1.39	1.68
M10	0.74	1.56	1.63	1.58	1.45	1.47
	1.00	1.52	1.54	1.51	1.39	1.44
	1.20	1.49	1.47	1.45	1.35	1.41

*According to ISO 2631-1 the frequency weighted acceleration values corresponding to the lower and upper limits of the Health Guidance Caution Zone (for 8 h of exposure) are 0.45 and 0.90 m/s^2 respectively

Table III

The working hours to reach the upper limit of the ISO 2631-1 health guidance caution zone (HGCZ) for 8-hour working duration

LHDs	*BMI Prime*	Hours				
		Access	Amobi	CAT	KAB301	KAB525
M1	0.74	5.31	4.52	4.69	10.04*	6.98
	1.00	5.72	5.28	5.31	11.68*	7.58
	1.20	6.07	6.01	5.89	13.23*	8.09*
M2	0.74	5.99	4.91	4.41	10.18*	7.68
	1.00	6.48	5.79	4.98	11.88*	8.38*
	1.20	6.89	6.62	5.49	13.50*	8.98*
M3	0.74	5.21	4.34	8.17*	7.67	4.78
	1.00	5.59	5.03	9.65*	8.71*	5.09
	1.20	5.92	5.67	11.07*	9.65*	5.36
M4	0.74	17.96*	13.80*	25.45*	14.90*	13.72*
	1.00	20.45*	18.08*	33.71*	17.88*	15.33*
	1.20	22.70*	22.78*	42.79*	20.80*	16.75*
M5	0.74	1.82	1.84	3.05	3.37	1.91
	1.00	1.89	2.02	3.36	3.67	1.99
	1.20	1.96	2.17	3.62	3.92	2.05
M6	0.74	2.72	2.61	3.34	4.89	3.15
	1.00	2.86	2.92	3.70	5.42	3.32
	1.20	2.98	3.21	4.01	5.88	3.47
M7	0.74	2.27	2.18	2.53	3.96	2.80
	1.00	2.37	2.40	2.75	4.33	2.94
	1.20	2.45	2.60	2.94	4.64	3.05
M8	0.74	4.25	3.83	4.87	8.58*	5.20
	1.00	4.54	4.42	5.53	9.86*	5.58
	1.20	4.78	4.96	6.13	11.05*	5.90
M9	0.74	2.00	1.97	3.03	2.92	2.13
	1.00	2.09	2.18	3.33	3.16	2.22
	1.20	2.16	2.36	3.60	3.37	2.30
M10	0.74	2.66	2.43	2.60	3.07	2.98
	1.00	2.81	2.72	2.86	3.33	3.14
	1.20	2.92	2.98	3.08	3.56	3.28

*Indicates exposures that require more than 8 working hours to exceed the upper limit of the HGCZ for five industrial seats with different driver anthropometrics (*BMI Primes*) in the underground mining environment

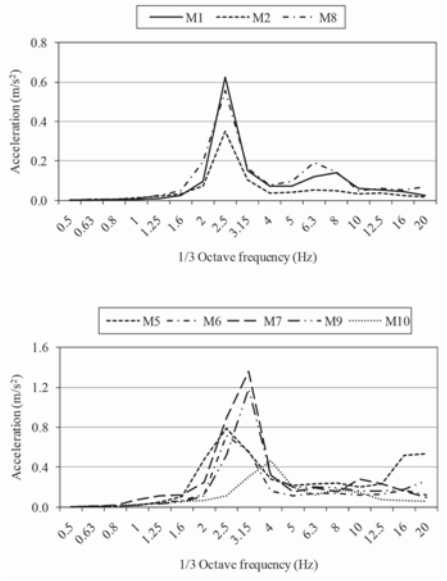

Figure 1—Chassis r.m.s. acceleration data for (a) three LHDs (M1, M2, and M8) and (b) five LHDs (M5, M6, M7, M9, and M10) at each one-third octave frequency band between 0.5 and 20 Hz. The KAB301 seat effectively attenuated the vibrations for the mining vehicles in Figure 1a, but not for those in Figure 1b

the KAB301 seat. These forestry vehicles had a dominant frequency of 2 Hz, while the mining vehicles had a dominant frequency of 2.5 Hz.

The $A(8)$ results for the LHDs are presented in Table II and the corresponding data for the skidder vehicles in the Appendix. The predicted $A(8)$ values from the sensitivity analyses (using the perturbed vibration amplitudes for each of the one-third octaves) for the CAT and KAB301 seats are presented in Figure 3. We focused on the three LHDs where the KAB301 seat effectively attenuated the vibrations (M1, M2, and M8); all three of these LHDs showed similar responses. The magnitude of the accelerations at 2.0, 2.5, 3.1, and 16.0 Hz resulted in large changes in the $A(8)$ values for both industrial seats. The KAB301 seat is highly sensitive to increases in magnitude of the 2 Hz and 3.15 Hz components (26% and 22% increase in $A(8)$, respectively) while the CAT seat is much less sensitive to increases in magnitude of these components (8% and 10% increase in $A(8)$, respectively). However, in the 2.5 Hz frequency band, the CAT seat is more sensitive to increases than the KAB 301 seat.

Discussion

Operators of heavy mobile machinery in the underground mining environment are subjected to large vibrations (Eger, Kociolek, and Dickey, 2013; Kumar, 2004; van Niekerk, Heyns, and Heyms, 2000). Seat selection is an important factor for reducing drivers' exposure to vibration (Gunaselvam and van Niekerk, 2005), but it is difficult to identify optimal seats due to the complexity of the seats' performance. We developed NN models characterizing the vertical attenuation properties of five common industrial seats (Ji, Eger, and Dickey, 2015) and predicted their performance for LHD vehicles from our library of occupational vibration exposures (Dickey, Eger, and Oliver, 2010). We evaluated the performance of five industrial seats based on the chassis vibrations measured for each of ten specific LHD vehicles and three variations of driver anthropometrics. Overall, the vibration environment for these ten vehicles was such that relatively few of the seats were effective at reducing the vibration exposure such that the workers could be exposed for 8 or more hours (32 of 150 seat-operator-vehicle combinations). Among the five seats tested in this study, our predictions indicate that the KAB301 seat was the best choice in the mining environment; it had the lowest $A(8)$ and largest number of hours to reach the upper boarder to the HGCZ for seven of the vehicles, and was ranked second for two other vehicles, although the vibration magnitudes were similar to the best-ranked seat. All of the seats were predicted to perform well for one of the vehicles. In terms of absolute vibration magnitude, the KAB301 seat allowed approximately half of the specific operator/vehicle combinations (14 of 30) to be operated for over 8 hours in the mining environment. The KAB301 seat attenuated the magnitudes of the vibration exposures for these operator-vehicle combinations below the upper limit (0.9 m/s²) of ISO 2631-1 HGCZ, which minimized the health risks of exposure for heavy machine operators. This is similar to the vibration magnitudes reported in other mining environments; for example, Aye and Heyns (2011)

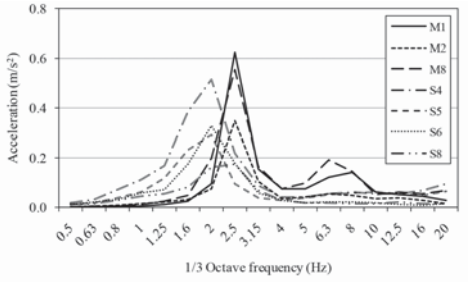

Figure 2—Chassis r.m.s. acceleration data for three LHDs and four skidders at each one-third octave frequency band between 0.5 and 20 Hz. The KAB301 seat performed much better than the CAT seat with LHDs M1, M2, and M8, but the CAT seat performed much better with skidders S4, S5, S6, and S8

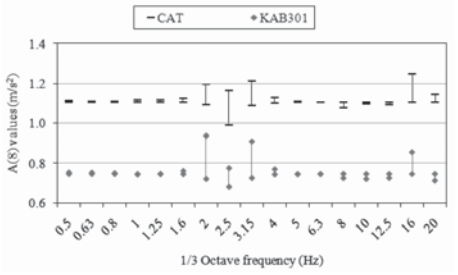

Figure 3—Influence of each vibration frequency band (one-third octave frequency between 0.5 and 20 Hz) on the $A(8)$ results for CAT and KAB301 seats for one representative LHD vehicle (M1) in the mining vibration environment. The KAB301 attenuated the vibrations more effectively than the CAT seat for this vehicle. The upper and lower points at each frequency reflect the predicted seatpan $A(8)$ magnitudes when the chassis acceleration at that one-third octave band was increased and decreased respectively

reported that approximately 50% of the heavy equipment used in mining causes vibration exposures that exceed exposure action values. Although the vibration exposure for the remaining operator-vehicle combinations did not permit the specific operator-vehicle combinations to be operated for over 8 hours, the KAB301 seat performed better than the other industrial seats (except for near-ties for two vehicles, and for the vehicle where all the seats performed well). These findings are in stark contrast to a parallel study evaluating the effectiveness of these same seats for attenuating vibration exposures in forestry skidder vehicles (Ji, Eger, and Dickey, 2015). We observed that the CAT seat was the best choice for the forestry skidders (between the five seat models that we tested); it limited 96% of the vibrations below the upper limit of the ISO2631-1 HGCZ range. These contrasting findings affirm that seat selection is not universal – the performance and ranking of industrial seats varies between vibration environments. Given that the magnitudes of the vibration total values (a_v) are relatively similar in these two environments (Plewa *et al.*, 2012), it appears that the performance of the seats may depend upon specific features of the vibration environment, such as the frequency spectra. The vibration spectra are different for forestry vehicles and mining vehicles; the dominant frequencies are 2 Hz for the forestry environment and 2.5 Hz for the mining environment (Figure 2). The sensitivity analysis (Figure 3) revealed that the seats had heightened sensitivity for the 2, 2.5, and 3.15 Hz frequency bands. The CAT seat performed better with the forestry vehicles (Ji, Eger, and Dickey, 2015) because the forestry vehicles have dominant 2 Hz vibrations, and higher 3.15 Hz vibrations than the mining vehicles (Figure 2), and the CAT seat was much less sensitive to increases in the magnitude of these two frequency components than the KAB 301 seat (Figure 3). Similarly, the KAB 301 seat performed better with the mining vehicles because the dominant frequency for LHDs was 2.5 Hz (Figure 2), and the KAB 301 seat was less sensitive to this frequency than the CAT seat (Figure 3). Our results are consistent with the previous report (Griffin *et al.*, 2006) that each seat suspension system amplifies the vibration in specific frequency ranges. Seat selection must be optimized by matching the performance of specific industrial seats with the frequency spectra for the vibration environments.

The number of vehicles was rather limited (10 LHDs) and we analysed a relatively small number of industrial seats. However, the seats evaluated were previously identified as the most common type currently used in the underground mining environment in Ontario. Although the current study has identified differences in performance between these five seats, this project is not intended to endorse specific seats – rather, we intend to emphasize the important point that industrial seats must be matched to the specific vibration environment. It is impossible to make universal recommendations about seat selection, as each seat's performance varies depending on the vibration exposure. Given that our study was limited to five seats, it would be helpful to expand our modelling approach to a larger number of seats. We propose to continue efforts to extend our seat selection investigations into other vibration environments, and to evaluate the responses and health risks of heavy machine operators with multi-axis vibrations.

Acknowledgements

We acknowledge funding from the Workplace Safety and Insurance Board of Ontario, and the assistance of all the volunteers. We also acknowledge in-kind contribution of seats from underground mining companies association with Workplace Safety North's Technical Advisory Committee for Underground Mining Equipment.

References

Aye, S.A. and Heyns, P.S. 2011. The evaluation of whole-body vibration in a South African opencast mine. *Journal of the Southern African Institute of Mining and Metallurgy*, vol. 111. pp. 751–758.

Bovenzi, M. and Betta, A. 1994. Low-back disorders in agricultural tractor drivers exposed to whole-body vibration and postural stress. *Applied Ergonomics*, vol. 25. pp. 231–241.

Burgess-Limerick, R. 2005. Reducing injury risks associated with underground coal mining equipment. *Ergonomics Australia*, vol. 19. pp. 14–20.

Cation, S., Jack, R., Oliver, M., Dickey, J.P., and Lee Shee, N.M. 2008. Six degree of freedom whole-body vibration during forestry skidder operations. *International Journal of Industrial Ergonomics*, vol. 38. pp. 739–757.

Davis, K.G. and Jorgensen, M.J. 2005. Biomechanical modeling for understanding of low back injuries: a systematic review. *Occupational Ergonomics*, vol. 5. pp. 57–76.

Dickey, J.P., Eger, T.R., and Oliver, M. L. 2010. A systematic approach for studying occupational whole-body vibration: A combined field and laboratory based approach. *Work*, vol. 35. pp. 15–26.

Donati, P. 2002. Survey of technical preventative measures to reduce whole-body vibration effects when designing mobile machinery. *Journal of Sound and Vibration*, vol. 253. pp. 169–183.

Eger, T., Salmoni, A., Cann, A., and Jack, R. 2006. Whole-body vibration exposure experienced by mining equipment operators. *Occupational Ergonomics*, vol. 6. pp. 121–127.

Eger, T., Stevenson, J.M., Grenier, S., Boileau, P.M., and Smets, M.P. 2011. Influence of vehicle size, haulage capacity and ride control on vibration exposure and predicted health risks for LHD vehicle operators. *Journal of Low Frequency Noise, Vibration and Active Control*, vol. 30. pp. 45–62.

Eger, T.R., Contratto, M.S., and Dickey, J.P. 2011. Influence of driving speed, terrain, seat performance and ride control on predicted health risk based on ISO 2631-1 and EU Directive 2002/44/EC. *Journal of Low Frequency Noise, Vibration and Active Control*, vol. 30. pp. 291–312.

Eger, T.R., Kociolek, A.M., and Dickey, J.P. 2013. Comparing health risks to load-haul-dump vehicle operators exposed to whole-body vibration using EU Directive 2002/44EC, ISO 2631-1 and ISO 2631-5. *Minerals*, vol. 3. pp. 16–35.

Gadzik, J. 2006. How much should I weigh? Quetelet's equation, upper weight limits, and BMI prime. *Connecticut Medicine*, vol. 70. pp. 81–88.

Griffin, M.J., Howarth, H.V.C., Pitts, P.M., Fischer, S., Kaulbars, U., Donati, P.M., and Bereton, P.F. 2006. Guide to good practice on whole-body vibration. Contract VC/2004/0341, European Commission Directorate General Employment, Social Affairs and Equal Opportunities, Brussels.

Gunaselvam, J. and Van Niekerk, J.L. 2005. Seat selection guidelines to reduce whole-body vibration exposure levels in the SA mining industry. *Journal of the South African Institute of Mining and Metallurgy*, vol. 105. pp. 675–686.

ISO 2631-1. 1997. Mechanical vibration and shock - Evaluation of human exposure to whole-body vibration - Part 1: General requirements. International Organization for Standardization, Geneva.

Jack, R.J., Oliver, M., Dickey, J.P., Cation, S., Hayward, G., and Lee-Shee, N. 2010. Six-degree-of-freedom whole-body vibration exposure levels during routine skidder operations. *Ergonomics*, vol. 53. pp. 696–715.

Ji, X., Eger, T.R.. and Dickey, J.P. 2015. Development of a seat selection algorithm to match industrial seats with specific forestry vibration exposures. *International Journal of Forest Engineering*, vol. 26. pp. 48–59.

Johanning, E. 2011. Diagnosis of whole-body vibration related health problems in occupational medicine. *Journal of Low Frequency Noise, Vibration and Active Control*, vol. 30. pp. 207–220.

Kumar, S. 2004. Vibration in operating heavy haul trucks in overburden mining. *Applied Ergonomics*, vol. 35. pp. 509–520.

Lee, P., Helewa, A., Goldsmith, C.H., Smythe, H.A., and Stitt, L.W. 2001. Low back pain: prevalence and risk factors in an industrial setting. *Journal of Rheumatology*, vol. 28. pp. 346–351.

Lis, A.M., Black, K.M., Korn, H., and Nordin, M. 2007. Association between sitting and occupational LBP. *European Spine Journal*, vol. 16. pp. 283–298.

Mandal, B.B. and Srivastava, A.K. 2010. Musculoskeletal disorders in dumper operators exposed to whole body vibration at Indian mines. *International Journal of Mining, Reclamation and Environment*, vol. 24. pp. 233–243.

May, P., Zhou, E., and Lee, C. W. 2012. Learning in fully recurrent neural networks by approaching tangent planes to constraint surfaces. *Neural Networks*, vol. 34. pp. 72–79.

Morgan, L.J. and Mansfield, N.J. 2011. A Summary of Current Knowledge on Effects of Simultaneous Whole-body Vibration and Trunk Rotation on Off-road Driving Tasks. CRC Press.

Paddan, G.S. and Griffin, M.J. 2002. Effect of seating on exposures to whole-body vibration in vehicles. *Journal of Sound and Vibration*, vol. 253. pp. 215–241.

Plewa, K.M., Eger, T.R., Oliver, M.L., and Dickey, J.P. 2012. Comparison between ISO 2631-1 comfort prediction equations and self-reported comfort values during occupational exposure to whole-body vehicular vibration. *Journal of Low Frequency Noise, Vibration and Active Control*, vol. 31. pp. 43–54.

Seidel, H. 2005. On the relationship between whole-body vibration exposure and spinal health risk. *Industrial Health*, vol. 43. pp. 361–377.

Smets, M.P., Eger, T.R., and Grenier, S.G. 2010. Whole-body vibration experienced by haulage truck operators in surface mining operations: a comparison of various analysis methods utilized in the prediction of health risks. *Applied Ergonomics,* vol. 41. pp. 763–770.

Van Niekerk, J.L., Heyns, P.S, and Heyns, M. 2000. Human vibration levels in the South African mining industry. *Journal of the South African Institute of Mining and Metallurgy*, vol. 100. pp. 235–242.

Village, J., Morrison, J.B., and Leong, D.K.N. 1989. Whole-body vibration in underground load-haul-dump vehicles. *Ergonomics*, vol. 32. pp. 1167–1183.

Widrow, B., Greenblatt, A., Kim, Y., and Park, D. 2013. The No-Prop algorithm: A new learning algorithm for multilayer neural networks. *Neural Networks*, vol. 37. pp. 182–188.

Won, S.H., Song, L., Lee, S.Y., and Park, C.H. 2010. Identification of finite state automata with a class of recurrent neural networks. *IEEE Transactions on Neural Networks*, vol. 21. pp. 1408–1421.

Appendix

A(8) results and the corresponding working hours to reach the upper limit of the ISO 2631-1 health guidance caution zone (HGCZ) for 8-hour working duration. Values in bold indicate exposures that require more than 8 working hours to access the upper limit of the HGCZ for five industrial seats with different driver anthropometrics (*BMI Primes*) in the forestry vibration environments. Reproduced from Ji, Eger, and Dickey (2015) with permission from the publisher. ◆

Skidders	*BMI*	Access		Amobi		CAT		KAB301		KAB525	
	Prime	*A*(8) m s^{-2}	Hours	*A*(8) m s^{-2}	Hours	*A*(8) m s^{-2}	Hours	*A*(8) m s^{-2}	Hours	*A*(8) m s^{-2}	Hours
S1	0.74	0.80	**10.07**	0.99	6.67	0.68	**13.94**	0.81	**9.96**	0.87	**8.64**
	1.00	0.76	**11.16**	0.90	**8.07**	0.61	**17.43**	0.75	**11.59**	0.83	**9.48**
	1.20	0.73	**12.13**	0.83	9.48	0.55	**21.08**	0.70	**13.13**	0.80	**10.20**
s2	0.74	0.80	**10.01**	0.95	7.20	0.70	**13.32**	0.79	**10.32**	0.88	**8.45**
	1.00	0.76	**11.10**	0.86	**8.81**	0.63	**16.58**	0.73	**12.06**	0.84	**9.26**
	1.20	0.73	**12.07**	0.79	**10.45**	0.57	**19.97**	0.69	**13.71**	0.81	**9.97**
S3	0.74	0.79	**10.46**	0.98	6.73	0.81	**9.81**	0.90	7.96	0.86	**8.74**
	1.00	0.75	**11.62**	0.89	**8.17**	0.74	**11.79**	0.84	**9.12**	0.82	**9.59**
	1.20	0.72	**12.65**	0.82	**9.61**	0.69	**13.75**	0.80	**10.19**	0.79	**10.34**
S4	0.74	1.34	3.60	1.63	2.43	0.97	6.89	1.37	3.44	1.58	2.59
	1.00	1.30	3.83	1.54	2.72	0.90	**8.02**	1.32	3.75	1.54	2.72
	1.20	1.27	4.01	1.48	2.97	0.84	**9.09**	1.27	4.02	1.51	2.83
S5	0.74	1.11	5.28	1.33	3.69	0.86	**8.77**	1.13	5.11	1.30	3.84
	1.00	1.07	5.68	1.24	4.25	0.79	**10.44**	1.07	5.69	1.26	4.08
	1.20	1.04	6.03	1.17	4.77	0.73	**12.07**	1.02	6.20	1.23	4.28
S6	0.74	1.03	6.15	1.30	3.85	0.69	**13.45**	1.08	5.53	1.21	4.43
	1.00	0.99	6.67	1.21	4.46	0.62	**16.77**	1.02	6.19	1.17	4.73
	1.20	0.95	7.11	1.14	5.02	0.57	**20.23**	0.98	6.78	1.14	4.99
S7	0.74	0.87	**8.51**	0.99	6.55	0.77	**11.06**	0.84	**9.16**	0.94	7.29
	1.00	0.83	**9.35**	0.90	7.93	0.69	**13.47**	0.78	**10.60**	0.90	7.93
	1.20	0.80	**10.09**	0.83	**9.30**	0.64	**15.90**	0.74	**11.95**	0.87	**8.49**
S8	0.74	0.94	7.27	1.17	4.77	0.66	**14.85**	0.99	6.66	1.08	5.59
	1.00	0.90	7.94	1.07	5.61	0.59	**18.73**	0.93	7.54	1.04	6.02
	1.20	0.87	**8.52**	1.00	6.42	0.53	**22.86**	0.88	**8.34**	1.01	6.39

http://dx.doi.org/10.17159/2411-9717/2016/v116n8a12

The prediction of penetration rate for percussive drills from indirect tests using artificial neural networks

by S. Kahraman*

Synopsis

Percussive drills are widely used in engineering projects such as mining and construction. The prediction of penetration rates of drills by indirect methods is particularly useful for feasibility studies. In this investigation, the predictability of penetration rate for percussive drills from indirect tests such as Shore hardness, P-wave velocity, density, and quartz content was investigated using firstly multiple regression analysis, then by artificial neural networks (ANNs). Operational pressure and feed pressure were also used in the analyses as independent variables. ANN analysis produced very good models for the prediction of penetration rate. The comparison of ANN models with the regression models indicates that ANN models are the more reliable. It is concluded that penetration rate for percussive drills can be reliably estimated from the Shore hardness and density using ANN analysis.

Keywords

percussive drills, penetration rate, indirect rock properties, regression analysis, artificial neural network.

Introduction

Percussive drills are extensively used in open pits, quarries, and on construction sites. The prediction of the penetration rate of drilling machines is very important for cost estimation and planning of rock excavation projects. Many researchers have investigated percussive drilling theoretically or experimentally and correlated the penetration rate with various rock properties.

Protodyakonov (1962) developed drop tests and described the coefficient of rock strength (CRS) used as a measure of the resistance of rock to impact. The Protodyakonov test was subsequently modified by Paone, Madson, and Bruce (1969), Tandanand and Unger (1975), and Rabia and Brook (1980, 1981). Paone, Madson, and Bruce (1969) conducted research work on percussion drilling in the field. They concluded that uniaxial compressive strength (UCS), tensile strength, Shore hardness, and static Young's modulus correlated tolerably well with penetration rates in nine hard and abrasive rocks. A much better correlation was obtained by using the CRS. Paone, Madson, and Bruce stated that no single property of a rock was completely satisfactory as a predictor of penetration rate. Tandanand and Unger (1975) developed an estimation equation that showed good correlation with actual penetration rates of percussive drills. They concluded that CRS was useful in predicting penetration rate and had a higher reliability than other rock properties. Rabia and Brook (1980, 1981) used a modified test apparatus to determine the rock impact hardness number and developed an empirical equation for predicting drilling rates for both down-the-hole and drifter drills. The equation relating penetration rate to drill operating pressure, Shore hardness, and rock impact hardness number was found to give excellent correlation for field data obtained from down-the-hole and drifter drills.

Selmer-Olsen and Blindheim (1970) conducted percussion drilling tests in the field using light drilling equipment with chisel bits. They established a good correlation between penetration rate and the drilling rate index (DRI) and found that rock hardness, strength, brittleness, and abrasivity were important in drilling. Selim and Bruce (1970) carried out percussive drilling experiments on nine rocks in the laboratory. They correlated the penetration rate for a specific drill rig with compressive strength, tensile strength, Shore hardness, apparent density, static and dynamic Young's modulus, shear modulus, CRS, and percentage of quartz, and established linear predictive equations. They stated that the established equations could be used for predicting the performance of percussive drills. Schmidt (1972) correlated the penetration rate with compressive strength, tensile strength, Shore hardness, density, static and dynamic Young's modulus, shear modulus, longitudinal velocity, shear velocity, and Poisson's ratio. He found that only compressive strength and those properties highly correlated with it, such as tensile strength and Young's modulus,

* *Hacettepe University, Mining Engineering Department, Ankara, Turkey.*

 ISSN 2225-6253. Paper received Aug. 2015; revised paper received May 2016.

exhibited good correlations with penetration rate. Pathinkar and Misra (1980) correlated several rock properties with the penetration rate obtained from laboratory-scale drilling in five different rock types, and concluded that conventional rock properties such as compressive strength, tensile strength, specific energy, Shore hardness, and Mohs hardness did not individually provide good correlation with penetration rate. They developed a good correlation between penetration rate and a set of rock properties, but the relationship was complex.

Howarth, Adamson, and Brendt (1986) correlated penetration rate with rock properties and found that bulk density, saturated compressive strength, apparent porosity, and saturated P-wave velocity exhibited strong corrrelations with penetration rate. However, the correlations of penetration rate, Schmidt hammer value, and dry compressive strength were not strong. They stated that porosity could influence drillabillity, since high porosity was likely to assist the formation of fracture paths and networking of such paths. Howarth and Rowland (1987) developed a quantitative measure of rock texture – the texture coefficient – and found a close relation between the texture coefficient and percussion drill penetration rates. They found that a rock with a high texture coefficient has a low drillability and a high compressive strength. Thuro and Spaun (1996) measured drilling rates using 20 kW and 15 kW borehammers (Atlas Copco COP 1440 and COP 1238 ME) together with the geological documentation of the tunnel face. They correlated specific rock properties with the penetration rates of percussive drills and concluded that penetration rate exhibits strong logarithmic relationships with compressive and tensile strength. They also introduced a new rock property, termed 'destruction work', for toughness referring to drillability, and found a highly significant correlation between destruction work and drillability. Kahraman (1999) developed penetration rate models for down-the-hole and hydraulic top-hammer drills using multiple curvilinear regression analysis. The results showed that the parameters significantly affecting penetration rate of down-the-hole drills were operating pressure, piston diameter, and Schmidt hammer value. For hydraulic top-hammer drills, the most significant parameters were blow frequency, compressive strength, and quartz content of the rock. Kahraman (2002) statistically investigated the relations between penetration rate of percussive drills and three different measures of brittleness obtained from compressive strength, tensile strength, and percentage of fines formed in the Protodyakonov test using the raw data obtained from the experimental work of different researchers. He showed that there was no correlation between penetration rate and the brittleness values derived from compressive strength and tensile strength. However, he found a strong correlation between penetration rate and the brittleness value derived from compressive strength and percentage of fines formed in the Protodyakonov test. He concluded that each method of measuring brittleness has its usage in rock drilling, depending on practical utility, *i.e.* one method of measuring brittleness shows good correlation with the penetration rate of percussive drills, while the other method does not. Kahraman, Bilgin, and Feridunoglu (2003) observed percussive blast-hole drills in eight rock types at open pit mines and three motorway sites and correlated penetration rates with rock properties. They found good correlations between the penetration rate and some rock properties.

Compared to the traditional expert systems, artificial neural networks (ANNs) are highly simplified models of nervous systems in the human brain and have some important features such as self-learning, adaptive recognition, and nonlinear dynamic processing. For this reason, ANNs have been used extensively in science and engineering applications in recent years. ANNs have also been applied in geotechnical engineering (Yuanyou, Yanming, and Ruigeng, 1997; Yang and Zhang, 1998; Singh, Singh, and Singh, 2001; Sonmez *et al.,* 2006; Zorlu *et al.*, 2008; Kahraman *et al.*, 2005, 2009, 2010).

There are few studies in the literature on the predictability of drilling rate from ANNs. Akin and Karpuz used an ANN to estimate major drilling parameters such as weight on bit, rotational speed, and bit type for diamond drilling. They concluded that the proposed methodology provided satisfactory results both in relatively less-documented and drilled formations as well as in well-known formations. Monazami, Hashemi, and Shahbazian (2012) investigated the predictability of penetration rate in oil well rotary drilling by using an ANN. They constructed an ANN model and showed that penetration rate could be estimated by using the derived model. Aalizad and Rashidinejad (2012) studied the predictability of penetration rates of rotary-percussive drill using an ANN. Their model includes intact rock properties, rock mass characteristics, the operational variables of the drill, and some blast-hole parameters. They stated that the ANN was a suitable tool for the prediction of the penetration rate of percussive drills. Basarir, Tutluoglu, and Karpuz (2014) evaluated penetration rate prediction for diamond bit drilling by adaptive neuro-fuzzy inference system (ANFIS) and multiple regression. They found that the prediction performances of the ANFIS model were better than those derived from the traditional multiple regression model, and that the constructed models can be used for an initial estimation of the penetration rate for similar cases. Khandelwal and Armaghani (2016) investigated the predictability of drilling rate index (DRI), which is a measure of percussive drilling rate, from hybrid genetic algorithm and artificial neural network (GA-ANN) models. They reported that hybrid GA-ANN technique performed better in predicting DRI compared to other developed models such as multiple regression and ANN.

Although there are some studies in the literature on drillability prediction from ANNs, only one of these (Aalizad, and Rashidinejad, 2012) is related to percussive drilling and includes numerous direct and indirect test results. In the current study, because indirect tests are easy and economical to carry out, the predictability of penetration rate for percussive drills from indirect tests such as Shore hardness, P-wave velocity, density, and quartz content is investigated using an ANN.

Data analysis

The raw data was obtained from the study by Selim and Bruce (1970). They reported the penetration rate data for percussive drills used in the laboratory. Two drills were used for drilling nine different rocks in the experiments. The drill

included in this study was a 6.67 cm bore jackleg type, which drill is a backstroke rifle-bar-rotation machine and bit diameter is confined to 3.81 cm cross-bits. Operational pressure was changed from 4.8 bar to 6.9 bar and feed pressure was changed from 4.1 bar to 6.2 bar during drilling tests for each rock type.

The descriptive statistics for the rock sample data are listed in Table I, showing minimum, maximum, and average values together with the standard deviations for each test type. The skewness values of each test are also given.

Regression analysis

Firstly, the correlation matrix was constructed for the rock properties to determine whether high redundancies exist between these independent variables. As shown in Table II, the correlation coefficients between the rock properties are weak, indicating there is no redundancy between the parameters. However, the correlation coefficients for density and P-wave velocity, and quartz content and Shore hardness, are not very weak. This may give rise to multicollinearity. For this reason, density and Shore hardness were selected for regression analysis since it is simpler to test these variables than the others.

Multiple regression analysis was performed for the estimation of penetration rate, including the parameters operational pressure, feed pressure, and rock properties, and three models were developed. Since the operational pressure and feed pressure are intrinsic drilling parameters, they were included in all models. A total of 100 data points were used in the regression analysis. 22 data points that were used in the ANN analysis were used for the validation of the derived models. The derived models, together with the correlation coefficients (r) and standard errors (SE), are as follows:

Table I

Descriptive statistics of the rock data (modified from Selim and Bruce (1970)

Statistical parameter	Shore hardness	P-wave velocity (km/s)	Density (g/cm³)	Quartz content (%)
Number of data	144	144	144	144
Minimum	36.0	5.0	2.5	1.0
Maximum	92.0	6.6	3.8	98.0
Average	76.6	5.8	2.9	32.9
Standard deviation	± 19.9	± 0.5	± 0.4	± 30.7
Skewness	–1.24	0.04	1.46	0.79

Table II

Correlation matrix for the rock properties

	Shore hardness	P-wave velocity (km/s)	Density (g/cm³)	Quartz content (%)
Shore hardness	1.00			
P-wave velocity (km/s)	0.38	1.00		
Density (g/cm³)	0.26	0.59	1.00	
Quartz content (%)	0.53	–0.24	0.25	1.00

$$PR = 95.0 + 10.9OP - 0.33FP - 0.79SH - 18.3\rho \quad [1]$$
$$r = 0.92;\ SE = 9.42$$

$$PR = 62.8 + 8.8OP - 0.64FP - 0.88SH \quad [2]$$
$$r = 0.80;\ SE = 12.78$$

$$PR = 74.2 + 11.2OP - 0.33FP - 32.8\rho \quad [3]$$
$$r = 0.64;\ SE = 19.42$$

where *PR* is the penetration rate (cm/dk), *OP* is the operational pressure (bar), *FP* is the feed pressure (bar), *SH* is the Shore hardness, and ρ is the density (g/cm³).

Equations [1] and [2] have very strong and strong correlation coefficients, respectively. However, the correlation coefficient of Equation [3] is weak. All regression equations were evaluated in the ANN analysis.

The regression models were validated by drawing scatter diagrams of the observed and estimated values. Ideally, on a plot of observed *versus* estimate values, the points should be scattered around the 1:1 diagonal straight line. A point lying on the line indicates an exact estimation. A systematic deviation from this line may indicate, for example, that larger errors tend to accompany larger estimations, suggesting nonlinearity in one or more variables. The plots of estimated *versus* observed values for the three equations are shown in Figures 1–3. For all models, although some of the data points are scattered uniformly about the diagonal line, others deviate somewhat from the line, showing that there may be some doubt about the model.

Artificial neural network (ANN) analysis

ANN models consist of an interconnected assembly of simple processing elements, neurons, which are organized in a

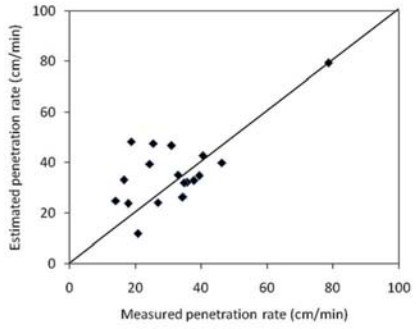

Figure 1—Estimated *versus* measured penetration rate for Equation [1]

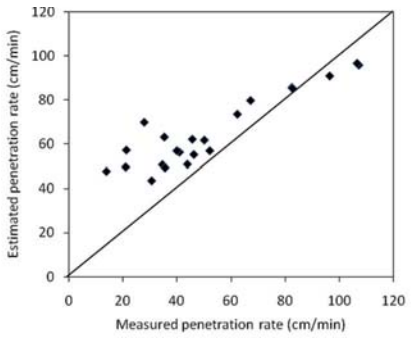

Figure 2—Estimated *versus* measured penetration rate for Equation [2]

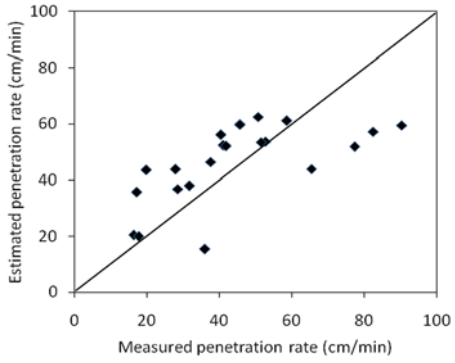

Figure 3—Estimated *versus* measured penetration rate for Equation [3]

layered fashion. Each neuron in a layer is connected to the neurons in the subsequent layer and so on, as seen in Figure 4. The interconnection between *i*th and *j*th layers is labelled as w_{ij} and is called 'weight'. These interconnections between layers provide a powerful tool for prediction and classification. During the learning phase, these interconnections are optimized in order to minimize a predefined cost function. The weighted sum of inputs to a neuron is calculated and the output of a neuron, the activation of the neuron, is determined by an activation function, which is illustrated in Figure 4 as f ().

There are different types of neural network models. The type of neural network used in this study is the multilayered perception (MLP). A MLP neural network is shown in Figure 5. A MLP network consists of an input layer, one or more hidden layers, and an output layer. Each layer has a number of processing units (neurons) and each unit is fully interconnected with weighted connections to units in the subsequent layer. The MLP transforms *i* inputs into *k* outputs through nonlinear mapping functions.

The back-propagation algorithm (Rumelhart and McClelland, 1986) is used in this study, because it is one of the most common network types used in feed-forward multilayer neural networks, and many other types are derived from it. The Levenberg-Marquardt (LM) algorithm is the fastest training algorithm. It is a Hessian-based algorithm for nonlinear least squares optimization. Hessian-based algorithms are used to allow ANNs to learn more suitable features of a complicated mapping (Hagan and Menhaj, 1994; Suratgar *et al.*, 2005). LM is used as the training algorithm in this study, since the training process converges quickly as the solution is approached. Regarding the number of hidden layers, there is no reason to use more than one hidden layer for many practical problems (Heaton Research, 2016). For this reason, one hidden layer is selected in this analysis. There is no strict rule for selecting the number of neurons in a hidden layer. Some rule-of-thumb methods to determine the number of neurons for the hidden layers can be found in the literature (Heaton Research, 2016).

The selected rule in this study is 'the number of hidden neurons should be between the size of the input layer and the size of the output layer'. As a transfer function, a sigmoidal function is selected because it is the most recommended activation function for back-propagation learning (Joarder and Aziz, 2002).

Some researchers (Kumar, 2005; Altun, Bilgil, and Fidan, 2007) have shown that ANN models are not consistently good in prediction in the case of highly skewed data. If the data is skewed, some transformation, such as a power transformation, can be used to reduce the skewness before performing neural network analysis. Skewness is a measure of the degree of symmetry in a normal distribution. If the skewness coefficient is zero, the distribution is symmetric (not skewed). Positive skewness indicates the distribution is skewed to the right, and negative skewness indicates the distribution is skewed to the left. As indicated in Table I, the skewness of rock parameters can be accepted as low. Therefore, the transformation or the treatment of data is not necessary.

A total of 144 data points were used in the ANN analysis. The first group, consisting of 100 data points, was used to train the network ANN models. 22 data points were used for the validation, and the remaining 22 were used for testing.

As shown in Figures 6–8, three different types of neural network structure are implemented in the MATLAB environment for the prediction of penetration rate to compare with the regression models (Equations [1]–[3]). The structures of the ANN models, namely the number of input

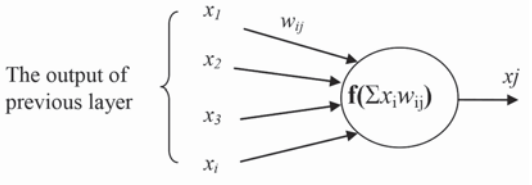

Figure 4—A simple block diagram of a neuron

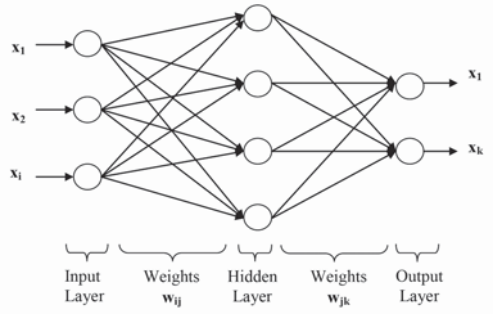

Figure 5—A multilayered perception neural network

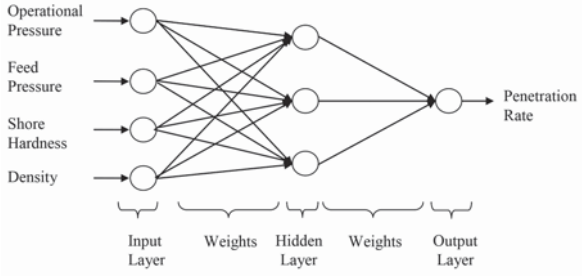

Figure 6—The structure of ANN Model I

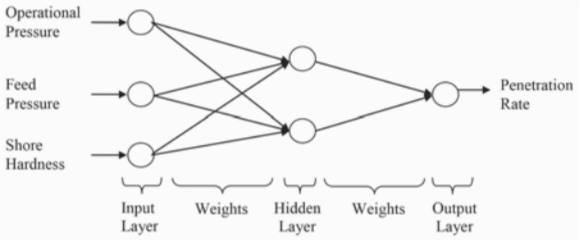

Figure 7—The structure of ANN Model II

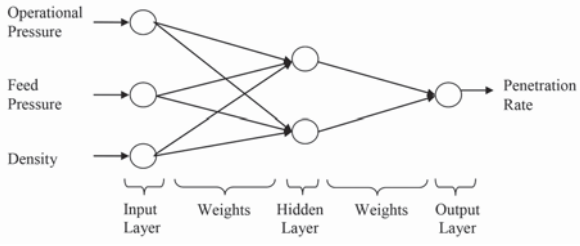

Figure 8—The structure of ANN Model III

Table III

The structures of the ANN models for the prediction of penetration rate

Model no.	Number of input neurons	Number of hidden neurons	Number of output neurons	Network type	Transfer function	Training parameters	Training algorithm
I	4	3	1	Feed-forward back-propagation	Tangent sigmoid Epochs: 17	Learning rate: adaptive. Gradient: 15.6 (trainlm)	Levenberg-Marquardt back-propagation algorithm
II	3	2	1	Feed-forward back-propagation	Tangent sigmoid Epochs: 26	Learning rate: adaptive. Gradient: 0.33 (trainlm)	Levenberg-Marquardt back-propagation algorithm
III	3	2	1	Feed-forward back-propagation	Tangent sigmoid Epochs: 16	Learning rate: adaptive. Gradient: 4.00 (trainlm)	Levenberg-Marquardt back-propagation algorithm

layer neurons, the number of hidden layer neurons. and the number of output layer neurons, are given in Table III. The training parameters and the algorithm that were employed in the training phase are also shown Table III.

In the first trial, a neural network with the structure 4-3-1 (Model I in Table III) is employed. This structure is used to construct a model that delineates the nonlinear relation between the independent variables and the penetration rate. The model is as follows:

$$PR = f(OP, FP, SH, \rho) \quad [4]$$

where *PR* is the penetration rate (cm/dk), *OP* is the operational pressure (bar), *FP* is the feed pressure (bar), *SH* is the Shore hardness, and ρ is the density (g/cm^3).

In the second trial, a neural network with the structure 3-2-1 (Model II in Table III) is constructed. The model is as follows:

$$PR = f(OP, FP, SH) \quad [5]$$

In the third trial, a neural network with the structure 3-2-1 (Model III in Table III) is constructed. The model is as follows:

$$PR = f(OP, FP, \rho) \quad [6]$$

The estimation capability of the derived models can be shown using scatter diagrams of the observed and estimated values. Ideally, on a plot of observed *versus* estimated values, the points should be scattered around the 1:1 diagonal straight line. A point lying on the line indicates an exact estimation. A systematic deviation from this line may indicate, for example, that larger errors tend to accompany larger estimations, suggesting nonlinearity in one or more variables. The plots of estimated *versus* observed penetration rate for models I–III are shown in Figures 9–11. In the plots the points are scattered uniformly about the diagonal line, suggesting that the models are reasonable.

Comparison of regression and ANN models

The models produced from ANN and regression analysis were compared using the correlation coefficients, the estimation capabilities, and the standard errors of estimates. The correlation coefficients of Equations [1] and [2] are strong, as shown in Table IV. However, the estimation capabilities of these equations are not good, as shown in Figures 1 and 2. Nevertheless, the corresponding ANN models (Model I and II) have much stronger correlation coefficients than those of the regression models and their estimation capabilities are very good, as shown in Figures 9 and 10. Although the correlation coefficient and the estimation capability of Equation [3] are not good, the corresponding ANN model (Model III) has a very strong correlation coefficient and its estimation capability is good, as shown in Figure 11.

The standard errors of estimates, which are the other criteria for the comparison, are also indicated in Table IV. The values of standard error of estimates for the ANN models are much lower than those of the regression models.

The comparison of the models produced from ANN and regression analysis using the correlation coefficients and the standard error of estimates indicates that ANN models for the prediction of penetration rate are more reliable than the regression models.

Comparison of derived models and previous models

Most of the previous regression models were derived for

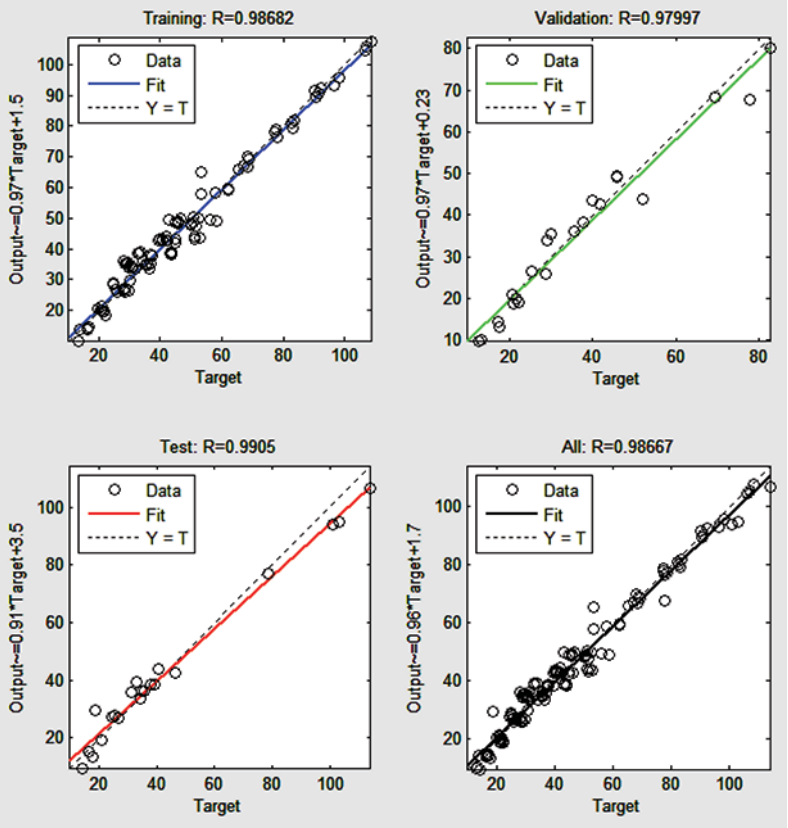

Figure 9—Estimated *versus* measured penetration rate for ANN Model I

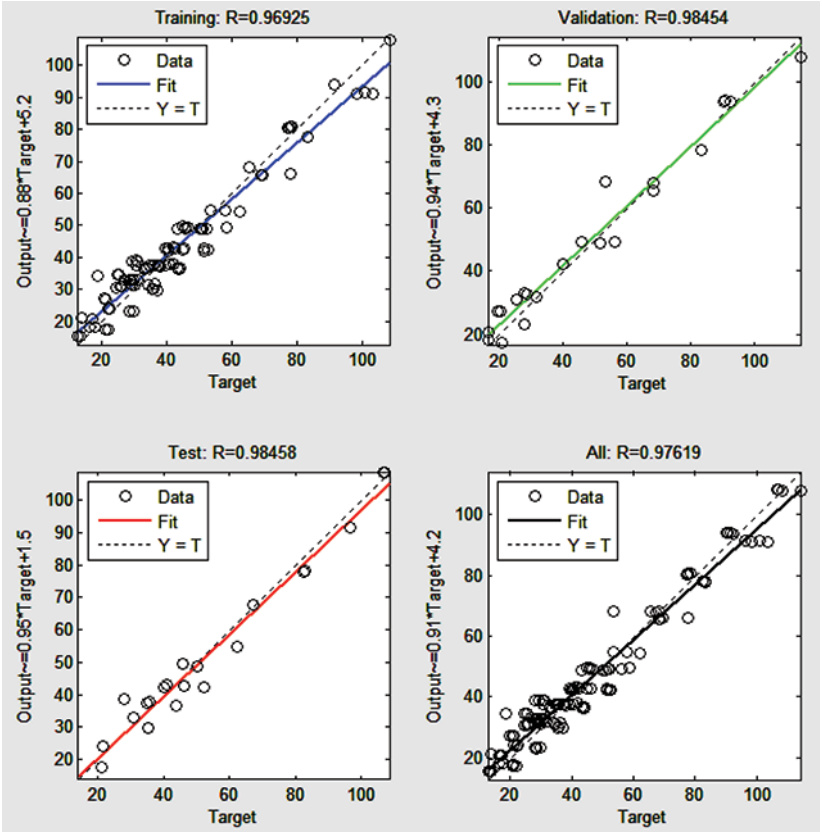

Figure 10 –Estimated *versus* measured penetration rate for ANN Model II

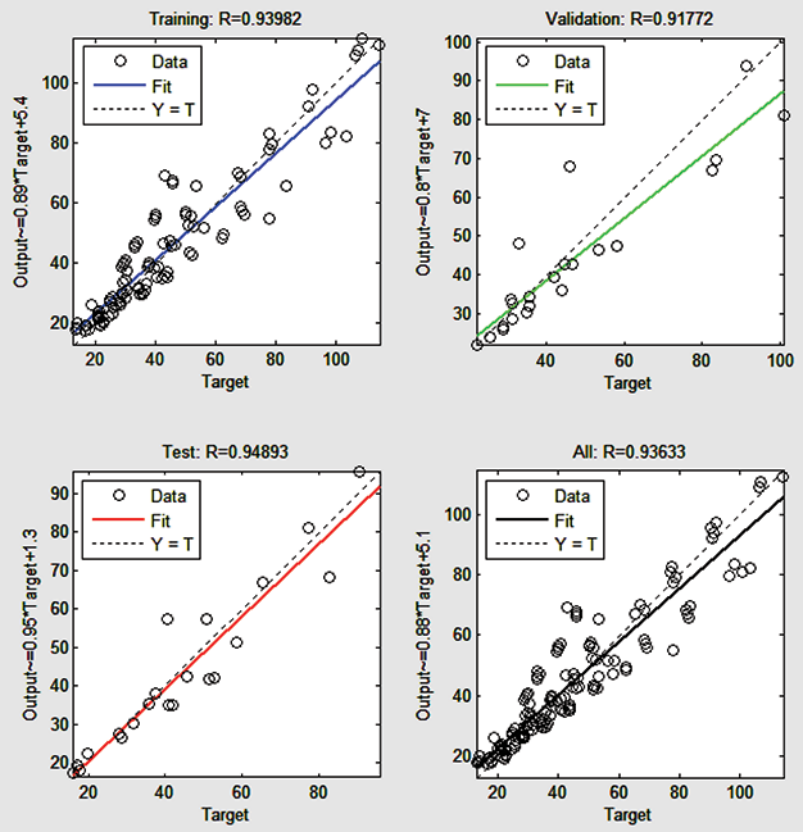

Figure 11 – Estimated versus measured penetration rate for ANN Model III

Table IV

Correlation coefficients and standard error of estimates for the models produced from ANN and regression analysis

Model type	Model no.	Coefficient of correlation (*r*)	Standard error of estimate
Regression models	Eq. [1]	0.92	9.42
	Eq. [2]	0.80	12.78
	Eq. [3]	0.64	19.42
ANN models	Model I	0.99	2.57
	Model II	0.98	4.79
	Model II	0.95	6.06

specific cases. For example, while some of them are valid for pneumatic drills, others are valid for hydraulic drills. The rock bit type may also change from one study to another. On the other hand, some previous models were derived for constant operational variables and only include rock properties. The examples of specific cases can be increased. For this reason, a direct comparison between the models derived in this study and the models suggested by other authors is difficult – only a general comparison can be made. Compared to the some previous models, the derived models include operational variables such as operational pressure and feed pressure. This makes the models more generalized. Another advantage of the derived models is that they include indirect test values, which can be easily determined.

Regarding the studies on the predictability of drilling rate from ANN, making a direct comparison between the ANN models constructed in this study and the models suggested by other authors is also difficult. As stated above, there are very limited studies on this subject. Some of the derived models are valid for diamond drilling (Akin and Karpuz, 2008; Basarir, Tutluoglu, and Karpuz, 2014) or oil well rotary drilling (Monazami, Hashemi, and Shahbazian, 2012). There is another available model (Khandelwal and Armaghani, 2016) which is related to DRI, and is an indirect measure of penetration rate. The ANN model constructed in this study can only be compared to the ANN model suggested by Aalizad and Rashidinejad (2012). The strength of the Aalizad and Rashidinejad model is that it includes rock mass and hole properties together with operational variables. However, because the model includes seven intact rock properties, it is too complex and not practical. Determining seven rock properties is time-consuming and expensive. On the other hand, it is known from the literature that there are generally strong correlations among some of these seven rock properties, such as uniaxial compressive strength, Brazilian tensile strength, and P-wave velocity. As a result, it can be said that because the ANN model constructed in this study includes one or two indirect test values, it is more practical than Aalizad and Rashidinejad's model.

Conclusion

The predictability of penetration rate for percussive drills from indirect tests such as Shore hardness, P-wave velocity,

density, and quartz content was investigated using ANNs and the results were compared with the derived regression models. Very good models were derived from ANN analysis for the prediction of penetration rate. The comparison of ANN models with the regression models showed that ANN models are more reliable than the derived regression models. This is because the drillability of rock is a nonlinear multivariable problem and ANNs show good performance in the solving such problems.

This research has shown that the penetration rate for percussive drills can be reliably estimated from the operational pressure, feed pressure, Shore hardness, and density by using ANN analysis. Three ANN models that are reliable were derived. One of these models can be alternatively used for the estimation purpose. Because the constructed ANN models have little input, they can be used practically. On the other hand, the rock properties included in the ANN models are indirect test values which are easy and cheap to obtain. Therefore, it can be said that the derived ANN models will be useful for practitioners and researchers studying rock drilling.

In conclusion, the ANN is a useful method for the estimation of the penetration rate for percussive drills. Further research should be carried out for different drilling machines and different cases.

References

Aalizad, S.A. and Rashidinejad, F. 2012. Prediction of penetration rate of rotary-percussive drilling using artificial neural networks – a case study. *Archives of Mining Science*, vol. 57. pp. 715–728.

Akin, S. and Karpuz, C. 2008. Estimating drilling parameters for diamond bit drilling operations using artificial neural networks. *International Journal of Geomechanics*, vol. 8. pp. 68–73.

Altun, H., Bilgil, A., and Fidan, B.C. 2007. Treatment of skewed multi-dimensional training data to facilitate the task of engineering neural models. *Expert Systems with Applications*, vol. 33. pp. 978–983.

Basarir, H., Tutluoglu, L., and Karpuz, C. 2014. Penetration rate prediction for diamond bit drilling by adaptive neuro-fuzzy inference system and multiple regressions. *Engineering Geology*, vol. 173. pp. 1–9.

Hagan, M.T. and Menhaj, M.B. 1994. Training feed forward networks with the Marquardt algorithm. *IEEE Transaction on Neural Network*, vol. 5. pp. 989–993.

Heaton Research. 2016. https://web.archive.org/web/20140721050413/http:/www.heatonresearch.com/node/707 May 2016.

Howarth, D.F. and Rowland, J.C. 1987. Quantitative assessment of rock texture and correlation with drillability and strength properties. *Rock Mechanics and Rock Engineering*, vol. 20. pp. 57–85.

Howarth, D.F., Adamson, W.R., and Brendt, J.R. 1986. Correlation of model tunnel boring and drilling machine performances with rock properties. *International Journal of Rock Mechanics and Mining Sciences*, vol. 23. pp. 171–175.

Joarder, K. and Aziz, S.M. 2002. A note on activation function in multilayer feed forward learning. *Proceedings of the International Joint Conference on Neural Networks: IJCNN '02*, vol. 1. IEEE, New York. pp. 519–523.

Kahraman, S. 1999. Rotary and percussive drilling prediction using regression analysis. *International Journal of Rock Mechanics and Mining Sciences*, vol. 36. pp. 981–989.

Kahraman, S. 2002. Correlation of TBM and drilling machine performances with rock brittleness. *Engineering Geology*, vol. 65. pp. 269–283.

Kahraman, S., Altun, H., Tezekici, B.S., and Fener, M. 2005. Sawability prediction of carbonate rocks from shear strength parameters using artificial neural networks. *International Journal of Rock Mechanics and Mining Sciences*, vol. 43. pp. 157–164.

Kahraman, S., Alber, M., Fener, M., and Gunaydin, O. 2010. The usability of Cerchar abrasivity index for the prediction of UCS and E of Misis Fault breccia: regression and artificial neural networks analysis. *Expert Systems with Applications*, vol. 37. pp. 8750–8756.

Kahraman, S., Bilgin, N., and Feridunoglu, C. 2003. Dominant rock properties affecting the penetration rate of percussive drills. *International Journal of Rock Mechanics and Mining Sciences*, vol. 40. pp. 711–723.

Kahraman, S., Gunaydin, O., Alber, M., and Fener, M. 2009. Evaluating the strength and deformability properties of Misis Fault Breccia using artificial neural networks. *Expert Systems with Applications*, vol. 36. pp. 6874–6878.

Khandelwal, M. and Armaghani, D.J. 2016. Prediction of drillability of rocks with strength properties using a hybrid GA-ANN technique. *Geotechnical and Geological Engineering*, vol. 34. pp. 605–620.

Kumar, U.A. 2005. Comparison of neural networks and regression analysis: a new insight. *Expert System with Applications*, vol. 29. pp. 424–430.

Monazami, M., Hashemi, A., and Shahbazian, M. 2012. Drilling rate of penetration prediction using artificial neural network: a case study of one of Iranian southern oil fields. *Oil and Gas Business*, no. 6. pp. 21–31.

Paone, J., Madson, D., and Bruce, W.E. 1969. Drillability studies – laboratory percussive drilling. *Report of Investigation* RI 7300. US Bureau of Mines.

Pathinkar, A.G. and Misra, G.B. 1980. Drillability of rocks in percussive drilling from energy per unit volume as determined with a microbit. *Mining Engineering*, vol. 32. pp. 1407–1410.

Protodyakonov, M.M. 1962. Mechanical properties and drillability of rocks. *Proceedings of the 5th Symposium on Rock Mechanics*, University of Minnesota. pp. 103–118.

Rabia, H. and Brook, N. 1980. An empirical equation for drill performance prediction. The State of The Art in Rock Mechanics. *Proceeding of the 21st US Symposium on Rock Mechanics, University of of Missouri-Rolla*. pp. 103–111.

Rabia, H. and Brook, N. 1981. The effects of apparatus size and surface area of charge on the impact strength of rock. *International Journal of Rock Mechanics and Mining Sciences*, vol. 18. pp. 211–220.

Rumelhart, D. and McClelland, J. 1986. Parallel distributed processing. MIT Press, Cambridge, Mass.

Schmidt, R.L. 1972. Drillability studies - percussive drilling in the field. *Report of Investigation* RI 7684, US Bureau of Mines.

Selim, A.A. and Bruce, W.E. 1970. Prediction of penetration rate for percussive drilling. *Report of Investigation* RI 7396, US Bureau of Mines.

Selmer-Olsen, R. and Blindheim, O.T. 1970. On the drillability of rock by percussive drilling. *Proceeding of the 2nd Congress of the International Society for Rock Mechanics*. pp. 65–70.

Singh, V.K., Singh, D., and Singh, T.N. 2001. Prediction of strength properties of some schistose rocks from petrographic properties using artificial neural networks. *International Journal of Rock Mechanics and Mining Sciences*, vol. 38. pp. 269–824.

Sonmez, H., Gokceoglu, C., Nefeslioglu, H.A., and Kayabasi, A. 2006. Estimation of rock modulus: for intact rocks with an artificial neural network and for rock masses with a new empirical equation. *International Journal of Rock Mechanics and Mining Sciences*, vol. 43. pp. 224–235.

Suratgar, A.A., Tavakoli, M.B., and Hoseinabadi, A. 2005. Modified Levenberg-Marquardt method for neural networks training. *Proceedings of the World Academy of Science, Engineering and Technology*. pp. 46–48.

Tandanand, S. and Unger, H.F. 1975. Drillability determination – a drillability index of percussive drills. *Report of Investigation* RI 8073. US Bureau of Mines.

Thuro, K. and Spaun, G. 1996. Introducing the 'destruction work' as a new rock property of toughness referring to drillability in conventional drill and blast tunnelling. *Proceedings of Eurock'96: Prediction and Performance in Rock Mechanics and Rock Engineering*, vol. 2. pp. 707–713.

Yang, Y. and Zhang, Q. 1998. The applications of neural networks to rock engineering systems (RES). *International Journal of Rock Mechanics and Mining Sciences*, vol. 35. pp. 727–745.

Yuanyou, X., Yanming, X., and Ruigeng, Z. 1997. An engineering geology evaluation method based on an artificial neural network and its application. *Engineering Geology*, vol. 47. pp. 149–156.

Zorlu, K., Gokceoglu, C., Ocakoglu, F., Nefeslioglu, H.A., and Acikalin, S. 2008. Prediction of uniaxial compressive strength of sandstones using petrography-based models. *Engineering Geology*, vol. 96. pp. 141–158. ◆

http://dx.doi.org/10.17159/2411-9717/2016/v116n8a13

Where to make the transition from open-pit to underground? Using integer programming

by J. Chung*, E. Topal*, and A.K. Ghosh†

Synopsis

The transition from open pit (OP) to underground (UG) operation is one of the challenging mining engineering issues. Mines that have the potential to transition from OP mining to UG mining will eventually come to a 'transition point' where the decision needs to be taken whether to extend the pit or switch to UG mining. In this paper we present a new integer programming (IP) formulation to obtain the optimal transition point from OP to UG mining. The proposed model is implemented on a three-dimensional (3D) gold deposit and a two-dimensional (2D) case study is used to demonstrate the validity of the model. Due to the large number of variables, strategies are proposed to shorten the solution time. The proposed model has successfully determined the optimal transition point and generated a significantly better undiscounted profit than that of the traditional approach.

Keywords
open pit, underground, transition point, mine optimization, integer programming.

Introduction

A mining project starts with an exploration stage that defines the location of the orebody and its properties that help to develop the geological block model. The geological block model can then be converted into an economic block model by including economic parameters such as mineral price and mining and processing cost. Later, the determination of the best possible mining strategy is emphasized.

The strategy for mining method selection plays an important role as it will directly affect the profit of the operation. Therefore, at this stage, the question is often 'Is the optimal mining method by open pit (OP), underground (UG) or combination of both?' (Topal, 2008). Globally, shallow deposits are generally mined by the OP method as it is economically superior to most UG mining methods with respect to production rate, dilution, safety, and other technical issues. However, OP mining is fairly sensitive to the mining depth because of haulage cost; thus, UG mining is usually applied for deep deposits.

Some shallow deposits extend vertically to considerable depth and thus have the potential to make the transition from OP to UG mining. Combining the OP and UG mining methods is referred to as combination mining. Worldwide, there are a few mines that have the potential to make the transition, or the transition has already been made, such as Kanowna Bell Western Australia, Chuquicamata in Chile, Grasberg in Indonesia, and Sunrise Dam in Western Australia.

The deposits that have the potential to make the transition from OP to UG will usually confront the 'transition problem'. In the combination mining method, 'transition point' refers to the point at which the decision has to be taken whether to (1) extend the pit or (2) switch from OP to UG. The determination of the optimum transition point is the 'transition problem'. The general view of the transition problem is illustrated in Figure 1.

In the current traditional approach to combined mining, the ultimate pit boundary will be determined and pit design will be accomplished as the first step. At this stage, the ultimate pit limit can be determined optimally by using algorithms such as the Lerchs-Grossman (LG) algorithm (Lerchs and Grossman, 1964) or maximum flow-based algorithms *e.g.*, pseudoflow algorithm (Hochbaum and Chen, 2000). The UG mine optimization and design will be started after the standard ultimate pit limit. However, according to Fuentes (2004), if the economic potential associated with the UG resources is taken into account, the final pit can be significantly diminished as shown in Figure 2. Therefore, it is essential to consider both OP and UG mining potential simultaneously, in

* *Department of Mining Engineering and Metallurgical Engineering, Western Australian School of Mines, Curtin University, Bentley Campus, WA, Australia.*

† *Department of Mining Engineering and Metallurgical Engineering, Western Australian School of Mines, Curtin University, Kalgoorlie Campus, WA, Australia.*

 ISSN 2225-6253. Paper received Jan. 2016; revised paper received Feb. 2016.

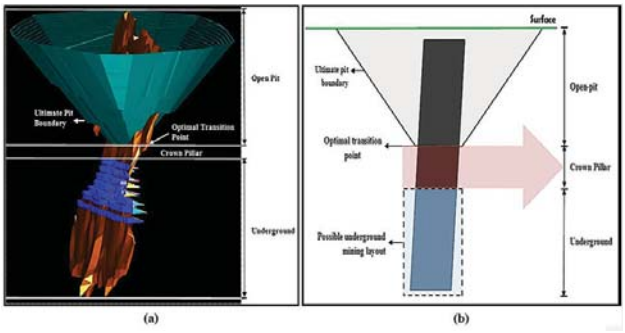

Figure 1—Schematic of Transition from OP to UG

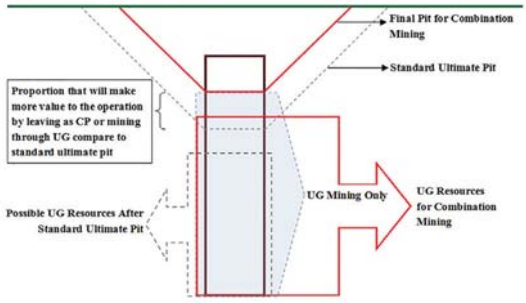

Figure 2—Resource configuration

order to maximize the project profit. In this paper we propose a new mathematical model in order to not only determine optimal transition point in three-dimensional space, but also the optimal mining strategy.

We firstly review the relevant literature to provide the context for the transition problem. The methodology used to formulate the transition problem and the formulation of the proposed integer programming (IP) model which optimizes the transition problem is then presented. The application of the proposed model in a two-dimensional (2D) case study is then illustrated, followed by a three-dimensional (3D) implementation along with strategies to reduce the computational size of the model. The paper concludes with a summary of the research findings and recommendations for future work.

Literature review and problem definition

Several research studies have been carried out previously to solve the transition problem. The first method was introduced by Soderberg and Rausch (1968), and involves the break-even cost differential between two mining methods as shown in the following formula:

$$Indicated\ Stripping\ Ratio = \frac{UG\ mining\ cost/ton\ ore - OP\ mining\ cost/ton\ ore}{OP\ stripping\ cost/ton\ waste}$$

This method emphasizes the relationship between the mining costs of 1 t of ore in both OP and UG compared to the waste removal cost. For instance, if the stripping ratio for any part of the deposit is less than the indicated stripping ratio; mining should be by OP. The shortcoming of this method is that it does not consider the cost of leaving a crown pillar and UG development work.

A methodology based upon cash flow was introduced by Nilsson (1982). This method takes the variations in the economic situation into consideration, including the impact of stripping ratio, interest rate, mining cost, and other components (Nilsson 1992, 1997). This is a trial-and-error method which is mainly based on the experience of the mine planner, and does not include any optimization strategy. Furthermore, the location of the crown pillar and the timing of transition are unknown.

Camus (1992) presented an innovative way to estimate block economic value (BEV) for block *i* which includes the profit on OP, UG, and stripping ratio as shown in the formula:

$$BEV\ of\ Block(i) = BEV\ (i)_{OP} - BEV\ (i)_{UG} - Stripping\ Cost$$

By using the traditional ultimate pit optimization methods, the pit boundary for a combined mining method can be determined. This approach is advantageous in large-scale case studies as it uses only a single block economic model, which reduces the size of the problem by 50%. However, this method has difficulty in crown pillar location and also takes no consideration of the UG mining process.

A heuristic approach has been used to solve the transition problem (Bakhtavar and Shahriar, 2007). In this method, the optimal pit limit is solved by using the Korabov algorithm and the blocks in the final pit level are divided into small sub-blocks and compared with the UG block values. These steps can help to define the transition depth. In addition, Abdollahisharif *et al.* (2008) also introduced a heuristic approach that outlines all the possible mining layout options and compares the profit generated by each option. A case study that employed this method was presented by Bakhtavar *et al.* (2010). The disadvantage of the heuristic approach is that the result is not optimal due to the nature of the methodology.

Mathematical modelling techniques are also used to solve the transition problem. For example, Bakhtavar *et al.* (2012) developed the binary integer programming model to define the optimal transition depth. The objective of the model is to maximize the overall profit by taking into account both the technical and the economic aspects of OP and UG mining methods. However, there are flaws in this mathematical model such as: (1) there is no consideration of an OP and crown pillar contiguous row of blocks, which will result in the location of the crown pillar away from bottom of the pit, and (2) the model is difficult to apply in real case studies due to its scale problem and computational intensity. Lastly, the model is formulated in 2D.

Opoku and Musingwini (2013) presented a structured approach to address the indicators to guide the decision-making process for the transition problem. The method chooses the most significant qualitative factors for the transition problem and incorporates them. Case scenarios are considered in the study for evaluation purposes. In the evaluation process, a comparison technique is utilized to overcome the transition problem. The authors introduced the term 'transition indicator' to guide the decision-making process. However, this approach depends heavily on the predetermined transition indicators and is not a true optimization process.

Where to make the transition from open-pit to underground?

Newman *et al.* (2013) evaluated the transition problem via a series of small longest-path problems with the objective of maximizing the profit, which is the discounted gross margin from the mined level minus the discounted UG development cost. The main objectives of this method are which level to mine by OP or UG and when to make the transition, as well as when to start UG mine development. The drawback of this approach is the scheduling that is developed per level/stratum is not practical.

Carli and Peroni (2014) proposed a preliminary analysis for the transition problem. The approach firstly generates the optimum ultimate pit by using the cut-off grade for OP mining and then estimates the UG resources (after pit exhaustion) considering the cut-off grade for UG mining. This approach considers OP and UG separately, which is not appropriate; as mentioned above, OP, UG, and crown pillar designs need to be considered simultaneously.

Dagdelen and Traore (2014) presented an iterative approach to determine the transition depth through an analysis of production scheduling for both OP and UG. The method starts the iteration process using the Whittle software to generate an ultimate pit boundary. Studio 5 and EPS software from CAE are then used to generate the stope layouts for UG mining, and OptiMine scheduler for the life-of-mine production schedule. Even though, the method aims to answer the questions 'where' and 'when' to transit from OP to UG, the methodology has some drawbacks. For example, it is based on an iterative process that does not generate an optimal solution; it assumes that transition will occur only after the ultimate pit boundary, which is not the case in most applications; and the crown pillar is unlikely to be at the optimum location.

Morales *et al.* (2015) assessed the optimal economic envelope for the combination mining method by creating a mathematical model. In order to solve the model, an algorithm that parameterizes the problem with regard to the location of the crown pillar and production level is developed. The framework of the algorithm uses the ultimate pit computations to search both the OP and UG mine plans. The iterative calculations are used to compute the different combinations of the OP mining level, UG mining level, and crown pillar location by placing the crown pillar at different locations. Evaluation of the results generated by different combinations will indicate the optimal transition envelope. The only criticisms of this method are that it is an iterative process, and also it does not consider the UG mine design, which leads to the impracticality of the transition envelope.

As many OP operations are approaching the final pit limit and/or have the potential to make the transition to UG mining, a competent method to handle the transition problem is required to maximize the project value and the resource utilization. This paper presents a new mathematical model that defines and resolves the transition problem for the combination mining method. Furthermore, the proposed model also helps to determine the best possible mining option for the deposit. The objective of the proposed model is to maximize the project's undiscounted profit among the options of (a) OP mining only, (b) UG mining only, or (c) a combination of OP and UG mining. Furthermore, if the model suggests combination mining as the preferred method, it will further define the mining layouts for OP and UG, including the position of the crown pillar.

Proposed model for the transition problem

The aim of a mathematical model is to represent a real-world problem through mathematical formulations. As the demand for mine planning optimization techniques increases in line with the number of shallow deposits approaching the designed final pit, the establishment of a mathematical model for the transition problem becomes more and more significant. IP, which is a well-recognized optimization technique in operation research, has the ability to find the optimal solution for the complex problem. Therefore, a special version of IP, namely the binary integer programming technique, is utilized in this paper to solve the transition problem optimally.

The IP technique is a branch of linear programming (LP). Generally, a LP problem is built with an objective function, a set of linear constraints, and a set of non-negativity restrictions which are shown as follows:

$$Max\ (Min)\ z = \sum_{n=1}^{n} c_n x_n$$

$$\text{subject to} \quad a_{11}x_1 + a_{12}x_2 + \cdots + a_{1n}x_n \le b_1$$

$$a_{21}x_1 + a_{22}x_2 + \cdots + a_{2n}x_n \le b_2$$

$$\vdots \quad \vdots \quad \vdots$$

$$a_{m1}x_1 + a_{m2}x_2 + \cdots + a_{mn}x_n \le b_m$$

$$Non-negativity\ restrictions: x_1, x_2, \cdots, x_n \ge 0$$

where z represents the objective function, which aims to maximize the profits or minimize the costs, x_i represents the decision variable for which values are to be determined by the model, a_{ij} and c_j are the constant coefficients representing the nature of the problem, and b_i is the right-hand side constant representing the availability of the resource for a constraint. Generally, an IP problem is a subcategory of an LP problem in which all the decision variables must be integer values as they represent entities that cannot be divided, such as people or machinery. A binary IP model is formed to capture the binary decisions 'yes' (0) and 'no' (1) such as if the block needs to be mined or not. Therefore, it is formed as a decision-making process, and 0 and 1 will be attributed to a decision of not extracting and extracting, respectively.

Notation and variables

Subscript notations

i, i'	Block reference name for OP mining
j, j'	Stope reference name for UG mining
k, k'	Mining level
m	Mining method; = 1 for OP mining and 2 for UG mining

Sets

M_i	Set of all blocks i in block model for OP mining
N_j	Set of all possible stopes j in block model for UG mining

O_i Set of overlying blocks should be removed in order to mine block i
B_j Set of the all stopes that share common blocks with stope j
LO_k Set of all OP blocks on level k
LU_k Set of all UG stopes on level k

Parameters

C_i The undiscounted profit to be generated by mining i
S_j The undiscounted profit to be generated by mining j
A Number of overlying blocks that need to be removed in order to mine ore block i
ℓ Number of rows that should successively remain as crown pillar

Decision variables

$$x_i = \begin{cases} 1, if\ block\ i\ mined\ through\ OP\ mining \\ 0, \quad otherwise \end{cases}$$

$$y_j = \begin{cases} 1, if\ stope\ j\ mined\ through\ UG\ mining \\ 0, \quad otherwise \end{cases}$$

$$T_{k,m} = \begin{cases} 1, if\ level\ k\ mined\ by\ mining\ method\ m \\ 0, \quad otherwise \end{cases}$$

$$H_k = \begin{cases} 1, if\ the\ level\ k\ leave\ as\ crown\ pillar \\ 0, \quad otherwise \end{cases}$$

Formulation

Objective function:

$$Max\ Z = \sum_{i \in M_i} C_i x_i + \sum_{j \in N_j} S_j y_j$$

Subject to:

OP slope constraints

$$A \cdot x_i - \sum_{i' \in O_i} x_{i'} \leq 0 \qquad \forall\, i, i' \in O_i \qquad [1]$$

UG stope design constraints

$$y_j + \sum_{j' \in B_j} y_{j'} \leq 1 \qquad \forall\, j, j' \in B_j \qquad [2]$$

Reserve restriction and 'one mining method for each level' constraints

$$T_{k,m} - x_i \geq 0 \quad \forall\, i | i \in LO_k, \quad m = 1 \qquad [3]$$

$$T_{k,m} - y_j \geq 0 \quad \forall\, j | j \in LU_k, \quad m = 2 \qquad [4]$$

$$\sum_{m=1}^{2} T_{k,m} + H_k \leq 1 \qquad \forall\, k \qquad [5]$$

Crown pillar location constraints

$$\ell \cdot T_{k,m} + \sum_{k'=0}^{k} H_{1+k'} \geq \ell \quad \forall\, k, k', m = 1 \qquad [6]$$

$$\ell \cdot T_{\ell+1,m} - \sum_{k'=1}^{\ell} H_{k'} \leq 0 \quad \forall k, m = 2 \qquad [7]$$

Non-negativity and integer constraints

$$x_i, y_j, T_{k,m}, H_k \in \{0,1\} \quad \forall\, i, j, k, m \qquad [8]$$

The objective function is formulated to maximize the profit gained through OP and UG mining operations. C_i and S_i are the constants that represent the undiscounted profit of OP and UG mining, respectively. These values will associate with one decision variable from either OP (x_i or UG y_i to form the equation representing the objective function.

The constraint [1] is established to hold the OP slope restriction. It forces all the overlying blocks to be mined in order to extract a given block. Conventionally, a 45-degree slope angle is considered. Therefore, in a three-dimensional case, it can be 1 to 5 or 1 to 9, which means that in order to mine an ore block, 5 or 9 overlying blocks will need to be removed.

Constraint [2] ensures that there is no overlapping stope is the final stope layout – only one stope can be removed from all possible stopes which share at least one common block. For further explanation, if the stope j which is formed by blocks 1–8 is selected to be mined, none of these blocks can be part of another mineable stope to avoid overlapping in the final stope layout.

Constraints [3], [4], and [5] are formed for the purpose of reserve restriction and to ensure that only one mining method (OP or UG) is employed for each row. Constraints [3] and [4] enforce that if a block or a stope is selected to be mined, the entire row will be mined through the same mining method. As an example, if block i located at level k is removed with OP mining, the entire k level will be mined through OP mining, and if one of the blocks within the mineable stope j located at level k is mined with UG mining, the entire k level will be mined through UG only. Constraint [5] is used to ensure that each row can be mined either through OP or UG or left as crown pillar.

The crown pillar plays an important role in the transition problem as it is used for strata control and to prevent inrush of water. Therefore, a good crown pillar design will reduce or even eliminate most of the geotechnical issues, particularly in the combination mining method. Constraint [6] is used to make sure that an appropriate number of rows remain as crown pillar, as dictated by the geotechnical requirements of the deposit. It also ensures that the crown pillar is located between the UG layout and final pit limit.

Furthermore, constraint [7] is structured to guarantee that if the whole deposit is mined through the UG method, an adequate thickness of roof remains.

Constraint [8] ensures non-negativity and integer nature of the variables, as required.

Validation of the proposed model

In order to demonstrate the validation of the proposed IP formulation, a 2D hypothetical block model has been developed and utilized. This section discusses the results generated by the model and compares the results of the combination mining method and single mining method, as well as the traditional transition approach. The IP model and its data file were written using Microsoft Excel VBA (2010) programming code. IBM CPLEX ILOG Corp. (2013) was used to solve the optimization model on a standard office computer (Dell OPTIPLEX 9020 with Intel Core i7 3.40 GHz CPU and 8 GB installed RAM).

The 2D hypothetical deposit containing 204 blocks with a size of 20 x 20 m and a stope size of 2 x 2 was used. The

Where to make the transition from open-pit to underground?

BEVs of both OP and UG have been calculated and are shown in Figure 3 and Figure 4 respectively.

For the 2D case study, the number of decision variables and constraints required to solve the proposed model is 444 and 841 respectively. The solution time for this case is less than a minute with 0% gap. As can be seen from Figure 5, the model recommends that levels 1 to 5 should be mined through OP, two levels below the pit will be reserved as a crown pillar, and the remaining levels will employ UG mining. Therefore, the optimal transition depth is 80 m. According to Figure 6, all the constraints included in the model are satisfied. Thus, the validity of the model has successfully been verified through the 2D hypothetical case.

Furthermore, three other mining strategies have been considered: (1) OP mining only, (2) UG mining only, and (3) the traditional approach which utilizes OP mining until the ultimate pit boundary is determined via LG, then switches to UG mining. The results generated by these mining strategies are shown in Figure 6.

1	1	1	1	1	4	4	-1	2	4	4	4	-2	-2	-2	-2	-2
-3	-3	-3	1	2	1	0	3	5	5	0	-1	-2	-3	-3	-3	-3
-4	-3	-4	-4	-3	1	3	5	6	5	1	-1	-3	-3	-4	-4	-3
-4	-3	-4	-4	-3	-1	9	8	5	3	8	-2	5	-4	-4	-4	-4
-5	-5	-5	-5	-5	0	1	1	2	2	-1	8	-4	-5	-5	-5	-5
-5	0	-5	-5	0	11	7	1	3	-1	6	-5	-5	-5	-5	-5	-5
-6	-2	-6	-6	-2	-1	2	2	2	4	-6	-6	-6	-6	-6	-6	-6
-8	-4	-8	-8	1	1	1	2	2	2	-7	-8	-8	-8	-8	-8	-8
-9	-6	-9	-9	-6	1	1	-9	-9	-9	-9	-9	-9	-9	-9	-9	-9
-9	-6	-9	-9	-6	-3	-6	-9	-9	-9	-9	-9	-9	-9	-9	-9	-9
-9	-6	-9	-9	-6	-3	-6	-9	-9	-9	-9	-9	-9	-9	-9	-9	-9
-9	-6	-9	-9	-6	-3	-6	-9	-9	-9	-9	-9	-9	-9	-9	-9	-9

Figure 3—OP economic block model

-1	-1	-1	-1	-1	-2	-1	1	1	2	0	0	-1	-1	-1	-1	-1
-1	-1	-1	-1	0	1	1	0	1	-1	-1	-1	-1	-1	-1	-1	-1
-2	-2	-2	-2	-2	-2	-1	1	0	2	1	-1	-2	-2	-2	-2	-2
-2	-2	-2	-2	-2	-1	2	1	0	-1	0	-1	-2	-2	-2	-2	-2
-2	-2	-2	-2	-2	-1	1	2	0	2	0	-1	-2	-2	-2	-2	-2
-2	-2	-2	-2	-2	-1	-1	-1	-1	0	-1	-2	-2	-2	-2	-2	-2
-3	-3	-3	-3	1	-2	2	5	2	-4	-5	-3	-3	-3	-3	-3	-3
-3	-3	-3	-3	-2	-1	1	2	3	-3	-3	-3	-3	-3	-3	-3	-3
-3	-3	-3	-3	-2	-1	1	12	4	-3	-3	-3	-3	-3	-3	-3	-3
-3	-3	5	-3	5	5	2	12	7	-3	-3	-3	-3	-3	-3	-3	-3
-3	-3	-3	5	-1	5	5	6	7	-3	-3	-3	-3	-3	-3	-3	-3
-3	-3	5	-3	-1	5	2	6	1	-3	-3	-3	-3	-3	-3	-3	-3

Figure 4—UG economic block model

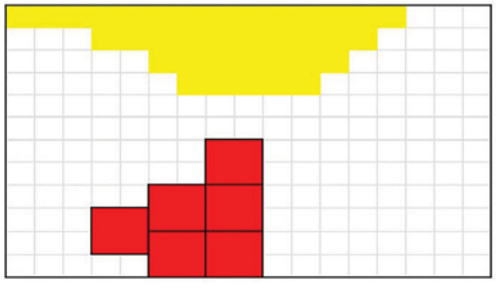

Figure 5—Mining layout of combination mining for two-dimensional case study

The result generated by each mining strategy is shown in Table I. It demonstrates that by using the proposed IP model, the profit generated by the 2D hypothetical case study can maximize the undiscounted profit up to 186 units. The proposed method has successfully improved the undiscounted profit by more than 30% for the traditional approach, and more than 75% and 84% for UG mining and OP mining respectively.

Implementation of proposed model in a 3D case study

The proposed IP model is applied to a gold deposit in 3D consisting of 83 025 blocks with average grade of 1 g/t. The block size is 20 × 20 × 20 m and each stope size consists of 2 × 2 × 2 blocks totalling 8 blocks. Figure 7 presents the grade distribution of the resource model.

The computational time required to obtain an optimized solution depends heavily on the decision variables; as the number of variables increases, the solution time increases

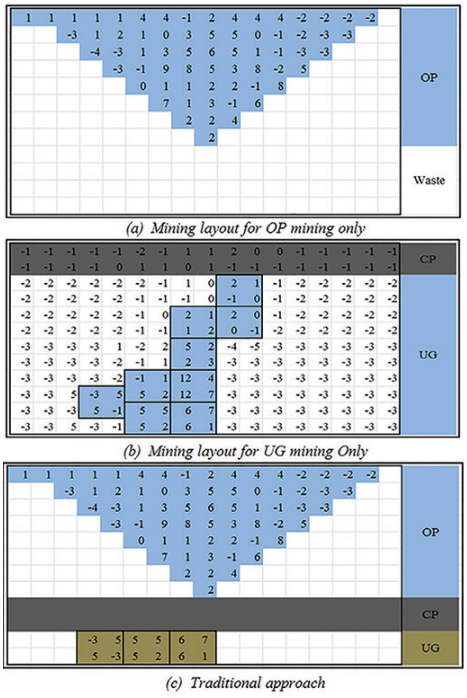

Figure 6—Mining layout for (a) OP mining only, (b) UG mining only, (c) Traditional approach

Table I

The results generated by each possible mining strategy: OP only, UG only, traditional approach, and combination mining (proposed IP model) in 2D case study

Mining method	Undiscounted profit ($)
New IP model	186
Traditional transition from OP to UG approach	142
UG mining method only	106
OP mining method only	101

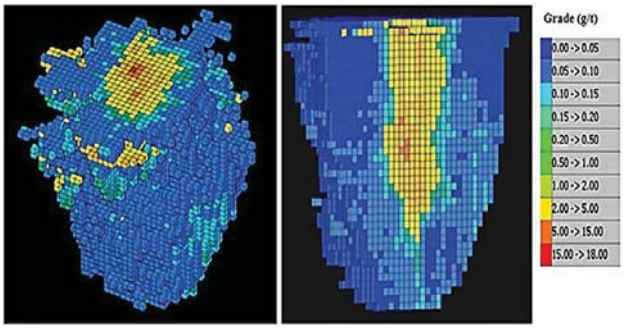

Figure 7—Resource model configurations

exponentially. Therefore, in order to keep the solution time reasonable, reduction of the problem size is crucial.

For the 3D case study, 166 173 decision variables and 332 183 constraints are required to formulate the problem to obtain the optimal solution, which requires approximately 34.5 hours. Therefore, some strategies are suggested in the next section to reduce the solution time while maintaining optimality of the results.

Strategies to handle a large-scale IP problem

The IP technique has been recognized as the method that has the potential to optimally solve real case problems; however, it requires a large number of variables and constraints to formulate the large-scale models. Furthermore, the magnitude of the variables can increase substantially when the stochastic models are considered (Groeneveld and Topal, 2011). It may, in some instances, preclude obtaining an optimal solution considering today's computing power. In order to overcome the deficiencies of the IP model, some tactics have been employed to keep the number of variables at the minimum level. With the assistance of these tactics, the efficiency of the proposed model can be maintained and it will be able to generate the optimal solution that satisfies the model integrity. The main techniques applied in the proposed model are focused on UG mine design and optimization as follows.

- Stope-based modelling is introduced instead of block-based modelling, as shown in Figure 8. The idea, which was proposed by Little and Topal (2011), is an innovative way to reduce the number of variables in the optimization model. For instance, instead of considering eight decision variables in 2 x 2 x 2 stope design, only one variable is considered for each stope, which represents eight blocks. The naming of the stope is X (first block coordinate) / (last block coordinate); using Figure 8 as an example, the stope is referenced as X (1,1,1)/(2,2,2)
- The predetermination of the positive value stope strategy is also utilized. This determines all the positive stopes in the prior stage of the mathematical model for UG mining. This strategy successfully reduces the variables in the proposed model by taking only the positive stopes into consideration and removing all the unprofitable stopes, which shortens the solution time (Little *et al.*, 2013). This strategy provides the optimality of the proposed model by considering all the positive stopes and discarding the stopes formed by waste (meaningless variables) in the model.

Gap is often represented as x% which means that the feasible solution is to be within x% optimality. To solve large-scale models, it is usually thought that a proved optimum is unlikely to be obtained within a reasonable amount of computational time. Thus, a gap (x%) can be chosen to reduce the solution times.

Model implementation and discussion of results

As many hours are required for obtaining an optimal solution of a larger model, the strategies discussed in the previous section have been adopted for the purpose of reduction the scale of the problem and solution time.

1. A stope-based mathematical model is used for UG mine planning and optimization. This approach has reduced the number of constraints drastically by one-eighth
2. A pre-processing step to determine the qualified stope has been included. This has successfully excluded all the non-profitable stopes and reduced the variables in the mathematical model. In the 3D case study, the mathematical model for UG mine optimization has 86 562 blocks. The process of obtaining the positive stopes takes approximately 1 hour, with 2910 positive stopes obtained. This strategy helps to reduce the 86 562 UG variables to 2910 variables in the proposed IP model. The profitable stopes thus determined will be substituted into the proposed IP model.
3. Often, an improvement of 1% gap will take quite a lot of time but may not improve the optimal result. Therefore, a 5% gap is used in this paper.

The whole process for solving the transition problem and associated size reduction strategies is demonstrated in Figure 9. Firstly, the block economic model (BEM) of both OP and UG mining is established. Then, the size reduction strategies are implemented:

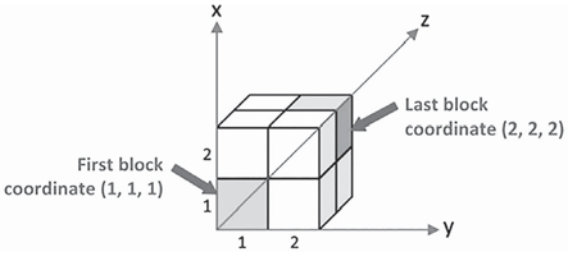

Figure 8—Stope reference terminology example (Little and Topal, 2011)

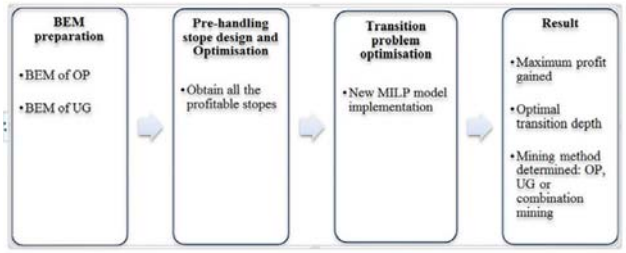

Figure 9—Process to solve the transition problem with the pre-handling technique

1. Find all the possible stopes in the UG BEV
2. Obtain all the profitable stopes out of all possible stopes.

Then, by substituting the outcome from the pre-handling stope design and optimization step, and the OP's BEM into the proposed model, the IP model for the transition problem is formulated. The model is solved by using one of the commercially available solvers, in this case CPLEX. CPLEX is used to solve the IP model to find optimal transition depth that creates the maximum profit for the project.

By employing all the suggested strategies, the decision variables required to solve the 3D case study have successfully been reduced from 166 173 to 86 058. The optimal result with less than 5% gap is obtained in approximately 2.5 hours with an $8.813 million undiscounted profit. The result obtained by the proposed model is compared with the result from other mining strategies in Table II. The result generated by the proposed model provides a much higher undiscounted profit compared to any other options.

Currently, mines that have the potential to make the transition mostly exercise the traditional approach – obtain the optimal pit limit first and observe the transition later. However, the traditional approach may not generate the maximum profit for the operation. This can be observed from the result presented in Table II; the proposed model generated approximately 5% more undiscounted profit than the UG mining method only, and 50% and 144% better than the traditional approach and OP mining method, respectively. Therefore, in order to maximize the value of the operation, it is essential to consider OP and UG mining methods simultaneously.

Furthermore, as indicated previously, the proposed model gives guidance for mining strategy selection by means of the maximized profit generated by the deposit through OP, UG, or combination mining strategy. Table II shows that UG mining results in a better undiscounted profit than OP mining, while the traditional approach also does not achieve as much as UG mining. Figure 2 illustrates the resource split for different mining strategies. It shows that there is a proportion of the resource to be left as the crown pillar or mined by UG methods in order to generate the maximized profit.

Figure 10 presents the result generated by the model for different mining strategies. It recommends that the first seven levels should be mined by OP, and then two levels left for the crown pillar followed by UG mining starting from level 10 and ceasing at level 41. The optimal transition point is at level 7 and the transition depth is 140 m – 7 (levels) x 20 *m*.

For the 3D case study, to obtain the optimal solution for the transition problem, the process presented in Figure 9 was followed. The whole process took approximately 3.5 hours (1 hour for UG optimization plus 2.5 hours to solve the new IP model) to generate the optimal solution for the transition problem, which is a significant improvement as it is a reduction of approximately 90% on the initial computation time (34.5 hours). Consequently, these strategies help to reduce the variables handling in the proposed IP model and improve the solution time drastically for a large-scale implementation.

Table II

The results generated by each possible mining strategy: OP only, UG only, traditional approach, and combination mining (proposed IP model) in 3D case study

Mining method	Undiscounted profit ($ million)
New IP model	8.813
UG mining method only	8.397
Traditional approach	5.867
OP mining method only	3.603

Conclusion and recommendations

Over the years, the optimization of the transition from OP to UG operation has become a significant issue and created a new challenge for the mine design process. A new IP model is proposed to provide a tool to solve the transition problem, which is able to maximize the profit gained from the operation within a reasonable solution time. The framework of the proposed model is on a 3D basis. It uses the block economic values as the coefficients in the objective function associated with a set of constraints for OP mining, UG stope mining, mining method, and reserve restriction.

A hypothetical 2D model was generated and utilized as the inputs to the proposed model to demonstrate the validity of the model. The result generated by the proposed model – combination mining method ($186) was compared with the results from other considered mining methods, which included the traditional transition approach ($146), UG mining method only ($106), and OP mining method only ($101). This showed that in the hypothetical case study, the combination mining method would generate the maximum profit for the operation. It also proved that it is essential to consider both OP and UG simultaneously.

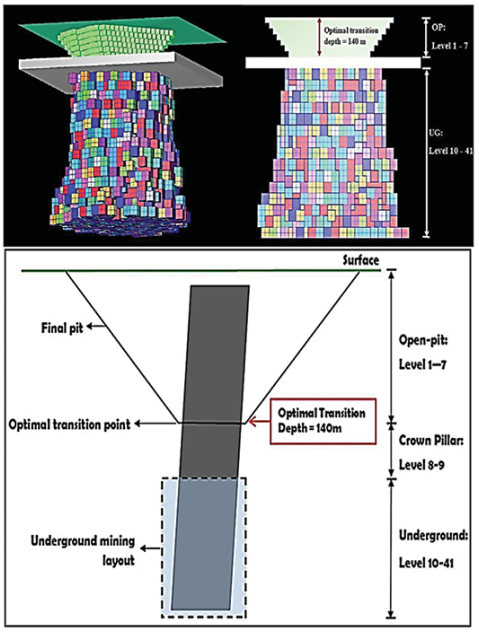

Figure 10—Mining layout generated by the new IP model

The 3D case study, which had 83 025 blocks, required roughly 27.5 hours to solve. It was shown that an increase in the number of decision variables will increase the solution time exponentially. Therefore, stope reference and pre-handling stope design and optimization strategies are employed to reduce the number of decision variables required for the proposed model. The solution time for the IP model, which employed the proposed strategies, was reduced to 3.5 hours. The 3D case study generated approximately $8.813 million undiscounted profit with a 5% gap, with an optimal transition depth of 140 m. This is approximately 50% higher than the undiscounted profit generated by the traditional approach to the transition problem. Furthermore, the approach proposed in this paper is equally effective in both greenfield and brownfield projects.

Although this research has demonstrated that IP modelling is an effective technique for solving the transition problem, there is a need to improve the practicality and performance of the current model. Further research is underway that focuses on the timing of the transition to maximize the NPV of the project, as well as methodologies to reduce the solution time further. Future research will also study the effect of the uncertainties involved in mining projects that affects the transition points. Changes in uncertain variables such as commodity price, operating cost, and geological uncertainty will influence the transition point directly. For instance, grade uncertainty has a great impact on the determination of the transition point (Chung *et al.*, 2015).

References

Abdollahisharif, J., Bakhtavar, E., Shahriar, K., Sobczyk, J., and Kicki, J. 2008. Open-pit to underground mining – where is the optimum transition depth. *Proceedings of the 21st World Mining Congress & Expo 2008*. pp. 189–196.

Bakhtavar, E., Namin, F.S., and Oraee, K. 2010. Practical final pit depth considering the future underground mining – a case study. *SME Annual Meeting and Exhibit*. Society for Mining, Metallurgy and Exploration, Littleton, Colorado.

Bakhtavar, E. and Shahriar, K. 2007. Optimal ultimate pit depth considering an underground alternative. *Proceedings of the Fourth Aachen International Mining Symposium on High Performance Mine Production*, Germany. pp. 213–221.

Bakhtavar, E., Shahriar, K., and Mirhassani, A. 2012. Optimization of the transition from open-pit to underground operation in combined mining using (0-1) integer programming. *Journal of the Southern African Institute of Mining and Metallurgy*, vol. 112, no. 12. pp. 1059–1064.

Camus, J.P. 1992. Open pit optimization considering an underground alternative. *Proceedings of the 23th International APCOM Symposium*, Tucson, AZ. Society for Mining, Metallurgy and Exploration, Littleton, Colorado. pp. 435–441.

Carli, C.D. and Peroni, R.L. 2014. An approach to define the optimal transition point from open pit to underground mining. *Proceedings of the 36th APCOM Symposium*, Porto Alegre, Brazil. pp. 367–377.

Chung, J., Topal, E. and Erten, O. 2015. Transition from open-pit to underground – using Integer Programming considering grade uncertainty. *Proceedings of the 17th Annual Conference of the International Association for Mathematical Geosciences*, Freiberg, Germany. Schaeben, H., Delgado, R.T., Boogart, K. G., and Boogart, R. (eds.). pp. 268–277.

Dagdelen, K. and Traore, I. 2014. Open pit transition depth determination through global analysis of open pit and underground mine scheduling. *Proceedings of Orebody Modelling and Strategic Mine Planning*, Perth, Australia, Dimitrakopoulus, R. (ed.). Australasian Institute of Mining and Metallurgy, Melbourne. pp. 195–200.

Fuentes, S.S. 2004. Going to an underground (UG) mining method. *Proceedings of MassMin 2004*, Santiago, Chile. pp. 633–636.

Groeneveld, B. and Topal, E. 2011. Flexible open-pit mine design under uncertainty. *Journal of Mining Science*, vol. 47, no. 2. pp. 212–226.

Hochbaum, D.S. and Chen, A. 2000. Performance analysis and best implementations of old and new algorithms for the open-pit mining problem. *Operations Research*, vol. 48, no. 6. pp. 894–914.

Ibm Cplex Ilog Corp. 2013. Version 12.6.

Lerchs, H. and Grossmann, F.I. 1964. Optimum design of open-pit mines. *CIM Bulletin*, vol. 58. pp. 47–54.

Little, J., Knights, P., and Topal, E. 2013. Integrated optimization of underground mine design and scheduling. *Journal of the Southern African Institute of Mining and Metallurgy*, vol. 113, no. 10. pp. 775–785.

Little, J. and Topal, E. 2011. Strategies to assist in obtaining an optimal solution for an underground mine planning problem using Mixed Integer Programming. *International Journal of Mining and Mineral Engineering*, vol. 3, no. 2. pp. 152–172.

Morales, N., Julio, C., Amaya, J., and Lamghari, A. 2015. Optimal economic envelope of joint open pit and underground mines. *Proceedings of the 37th APCOM Symposium*, Fairbanks, Alaska. Society for Mining, Metallurgy and Exploration, Littleton, Colorado. pp. 343–351.

Newman, A.M., Yano, C.A., and Rubio, E. 2013. Mining above and below ground: timing the transition. *IIE Transactions*, vol. 45, no. 8. pp. 865–882.

Nilsson, D. 1982. Open-pit or underground mining. *Underground Mining Methods Handbook*. Hustrulid, W.A. (ed.). American Institute of Mining, Metallurgical, and Petroleum Engineers, New York. pp. 70–87.

Nilsson, D. 1992. Surface *vs.* underground methods. SME Mining Engineering Handbook. Hartman, H.L. (ed.). Society for Mining, Metallurgy, and Exploration, Littleton, Colorado. vol. 2. pp. 2058–2069.

Nilsson, D. 1997. Technical note: Optimal final pit depth: once again. *Mining Engineering*, vol. 49, no. 1. pp. 71–72.

Opoku, S. and Musingwini, C. 2013. Stochastic modelling of the open pit to underground transition interface for gold mines. *International Journal of Mining Reclamation and Environment*, vol. 27, no. 6. pp. 407–424.

Soderberg, A. and Rausch, D.O. 1968. Pit planning and layout. *Surface Mining*. Pfleider, E.P. (ed.). American Institute of Mining, Metallurgical, and Petroleum Engineers, New York. pp. 142–143.

Topal, E. 2008. Early start and late start algorithms to improve the solution time for long-term underground mine production scheduling. *Journal of the Southern African Institute of Mining and Metallurgy*, vol. 108, no. 2. pp. 99–107. ◆

INTERNATIONAL ACTIVITIES

2016

27 August–4 September 2016 — **35th International Geological Congress**
Cape Town, South Africa
Contact: Craig Smith
Tel: +27 11 492-3370, Fax: +27 11 492-3371
E-mail: craig.smith@gssa.org.za

31 August–2 September 2016 — **MINESafe Conference Striving for Zero Harm**
Emperors Palace, Hotel Casino Convention Resort
Contact: Raymond van der Berg
Tel: +27 11 834-1273/7, Fax: +27 11 838-5923/833-8156
E-mail: raymond@saimm.co.za,
Website: http://www.saimm.co.za

12–13 September 2016 — **Mining for the Future 2016 'The Future for Mining starts Now'**
Electra Mining, Nasrec, Johanannesburg
Contact: Camielah Jardine
Tel: +27 11 834-1273/7, Fax: +27 11 838-5923/833-8156
E-mail: camielah@saimm.co.za,
Website: http://www.saimm.co.za

12–14 September 2016 — **8th International Symposium on Ground Support in Mining and Underground Construction**
Kulturens Hus – Conference & Congress, Luleå, Sweden
Contact: Erling Nordlund
Tel: +46-920493535, Fax: +46-920491935
E-mail: erling.nordlund@ltu.se,
Website: http://groundsupport2016.com

27 September 2016 — **Global Mining Standards and Guidelines Group '*Underground Mining Forum*'**
Wits Club, University of the Witwatersrand, Johannesburg
Contact: Raymond van der Berg
Tel: +27 11 834-1273/7, Fax: +27 11 838-5923/833-8156
E-mail: raymond@saimm.co.za,
Website: http://www.saimm.co.za

19–21 October 2016 — **AMI Ferrous and Base Metals Development Network Conference 2016**
Southern Sun Elangeni Maharani, KwaZulu-Natal, South Africa
Contact: Raymond van der Berg
Tel: +27 11 834-1273/7, Fax: +27 11 838-5923/833-8156
E-mail: raymond@saimm.co.za,
Website: http://www.saimm.co.za

25 October 2016 — **14th Annual Student Colloquium**
Mintek, Randburg
Contact: Raymond van der Berg
Tel: +27 11 834-1273/7, Fax: +27 11 838-5923/833-8156
E-mail: raymond@saimm.co.za,
Website: http://www.saimm.co.za

2017

9–10 March 2017 — **3rd Young Professionals Conference**
Innovation Hub, Pretoria, South Africa
Contact: Camielah Jardine
Tel: +27 11 834-1273/7, Fax: +27 11 838-5923/833-8156
E-mail: camielah@saimm.co.za,
Website: http://www.saimm.co.za

9–12 May 2017 — **6th Sulphur and Sulphuric Acid 2017 Conference**
Cape Town, South Africa
Contact: Camielah Jardine
Tel: +27 11 834-1273/7, Fax: +27 11 838-5923/833-8156
E-mail: camielah@saimm.co.za,
Website: http://www.saimm.co.za

25–28 June 2017 — **Emc 2017: European Metallurgical Conference**
Leipzig, Germany
Contact: Paul-Ernst-Straße
Tel: +49 5323 9379-0, Fax: +49 5323 9379-37
E-mail: EMC@gdmg.de,
Website: http://emc.gdmb.de

27–29 June 2017 —**4th Mineral Project Valuation Colloquium**
Mine Design Lab, Chamber of Mines Building,
The University of the Witwatersrand, Johannesburg
Contact: Raymond van der Berg
Tel: +27 11 834-1273/7, Fax: +27 11 838-5923/833-8156
E-mail: raymond@saimm.co.za,
Website: http://www.saimm.co.za

2–7 October 2017 — **AfriRock 2017: ISRM International Symposium 'Rock Mechanics for Africa'**
Cape Town Convention Centre, Cape Town
Contact: Raymond van der Berg
Tel: +27 11 834-1273/7, Fax: +27 11 838-5923/833-8156
E-mail: raymond@saimm.co.za,
Website: http://www.saimm.co.za

25–27 October 2017 — **AMI Precious Metals 2017 'The Precious Metals Development Network (PMDN)'**
Gauteng, South Africa
Contact: Raymond van der Berg
Tel: +27 11 834-1273/7, Fax: +27 11 838-5923/833-8156
E-mail: raymond@saimm.co.za,
Website: http://www.saimm.co.za

Company Affiliates

The following organizations have been admitted to the Institute as Company Affiliates

3 M South Africa

AECOM SA (Pty) Ltd

AEL Mining Services Limited

Air Liquide (PTY) Ltd

AMEC GRD SA

AMIRA International Africa (Pty) Ltd

ANDRITZ Delkor (Pty) Ltd

Anglo Operations (Pty) Ltd

Arcus Gibb (Pty) Ltd

Aurecon South Africa (Pty) Ltd

Aveng Engineering

Aveng Mining Shafts and Underground

Axis House Pty Ltd

Bafokeng Rasimone Platinum Mine

Barloworld Equipment -Mining

BASF Holdings SA (Pty) Ltd

BCL Limited

Becker Mining (Pty) Ltd

BedRock Mining Support Pty Ltd

Bell Equipment Limited

Blue Cube Systems (Pty) Ltd

Caledonia Mining Corporation

CDM Group

CGG Services SA

Concor Mining

Concor Technicrete

Cornerstone Minerals Pty Ltd

Council for Geoscience Library

Cronimet Mining Processing SA (Pty) Ltd

CSIR Natural Resources and the Environment (NRE)

Data Mine SA

Department of Water Affairs and Forestry

Digby Wells and Associates

DRA Mineral Projects (Pty) Ltd

DTP Mining

Duraset

Elbroc Mining Products (Pty) Ltd

eThekwini Municipality

Exxaro Coal (Pty) Ltd

Exxaro Resources Limited

FLSmidth Minerals (Pty) Ltd

Fluor Daniel SA (Pty) Ltd

Franki Africa (Pty) Ltd-JHB

Fraser Alexander Group

Geobrugg Southern Africa (Pty) Ltd

Glencore

Goba (Pty) Ltd

Hall Core Drilling (Pty) Ltd

Hatch (Pty) Ltd

Herrenknecht AG

HPE Hydro Power Equipment (Pty) Ltd

IMS Engineering (Pty) Ltd

Ivanhoe Mines SA

Joy Global Inc.(Africa)

Kudumane Manganese Resources

Leco Africa (Pty) Limited

Longyear South Africa (Pty) Ltd

Lonmin Plc

MAGOTTEAUX (PTY) LTD

MBE Minerals SA Pty Ltd

MCC Contracts (Pty) Ltd

MD Mineral Technologies SA (Pty) Ltd

MDM Technical Africa (Pty) Ltd

Metalock Engineering RSA (Pty) Ltd

Metorex Limited

Metso Minerals (South Africa) Pty Ltd

MineRP Holding (Pty) Ltd

Mintek

MIP Process Technologies (Pty) Ltd

MSA Group (Pty) Ltd

Multotec (Pty) Ltd

Murray and Roberts Cementation

Nalco Africa (Pty) Ltd

Namakwa Sands(Pty) Ltd

New Concept Mining (Pty) Limited

Northam Platinum Ltd - Zondereinde

PANalytical (Pty) Ltd

Perkinelmer

Polysius A Division Of Thyssenkrupp Industrial Sol

Precious Metals Refiners

Rand Refinery Limited

Redpath Mining (South Africa) (Pty) Ltd

Rocbolt Technologies

Rosond (Pty) Ltd

Royal Bafokeng Platinum

Roymec Global (Pty) Ltd

RungePincockMinarco Limited

Rustenburg Platinum Mines Limited

Salene Mining (Pty) Ltd

Sandvik Mining and Construction Delmas (Pty) Ltd

Sandvik Mining and Construction RSA(Pty) Ltd

SANIRE

SENET (Pty) Ltd

Senmin International (Pty) Ltd

Smec South Africa

SMS group Technical Services South Africa (Pty) Ltd

Sound Mining Solution (Pty) Ltd

South 32

SRK Consulting SA (Pty) Ltd

Technology Innovation Agency

Time Mining and Processing (Pty) Ltd

Tomra (Pty) Ltd

Ukwazi Mining Solutions (Pty) Ltd

Umgeni Water

Vietti Slurrytec (Pty) Ltd

Webber Wentzel

Weir Minerals Africa

Worley Parsons RSA (Pty) Ltd

Forthcoming SAIMM events...

EXHIBITS/SPONSORSHIP
Companies wishing to sponsor and/or exhibit at any of these events should contact the conference co-ordinator as soon as possible

For the past 120 years, the Southern African Institute of Mining and Metallurgy, has promoted technical excellence in the minerals industry. We strive to continuously stay at the cutting edge of new developments in the mining and metallurgy industry. The SAIMM acts as the corporate voice for the mining and metallurgy industry in the South African economy. We actively encourage contact and networking between members and the strengthening of ties. The SAIMM offers a variety of conferences that are designed to bring you technical knowledge and information of interest for the good of the industry. Here is a glimpse of the events we have lined up for 2016. Visit our website for more information.

SAIMM
THE SOUTHERN AFRICAN INSTITUTE OF MINING AND METALLURGY

For further information contact:
Conferencing, SAIMM
P O Box 61127, Marshalltown 2107
Tel: (011) 834-1273/7
Fax: (011) 833-8156 or (011) 838-5923
E-mail: raymond@saimm.co.za

SAIMM DIARY

2016

- **CONFERENCE**
  MINESafe Conference Striving for Zero Harm
  31 August–2 September 2016, Emperors Palace, Hotel Casino Convention Resort,
- **CONFERENCE**
  Mining for the Future 2016 *'The Future for Mining starts Now'*
  12–13 September 2016, Electra Mining, Nasrec, Johannesburg
- **Forum**
  Global Mining Standards and Guidlines Group '*Underground Mining Forum*' Conference 2016
  27 September 2016, Wits Club, University of the Witwatersrand, Johannesburg
- **CONFERENCE**
  AMI Ferrous and Base Metals Development Network Conference 2016
  19–21 October 2016, Southern Sun Elangeni Maharani, KwaZulu-Natal
- **COLLOQUIUM**
  14th Annual Student Colloquium
  25 October 2016, Mintek, Randburg

2017

- **CONFERENCE**
  3rd Young Professionals Conference
  9–10 March 2017, Innovation Hub, Pretoria
- **CONFERENCE**
  6th Sulphur and Sulphuric Acid 2017 Conference
  9–12 May 2017, Cape Town, South Africa
- **CONFERENCE**
  4th Mineral Project Valuation Colloquium
  27–29 June 2017, The University of the Witwatersrand, Johannesburg
- **SYMPOSIUM**
  AfriRock 2017: ISRM International Symposium *'Rock Mechanics for Africa'*
  2–7 October 2017, Cape Town Convention Centre, Cape Town
- **CONFERENCE**
  Precious Metals 2017 'The Precious Metals Development Network (PMDN)'
  25–27 October 2017, Gauteng, South Africa

CM solutions

metallurgical consultancy & laboratories

maximizing metallurgy

Our four-in-one solution.
We do your test work,
interpret it,
model it
and integrate the results
in metallurgical designs.

Our laboratory areas of expertise

- Mineral processing
- Hydrometallurgy
- Chemical analysis
- Process development
- Solid liquid separation
- Pyrometallurgy

CM SOLUTIONS IS AN
ISO 9001:2008
ACCREDITED COMPANY
Certificate 91215729,
audited by DEKRA GmbH, Stuttgart

T 011 608 0019
F 011 608 4067
C 082 441 2788
E consultants@cm-solutions.co.za

Pinelands Office Park
Unit T5, 1 Ardeer Road
Modderfontein, 1609
South Africa

Find us on www.cm-solutions.co.za

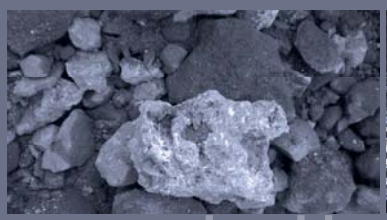


conductivity leaching test rig calcining wet chemistry sulfides shaking agitation electrowinning filtration furnace ion exchange open tanks roasting solvent extraction batch tests milling DMS pressure oxidation TCLP cyclone Isotherms PSD pilot plant cathode kinetics cell design flocculant screening flotation crushing ICP-OES crushing pyrometallurgy cyanidation attritioning water analysis thickening pressure oxidation heap pH control solid liquid separation